Accessing molecule-metal and hetero-molecular interfaces with direct and resonant photoelectron spectroscopy

Dissertation

zur Erlangung des naturwissenschaftlichen Doktorgrades der

Julius-Maximilians-Universität Würzburg

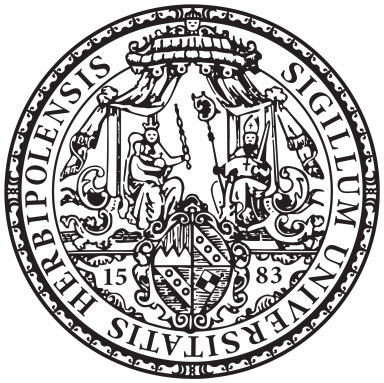

vorgelegt von

Christoph Sauer

aus Würzburg

Würzburg 2014

Eingereicht am: 27.08.2014
bei der Fakultät für Physik und Astronomie

1. Gutachter: PD Dr. Achim Schöll
2. Gutachter: Prof. Dr. Matthias Bode
der Dissertation

Vorsitzende(r):

1. Prüfer: PD Dr. Achim Schöll
2. Prüfer: Prof. Dr. Matthias Bode
3. Prüfer: Prof. Dr. Giorgio Sangiovanni
im Promotionskolloquium

Tag des Promotionskolloquiums: 19.12.2014

Doktorurkunde ausgehändigt am:

Contents

1 Introduction

Regarding an issue from different perspectives can lead to an enlightening enrichment of existing views and pave the way for stimulating discussions. In organic semiconductor based electronic devices the challenge of seeing things from different viewpoints is obviously posed since organic materials and metal surfaces necessarily touch at metal-organic interfaces. These can include polymers and π-conjugated molecules who themselves often form hetero-organic interfaces in organic electronic devices such as organic light emitting diodes or organic photovoltaics [1–8]. Many advantages have been attributed to this rather new class of devices compared to the traditional anorganic semiconductor based electronics. These are for example improved light absorption and emission as well as lighter and more flexible mechanical structure in combination with lower production costs. Which of these promising aspects will actually be achieved in everyday life products will, among other things, also depend on finding answers for fundamental research questions. One of these questions deals with charge transport across metal-organic and hetero-organic interfaces. For that charge transfer (CT) in the ground state as well as dynamical CT as a reaction on an excitation is an important issue. The latter dynamical effect can be investigated either with pump probe techniques or with resonant photoelectron spectroscopy (RPES). The former require precise control of the time delay between the excitation (pump) and the measurement pulse (probe) while the latter takes advantage of the core hole lifetime as an internal clock to which a CT time can be compared. The existence of this core hole does modify the dynamical reaction of the total interface system with respect to an excitation only within the valence band, i.e. optical adsorption. However, the comparison of different systems and to other experimental techniques allows to extract valuable information for charge transport phenomena. With the core-hole-clock technique it is in principal possible to study CT on a femtosecond [9, 10] and even an attosecond time scale [11–13]. In order to perform such an investigation at a hetero-organic interface several prerequisites need to be fulfilled. First of all a well defined hetero-organic interface is required since a complicated spectroscopic technique like RPES will almost certainly pose many questions that might not be answerable for an interface system which is inhomogeneous or for which the geometric structure itself is not sufficiently known. This matter can be dealt with by investigating extensively studied model systems because for these the desired structural information either already exists or can be gained in satisfactory detail. Hence I choose π-conjugated molecules on single crystal surfaces since for these materials the formation of a well ordered interface appears to be more likely than for polymers and polycrystalline surfaces. Finding a proper hetero-molecular interface (vertical [14–24] or lateral [25–32]) consisting of these model systems will constitute the first part of this thesis. The second part will start with

the identification of criteria for a CT analysis with RPES. This demands an RPES study of homo-molecular multilayer and molecule-metal interface systems. The knowledge gained by this study can then be applied to the identified well defined hetero-molecular interface. For both the characterization of hetero-molecular interfaces and the attempt to understand RPES of the homo-molecular systems a decision about the initially mentioned perspective needs to be made. Whether molecules on metal surfaces should be described within established concepts of molecular or solid state physics is not entirely clear at this point. Both viewpoints can be justified but throughout this thesis it will become more and more evident that switching the perspective and taking advantage of both concepts is necessary for an advancement in the understanding of the applied techniques and the investigated systems.

In chapter 2 the theoretical concepts which lay the foundation for the following discussion of the experimental data are presented. Hereby the theory of the used experimental techniques photoelectron spectroscopy (PES), near edge x-ray absorption fine structure (NEXAFS) spectroscopy, and RPES is briefly introduced. Thereafter the theory of the excitation of molecular vibrations in RPES is illustrated in more detail in subsection 2.1.4. This molecular physics concept will allow to relate part of the RPES data of chapter 5 to RPES data of small molecules in the gas phase and enable a comparative discussion. In section 2.2 the *Molecular Gunnarsson-Schönhammer* theory is introduced. This theory is derived from solid state physics concepts. In this work it is employed to connect core level and valence PES and to demonstrate a direct correspondence of the two techniques which is used in chapter 4 to assign specific states to features in valence PES data. This assignment relies on the *fingerprint approach* analysis for which the *Molecular Gunnarsson-Schönhammer* theory also constitutes the theoretical basis. Therein the core level PES data of hetero-molecular systems is reproduced with reference spectra of homo-molecular systems that can be seen as true fingerprints. The thereby identified contributions to the core level PES data also need to be present in the valence PES data due to the direct correspondence of both techniques. Furthermore, the potential of the *fingerprint approach* analysis of core level PES data for a structural characterization of hetero-molecular films on metal surfaces is explicitly shown with data of model systems. The investigations of hetero-molecular systems on Ag surfaces in chapter 4 utilizes this way of comparative core level data analysis to unambiguously determine which molecule is in direct contact to the Ag surface and which one is situated in higher layers. Other surface sensitive techniques like scanning tunneling microscopy (STM) and low energy electron diffraction (LEED) can provide analogue information. However, for a system without long range order LEED will not be able to do so. Moreover, STM measurements of hetero-molecular systems are experimentally quite demanding and usually require very low measurement temperatures (liquid He cooled). Consequently, this work demonstrates the power of the *fingerprint approach* analysis for the characterization of hetero-molecular films on metal substrates. In addition to this, the *Molecular Gunnarsson-Schönhammer* theory is the foundation for the *Molecular Cluster Model* which evolves from the former theory through a simplification. In section 2.3 a common description of PES, NEXAFS spectroscopy, and RPES is introduced within this *Molec-*

ular Cluster Model. Since this theoretical treatment is only established in solid state physics and thus quite uncommon for molecular systems it is presented in some detail. It is used in subsection 5.3.1 for a quantitative consistency check of the assignment of a particular final state to a metal-organic interface feature and to relate this feature to CT. After that the *Molecular Cluster Model* is transformed into a multichannel model which is closer to the established concept of CT during the time scale of the lifetime of an intermediate state. In this case it is also a question of the perspective whether a quantum mechanical superposition or several channels are considered for the theoretical description of the same process.

All experimental information necessary for the discussion of the data in chapters 4 and 5 is summarized in chapter 3. The main result of the *fingerprint approach* analysis of hetero-molecular systems in chapter 4 is the identification of two hetero-organic interfaces which are suitable for a subsequent analysis with RPES. These are the lateral hetero-molecular system CuPc + PTCDA/Ag(111) and the vertical hetero-molecular system CuPc/1 ML PTCDA/Ag(111) (for details about the molecules of these systems see section 3.2). During the search for these systems additional information on the stability and instability of hetero-molecular films at 300 K and at elevated temperatures (420–570 K) is gained for a large number of systems. This information is discussed in section 4.3 in the context of molecule-metal and molecule-molecule interactions and their importance for the energy balance of a hetero-molecular film. The initial RPES investigations of homo-molecular systems in chapter 5 deal with the $h\nu$ dependent intensity variation of features in the RPES data and the $h\nu$ dependent line-shape evolution of energetically separable molecular orbital signals. The latter does also influence the discussion of CT related features since an alternative interpretation of the observed $h\nu$ dependence includes such features. However, the comprehensive analysis of the large data set allows to exclude this explanation and favors a description of the effect with the excitation of molecular vibrations [33]. The desired CT analysis with RPES of hetero-molecular interfaces is then performed in section 5.4 for the systems identified in chapter 4. None of the features related to dynamical CT in section 5.3 can be used in section 5.4 to confirm such dynamical CT at one of the hetero-molecular interfaces. From the point of view of the RPES data it appears that in the system CuPc + PTCDA/Ag(111) the molecule-metal interaction dominates while in the system CuPc/1 ML PTCDA/Ag(111) no significant hybridization at the CuPc-PTCDA interface takes place.

So far the perspective of solid state physics concepts described in this work could not be introduced into the literature on RPES applied to π-conjugated molecules on metal substrates. Merely the molecular concept based explanation of the $h\nu$ dependent line-shape evolution of molecular orbital signals and its modification on different surfaces has been published in Ref. [33].

2 Theoretical concepts

In this chapter I introduce the theoretical concepts that will later on be used as a basis for the discussion of the data in chapters 4 and 5. First I give a brief overview of the basic theory of the applied experimental techniques of photoelectron spectroscopy (PES), near edge x-ray absorption fine structure (NEXAFS) spectroscopy, and resonant photoelectron spectroscopy (RPES). For the latter the issue of the excitation of vibrations is discussed in a separate subsection. In the following sections 2.2 and 2.3 I will present two possible approaches to treat electronic excitations in the final states of the discussed experimental techniques. In section 2.2 I construct a *Molecular Gunnarsson-Schönhammer* Hamiltonian which constitutes the basis for the *fingerprint approach* I will use in chapter 4 for analyzing hetero-molecular films on metal substrates. Starting from the *Molecular Gunnarsson-Schönhammer* Hamiltonian I will then develop a *Molecular Cluster Model* theory in section 2.3. The formulas deduced in this section relate the signals observed in the experimental techniques used in this work to Cluster Model parameters. This allows a consistent treatment of valence PES, core level PES, NEXAFS spectroscopy and RPES within a common set of parameters that originate from the *Molecular Cluster Model* Hamiltonian.

2.1 Basic theory of the applied experimental techniques

From the experimentalists point of view RPES is performing PES with a photon energy ($h\nu$) close to or equal to an energy necessary to resonantly excite an electron from a core level into a previously unoccupied valence orbital. This is the energy region which is investigated in NEXAFS spectroscopy. So in order to introduce the theoretical background of RPES I first give a brief introduction to direct PES and NEXAFS spectroscopy. A detailed treatment of the former is given in Refs. [34, 35] while the latter is extensively discussed in Ref. [36]. Furthermore, the following description of PES clarifies the approaches given in sections 2.2 and 2.3 of this chapter.

2.1.1 Photoelectron spectroscopy

PES is based on the photoelectric effect [37] which describes the excitation of bound electrons in any form of matter into vacuum by a photon. The kinetic energy (E_K) of the emitted photoelectrons is measured and their binding energy (E_B) is given by

$$E_K = h\nu - |E_B| - \Phi \tag{2.1}$$

Hereby Φ is the work function of a solid. In time dependent first order perturbation theory [38] the transition probability w from an initial state Ψ_i to a final state Ψ_f of an N electron system can be described by Fermi's golden rule [34, 35, 39]

$$w \propto \frac{2\pi}{\hbar} \left| \left\langle \Psi_f(N) \left| H' \right| \Psi_i(N) \right\rangle \right|^2 \delta\left(E_f - E_i - h\nu\right) \tag{2.2}$$

where H' is the perturbation operator and E_i and E_f are the energies of the states Ψ_i and Ψ_f, respectively. H' describes the photon field which excites an electron from the initial state orbital $\phi_{i,k}$ into a photoelectron final state with the wave function ϕ_{f,E_K}. In order to give a simple discussion of the PES process $\Psi_i(N)$ is written as a product of the active one-electron orbital $\phi_{i,k}$ and the remaining $N-1$ electron wave function $\Psi_i^k(N-1)$

$$\Psi_i(N) = C \cdot \phi_{i,k} \cdot \Psi_i^k(N-1) \tag{2.3}$$

with the operator C that ensures antisymmetry of the (fermionic) wave function. The index k represents a quantum number that labels the active orbital $\phi_{i,k}$ which is not included in the $N-1$ electron wave function $\Psi_i^k(N-1)$. In the final state such a factorization of the N electron wave function is known as the sudden approximation. It is based on the assumption that the photoelectron does not interact with the remaining $N-1$ electron system. So the final state is written as

$$\Psi_f(N) = C \cdot \phi_{f,E_K} \cdot \Psi_f^k(N-1) \tag{2.4}$$

The photocurrent I can then be written as a sum over all initial states i, final states f and orbitals with quantum number k in w given in Eq. 2.2. Additionally, a summation over possible excitations s in the final state $\Psi_{f,s}^k(N-1)$ has to be performed if an interaction of the photohole with the remaining $N-1$ electrons is not neglected. Hence with the wave functions of Eq. 2.3 and Eq. 2.4 inserted into w of Eq. 2.2 the photocurrent takes the form

$$I \propto \sum_{f,i,k} \underbrace{\left| \left\langle \phi_{f,E_K} \left| H' \right| \phi_{i,k} \right\rangle \right|^2}_{\text{PES matrix element}} \cdot \underbrace{\sum_s \left| \left\langle \Psi_{f,s}^k(N-1) \,|\, \Psi_i^k(N-1) \right\rangle \right|^2 \delta\left(E_f - E_i - h\nu\right)}_{\text{spectral function}} \tag{2.5}$$

The first part of I is called the PES matrix element. It describes the PES intensity of different orbitals k and effects of the light polarization and sample orientation in a particular measurement geometry of light incidence, sample, and detector. The second part is

usually referred to as the spectral function. Its first part, the matrix element of the $N-1$ electron wave functions Ψ takes the excitations s into account. Hence each PES signal of orbital k is accompanied by s satellite features whose relative intensities are governed by the particular matrix element. The theoretical approaches in the following sections 2.2 and 2.3 concentrate on such satellite excitations in the PES spectrum. The second part of the spectral function is the delta function which takes care of the conservation of energy in the PES process.

2.1.2 Near edge x-ray absorption fine structure spectroscopy

The theoretical description of NEXAFS spectroscopy can also be performed on the basis of Eq. 2.5. In contrast to PES the final state in NEXAFS spectroscopy is not a product of a photolelectron with a wave function ϕ_{f,E_K} and the remaining $N-1$ electron wave function as in Eq. 2.4. Here the electron from the active orbital $\phi_{i,k}$ is resonantly excited into a previously unoccupied orbital $\phi_{f,k'}$. In NEXAFS spectroscopy the probability of such a resonant absorption of a photon depending on $h\nu$ is measured by the detection of a signal produced by the decay of the unstable final state.

2.1.3 Resonant photoelectron spectroscopy

In part of the literature on RPES the term RPES is used exclusively for the emergence of actual resonance effects [40, 41] which can occur in PES spectra when $h\nu$ is tuned over an electronic transition in NEXAFS spectroscopy. As stated in the beginning of this section I will use the term more loosely. Whenever PES is performed with an $h\nu$ close to or matching a NEXAFS resonance (a peak in the NEXAFS spectrum which corresponds to one or more electronic transitions) I will call it RPES. When $h\nu$ is far below a NEXAFS resonance I will use the term PES or in a comparison to RPES explicitly utilize the wording direct or off-resonant PES. The theoretical description of RPES is more complicated than the above given treatment of PES. In the latter a single matrix element (see Eq. 2.2) is the starting point for the following simplifications while for the former the involvement of an intermediate state has to be considered. This requires multiple matrix elements in a theoretical description of the additional channels that produce photoelectrons. Additionally, the simultaneous contribution of the direct PES term and the additional terms at resonance can lead to interference effects in RPES. This constitutes a further complication of the theoretical treatment. In the following I will give a short summary of the two major theoretical approaches with selected examples from literature and discuss their relation.

A possible formalism used for the calculation of RPES is based on the work of Fano [42]. In the center of this approach the consequences of an energetic overlap of a continuous and a discrete final state are theoretically investigated and the analogy to scattering theory is discussed. An application of the results of this work to RPES on metals can for example be found in Refs. [43–45]. Hereby the final state of direct PES constitutes

the energetically continuous state of the Fano picture and the final state of the (resonant) Auger decay represents the energetically discrete state. The application of the Fano picture for these metallic solids is obviously reasonable since it properly predicts the observed antiresonance in the constant initial state (CIS) spectra which originates from the interference of the discrete Auger channel and the continuous PES channel. In Ref. [46] it is shown that a Fano contribution is included in the formula used for example in Refs. [9, 40, 41] (see Eq. (762) in Ref. [46] and discussion that follows). The formula used in Refs. [9, 40, 41] to describe RPES consists of a sum of a direct PES matrix element analogous to Eq. 2.2 and a term of the same form as the Kramers-Heisenberg formula [47] in the square of their absolute value (see Eq. 2.6). In this approach the interference appears in the cross terms of the two parts [40, 41, 46] and in general the intensity variation of a CIS signal is a mixture of a Fano and a Lorentzian contribution [46]. For discrete intermediate states that are energetically well separated this can be explicitly shown. In this case the scattering amplitude τ_{fi} can be written as [46]

$$\left|\tau_{fi}\right|^2 = \left|A + \frac{B + iC}{\varepsilon + \frac{i\Gamma}{2}}\right|^2 = \frac{\left(A\varepsilon + B\right)^2 + \left(\frac{\Gamma}{2}A + C\right)^2}{\varepsilon^2 + \left(\frac{\Gamma}{2}\right)^2} \tag{2.6}$$

Hereby A, B, and C are real, Γ is the (real) lifetime width, and ε denotes the energetic difference of the initial and the intermediate state. With Eq. 2.6 the two extreme cases can be discussed. For $A = 0$ (no direct PES contribution) a pure Lorentzian line-shape is obtained while for $\frac{\Gamma}{2}A + C = 0$ Eq. 2.6 describes a pure Fano line-shape ($\left|\tau_{fi}\right|^2 \propto (q+\varepsilon)^2 / \left(\varepsilon^2 + 1\right)$ [42, 46]). Hence the physics of the Fano approach is imbedded in the formula given in Refs. [9, 40, 41]. The theoretical treatment in Refs. [9, 40, 41] has the advantage that it has a rather easily interpretable form for the discussion of the excitation of molecular vibrations. Hence I will use this form in subsection 2.1.4. Electronic resonance effects are also found in RPES data of molecules [48, 49] and treated theoretically within the Fano approach (or the analogous scattering theory). For further details about the calculation of RPES I would like to refer the reader to the above given references. A detailed discussion of electronic resonance effects in RPES seems useless at this point. So far, to my best knowledge, these have not been reported for the π-conjugated molecules investigated in this work. Furthermore, full RPES calculations for such large molecules (analogous to the references given above) are to my best knowledge not possible at this point.

In the previous paragraph RPES is discussed as a coherent and energy conserving one-step process. The involvement of an intermediate state must not be interpreted as a picture of two separated steps of excitation and deexcitation. Such a two-step process is a proper picture when $h\nu$ is larger than the core level ionization potential, i.e. a core hole is created by direct PES and a photoelectron is excited into vacuum. Then the entire RPES process consists of direct PES and the subsequent (regular) Auger decay and can be described in two separated steps. In this case the emitted electron will be an Auger electron and hence remain at constant E_K. So for the deexcitation in this two-step process I will consequently use the term Auger decay throughout this work.

When $h\nu$ is smaller than the core level ionization potential it is a question of localization of the excited electron whether the RPES process is coherent or incoherent and thus energy conserving or not energy conserving, respectively. The former scenario is for example found for RPES of metals where the electron is exited into a localized f-orbital [45, 50, 51]. Here strongly resonantly enhanced signals at constant E_B are observed in the valence regime when $h\nu$ is tuned over a NEXAFS resonance. In contrast to that the resonant excitation of an electron into a delocalized d-band of a metal results in an enhancement of a valence signal that disperses with constant E_K on an E_B scale [40, 52–54]. So delocalization of the electron excited in an electronic transition in NEXAFS spectroscopy leads to a non energy conserving process since the excess energy of the photon does not lead to a higher E_K of the emitted electron. Thus the delocalization of the excited electron results in the same dissipation of energy as if this electron was excited into vacuum. For the localized RPES process on the other hand the energy of the excited electron is translated to the emitted electron which leads to a conservation of energy for the full RPES process. A proper term to describe both possible processes with $h\nu$ smaller than the core level ionization potential is autoionization. For adsorbates on metal substrates the case of intermediate localization has been observed [11–13, 55]. Consequently, both a signal that disperses with constant E_K and a signal that remains at constant E_B are found. The issue of localization and delocalization is discussed as charge transfer (CT) in these systems because delocalization from the adsorbate can be interpreted as transfer of the excited electron into the substrate. A quantitative extraction of relative intensities of the two signals can be used for a quantitative determination of CT times with respect to the core hole lifetime of the particular RPES process [9]. The application of this so-called core-hole-clock technique to π-conjugated molecules will be discussed in the introductory part of chapter 5.

2.1.4 Excitation of molecular vibrations in resonant photoelectron spectroscopy

The application of PES and NEXAFS spectroscopy to molecules allows to observe the excitation of molecular vibrations in the final state [34, 36]. For these techniques this excitation of vibrations accompanying electronic transitions can be explained within the Born-Oppenheimer approximation [56] and by the Franck-Condon principle [34, 36] through the overlap of nuclear wave functions of the initial and the final state. Hereby the character of the initial and final state potential energy surfaces results in characteristic nuclear wave functions which govern the magnitude of the particular overlap integrals. The relative values of these so-called Franck-Condon factors manifest themselves in the observed relative intensities of excited vibrational states. A detailed derivation and schematic pictures describing the Franck-Condon scheme for PES can be found in Refs. [57–59] and for NEXAFS spectroscopy in Refs. [60, 61]. For small molecules in the gas phase separated single vibrational final states can be observed in PES [62] and NEXAFS spectra [63]. Due to several broadening mechanisms [57, 58], the simultaneous excitation of many vibrational modes, and the possibility of a coupling in

between them this is usually not possible for π-conjugated molecules [64–66]. However, an effective single mode analysis can be performed for those systems [57–59, 64, 67].

In RPES additional effects can be involved in the excitation of molecular vibrations with respect to PES and NEXAFS spectroscopy. First of all the validity of the Born-Oppenheimer approximation can be limited and vibronic and electronic excitations might no longer be separable. For a theoretical treatment of RPES within a time dependent Kramers-Heisenberg formalism covering such effects in N_2 I would like to refer the reader to Ref. [68]. Furthermore, analogue to the electronic interference effects discussed in subsection 2.1.3 there is the possibility for vibronic interference through cross terms of the direct PES term and the resonant term given in Eq. 2.7. However, both of the just mentioned effects are beyond the scope of this work and will not be considered in the analysis of the RPES data of π-conjugated molecules in section 5.2.

The excitation of molecular vibrations observed in this work will be discussed in comparison to small molecules since calculations for the actually investigated systems are not available and, to my best knowledge, not possible at this point. The investigation of vibrational excitations in small molecules by RPES is based on a formula originating from Eq. (762) in Ref. [46]. After neglecting the direct PES term and a factorization of the electronic and the vibronic part of the total wave functions (Born-Oppenheimer approximation) the intensity $I_f(h\nu)$ of the vibrational final state $|f\rangle$ as a function of $h\nu$ is given by [62]

$$I_f(h\nu) \propto M(h\nu) \left| \sum_n \frac{\langle f|\, n\rangle \langle n|\, 0\rangle}{h\nu - (E_n - E_0) - \frac{i\Gamma}{2}} \right|^2 \tag{2.7}$$

Here M is a function of $h\nu$ (E_{exc} in Ref. [62]) which describes the profile of the exciting photon beam. E_n and E_0 are the energies of the intermediate vibrational state $|n\rangle$ and the initial vibrational state $|0\rangle$, respectively. Γ denotes the energetic width (lifetime broadening) of the excited state. The intensity of one electronic final state measured in RPES $I(E_K)$ as a function of E_K (E_{emi} in Ref. [62]) is then obtained by a sum over all f as [62]

$$I(E_K) \propto \sum_f I_f[h\nu - (E_f - E_0)] \tag{2.8}$$

Considering this equation together with Eq. 2.7 it becomes obvious that the excitation of vibrations in RPES depends on $h\nu$. This means that for different $h\nu$ a different intensity of a particular final state vibrational excitation is produced in RPES. If the vibrational contributions can be resolved they will be visible in the RPES data as separated peaks whose relative intensities within an electronic final state signal will change for different $h\nu$. For overlapping vibrational contributions their envelope and hence the line-shape of the electronic final state shows such a dependence on $h\nu$.

Eq. 2.7 can be expanded and separated into two parts [62]. The first part only consists of transitions that include a single vibrational intermediate state $|n\rangle$ while the second term includes cross terms which stem from a nonvanishing energetic overlap of different $|n\rangle$. This second term is responsible for the effect called lifetime vibrational interfer-

ence [62, 69] and will be discussed at the end of this paragraph. First I only consider the consequence of the first term which has no contribution of vibronic interference. In the first term the intensity distribution among the vibronic final states for a particular $h\nu$ is governed by the Franck-Condon factors of the vibronic intermediate state and the vibronic final states. In other words the matrix elements $\langle f|\, n\rangle$ determine the intensities of the different vibrational excitations in the final state. Here a particular state $|n\rangle$ is produced by the excitation ($\langle n|\, 0\rangle$) and thus depends on $h\nu$. Hence for a different $h\nu$ a different $|n\rangle$ is realized and a characteristic set of Franck-Condon factors results from the matrix elements $\langle f|\, n\rangle$. So the observed vibronic excitations in RPES undergo an evolution with changing $h\nu$ that is a consequence of two Franck-Condon matrix elements. For schematic diagrams illustrating this mechanism for a single vibrational mode see Figs. 3 and 5 in Ref. [70]. Considering the second term (vibronic interference term) leads to deviations from this simple double Franck-Condon picture. A helpful analogy is given by a the famous double slit experiment (for example chapter 2.1 in Ref. [38]). There it is also an interference term which produces a deviation from the simple superposition of intensities of both slits. Similarly the energetic overlap of two neighboring intermediate vibronic states results in an interference effect in the excitation of vibrational final states. If the lifetime broadening Γ is larger than the energetic separation of the intermediate vibronic states two neighboring vibronic states will be simultaneously exited. Consequently, the relative intensities of the vibrations exited in the final state are changed with respect to the ones given by the pure double Franck-Condon mechanism in the first term. The magnitude of this lifetime vibrational interference effect for small molecules is shown through a comparison of calculations including and excluding this effect [62, 69]. The larger influence of this effect on RPES spectra of O_2 with respect to N_2 and CO at the carbon K-edge is explained by the larger lifetime broadening of the core hole in the oxygen atom [69]. This means that a change in the lifetime broadening of a core hole in a molecule can have an influence on the line-shape of an electronic final state measured in RPES. For example the adsorption on a metal surface can lead to such a variation of hole lifetime broadening for π-conjugated molecules [59]. Note that the effect of lifetime vibrational interference is a consequence of the form of Eq. 2.7 and hence of mathematical origin in the above discussion. For a discussion of the effect based on a wave packet concept I would like to refer the reader to Ref. [69].

2.2 From the Gunnarsson-Schönhammer theory to the *fingerprint approach* analysis of hetero-molecular systems

A possible approach for the theoretical description of PES is given by the Gunnarsson-Schönhammer theory [71, 72]. It is based on the single impurity Anderson model [73] and was originally used to calculate core level and valence PES spectra of metal compounds with localized valence orbitals [74, 75]. Thereby the metal atom is treated as

a single impurity coupled to a delocalized metallic background while a coupling to another metal atom is not taken into account. Core level and valence PES spectra are calculated with the same set of parameters that characterize the material. Thus there is a direct correspondence of core level and valence PES spectra of a particular material since both are determined by the Hamiltonian which includes the same parameters. This direct correspondence between core level and valence PES is of special interest for my work on metal-organic interface systems. It will be discussed explicitly for two molecular model systems after the introduction of the Hamiltonian that describes the molecule-metal interface. For metal compounds the analysis of the core level PES spectra allows to deduce parameters of the valence band region such as the occupation of a particular level and the coupling parameter between the localized orbital and the metallic band [72, 74–76]. The reason for the possibility of investigating valence band properties by core level PES is given by the reaction of the valence region to the creation of the core hole. Hence the character of the valence band is imprinted on the core level spectrum.

The Gunnarsson-Schönhammer theory [71, 72] can be applied to π-conjugated molecules adsorbed on metal surfaces when the molecule is treated as a single impurity and the metal s-p bands are seen as a metallic background coupled to the valence orbitals of the molecule. Analogous to the Gunnarsson-Schönhammer Hamiltonian [71, 72] I can write down a Hamiltonian for the single impurity molecule-metal interface system in second quantization [77] as

$$\begin{aligned}\mathscr{H}_{MGS} = &\sum_{k,\sigma} \varepsilon_k \mathbf{n}_{k,\sigma} + \sum_{m,\sigma} \varepsilon_m \mathbf{n}_{m,\sigma} + \varepsilon_c \sum_{\sigma} \mathbf{n}_{c,\sigma} + \sum_{m,k,\sigma} V_{k,m} \left(\mathbf{c}^{\dagger}_{k,\sigma} \mathbf{c}_{m,\sigma} + \mathbf{c}^{\dagger}_{m,\sigma} \mathbf{c}_{k,\sigma} \right) \\ &+ \frac{1}{2} \sum_{m,\sigma \neq m',\sigma'} U_{m,m'} \mathbf{n}_{m,\sigma} \mathbf{n}_{m',\sigma'} - U_{m,c} \left(2 - \sum_{\sigma} \mathbf{n}_{c,\sigma} \right) \sum_{m,\sigma} \mathbf{n}_{m,\sigma}\end{aligned} \tag{2.9}$$

The subscript *MGS* stands for *Molecular Gunnarsson-Schönhammer*, ε is a single particle energy, $\mathbf{n}$ the number operator, $\mathbf{c}^{\dagger}$ the creation operator and $\mathbf{c}$ the annihilation operator. The subscript k represents a state of the metal s-p band, m stands for a molecular orbital, c for the molecular core level from which PES is performed and σ denotes the spin. Hence $V_{k,m}$ is the hopping matrix element of the molecular orbital m to the metal s-p band state k, $U_{m,m'}$ is the Coulomb repulsion of the molecular orbitals m and m' and $U_{m,c}$ the Coulomb attraction of the hole in the core level c and the electron in the molecular orbital m. For the π-conjugated molecules investigated in this work each of the above considered terms can be justified by experimental observations. The existence of a non vanishing $V_{k,m}$ is demonstrated by the observation of a (partially) occupied lowest unoccupied molecular orbital (LUMO) in valence PES and tunneling spectroscopy [78–83]. If $V_{k,m}$ was vanishing the molecule would be isolated and hence the feature with the smallest E_B in the valence regime would be the highest occupied molecular orbital (HOMO) signal. Moreover, differences between the line-shape of core level PES spectra of molecules adsorbed on a metal surface with respect to the corresponding multilayer are observed (see Fig. 2.1 and Refs. [18, 78, 83–85]). This can be explained by the

emergence of satellite peaks in addition to the main peak in the case of the molecule-metal interface which points towards the involvement of a $U_{m,c}$ (and a $V_{k,m}$) of significant magnitude [84]. The existence of a $U_{m,m'}$ of a relevant size is shown by the finding of a Kondo resonance for several π-conjugated molecules adsorbed on metal surfaces [86–91].

From a mathematical viewpoint the direct correspondence of valence PES and core level PES can be explained with the Hamiltonian in Eq. 2.9 and the photocurrent of a PES measurement given by Eq. 2.5. A particular set of parameters of the Hamiltonian ($\mathscr{H}_{MGS}$) results in characteristic eigenfunctions ($\Psi^k_{f,s}$ and Ψ^k_i) and eigenenergies (E_f and E_i). The former determine the intensities of the signals in the PES spectrum while the latter are responsible for the energies (E_K or E_B) of these signals. Considering the terms in the Hamiltonian in Eq. 2.9 this direct correspondence can be discussed in a more intuitive way. The Coulomb attraction $U_{m,c}$ triggers a characteristic reaction of the valence orbitals when a core hole is created. Similarly $U_{m,m'}$ forces the valence orbitals to react on a valence hole. Hence a particular occupation of the valence orbitals results in both a characteristic core level and valence PES spectrum. Through the coupling of the molecular orbitals to the metal substrate states and the energy cost $U_{m,m'}$ for transferring an additional charge onto the molecule in combination with the single particle energies ε_m and ε_k the occupation of the valence orbitals is determined. Consequently, the valence PES and core level PES spectra are characteristic for a molecule-metal interface system. This means that the same molecule adsorbed on another metal substrate can exhibit significantly different PES spectra.

The explicit discussion of the direct correspondence between core level and valence PES is given with the examples of CuPc in Fig. 2.1 and PTCDA in Fig. 2.2 (for details about these molecules see section 3.2). In Fig. 2.1 core level and valence PES spectra are displayed for a CuPc multilayer and CuPc adsorbed on different metal substrates. The multilayer sample serves as a reference for vanishing couping to metal states because CuPc is in a pure homo-molecular environment. In this scenario the valence PES spectrum (Fig. 2.1(b)) shows no LUMO signal. Hence the line-shape of the C1s core level spectrum of the CuPc multilayer is a characteristic line-shape that goes together with no LUMO signal in valence PES. The C1s core level spectrum of the submonolayer (sub-ML) of CuPc on Au(111) in Fig. 2.1(a) exhibits the same line-shape (within measurement accuracy) as the CuPc multilayer. As expected no LUMO signal is observed in the valence PES spectrum of a sub-ML of CuPc on Au(111) in Fig. 2.1(b). The shift in E_B between the PES spectra of the CuPc multilayer and the sub-ML CuPc on Au(111) can be explained by the different work functions of Au(111) and Ag(111) [34]. The latter is the substrate of the multilayer sample. Since such systems mainly align their energetic levels to the vacuum level [92–95] the larger work function of Au(111) leads to the observed energetic shift to smaller E_B. In contrast to the valence PES spectra of the multilayer and sub-ML on Au(111) the CuPc monolayer (ML) sample on Ag(111) in Fig. 2.1(b) shows a LUMO signal at the Fermi energy (E_F). As expected from the *Molecular Gunnarsson-Schönhammer* Hamiltonian $\mathscr{H}_{MGS}$ in Eq. 2.9 the observed change in valence PES goes along with a significantly altered line-shape of the C1s core level PES

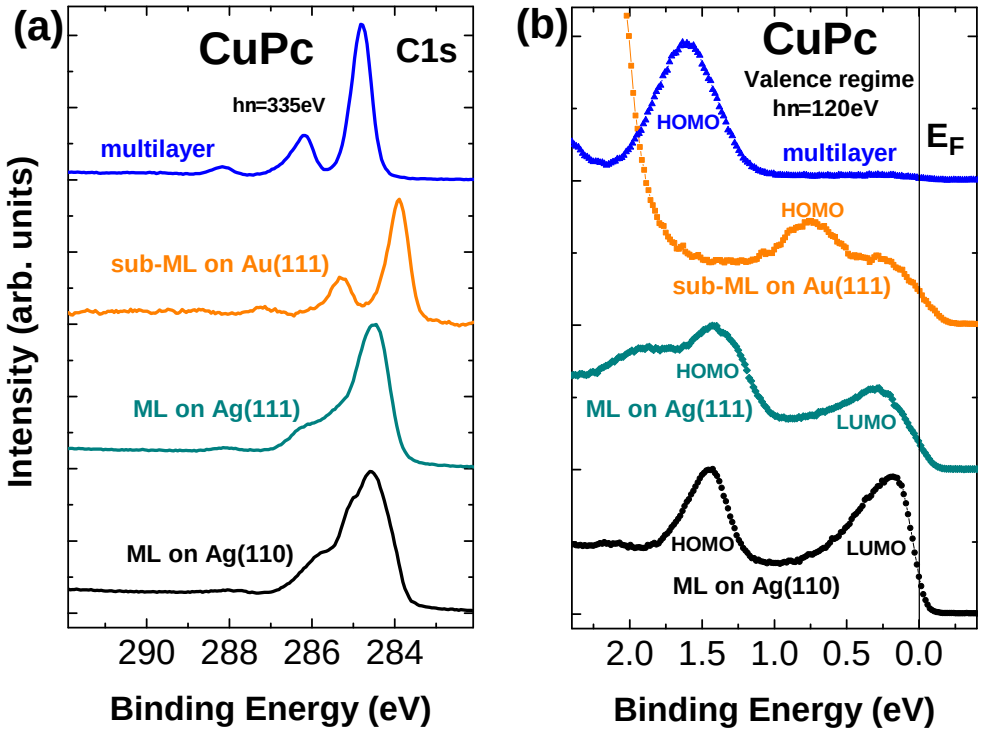

Figure 2.1: Comparison of C1s core level PES spectra and valence PES spectra of CuPc. **(a)** C1s core level spectra of a CuPc multilayer sample together with a sub-ML sample on Au(111) and ML samples on Ag(111) and Ag(110). The spectra are scaled to similar intensities for better comparability of the line-shape. For the sub-ML on Au(111) a power law background is subtracted while for the other spectra no background correction is performed. **(b)** Valence PES spectra of the corresponding samples in panel (a). The vertical line denotes E_F.

spectrum. Moreover, for CuPc adsorbed on Ag(110) a variation in the valence PES spectrum with respect to Ag(111) is found in Fig. 2.1(b). A change at the large E_B tail of the HOMO signal for the ML on Ag(111) with respect to Ag(110) is observed. The signal at $E_B \approx 2$ eV is assigned to the HOMO-1 split off band in Ref. [82]. Neither a reason for the decrease of intensity of this signal from Ag(111) to Ag(110) nor the explicit consequences for core level PES can be given here. More importantly, a LUMO signal is found for 1 ML CuPc/Ag(110) in Fig. 2.1(b). Furthermore, a line-shape variation of this LUMO signal is observed from Ag(111) to Ag(110). These changes in the valence PES spectra of CuPc on Ag(110) with respect to Ag(111) are reflected in a different line-shape of the corresponding C1s core level PES spectra in Fig. 2.1(a). However, compared to the change observed with respect to the samples without a LUMO signal in valence PES (multilayer and sub-ML on Au(111)) both core level PES spectra of the Ag samples can be considered similar. Consequently, it can be concluded that small changes observed in valence PES go together with small changes in the C1s core level PES. Strong changes, like the presence or absence of a LUMO signal, on the other hand

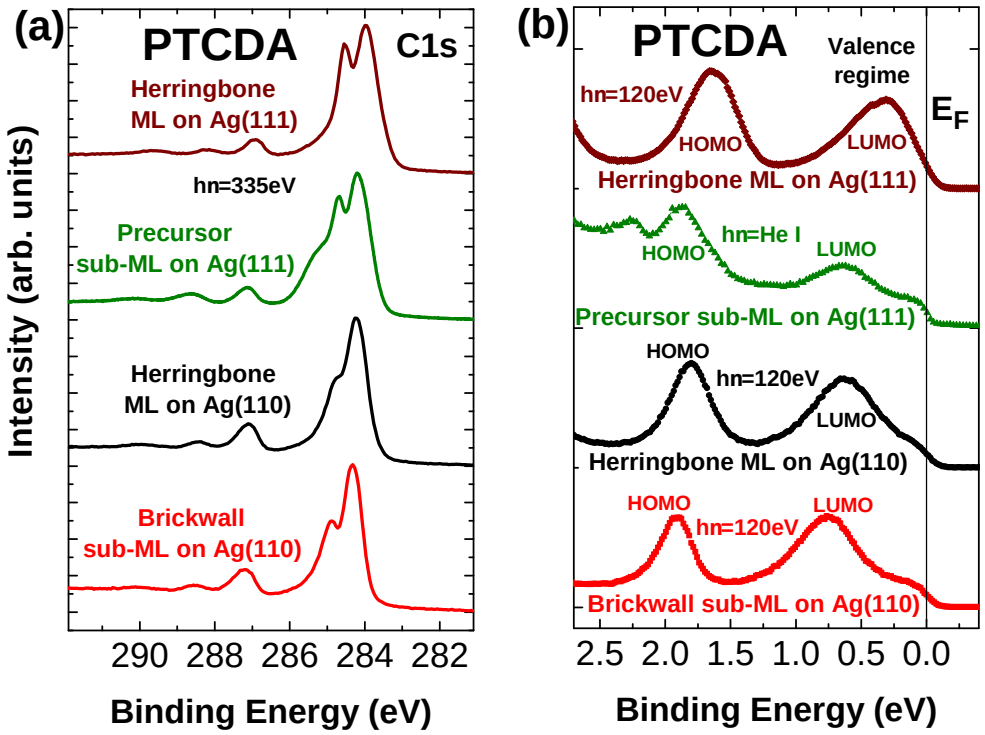

Figure 2.2: Comparison of C1s core level PES spectra and valence PES spectra of PTCDA adsorbed on Ag. **(a)** C1s core level spectra of PTCDA adsorbed on Ag(111) and Ag(110) in two different phases for each substrate. The spectra are scaled to similar intensities for better comparability of the line-shape. The C1s core level PES spectrum of the precursor sub-ML on Ag(111) is taken from Ref. [96]. **(b)** Valence PES spectra of the corresponding samples in panel (a). The vertical line denotes E_F. The feature at higher E_B than the HOMO for the precursor sub-ML on Ag(111) is a Ag4d satellite produced by He Iβ radiation. The valence PES spectrum of the precursor sub-ML on Ag(111) is taken from Ref. [79].

go together with strong changes in the C1s core level PES line-shape. So line-shapes of C1s core level PES spectra similar to the ones of 1 ML CuPc on Ag(111) and Ag(110) are the characteristic line-shapes that correspond to valence PES spectra with a LUMO signal. The discussed example of the model molecule CuPc shows that the expected direct correspondence of valence PES and core level PES exists for molecular systems of π-conjugated molecules.

The direct correspondence between valence PES and core level PES is also obvious for the model molecule PTCDA. Analog to CuPc the emergence of a LUMO signal in valence PES manifests itself in a characteristic line-shape of the C1s core level PES spectrum that differs substantially from the line-shape of the corresponding PES spectrum of a multilayer sample [78]. However, with PTCDA the magnitude of the consequences of changes in core level PES spectra for valence PES spectra (and vice versa) can be investigated in more detail. This investigation is possible because different structural phases

can be prepared for PTCDA on Ag(111) [79] and Ag(110) [97–99]. Hence not only the influence of a different surface but also the influence of a different structure on the same surface on the PES spectra can be discussed. The differences in the line-shapes of the C1s core level PES spectra in Fig. 2.2(a) are changes of the relative intensities of the two peaks of the most intense signal at $E_B \approx 284.5$ eV, the emergence of a shoulder at the tailing edge of this signal, and E_B shifts in the order of $100-300$ meV. These differences go together with E_B shifts of the molecular orbital signals in the order of $100-300$ meV in the valence PES spectra in Fig. 2.2(b).

The findings of Figs. 2.1 and 2.2 could be used for the analysis of hetero-organic systems on metal substrates if certain requirements were fulfilled. These are discussed in the following. The characteristic line-shape of PES spectra of the molecule-metal interface systems originates form their particular set of parameters in the *Molecular Gunnarsson-Schönhammer* Hamiltonian $\mathscr{H}_{MGS}$ in Eq. 2.9. Only if a molecule at the hetero-molecular interface and at the molecule-metal interface can be described by the same Hamiltonian and with a similar set of parameters the line-shapes of the corresponding PES spectra will be similar. Otherwise different line-shapes of the PES spectra are expected for a molecule in direct contact to the metal surface and those at a hetero-organic interface. If a molecule at such an interface and in the homo-molecular multilayer can be described by the same Hamiltonian and a similar set of parameters the line-shapes of PES spectra of all equal molecules not in direct contact to the metal surface will be similar. In this case the PES spectra of the particular homo-molecular multilayer can serve as a reference spectrum to reproduce the PES signals of all equal molecules not in direct contact to the metal surface. In any case PES spectra of the homo-molecular molecule-metal interface can be used as a reference spectrum that reproduces the PES signals of the corresponding molecules which are in direct contact to the metal surface. So the first requirement for a significant reproduction of a PES spectrum of a hetero-organic system on a metal substrate is a substantially different line-shape of the PES spectra of each molecule in the first and in higher layers. The second requirement is a substantially different line-shape of the PES spectra of the different molecules in the first and in higher layers. In other words the PES spectra of molecule A must be distinguishable from the PES spectra of molecule B in the first and in higher layers. The third requirement is a similar line-shape of the PES spectra of each molecule at a hetero-molecular and a homo-molecular interface. If a hetero-molecular interface does not exist in a system the fulfillment of this third requirement will be unnecessary. The first and the second requirement are fulfilled for the C1s core level PES spectra of CuPc and PTCDA on an Ag(111) and an Ag(110) surface (see Figs. 2.1 and 2.2 and Ref. [78]). The fulfillment of the third requirement can be discussed with the actual C1s core level PES measurement of the hetero-organic system of CuPc and PTCDA on the Ag(111) or Ag(110) surface. In chapter 4 it will be shown that this third requirement is either fulfilled for CuPc and PTCDA on Ag(111) or does not need to be fulfilled. Furthermore, the fulfillment of all three requirements is demonstrated for other molecules in chapter 4. All these molecules have in common that a LUMO signal is observed in direct valence PES for the molecule-Ag interface

while this signal is absent in the valence PES spectra of a homo-molecular and a hetero-molecular multilayer.

In the case of the fulfillment of all three requirements the manifold of peaks in an energy range of $5-10$ eV in the C1s core level PES spectra has the character of a true fingerprint for a molecule at a particular interface. Consequently, a significant deconvolution of C1s core level PES spectra that include two or more contributions is possible. In this *fingerprint approach* analysis the measured spectrum is reproduced with a linear combination of reference spectra of the particular homo-molecular samples. A successful reproduction of all features of the line-shape of the measured C1s core level PES spectrum immediately shows which molecule is in direct contact to the metal surface. Hence the *fingerprint approach* analysis permits statements about the layer order of the hetero-organic film on a metal substrate. Furthermore, due to the direct correspondence of core level and valence PES the *fingerprint approach* analysis of the C1s core level spectrum can be used to assign features in the valence PES spectrum. In the case of a hetero-organic film a direct assignment of the features in a valence PES energy distribution curve (EDC) through a comparison to the corresponding homo-molecular EDC might be very difficult. A significant assignment could be hindered by many energetically overlapping features and possible variations with respect to the corresponding homo-molecular EDC. The latter could be due to a change in the structure (see Fig. 2.2) which could be induced by the presence of the other molecule in the hetero-organic system. A similar *fingerprint approach* analysis can be performed with angular resolved valence PES spectra [80, 99–101] if the necessary order in the molecular orientation is realized for a significant deconvolution of the spectra in k-space. Additionally, the angular intensity distribution must fulfill the three requirements discussed above. Furthermore, effects of diffuse scattering and backscattering of photoelectrons must be negligible.

2.3 The molecule-metal interface in a cluster model

The goal of this section is to develop a consistent description of PES, NEXAFS spectroscopy and RPES on the basis of the cluster model [102–105] including parameters analogue to the ones of Eq. 2.9 discussed in section 2.2. Therefor the *Molecular Cluster Model* Hamiltonian $\mathscr{H}_{MCM}$ needs to be written in a matrix form with the particular chosen basis states. Diagonalization of the $\mathscr{H}_{MCM}$ matrix leads to the eigenstates and the corresponding eigenenergies for the initial state and final state of the particular experiment. With these the energetic separation and intensity ratio of the final states of this particular experiment are obtained as a function of the cluster model parameters from $\mathscr{H}_{MCM}$. This approach is a possible way to calculate the matrix elements in the spectral function given in Eq. 2.5. For each orbital $\phi_{i,k}$ the intensity ratios and energetic separation of the *s* excitations in the final state are obtained in this way. Since this approach is quite uncommon for π-conjugated molecules adsorbed on metal surfaces I will go through it in some detail in the following. Most calculations are analogue to Ref. [106] where core level PES from d-orbitals is discussed. However, the adjustments to the electronic struc-

ture of molecules results in some differences of the Hamiltonian. Thus after introducing the *Molecular Cluster Model* Hamiltonian I give a detailed discussion of all its terms. Then I will present a general solution for the eigenvalue equation which will then be used to calculate the energetic separation and the intensity ratio of the signals produced in valence PES, core level PES, NEXAFS spectroscopy and RPES. In subsection 5.3.1 the theoretical treatment presented in this section will be used for the interpretation of data on coronene adsorbed on Ag(111). The presented theoretical treatment in this section is restricted to a simple two state basis which is chosen for the discussion of this particular example. However, by considering other states or by extending the basis set the application to other electronic excitations, which might be important for a different molecule-metal system, is possible.

2.3.1 The *Molecular Cluster Model* Hamiltonian

The cluster model Hamiltonian is obtained from the Gunnarsson-Schönhammer Hamiltonian by setting the metallic band width to zero [102–105]. Hence the different energies ε_k in Eq. 2.9 are transformed into a single energy ε_M for all metal electrons. The molecule-metal system is treated as a cluster that consists of a single molecule which is coupled to several metal ligand atoms with a total of n electrons. For the sake of simplicity only one core level C, the HOMO H and the LUMO L of the molecule will be considered. The *Molecular Cluster Model* Hamiltonian $\mathscr{H}_{MCM}$ for these orbitals can be written as

$$\begin{aligned}\mathscr{H}_{MCM} =& \varepsilon_M \sum_{M,\sigma} \mathbf{n}_{M,\sigma} + \varepsilon_H \sum_{\sigma} \mathbf{n}_{H,\sigma} + \varepsilon_L \sum_{\sigma} \mathbf{n}_{L,\sigma} + \varepsilon_C \sum_{\sigma} \mathbf{n}_{C,\sigma} \\ &+ V_{L,M} \left(\mathbf{c}^{\dagger}_{M,\sigma} \mathbf{c}_{L,\sigma} + \mathbf{c}^{\dagger}_{L,\sigma} \mathbf{c}_{M,\sigma} \right) + V_{H,M} \left(\mathbf{c}^{\dagger}_{M,\sigma} \mathbf{c}_{H,\sigma} + \mathbf{c}^{\dagger}_{H,\sigma} \mathbf{c}_{M,\sigma} \right) \\ &+ U_{L,L} \mathbf{n}_{L,\sigma} \mathbf{n}_{L,\sigma'} + U_{H,H} \mathbf{n}_{H,\sigma} \mathbf{n}_{H,\sigma'} + U_{H,L} \sum_{\sigma} \mathbf{n}_{H,\sigma} \mathbf{n}_{L,\sigma} \\ &- U_{H,C} \left(2 - \sum_{\sigma} \mathbf{n}_{C,\sigma} \right) \sum_{\sigma} \mathbf{n}_{H,\sigma} - U_{L,C} \left(2 - \sum_{\sigma} \mathbf{n}_{C,\sigma} \right) \sum_{\sigma} \mathbf{n}_{L,\sigma}\end{aligned} \tag{2.10}$$

The sums over the molecular orbitals m are written out explicitly for a more transparent discussion of the cluster model parameters. The first row of Eq. 2.10 consists of the trivial energy terms of all orbitals. If the orbital is occupied with two electrons in a state the single particle energy of the orbital will contribute to the total energy twice. The terms in the second row describe hopping from M to L, M to H and vice versa for each orbital. The parameters $V_{L,M}$ and $V_{H,M}$ are the hopping matrix elements and proportional to the overlap of M with L and M with H, respectively. The third row includes all Coulomb repulsion terms within the molecular orbitals. (At this point these hopping matrix elements V and Coulomb parameters U are considered to be different. Simplifying assumptions for their relations will be made in subsection 5.3.1.) The terms which take the Coulomb attraction of a hole in C and electrons in H and L into account

are in the fourth row. Each electron in H is attracted by a hole in C with $U_{H,C}$ and each electron in L is attracted by a hole in C with $U_{L,C}$.

2.3.2 General calculations

For the description of valence PES, core level PES, NEXAFS spectroscopy and RPES different sets of basis states are necessary. The one for the initial state (denoted by the index I) is equal for all techniques while the one for the final state (denoted by the index F) can differ. For RPES a third state is necessary to describe the involvement of an intermediate state (denoted by the index Z). In order to use analogous formulas for all techniques I introduce indexes for the following calculations. The index h stands for the experimental technique and l denotes the state I, Z, or F. With the particular set of basis states the Hamiltonian $\mathscr{H}_{MCM,h,l}$ is written in matrix form by calculating the energy eigenvalue of each combination of basis states. The general matrix elements for a two state basis with the basis states $|h,l,0\rangle$ and $|h,l,1\rangle$ are

$$\begin{aligned}
\langle h,l,0|\,\mathscr{H}_{MCM}\,|h,l,0\rangle &= E_{h,l}\\
\langle h,l,1|\,\mathscr{H}_{MCM}\,|h,l,1\rangle &= E_{h,l}+\Delta_{h,l}\\
\langle h,l,0|\,\mathscr{H}_{MCM}\,|h,l,1\rangle &= V_{h,l}\\
\langle h,l,1|\,\mathscr{H}_{MCM}\,|h,l,0\rangle &= V_{h,l}
\end{aligned} \tag{2.11}$$

Hereby $E_{h,l}$ describes the energy of the basis state $|h,l,0\rangle$ and $\Delta_{h,l}$ the energetic difference of the basis states $|h,l,0\rangle$ and $|h,l,1\rangle$. $V_{h,l}$ can be interpreted as an energetic overlap of the basis states $|h,l,0\rangle$ and $|h,l,1\rangle$ which stems from the hopping terms in Eq. 2.10. This results in the Hamiltonian matrix

$$\mathscr{H}_{MCM,h,l} = \begin{pmatrix} E_{h,l} & V_{h,l} \\ V_{h,l} & E_{h,l}+\Delta_{h,l} \end{pmatrix} \tag{2.12}$$

In order to diagonalize the matrix in Eq. 2.12 the eigenvalue equation

$$\left(\mathscr{H}_{MCM,h,l} - \lambda_{h,l,i}\cdot\mathbf{1}\right)\left|\Psi_{h,l}\right\rangle = 0 \tag{2.13}$$

needs to be solved. Here $\mathbf{1}$ denotes the unity matrix, $\left|\Psi_{h,l}\right\rangle$ is the eigenvector of experiment h and state l and $\lambda_{h,l,i}$ stands for the corresponding eigenenergy. The index $i = 0,1$ names the two different eigenenergies $\lambda_{h,l,i}$ and eigenvectors $\left|\Psi_{h,l,i}\right\rangle$ that are obtained for the two state basis. Solving Eq. 2.13 results in the eigenenergies [106]

$$\lambda_{h,l,0} = E_{h,l} + \frac{\Delta_{h,l}}{2} - \frac{1}{2}\sqrt{\Delta_{h,l}^2+4V_{h,l}^2} \quad , \quad \lambda_{h,l,1} = E_{h,l} + \frac{\Delta_{h,l}}{2} + \frac{1}{2}\sqrt{\Delta_{h,l}^2+4V_{h,l}^2} \tag{2.14}$$

The difference of these eigenenergies and hence the energetic separation of the eigenstates is

$$\Delta E_{h,l} = \lambda_{h,l,1} - \lambda_{h,l,0} = \sqrt{\Delta_{h,l}^2+4V_{h,l}^2} \tag{2.15}$$

The eigenvectors are calculated as

$$\begin{aligned}\left|\Psi_{h,l,0}\right\rangle &= \alpha_{h,l,0}\left|h,l,0\right\rangle + \beta_{h,l,0}\left|h,l,1\right\rangle \\ \left|\Psi_{h,l,1}\right\rangle &= \alpha_{h,l,1}\left|h,l,0\right\rangle + \beta_{h,l,1}\left|h,l,1\right\rangle\end{aligned} \tag{2.16}$$

with the prefactors $\alpha_{h,l,i}$ and $\beta_{h,l,i}$. These are obtained as [106]

$$\begin{aligned}\alpha_{h,l,0} &= \frac{2V_{h,l}}{\sqrt{4V_{h,l}^2 + \left(\Delta_{h,l} - \sqrt{\Delta_{h,l}^2 + 4V_{h,l}^2}\right)^2}}\,,\ \beta_{h,l,0} = \frac{\Delta_{h,l} - \sqrt{\Delta_{h,l}^2 + 4V_{h,l}^2}}{\sqrt{4V_{h,l}^2 + \left(\Delta_{h,l} - \sqrt{\Delta_{h,l}^2 + 4V_{h,l}^2}\right)^2}} \\ \alpha_{h,l,1} &= \frac{2V_{h,l}}{\sqrt{4V_{h,l}^2 + \left(\Delta_{h,l} + \sqrt{\Delta_{h,l}^2 + 4V_{h,l}^2}\right)^2}}\,,\ \beta_{h,l,1} = \frac{\Delta_{h,l} + \sqrt{\Delta_{h,l}^2 + 4V_{h,l}^2}}{\sqrt{4V_{h,l}^2 + \left(\Delta_{h,l} + \sqrt{\Delta_{h,l}^2 + 4V_{h,l}^2}\right)^2}}\end{aligned} \tag{2.17}$$

All $\left|\Psi_{h,l,i}\right\rangle$ are properly normalized which can be tested by calculating

$$\alpha_{h,l,i}^2 + \beta_{h,l,i}^2 = 1 \tag{2.18}$$

The intensity ratio of the two final states produced in an experiment without intermediate state is calculated in the following way [106]

$$IR_h = \frac{\left|\left\langle\Psi_{h,F,1}\right| \mathscr{H}_h \left|\Psi_{h,I,0}\right\rangle\right|^2}{\left|\left\langle\Psi_{h,F,0}\right| \mathscr{H}_h \left|\Psi_{h,I,0}\right\rangle\right|^2} \tag{2.19}$$

Here $\mathscr{H}_h$ is the Hamiltonian for the experiment h. In Eq. 2.19 only the energetically lower initial state (ground state, $i = 0$) is considered for the intensity ratio of the two final states. For that it is assumed that the magnitude of energetic separation between both initial states is large enough to consider the energetically higher state as unoccupied. For energetically close lying initial states with a significant energetic broadening this assumption might not be justified. The involvement of an intermediate state in RPES complicates the calculation of the intensity ratio. My approach to include an intermediate state is presented in subsection 2.3.6.

2.3.3 Valence photoelectron spectroscopy

In valence PES an electron is removed from a molecular orbital of the initial state I which results in the final state F. The basis states for valence PES ($h = VPES$ in the indexes of the formulas) are hence

$$\begin{aligned} \text{basis of VPES initial state } I: \quad |VPES,I,0\rangle &= \left|C^2H^2L^0M^n\right\rangle \\ |VPES,I,1\rangle &= \left|C^2H^2L^1M^{n-1}\right\rangle \\ \text{basis of VPES final state } F: \quad |VPES,F,0\rangle &= \left|C^2H^1L^0M^n\right\rangle \\ |VPES,F,1\rangle &= \left|C^2H^2L^0M^{n-1}\right\rangle \end{aligned} \tag{2.20}$$

The superscript denotes the occupation of the particular level ($n \in \mathbb{N}$). The basis states constitute an orthonormal basis with

$$\begin{aligned} \left\langle C^2H^2L^0M^n \left| C^2H^2L^0M^n \right\rangle = \left\langle C^2H^2L^1M^{n-1} \left| C^2H^2L^1M^{n-1} \right\rangle &= 1 \\ \left\langle C^2H^2L^1M^{n-1} \left| C^2H^2L^0M^n \right\rangle = \left\langle C^2H^2L^0M^n \left| C^2H^2L^1M^{n-1} \right\rangle &= 0 \\ \left\langle C^2H^1L^0M^n \left| C^2H^1L^0M^n \right\rangle = \left\langle C^2H^2L^0M^{n-1} \left| C^2H^2L^0M^{n-1} \right\rangle &= 1 \\ \left\langle C^2H^2L^0M^{n-1} \left| C^2H^1L^0M^n \right\rangle = \left\langle C^2H^1L^0M^n \left| C^2H^2L^0M^{n-1} \right\rangle &= 0 \end{aligned} \tag{2.21}$$

A third basis state in the initial state I with two electrons transfered to the LUMO $\left|C^2H^2L^2M^{n-2}\right\rangle$ is not considered. In coronene/Ag(111) the contribution of such a state is believed to be very small. Furthermore, the basis state $\left|C^2H^1L^1M^{n-1}\right\rangle$ is omitted in the final state since no contribution to the RPES data on coronene/Ag(111) can be found (details will be given in the discussion in subsection 5.3.1). With the basis states from Eq. 2.20 and $\mathscr{H}_{MCM}$ given in Eq. 2.10 the energy matrix elements for the initial state I in valence PES are

$$\begin{aligned} \left\langle C^2H^2L^0M^n \right| \mathscr{H}_{MCM} \left| C^2H^2L^0M^n \right\rangle &= E_{VPES,I} \\ \left\langle C^2H^2L^1M^{n-1} \right| \mathscr{H}_{MCM} \left| C^2H^2L^1M^{n-1} \right\rangle &= E_{VPES,I} + \varepsilon_L - \varepsilon_M + 2U_{H,L} \\ &= E_{VPES,I} + \Delta_{VPES,I} \\ \left\langle C^2H^2L^1M^{n-1} \right| \mathscr{H}_{MCM} \left| C^2H^2L^0M^n \right\rangle &= V_{L,M} = V_{VPES,I} \\ \left\langle C^2H^2L^0M^n \right| \mathscr{H}_{MCM} \left| C^2H^2L^1M^{n-1} \right\rangle &= V_{L,M} = V_{VPES,I} \end{aligned} \tag{2.22}$$

In my discussion of data only the energetic separation of states will be considered. As shown in Eq. 2.15 the energy $E_{VPES,I}$ cancels out in the energetic separation of the final states. Hence the energy of the basis state $\left|C^2H^2L^0M^n\right\rangle$ can be summarized in $E_{VPES,I}$ and for the energy of the basis state $\left|C^2H^2L^1M^{n-1}\right\rangle$ only the change with respect to the basis state $\left|C^2H^2L^0M^n\right\rangle$ needs to be considered. According to the notation in Eq. 2.11 in subsection 2.3.2 the energetic difference between the basis states $\left|C^2H^2L^0M^n\right\rangle$ and $\left|C^2H^2L^1M^{n-1}\right\rangle$ is defined as $\Delta_{VPES,I}$. Furthermore, the energetic overlap $V_{L,M}$ is termed

$V_{VPES,I}$. Analogously to Eq. 2.22 the final state energy matrix elements for the basis vectors given in Eq. 2.20 are

$$\begin{aligned}
\left\langle C^2H^1L^0M^n\right| \mathscr{H}_{MCM} \left|C^2H^1L^0M^n\right\rangle &= E_{VPES,F} \\
\left\langle C^2H^2L^0M^{n-1}\right| \mathscr{H}_{MCM} \left|C^2H^2L^0M^{n-1}\right\rangle &= E_{VPES,F} + \varepsilon_H - \varepsilon_M + U_{H,H} \\
&= E_{VPES,F} + \Delta_{VPES,F} \\
\left\langle C^2H^2L^0M^{n-1}\right| \mathscr{H}_{MCM} \left|C^2H^1L^0M^n\right\rangle &= V_{H,M} = V_{VPES,F} \\
\left\langle C^2H^1L^0M^n\right| \mathscr{H}_{MCM} \left|C^2H^2L^0M^{n-1}\right\rangle &= V_{H,M} = V_{VPES,F}
\end{aligned} \tag{2.23}$$

With the eigenenergies in Eq. 2.14 and the energy matrix elements of Eq. 2.23 the energetic separation of the two states produced by the valence PES experiment is given according to Eq. 2.15 as

$$\begin{aligned}
\Delta E_{VPES,F} = \lambda_{VPES,F,1} - \lambda_{VPES,F,0} &= \sqrt{\Delta^2_{VPES,F} + 4V^2_{VPES,F}} \\
&= \sqrt{(\varepsilon_H - \varepsilon_M + U_{H,H})^2 + 4V^2_{H,M}}
\end{aligned} \tag{2.24}$$

With Eq. 2.24 the energetic separation of signals in a valence PES spectrum is related to the cluster model parameters. The second information from this experiment is the intensity ratio IR_{VPES} of the final state signals. According to Eq. 2.19 this can be calculated by

$$IR_{VPES} = \frac{\left|\left\langle \Psi_{VPES,F,1}\right| \mathscr{H}_{VPES} \left|\Psi_{VPES,I,0}\right\rangle\right|^2}{\left|\left\langle \Psi_{VPES,F,0}\right| \mathscr{H}_{VPES} \left|\Psi_{VPES,I,0}\right\rangle\right|^2} \tag{2.25}$$

The operator $\mathscr{H}_{VPES}$ which describes valence PES is the annihilation operator $\mathbf{c}_{m,\sigma}$. It annihilates an electron in the orbital m and hence reduces the occupation number of this orbital by 1. In the case of the here considered orbitals $\mathscr{H}_{VPES} = \mathbf{c}_{H,\sigma} + \mathbf{c}_{L,\sigma}$. Inserting the valence PES basis states of Eq. 2.20 into the form of the eigenvectors in Eq. 2.16 I obtain

$$\begin{aligned}
\left|\Psi_{VPES,I,0}\right\rangle &= \alpha_{VPES,I,0} \left|C^2H^2L^0M^n\right\rangle + \beta_{VPES,I,0} \left|C^2H^2L^1M^{n-1}\right\rangle \\
\left|\Psi_{VPES,I,1}\right\rangle &= \alpha_{VPES,I,1} \left|C^2H^2L^0M^n\right\rangle + \beta_{VPES,I,1} \left|C^2H^2L^1M^{n-1}\right\rangle \\
\left|\Psi_{VPES,F,0}\right\rangle &= \alpha_{VPES,F,0} \left|C^2H^1L^0M^n\right\rangle + \beta_{VPES,F,0} \left|C^2H^2L^0M^{n-1}\right\rangle \\
\left|\Psi_{VPES,F,1}\right\rangle &= \alpha_{VPES,F,1} \left|C^2H^1L^0M^n\right\rangle + \beta_{VPES,F,1} \left|C^2H^2L^0M^{n-1}\right\rangle
\end{aligned} \tag{2.26}$$

Inserting these and $\mathscr{H}_{VPES}$ into Eq. 2.25 the intensity ratio takes the form

$$IR_{VPES} = \frac{\left|\alpha_{VPES,F,1}\alpha_{VPES,I,0} + \beta_{VPES,F,1}\beta_{VPES,I,0}\right|^2}{\left|\alpha_{VPES,F,0}\alpha_{VPES,I,0} + \beta_{VPES,F,0}\beta_{VPES,I,0}\right|^2} \tag{2.27}$$

To obtain Eq. 2.27 the relations in Eq. 2.21 are used. Additionally, all matrix elements that contain states which are not considered in the chosen basis sets vanish. With the

general formulas for the prefactors presented in Eq. 2.17 and the obtained relations for $V_{VPES,l}$ and $\Delta_{VPES,l}$ of Eqs. 2.22 and 2.23 the measured intensity ratio in valence PES is related to cluster model parameters by Eq. 2.27.

2.3.4 Core level photoelectron spectroscopy

The theoretical description of core level PES is analogous to valence PES. Hence I will only give a brief presentation of the terms specific for core level PES in this subsection. In core level PES an electron is removed from a core level orbital C of the initial state I which results in the final state F. Thus the basis states for core level PES ($h = CPES$ in the indexes of the formulas) are

$$\begin{aligned} \text{basis of CPES initial state } I: \quad |CPES,I,0\rangle &= \left|C^2H^2L^0M^n\right\rangle \\ |CPES,I,1\rangle &= \left|C^2H^2L^1M^{n-1}\right\rangle \\ \text{basis of CPES final state } F: \quad |CPES,F,0\rangle &= \left|C^1H^2L^0M^n\right\rangle \\ |CPES,F,1\rangle &= \left|C^1H^2L^1M^{n-1}\right\rangle \end{aligned} \tag{2.28}$$

The final state energy matrix elements for the basis vectors given in Eq. 2.28 are

$$\begin{aligned} \left\langle C^1H^2L^0M^n\right| \mathscr{H}_{MCM} \left|C^1H^2L^0M^n\right\rangle &= E_{CPES,F} \\ \left\langle C^1H^2L^1M^{n-1}\right| \mathscr{H}_{MCM} \left|C^1H^2L^1M^{n-1}\right\rangle &= E_{CPES,F} + \varepsilon_L - \varepsilon_M + 2U_{H,L} - U_{C,L} \\ &= E_{CPES,F} + \Delta_{CPES,F} \\ \left\langle C^1H^2L^1M^{n-1}\right| \mathscr{H}_{MCM} \left|C^1H^2L^0M^n\right\rangle &= V_{L,M} = V_{CPES,F} \\ \left\langle C^1H^2L^0M^n\right| \mathscr{H}_{MCM} \left|C^1H^2L^1M^{n-1}\right\rangle &= V_{L,M} = V_{CPES,F} \end{aligned} \tag{2.29}$$

The operator that describes the core level PES experiment is $\mathscr{H}_{CPES} = \mathbf{c}_{C,\sigma}$. Both the energy separation (Eq. 2.24) and the intensity ratio (Eq. 2.27) are analogue to valence PES. Inserting $\Delta_{CPES,F}$ and $V_{CPES,F}$ instead of $\Delta_{VPES,F}$ and $V_{VPES,F}$ results in the formulas that relate the core level PES experiment to the cluster model parameters.

2.3.5 Near edge x-ray absorption fine structure spectroscopy

In NEXAFS spectroscopy an electron from a core level in the initial state I is transfered into the previously unoccupied level L in the final state F. Hence the basis states for NEXAFS spectroscopy ($h = NEX$ in the indexes of the formulas) are

$$\begin{aligned} \text{basis of NEX initial state } I: \quad |NEX,I,0\rangle &= \left|C^2H^2L^0M^n\right\rangle \\ |NEX,I,1\rangle &= \left|C^2H^2L^1M^{n-1}\right\rangle \\ \text{basis of NEX final state } F: \quad |NEX,F,0\rangle &= \left|C^1H^2L^1M^n\right\rangle \\ |NEX,F,1\rangle &= \left|C^1H^2L^2M^{n-1}\right\rangle \end{aligned} \tag{2.30}$$

The corresponding final state energy matrix elements for these basis vectors are

$$\begin{aligned} \left\langle C^1H^2L^1M^n\right| \mathscr{H}_{MCM} \left|C^1H^2L^1M^n\right\rangle &= E_{NEX,F} \\ \left\langle C^1H^2L^2M^{n-1}\right| \mathscr{H}_{MCM} \left|C^1H^2L^2M^{n-1}\right\rangle &= E_{NEX,F} + \varepsilon_L - \varepsilon_M + 2U_{H,L} + U_{L,L} - U_{C,L} \\ &= E_{NEX,F} + \Delta_{NEX,F} \\ \left\langle C^1H^2L^2M^{n-1}\right| \mathscr{H}_{MCM} \left|C^1H^2L^1M^n\right\rangle &= V_{L,M} = V_{NEX,F} \\ \left\langle C^1H^2L^1M^n\right| \mathscr{H}_{MCM} \left|C^1H^2L^2M^{n-1}\right\rangle &= V_{L,M} = V_{NEX,F} \end{aligned} \tag{2.31}$$

The NEXAFS spectroscopy operator is $\mathscr{H}_{NEX} = \mathbf{c}^{\dagger}_{L,\sigma}\mathbf{c}_{C,\sigma}$. Again Eqs. 2.24 and 2.27 connect the energetic separation and the intensity ratio of the final states of NEXAFS spectroscopy with the cluster model parameters when $\Delta_{VPES,F}$ and $V_{VPES,F}$ are replaced by $\Delta_{NEX,F}$ and $V_{NEX,F}$.

2.3.6 Resonant photoelectron spectroscopy

In Ref. [103] RPES is treated within a cluster model by introducing an intermediate state. Matrix elements describing the photon absorption and super-Coster-Kronig decay are then inserted into the formalism of Ref. [44]. By that a Fano shape with an antiresonance is produced for the calculated CIS spectra. I will neglect resonance effects and treat RPES as valence PES through an intermediate state Z. The first step of this energy conserving two step process is equal to NEXAFS spectroscopy as described in subsection

2.3.5. The second step is autoionization which leads to the same final states as in valence PES. Hence the basis vectors of all three states are

$$\begin{aligned}
\text{basis of RPES initial state } I: \quad |RPES,I,0\rangle &= \left|C^2H^2L^0M^n\right\rangle \\
|RPES,I,1\rangle &= \left|C^2H^2L^1M^{n-1}\right\rangle \\
\text{basis of RPES intermediate state } Z: \quad |RPES,Z,0\rangle &= \left|C^1H^2L^1M^n\right\rangle \\
|RPES,Z,1\rangle &= \left|C^1H^2L^2M^{n-1}\right\rangle \\
\text{basis of RPES final state } F: \quad |RPES,F,0\rangle &= \left|C^2H^1L^0M^n\right\rangle \\
|RPES,F,1\rangle &= \left|C^2H^2L^0M^{n-1}\right\rangle
\end{aligned} \tag{2.32}$$

The relations $\Delta_{RPES,Z}$ and $V_{RPES,Z}$ are hence equal to $\Delta_{NEX,F}$ and $V_{NEX,F}$ given in Eq. 2.31. Equally the relations $\Delta_{RPES,F}$ and $V_{RPES,F}$ are the same as $\Delta_{VPES,F}$ and $V_{VPES,F}$ of Eq. 2.23. Consequently I obatin for RPES

$$\begin{aligned}
\Delta_{RPES,Z} = \Delta_{NEX,F} &= \varepsilon_L - \varepsilon_M + 2U_{H,L} + U_{L,L} - U_{C,L} \\
V_{RPES,Z} = V_{NEX,F} &= V_{L,M} \\
\Delta_{RPES,F} = \Delta_{VPES,F} &= \varepsilon_H - \varepsilon_M + U_{H,H} \\
V_{RPES,F} = V_{VPES,F} &= V_{H,M}
\end{aligned} \tag{2.33}$$

Thus in my theoretical treatment of RPES the same energetic separation of the eigenstates of the final state is obtained as in valence PES (see Eq. 2.24). In contrast the intensity ratio can be altered due to the involvement of an intermediate state. Each of the two final states can be produced by autoionization (AI) from the two different intermediate states Z. Eq. 2.19 is thus modified in the following way

$$IR_{RPES} = \frac{|W(F,1;Z,1) + W(F,1;Z,0)|^2}{|W(F,0;Z,1) + W(F,0;Z,0)|^2} \tag{2.34}$$

with a short notation for the double matrix elements W

$$\begin{aligned}
W(F,1;Z,1) &= \left\langle \Psi_{RPES,F,1}\right| \mathscr{H}_{AI} \left|\Psi_{RPES,Z,1}\right\rangle \left\langle \Psi_{RPES,Z,1}\right| \mathscr{H}_{NEX} \left|\Psi_{RPES,I,0}\right\rangle \\
W(F,1;Z,0) &= \left\langle \Psi_{RPES,F,1}\right| \mathscr{H}_{AI} \left|\Psi_{RPES,Z,0}\right\rangle \left\langle \Psi_{RPES,Z,0}\right| \mathscr{H}_{NEX} \left|\Psi_{RPES,I,0}\right\rangle \\
W(F,0;Z,1) &= \left\langle \Psi_{RPES,F,0}\right| \mathscr{H}_{AI} \left|\Psi_{RPES,Z,1}\right\rangle \left\langle \Psi_{RPES,Z,1}\right| \mathscr{H}_{NEX} \left|\Psi_{RPES,I,0}\right\rangle \\
W(F,0;Z,0) &= \left\langle \Psi_{RPES,F,0}\right| \mathscr{H}_{AI} \left|\Psi_{RPES,Z,0}\right\rangle \left\langle \Psi_{RPES,Z,0}\right| \mathscr{H}_{NEX} \left|\Psi_{RPES,I,0}\right\rangle
\end{aligned} \tag{2.35}$$

Hereby the autoionization (AI) operator is $\mathscr{H}_{AI} = \left(\mathbf{c}_{H,\sigma} + \gamma \cdot \mathbf{c}_{L,\sigma'}\right) \mathbf{c}^{\dagger}_{C,\sigma} \mathbf{c}_{L,\sigma}$. So far the probabilities for producing the different final states were set equal. Specifically the creation of a hole in the HOMO and the LUMO in valence PES was assumed to be of equal probability. For the two different autoionization channels described by $\mathscr{H}_{AI}$ I drop this assumption and hence introduce the weighting factor γ. In this way the matrix element which involves the states C and L twice can be weighted by γ with respect to the matrix element that includes C, H and L. It is reasonable to assume a larger value for an au-

toionization matrix element containing the same molecular orbital twice with respect to an autoionization matrix element which includes two different molecular orbitals. With the given $\mathscr{H}_{AI}$, the above defined $\mathscr{H}_{NEX}$ and the form of the eigenvectors presented in Eq. 2.26 the matrix elements in Eq. 2.35 are calculated as

$$\begin{aligned}
W(F,1;Z,1) &= \left(\alpha_{RPES,F,1}\alpha_{RPES,Z,1} + \gamma\cdot\beta_{RPES,F,1}\beta_{RPES,Z,1}\right) \\
&\quad\times\left(\alpha_{RPES,Z,1}\alpha_{RPES,I,0} + \beta_{RPES,Z,1}\beta_{RPES,I,0}\right) \\
W(F,1;Z,0) &= \left(\alpha_{RPES,F,1}\alpha_{RPES,Z,0} + \gamma\cdot\beta_{RPES,F,1}\beta_{RPES,Z,0}\right) \\
&\quad\times\left(\alpha_{RPES,Z,0}\alpha_{RPES,I,0} + \beta_{RPES,Z,0}\beta_{RPES,I,0}\right) \\
W(F,0;Z,1) &= \left(\alpha_{RPES,F,0}\alpha_{RPES,Z,1} + \gamma\cdot\beta_{RPES,F,0}\beta_{RPES,Z,1}\right) \\
&\quad\times\left(\alpha_{RPES,Z,1}\alpha_{RPES,I,0} + \beta_{RPES,Z,1}\beta_{RPES,I,0}\right) \\
W(F,0;Z,0) &= \left(\alpha_{RPES,F,0}\alpha_{RPES,Z,0} + \gamma\cdot\beta_{RPES,F,0}\beta_{RPES,Z,0}\right) \\
&\quad\times\left(\alpha_{RPES,Z,0}\alpha_{RPES,I,0} + \beta_{RPES,Z,0}\beta_{RPES,I,0}\right)
\end{aligned} \tag{2.36}$$

The parameters included in $\Delta_{RPES,Z}$ and $V_{RPES,Z}$ have no influence on the intensity ratio IR_{RPES} as long as they are finite. Furthermore, $\gamma = 1$ represents the scenario of valence PES through two intermediate states with equal probability. Hence for $\gamma = 1$ the intensity ratio of RPES is equal to the intensity ratio of valence PES. For $\gamma > 1$ the autoionization channel that includes the state L twice is resonantly enhanced with respect to the other channel. This relative resonant enhancement changes the intensity ratio in RPES with respect to valence PES.

3 Experiment

My presentation of the experimental details starts with a summary of the setup at the UE52-PGM beamline where all data of this work was measured. After the characteristics of the beamline and the used detectors are given I discuss the measurement geometry for the applied experimental techniques. Thereafter I explain the preparation of homo- and hetero-molecular films on Ag and Au substrates with the previously introduced π-conjugated molecules. Thereby evaporation temperatures and a rough characterization of the particular growth mode are given for all used molecules. After that I present the data treatment of all applied experimental techniques with a special emphasis on the normalization of resonant photoelectron spectroscopy (RPES) data at the carbon K-edge. In the last section of this chapter I illustrate how core level photoelectron spectroscopy (PES) can be used for the determination of the thickness of adsorbate films. First the general formulas are given and then their application to the different systems examined in this work is explained.

3.1 Experimental setup at UE52-PGM

All measurements presented in this work were performed in a UHV chamber with a base pressure below 5×10^{-10} mbar at the undulator beamline UE52-PGM at BESSY II. The beamline was operated in the traditional mode with the beam focused on the beamline exit slit. For a detailed description of the beamline see Ref. [107]. At this beamline a resolving power of $E/\Delta E = 14000$ can be achieved at a photon energy ($h\nu$) of $h\nu = 400$ eV with an exit slit of 20 μm and a fix-focus constant (c_{ff}) of 10 [108]. With $c_{ff} = 10$ the possible $h\nu$ range is $120 - 1900$ eV. For all measurements in this work a beamline exit slit of 40 μm and p-polarized light was selected. In the RPES measurements photon energies of $h\nu \approx 280 - 300$ eV were used while for core level PES $h\nu$ was adjusted to obtain electrons with a kinetic energy (E_K) of $E_K = 50$ eV for the main signal. The valence region was recorded with the minimum $h\nu$ of 120 eV. Assuming linearity of the resolving power with the exit slit and a dependence on energy as $E/\Delta E \propto 1/\sqrt{E}$ for the plane grating monochromator [109, 110] a $h\nu$ resolution better than 40 meV is achieved in RPES measurements ($h\nu \approx 290$ eV). For $h\nu = 335$ eV, which is the energy used for C1s core level PES, a $h\nu$ resolution better than 45 meV can be estimated analogously. For $h\nu$ used to probe other signals the beamline resolution is much better than the intrinsic width of the signals. Hence no explicit values are given here. As an additional light source an x-ray tube with AlK_α light ($h\nu = 1486.6$ eV) is also available at the PES chamber at UE52-PGM.

(R)PES intensities were recorded with a VG-Scienta R4000 multi channel plate electron analyzer with an entrance slit of 300 μm. For valence PES the Angular mode was chosen in order to monitor possible angular dependent effects of the substrate or the adsorbates. In this mode electrons, which leave the sample at a certain angle with respect to the surface normal, are projected onto a certain point of the multi channel plate. Consequently, the electron intensity as a function of the binding energy (E_B) and angle is recorded in the 2D raw data. All other (R)PES measurements were performed in the Transmission mode which is optimized for maximum transmission and hence focuses as many electrons as possible onto the multi channel plate. In this mode no angular information is obtained. Instead spatial information is contained in one direction of the 2D raw data. With this it can be checked whether the sample position was properly set to the focus point of the analyzer. The energy resolution of the electron analyzer can be estimated assuming linearity of the resolving power as a function of the pass energy. Utilizing measured values for the VG-Scienta SES200 analyzer this results in $\Delta E \approx 30$ meV for 20 eV pass energy, $\Delta E \approx 75$ meV for 50 eV pass energy and $\Delta E \approx 150$ meV for 100 eV pass energy. In near edge x-ray absorption fine structure (NEXAFS) measurements the intensity of electrons stemming from the autoionization or Auger decay after photon absorption of the adsorbates were recorded. Therefor a partial electron yield detector was used. It consists of a channeltron, operated with a voltage of 2.76 kV, and a grid that can be set to a desired retarding voltage. For measurements at the carbon K-edge a retarding voltage of 150 eV was used.

The angle between the photon beam and the electron optical system of the R4000 analyzer is 55°. The manipulator can be turned around its axis to vary the angle ϕ in between the surface normal of the sample and the R4000 analyzer (and simultaneously the angle of light incidence with respect to the surface normal). Core level PES measurements have always been performed in normal emission geometry ($\phi = 0°$). For differences in ϕ a variation in the background to signal ratio and a change in the line-shape of core level PES signals is observed (see Fig. A1). Since such changes prohibit a proper normalization and line-shape analysis of the core level PES data the normal emission geometry was carefully obtained at the beginning of each beamtime by the reflection of light from the crystal. NEXAFS spectroscopy and RPES were performed for $\phi = 15°$ and an angle of light incidence of 70° with respect to the surface normal. In this geometry the cross section for the absorption of p-polarized light by flat lying molecules is higher than in normal emission geometry [36, 61]. Geometries of an even higher angle of incidence would lead to a higher absorption cross section but would also cause experimental problems due to a decreasing effective crystal size. Valence PES was either performed in normal emission or with $\phi = 15°$ (and an angle of light incidence of 70°). The latter was used to increase the intensity of signals stemming from the molecular orbitals with respect to the substrate. Such intensity variations as a function of the emission angle are extensively discussed in Refs. [59, 80, 99–101]. The spatial degree of freedom which moves the sample towards and away from the detector was always adjusted to the focus point of the detector. The two other spatial directions were used to scan the beam over the sample in order to avoid radiation damage and to gain information about the sample ho-

mogeneity. With the used manipulator a stable temperature minimum of approximately 100 K was reached with liquid N_2 cooling.

3.2 Sample preparation

The Ag and Au single crystal surfaces were cleaned by several sputter and annealing cycles. Ar-ion sputtering with an acceleration voltage of 700 V and a sample current of approximately 4 μA was performed at an angle of incidence of 45° with respect to the surface normal form both sides until no C1s signal could be detected with high resolution PES at $h\nu = 335$ eV. Ag(111) and Ag(110) were subsequently annealed in two steps. First the Ag crystals were heated to 800 K for 5–10 min and second to 750K for 10–20 min. Au(111) was heated to approximately 900 K for 20 min after the sputtering procedure.

Organic molecules were previously purified by sublimation and deposited from Knudson cells onto the cleaned surfaces at pressures below 10^{-8} mbar. For a ball and stick model of all molecules investigated in this work see Fig. 3.1. The simplest molecule investigated in this thesis is coronene which is a pure hydrocarbon molecule with the empirical formula $C_{24}H_{12}$. 1,4,5,8-naphthalene-tetracarboxylic-dianhydride (NTCDA) with the empirical formula $C_{14}H_4O_6$ and 3,4,9,10-perylene-tetracarboxylic-dianhydride (PTCDA) with the empirical formula $C_{24}H_8O_6$ contain functional groups with oxygen. Moreover, two metal-phthalocyanines, namely copper-phthalocyanine (CuPc) with the empirical formula $C_{32}H_{16}CuN_8$ and tin-phthalocyanine (SnPc) with the empirical formula $C_{32}H_{16}N_8Sn$, are used in this work. Since the tin atom is considerably larger than the copper atom SnPc is a bent and CuPc a flat molecule (see Fig. 3.1). 2,3,5,6-tetrafluoro-7,7,8,8-tetracyanoquinodimethane (F4TCNQ) with the empirical formula $C_{12}F_4N_4$ only contains one benzene ring to which nitrogen based functional groups and fluorine atoms are attached. All molecules have in common that they exhibit a π-conjugated structure which results in delocalized molecular valence orbitals.

Only approximate evaporation temperatures and the corresponding deposition rates can be given here for the used molecules since these did vary between different beamtimes. The exact combination of temperature and rate depends on the geometry of the evaporator with respect to the sample which obviously varies a little for different beamtimes. Furthermore, the point of the temperature measurement and the filling of the crucible in the Knudsen cell can lead to a variation of the deposition parameters. For all molecules deposition rates below one monolayer (ML) per minute were used. For submonolayer (sub-ML) samples the temperature was usually adjusted to reach a rate around 0.1 ML/min. Generally, it was observed that deposition rates had the tendency to decrease from deposition to deposition for the first couple of depositions. After that quite stable rates ($\pm \approx 10\%$) could be realized.

In general, detailed information on the roughness of the films investigated in this work cannot be given. However, a Frank-van-der-Merwe-like (layer-by-layer-like) film growth

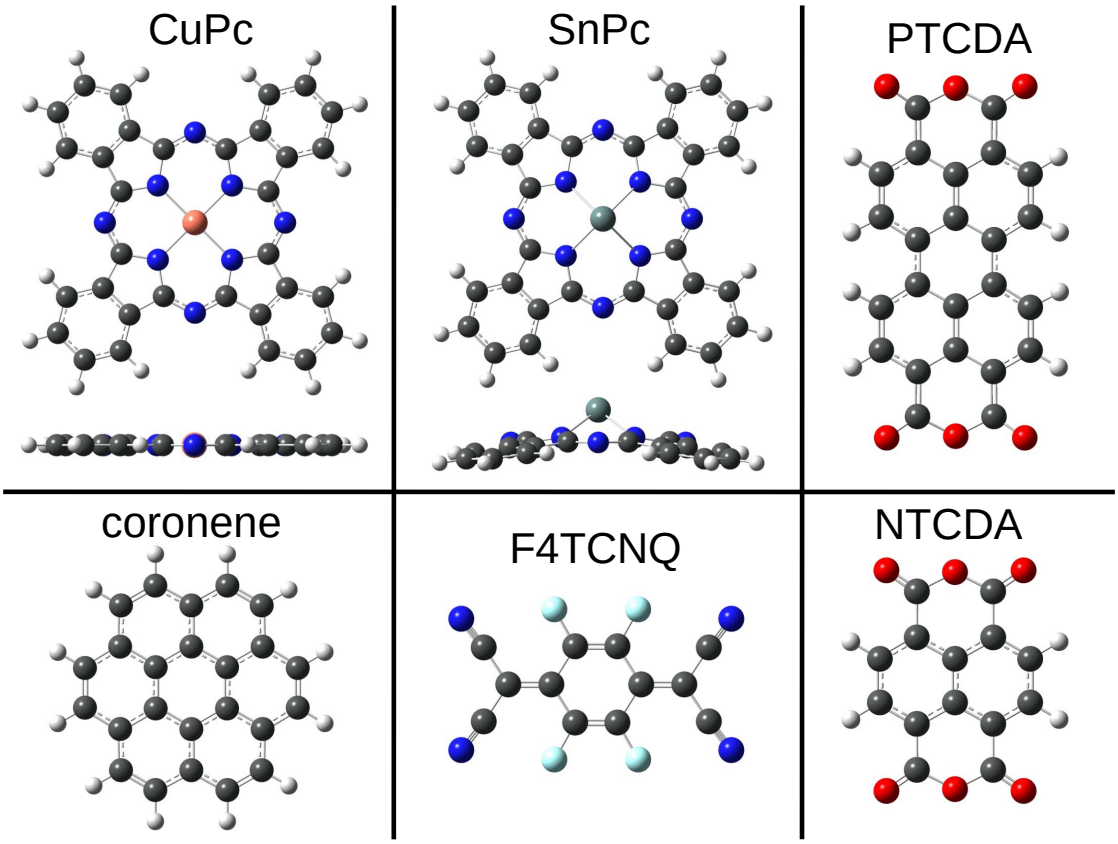

Figure 3.1: Ball and stick models of the investigated molecules CuPc, SnPc, PTCDA, coronene, F4TCNQ, and NTCDA (for empirical formulas and full names see text). The colors of the balls denote the following atoms: white = hydrogen, black = carbon, red = oxygen, dark blue = nitrogen, light blue = fluorine, brown = copper and dark cyan = tin. Below the top view of CuPc and SnPc both molecules are also illustrated from the side view. The side view demonstrates that SnPc is bent in contrast to the flat CuPc molecule.

[111, 112] can be confirmed with the attenuation of PES signals that originate from the substrate or the molecule-metal interface. These signals will decrease by the magnitude expected from Eq. 3.1 and the totally deposited material (estimated from the deposition rate) if the film grows roughly in a Frank-van-der-Merwe fashion. Whether a perfect Frank-van-der-Merwe growth is realized cannot be concluded in this way. Hence I will use the term Frank-van-der-Merwe-like growth when a film can be grown for which interface or substrate originated PES signals are (almost) fully attenuated and hence do not contribute significantly to the measured PES spectra. In contrast, a Stranski-Krastanov (closed layer(s) plus islands) or a Volmer-Weber (only islands) growth mode [111, 112] is identified by the inability to prepare samples without PES signals that originate from the substrate or the molecule-metal interface although enough organic material is deposited to completely attenuate these PES signals (according to Eq. 3.1).

For SnPc molecules a deposition temperature of $T_{evap} \approx 650$ K was used. At a substrate temperature $T_{sub} \approx 300$ K SnPc films can be grown for which PES signals of the substrate are almost vanishing due to the attenuation by the SnPc overlayer (see section 3.4). Hence a Stranski-Krastanow growth with a major fraction of the deposited molecules situated in 3D islands can be excluded for SnPc molecules. CuPc was also deposited at $T_{evap} \approx 650$ K but a Frank-van-der-Merwe-like grown film can only be realized at $T_{sub} \approx 100$ K. At $T_{sub} \approx 300$ K intense PES signals of the Au(111) and Ag(111) substrates are observed for films with a deposited amount of CuPc molecules for which these should be almost fully attenuated. This points towards Stranski-Krastanow growth with only one or two closed layers for CuPc molecules at $T_{sub} \approx 300$ K. PTCDA films were prepared with deposition temperatures of $T_{evap} \approx 640$ K and at $T_{sub} \approx 300$ K the attenuation of PES signals of the substrate allows to excluded Stranski-Krastanow growth dominated by 3D islands (as for SnPc films). The deposition temperature of NTCDA molecules was $T_{evap} \approx 485$ K. With that a Frank-van-der-Merwe-like film can be prepared at $T_{sub} \approx 100$ K. For detailed information about the growth of NTCDA multilayer films see Refs. [61, 113, 114]. Coronene films were prepared with $T_{evap} \approx 450$ K. A Frank-van-der-Merwe-like grown film could only be achieved with $T_{sub} \approx 100$ K which reveals 3D island dominated Stranski-Krastanow growth (as for CuPc films) for coronene molecules on Ag(111) at $T_{sub} \approx 300$ K. Sub-ML and ML films of F4TCNQ molecules were deposited onto Ag(110) at $T_{evap} \approx 400$ K. At $T_{sub} \approx 300$ K PES signals from the F4TCNQ multilayer with unexpectedly small PES intensities can be detected in core level PES. This could be a consequence of a low sticking coefficient [115, 116] or 3D island dominated Stranski-Krastanow growth (as for CuPc and coronene films). At $T_{sub} \approx 100$ K the preparation of an F4TCNQ multilayer without a significant contribution by the first layer of F4TCNQ molecules on Ag(110) is possible. Thus a Frank-van-der-Merwe-like growth mode is found for F4TCNQ molecules on Ag(110) at $T_{sub} \approx 100$ K.

Sub-ML films of SnPc and CuPc molecules on Au(111), coronene molecules on Ag(111) and F4TCNQ molecules on Ag(110) were prepared by direct deposition. In contrast, the preparation of ML films of SnPc, CuPc, and PTCDA molecules on Ag(111) and Ag(110) was achieved by depositing a multilayer in a first step and subsequently annealing these films at $T_{sub} \approx 520 - 570$ K. At these temperatures all molecules except the ones in direct contact to the Ag surface are desorbed for these systems. Hence exactly 1 ML remains. This preparation recipe was found to be very reproducible and the obtained films can be used as references for quantitative statements. The term 1 ML will only be used for ML films which are prepared by this annealing procedure. A full ML of a film that is directly deposited will be denoted as 1.0 ML. An NTCDA/Ag(111) ML was prepared by heating an NTCDA multilayer sample up to $T_{sub} \approx 400$ K with a rate of 1 K/s. According to Ref. [113] this results in the relaxed ML of NTCDA/Ag(111) [117, 118]. For the ML films prepared by annealing of a multilayer a remaining signal from the second and higher layers can be excluded by the absence of characteristic PES signals of the multilayer (see section 2.2 and chapter 4).

Vertical hetero-organic films were prepared by direct deposition of the second molecule on top an ML of the first molecule at $T_{sub} \approx 300$ K. For PTCDA, SnPc, and CuPc on Ag(111) and Ag(110) this 1 ML film was prepared by the annealing procedure described in the previous paragraph. For 1.0 ML F4TCNQ/Ag(110) such an annealing procedure was not performed since a partial decomposition of the F4TCNQ molecules is observed at temperatures above $T_{sub} \approx 420$ K (see subsection 4.2.2). Interestingly, no desorption of this small molecule in direct contact to the Ag(110) surface can be observed for $T_{sub} \approx$ 570 K.

Detailed information on the structure of the investigated organic-metal and hetero-organic interfaces will be given in chapters 4 and 5 if such information is of interest for the discussion of the presented data. A detailed summary of the investigations available in literature for all the above given systems would go far beyond the scope of this work.

3.3 Data treatment

In contrast to the fixed $h\nu$ of laboratory UV and x-ray light sources, $h\nu$ of the light produced by a synchrotron is adjustable continuously. Due to a finite mechanical accuracy and a possible hysteresis of the step motors that move the monochromator the desired $h\nu$ and the actual $h\nu$ can differ. Hence $h\nu$ has to be calibrated each time it is changed and the monochromator is moved. Furthermore, a possible drift of the monochromator position or the beam position on the monochromator could effect $h\nu$ even if it its not changed. Consequently, I calibrated $h\nu$ after each measurement with a substrate signal. For $h\nu \leq 335$ eV and an Ag substrate $h\nu$ is corrected so that the Fermi energy (E_F) becomes $E_F = 0$ eV while for $h\nu \geq 400$ eV it is adjusted so that E_B of the Ag3d lines is equal to the value given in Ref. [119]. When an Au substrate was used $h\nu$ is always shifted so that E_B of the Au4f lines is matching the value in Ref. [119] unless E_F is part of the measured data. In this case the energy calibration is performed with E_F. For NEXAFS spectroscopy and RPES the energy calibration is done after the data acquisition and all $h\nu$ are shifted rigidly by the obtained E_B offset. For multilayer films calibrated with E_F an accuracy better than $\Delta h\nu = \Delta E_B = 50$ meV is estimated. Here the low signal of the substrate s-p band at E_F limits the accuracy of the energy calibration. For all other samples the accuracy of the energy calibration is estimated to be better than $\Delta h\nu = \Delta E_B = 30$ meV.

The valence PES data is integrated over the angular direction after it has been checked for angle dependent features. Especially the influence of substrate bands, which could create additional peaks and line-shape changes of the molecular orbital signals, has been checked prior to the discussion of an angle integrated 1D energy distribution curve (EDC). A normalization which allows the extraction of quantitative intensities is very difficult in the valence regime. Complete knowledge of the angular dependence of the molecular orbital signals and possible scattering effects (diffuse scattering and backscattering) is required for quantitative statements. So the valence PES spectra in this work

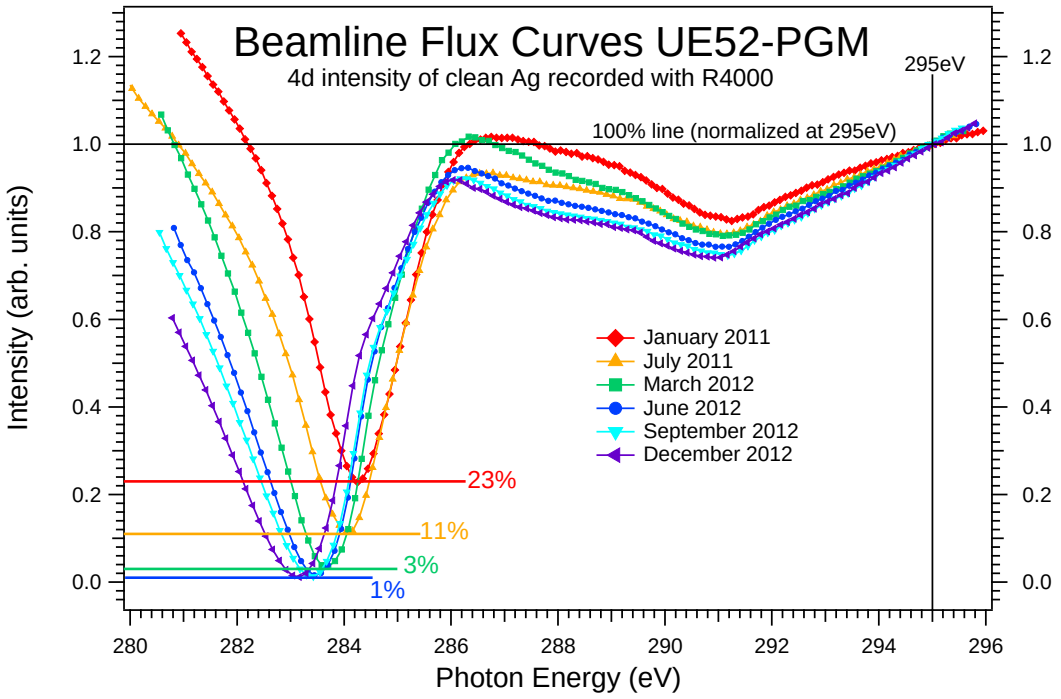

Figure 3.2: Flux curves of UE52-PGM for different beamtimes recorded with the R4000 electron analyzer. The intensity integrated over the measured E_B range mainly stems from the Ag4d bands. Different measurements of the clean Ag crystal recorded over a time scale of years are presented as a function of $h\nu$. All curves are energy calibrated and normalized at $h\nu = 295$ eV for a comparison to each other.

are simply scaled with respect to each other for best comparison of the discussed effect. This comparison of valence PES is always performed for EDCs recorded in the same measurement geometry (equal orientation within reading accuracy of ϕ of the crystal with respect to the detector). Thus the same area (within measurement accuracy) in reciprocal space is probed in these EDCs.

After checking proper focusing the core level PES data is integrated over the spatial direction. The resulting 1D core level PES EDCs are normalized at the pre-peak plateau at lower E_B than the signal with the smallest E_B of the particular core level. The intensity at this point consists of inelastically scattered secondary electrons. Different electron emission angles (see Fig. A1) and strong changes in the surface roughness are able to significantly alter the intensity at this E_B with respect to the core level PES signal. Whenever such effects can be excluded intensities of core level PES can be used for quantitative statements (see section 3.4). For C1s core level PES data no background is subtracted on Ag substrates (unless denoted differently) while for films in the ML coverage range on Au substrates a power law background is subtracted for a better comparability to the PES data of films on Ag substrates. The lower signal to background ratio of the other core level PES signals (N1s, O1s, F1s) also requires the subtraction of a power law background.

Analogous to the core level PES data the RPES data is integrated over the spatial direction after proper focusing has been confirmed. This results in a 2D PES map (raw RPES data is 3D) with PES intensity as a function of E_B and $h\nu$. The dependence on $h\nu$ requires special care in the normalization similar to NEXAFS spectroscopy. Hence the normalization procedure for both techniques is discussed together in the following. For the NEXAFS spectroscopy and RPES data at the carbon K-edge the intensity of the light undergoes a change in the order of 1-2 orders of magnitude as a function of $h\nu$. This is caused by carbon contaminations on the optical elements of the beamline. Since this changes over the time scale of months the flux curve of the beamline also does [119] and a normalization signal has to be recorded for each beamtime. For NEXAFS spectroscopy this is performed with the partial yield electron detector operated in the same settings and measurement geometry as for the actual NEXAFS measurements using a clean substrate sample. For RPES the beamline flux curve is recorded with the R4000 detector by measuring the Ag4d (or Au5d) PES intensity of the clean substrate as a function of $h\nu$ in the same geometry as the RPES measurements. A selection of different flux curves obtained by this method are presented in Fig. 3.2. With respect to the point of normalization at $h\nu = 295$ eV the intensity of the total minimum of the curve decreases with time. Furthermore, the $h\nu$ position of this total minimum simultaneously changes towards lower $h\nu$. Fig. 3.2 clearly demonstrates how delicate the normalization at the carbon K-edge is. Further changes of the intensity of the light during the NEXAFS and RPES measurement stem from the variation of the electron current in the storage ring. This variation also needs to be taken into account. So after the energy calibration of the NEXAFS spectroscopy and RPES data it is divided by the ring current and the energy calibrated beamline flux curve for proper normalization. In the case of RPES artifacts due to the normalization procedure might occur since PES signals from higher orders of light are also present in the data. Light with $n \cdot h\nu$ ($n \in \mathbb{N}$) is transmitted by the monochromator which leads to an additional structureless PES intensity background. Additionally, a C1s core level PES signal produced with $2 \cdot h\nu$ contributes to the RPES data. The intensity variation with $h\nu$ of the higher order PES signals is quite constant since the beamline flux curve at the corresponding $n \cdot h\nu$ is almost flat. Hence after the normalization with the beamline flux curve PES intensities of higher order signals are massively increased in the total minimum of the beamline flux curve with respect to other $h\nu$. This is seen as an increase of PES intensity of the background in the E_B region below the intense Ag4d and Au5d lines at the $h\nu$ of the total minimum of the beamline flux curve. At this $h\nu$ the second order C1s PES signal also shows an intensity maximum after the normalization with the flux curve. In cases where the higher order artifacts hinder the data evaluation they are subtracted after the normalization with the ring current and before the normalization with the beamline flux curve. For a reduction of artifacts stemming from the structureless higher order background a constant offset is subtracted from the PES map.

In the case of the PES detail map of a sub-ML of coronene/Ag(111) (see subsection 5.3.1) the second order C1s signal is subtracted. Therefor a C1s core level PES reference spectrum of the same sample is used. First I identify the proper intensity and E_B

position of this reference spectrum for the best possible subtraction at an E_B smaller than E_F. At this point no other PES signals exist which hinder a proper subtraction. Then the linear dispersion on the E_B scale and the almost constant intensity of second order PES signals allow me to subtract the second order C1s also in the vicinity of other PES signals.

3.4 Thickness calibration of adsorbates with photoelectron spectroscopy

There are several ways for the calibration of the thickness of an adsorbate film. Using core level PES data it depends on the thickness range of the adsorbate film and the coupling of the first adsorbate layer to the substrate which approach is the method of choice for a proper thickness calibration. In general the PES intensity of an adsorbate signal as well as the attenuation of PES signals of the substrate can be used. In special cases characteristic PES signals of a certain adsorbate layer can confirm its presence. The small mean free path of the measured photoelectrons results in a significant attenuation of core level PES lines [34]. The effective attenuation length λ, which depends on E_K of the photoelectrons, can be used to determine the thickness d of an overlayer with the formula [34]

$$I_{sub}(d) = I_{0,sub} \cdot exp\left(\frac{d}{\lambda}\right) \tag{3.1}$$

Here $I_{sub}(d)$ is the intensity of a core level PES signal of the substrate with an overlayer of thickness d and $I_{0,sub}$ is the corresponding core level PES intensity of the uncovered substrate sample. Eq. 3.1 treats the overlayer as a continuum and thus only describes thick overlayers (multilayers) properly for which this simplification is reasonable. Furthermore, layer-by-layer growth is assumed in Eq. 3.1. For samples below approximately 5 ML Eq. 3.1 can be modified to a more realistic form. Assuming a layer-by-layer grown overlayer of n ML ($n \in \mathbb{N}$) in which the nth layer has a coverage of θ ($\theta \in [0;1]$) I obtain

$$I_{sub}(\theta, n) = I_{0,sub} \cdot \left[\theta \cdot exp\left(\frac{n}{\lambda_{ML}}\right) + (1-\theta) \cdot exp\left(\frac{n-1}{\lambda_{ML}}\right)\right] \tag{3.2}$$

The effective attenuation length λ_{ML} is given in units of ML here. For other growth modes Eq. 3.2 can be modified according to the particular model which describes for example height and fractional coverage of islands. For the determination of n Eq. 3.2 with $\theta = 1$ can be used. The correct n is found when the measured PES intensity value of I_{sub} is between the calculated intensities for n and $n-1$. Inserting this n into Eq. 3.2 then yields θ. Similarly, formulas for the intensity of n overlayers $I_{ov,n}$ can be developed. For that the attenuation of the core level PES signal stemming from a certain layer by all layers above needs to be taken into account. The core level PES intensity

of a layer-by-layer grown adsorbate film of n ML with a coverage of θ for the nth layer is

$$\begin{aligned} I_{ov,1}(\theta) &= I_{0,ov} \cdot \theta \ ; \text{ for } n = 1 \\ I_{ov,2}(\theta) &= I_{0,ov} \cdot \left[1 + \theta \cdot exp\left(\frac{1}{\lambda_{ML}} \right) \right] \ ; \text{ for } n = 2 \\ I_{ov,3}(\theta) &= I_{0,ov} \cdot \left[1 + exp\left(\frac{1}{\lambda_{ML}} \right) + \theta \cdot exp\left(\frac{2}{\lambda_{ML}} \right) \right] \ ; \text{ for } n = 3 \\ &\text{... and so on for } n > 3 \end{aligned} \tag{3.3}$$

$I_{0,ov}$ denotes the intensity of one complete overlayer. Again, for the thickness calibration with Eq. 3.3 first the proper n needs to be found by calculating $I_{ov,n}$ for $\theta = 1$. When the measured PES intensity is between $I_{ov,n}$ and $I_{ov,n-1}$ the formula for $I_{ov,n}$ can be used to determine θ. However, for this approach $I_{0,ov}$ needs to be known. Moreover, a proper normalization procedure (see section 3.3) for the measured core level PES spectra must be possible for a quantitative evaluation of thicknesses with both Eq. 3.3 and Eq. 3.2. The uncertainty through improper normalization can be overcome by considering relative PES intensities since these are independent of the normalization. For example the thickness of a system of two different adsorbate layers with separable contributions to the same core level PES spectrum can be evaluated by the PES intensity ratio of both adsorbates. Through the thickness evaluation of such systems with core level PES ratios the applicability of the normalization described in section 3.3 is confirmed. The effective attenuation lengths λ for organic molecules are known for investigations of the model system PTCDA on Ag(111) [120]. The assumption that these values can be used for other π-conjugated molecules as well as for single layers is tested by cross checks with thickness evaluations by PES intensities of overlayers below 1.0 ML. Since these are independent of λ (see Eq. 3.3) the matching thickness values of both approaches confirm that the values in Ref. [120] can be used for all systems investigated in this work.

The thickness determination of homo-molecular multilayer (approximately 5-15 ML) films in this work is performed with Eq. 3.1. The intensities of the bare and the covered substrate lines (Ag3d or Au4f) are measured with AlK$_\alpha$ light. This combination of light source and signal leads to $E_K \approx 1100$ eV for Ag3d and $E_K \approx 1400$ eV for Au4f. According to Ref. [120] the effective electron attenuation lengths λ of an organic film for these E_K is close to the thickness of the investigated films. This match of thickness and λ is of advantage considering the exponential relation in Eq. 3.1. For a λ that is much smaller than the thickness d a small variation in intensity leads to a large difference in the obtained thickness. Moreover, the normalization itself proofed to be more robust for such large E_K with respect to those in the range of 100 eV. The obtained thickness by this high E_K damping method is then qualitatively cross checked with the attenuation of substrate s-p bands in the vicinity of E_F and characteristic PES signals of the first adsorbate layer (if present) measured with lower E_K of 50-120 eV. When substrate and interface features measured with low E_K are much less attenuated than expected by the thick-

ness obtained with the attenuation of PES signals with larger E_K, Stranski-Krastanow (or Volmer-Weber) growth can be concluded. In this case the obtained value can be seen as an effective thickness which only allows a comparison to other coverages of the same type of sample. Throughout this work both the Frank-van-der-Merwe-like grown thick films (5-10 ML) and the films exhibiting a Stranski-Krastanow growth mode are referred to as multilayer samples as long as interface signals do not significantly contribute to the discussed effect.

For homo-molecular systems for which a 1 ML film cannot be prepared by annealing a multilayer sample first a proper reference is needed for an accurate thickness calibration in the range of approximately 1.0 ML. For coronene on Ag(111) in this coverage range the C1s PES signal of 1 ML PTCDA/Ag(111) serves as a reference in this work. Since the same substrate is used and the only PES signals at lower E_B are the PES signals of the molecular orbitals (which are more than 200 eV away) the background of the C1s PES spectrum of the first layer of coronene and PTCDA molecules can be assumed to be equal at $E_K \approx 50$ eV. Hence the low E_B region of the C1s PES spectrum is a proper point of normalization. Furthermore, comparing the PTCDA herringbone structure [78] and the commensurate 1.0 ML structure of coronene on Ag(111) [59, 121] it is found that the surface density of carbon atoms is equal (within measurement accuracy) for both (difference of 1%). Hence the known intensity of 1 ML PTCDA/Ag(111) can be used as $I_{0,ov}$ in Eq. 3.3 to obtain the coverage for the coronene/Ag(111) film from its C1s PES spectrum. A change of the line-shape of the C1s PES spectrum due to the emergence of a second layer contribution is used to cross check the obtained thicknesses. The thickness of sub-ML films of CuPc/Au(111) is calibrated with the thickness dependent E_B of the HOMO signal in valence PES reported in Ref. [122]. The emergence of a HOMO signal with a larger E_B stemming from the second CuPc layer [122] serves as an indicator for molecules beyond a complete first layer. The thickness of a SnPc film on Au(111) is then calibrated with PES intensites of the core level PES signals (C1s and N1s). Herefor the corresponding PES intensities of PES spectra of the CuPc/Au(111) films with a calibrated thickness are used as a reference. All thicknesses of the homo-molecular films in the ML range for which a 1 ML film cannot be prepared by annealing a multilayer sample are further cross checked with the attenuation of Ag3d and Au4f PES signals. The coverage uncertainty for these systems is estimated to be 0.2 ML.

The thickness calibration of the system F4TCNQ/Ag(110) cannot be performed with a 1 ML sample prepared by annealing a multilayer film. The reason for this is the partial decomposition of the molecule at elevated temperatures (see subsection 4.2.2). In this case the 1.0 ML reference is found by a series of depositions around the 1.0 ML coverage range. Below 1 ML the low energy electron diffraction (LEED) pattern of this system changes with the F4TCNQ coverage until a characteristic LEED pattern for 1.0 ML is measured. This is the LEED pattern that does not change anymore with the deposition of additional F4TCNQ molecules. Hence the smallest PES intensities of a sample with this LEED pattern constitute a proper 1.0 ML reference. The determination of 1.0 ML with this method is confirmed with a change of the line-shape of the C1s core level PES spectrum that stems form a C1s PES signal of F4TCNQ molecules in higher layers. In

the case of F4TCNQ/Ag(110) less intensity than expected by Eq. 3.3 and the calibrated deposition rate is found in the core level PES spectra of samples with F4TCNQ coverages above 1.0 ML. This can either be explained by 3D island dominated Stranski-Krastanow growth or a low sticking coefficient for F4TCNQ molecules in the second and in higher layers. Although the PES intensity stemming from the contribution of the second and higher layers is small a significant line-shape variation above 1.0 ML can be significantly identified.

For SnPc, CuPc, and PTCDA molecules on Ag surfaces a 1 ML sample can be prepared by annealing a multilayer sample. Hence proper 1 ML reference signals for all core level PES signals are easily obtained. For the lateral hetero-organic systems investigated in chapter 4 this results in a straightforward thickness calibration with total core level intensities inserted into Eq. 3.3 for $n = 1$. Since only SnPc and CuPc molecules contain nitrogen and only PTCDA molecules contain oxygen the N1s and O1s PES spectra constitute exclusive signals for the particular molecule which can be used for the determination of the thickness of one molecular species in the lateral hetero-organic film. The intensity ratio of the two contributions to the C1s core level PES spectrum is then used for a cross check which is independent of the normalization. Since no uncertainty through an attenuation length enters this thickness calibration the uncertainty of the coverage of one molecular species in a lateral hetero-organic film can be estimated to be 0.1 ML. The thickness calibration of the upper molecular species (second or higher layers) in a vertical hetero-organic system can equally be performed by their total core level PES intensities inserted into Eq. 3.3 together with the 1 ML reference value. Moreover, the attenuation of the total PES intensity of the bottom molecular species (first layer) in the vertical hetero-organic systems can also be used (Eq. 3.2). In the case of the vertical hetero-organic systems the PES intensity ratio of the contributions of both molecular species to the C1s PES spectrum serves as an accurate cross check. For this the total PES intensity of the upper molecular species (Eq. 3.3) is divided by the attenuated PES intensity of the bottom molecular species (Eq. 3.2). As stated above this PES intensity ratio is independent of the normalization of the PES spectra and hence only the uncertainty in λ needs to be considered. Since λ does not enter the thickness evaluation for the first overlayer ($n = 1$) in Eq. 3.3 the vertical hetero-organic systems with a coverage of the upper molecular species below 1 ML are calibrated by truly independent approaches. This allows me to estimate an uncertainty of the coverage of only 0.1 ML for these systems.

4 Analyzing hetero-organic films on metal substrates with photoelectron spectroscopy - the *fingerprint approach* analysis

The goal of this chapter is to find well defined hetero-organic interfaces that are suitable for further investigations with powerful but complicated spectroscopic methods such as resonant photoelectron spectroscopy (RPES). Particularly in the latter case, a significant identification of signals is only possible for a well defined interface. This means that both molecular layers need to form an actual hetero-interface. In other words there must be a contact surface of the two different molecules instead of two separated homo-molecular domains. Additionally, the valence photoelectron spectroscopy (PES) spectrum of the hetero-molecular film should allow a separation of the signals from the two different molecules. This is vital when a quantitative extraction of PES intensities from the RPES data is required. Even the assignment of intensity to a particular molecule in the hetero-organic systems can be hindered by an energetic overlap of PES signals. A promising starting point is a monolayer (ML) on an Ag surface. For several molecules a complete and flat lying first layer can be prepared by annealing a multilayer sample (see section 3.2). This first layer can be the first step of the desired well defined hetero-organic interface. Finding a molecule that grows flat lying in a second layer, which completely forms before higher layers are occupied, constitutes the next step. If such a system exhibits separable PES signals in the valence regime it will be appropriate for a subsequent study with RPES.

The *fingerprint approach* introduced in section 2.2 can be employed to analyze hetero-organic systems on Ag with properly chosen molecules. These are the molecules which fulfill the requirements discussed in section 2.2. Whenever these requirements are fulfilled the *fingerprint approach* analysis of the hetero-organic system can be used to find out which molecule is in direct contact to the Ag surface. So the detection of the molecule deposited in the second preparation step in the first layer indicates a layer exchange and hence an instable and possibly insufficiently ordered interface. An analogous conclusion can be drawn from the finding of the molecule deposited in the first preparation step in higher layers. Moreover, a comparison of the measured core level PES intensity with the expected one from the deposition rate can be used to estimate whether the second layer exhibits the required wetting growth. Additionally, the intensity ratio of different PES

signals serves as a consistency check for the conclusions drawn by the *fingerprint approach* analysis. The existence of separable signals in the valence regime will be examined with valence PES. Only for a system that fulfills all these requirements a detailed investigation with RPES can lead to significant conclusions.

Previous to this work it was found that the hetero-organic system of an ML or a submonolayer (sub-ML) of SnPc on 1ML PTCDA/Ag(111) fulfills all the above explained requirements [17, 18]. However, a detailed analysis of the existing RPES data with a special emphasis on dynamical hetero-molecular interface charge transfer (CT) has not been performed for this system [123]. In chapter 5 a large RPES data set of several molecular systems is presented and discussed with regard to signals that are related to such an interface CT. In the light of this data the data of SnPc/1ML PTCDA/Ag(111) can be revised. I will show that statements about CT are possible for this system through a comparison to other systems investigated in chapter 5. At this point SnPc/1ML PTCDA/Ag(111) will serve as a starting point for the search for other well defined hetero-molecular interface systems.

In the following several hetero-organic systems on Ag(111) and Ag(110) are investigated with the *fingerprint approach* analysis and the results are discussed in relation to literature. First it is shown that not all combinations of metal-phthalocyanine (SnPc or CuPc) and PTCDA molecules on Ag(111) are stable at $T = 300$ K. The unexpected finding of a vertical exchange for PTCDA molecules on 1 ML CuPc/Ag(111) motivates an investigation of further hetero-organic systems consisting of PTCDA and F4TCNQ molecules on Ag(110). Since the observed behavior of the investigated systems points towards the existence of an energy barrier that hinders a vertical exchange a study at elevated temperatures is performed. Thereby I gain further information for the general discussion about the energy balance of a hetero-molecular film on a metal substrate which is given at the end of this chapter. Additionally, I find a way to prepare lateral hetero-organic systems on Ag(111) through the applied annealing procedure. Together with the vertical hetero-organic system of CuPc molecules on 1 ML PTCDA/Ag(111) the lateral hetero-organic system CuPc + PTCDA/Ag(111) is identified to be appropriate for the RPES investigations of hetero-organic interfaces in section 5.4.

4.1 *Fingerprint approach* analysis of vertical hetero-organic systems at 300 K

In previous studies it is shown by PES and near edge x-ray absorption fine structure spectroscopy studies that SnPc molecules grow flat lying on 1 ML PTCDA/Ag(111) [17, 18]. Furthermore, valence PES data reveals that the first layer of SnPc at this hetero-organic interface grows in a wetting mode [17]. This means that this first layer of SnPc is completed before a second layer starts to grow. This finding is corroborated by differential reflectance spectroscopy (DRS) investigations [124] which give a value of less than 10% of higher layer SnPc growth with respect to first layer SnPc growth on top

of 1 ML PTCDA/Ag(111). The fact that the signal of the highest occupied molecular orbital (HOMO) of SnPc is situated between the lowest unoccupied molecular orbtial (LUMO) and the HOMO signal of 1 ML PTCDA/Ag(111) allows a significant deconvolution of the valence PES spectra [18]. Hence this system exhibits the required well defined interface and proper energetic separation of signals in valence PES for an investigation with RPES. However, for the discussion of a quite complicated technique like RPES a comparison of different systems is highly desired. Hence in the following section I will analyze several hetero-organic systems with core level and valence PES in order to characterize them as appropriate or inappropriate for a detailed analysis with RPES.

4.1.1 Metal-phthalocyanine and PTCDA molecules on Ag(111)

A reasonable first attempt in order to find a proper system that fulfills the above discussed requirements is to start from SnPc/1 ML PTCDA/Ag(111). Since this system exhibits the desired growth properties it can be expected that a system with the same molecules but a change in the order of the layers also will. Thus my search for a proper interface system starts with PTCDA/1 ML SnPc/Ag(111). Exchanging the SnPc molecule in SnPc/1 ML PTCDA/Ag(111) with a similar molecule constitutes another way to obtain a similar but different hetero-organic system. The chosen molecule is CuPc because detailed structural data for CuPc/1 ML PTCDA/Ag(111) is known [20]. The third system investigated in the following is PTCDA on 1 ML CuPc/Ag(111). Here the expected similarities to PTCDA/1 ML SnPc/Ag(111) appear to facilitate a common interpretation.

PTCDA/1 ML SnPc/Ag(111)

In the coverage range of a (sub-)ML the system SnPc/Ag(111) has been well characterized by many techniques [83, 125–127]. It is found that the first layer on the Ag(111) surface is modified with respect to a SnPc multilayer. The most obvious modification of (sub-)ML SnPc/Ag(111) with respect to a SnPc multilayer observed by PES is the emergence of a LUMO signal in the valence PES spectrum of (sub-)ML SnPc/Ag(111) [83]. As expected from the direct correspondence of valence and core level PES (see discussion in section 2.2) this strong change in valence PES goes together with a significant variation of the line-shape of the core level PES data between (sub-)ML SnPc/Ag(111) and a SnPc multilayer. Especially the line-shape of the C1s core level PES spectrum of a SnPc molecule is substantially different for SnPc molecules in direct contact to Ag(111) and in higher layers of a homo-molecular SnPc multilayer [83]. Moreover, the line-shape of the C1s core level PES spectra of a SnPc multilayer and (sub-)ML SnPc/Ag(111) are distinguishable from the C1s PES spectra of a PTCDA multilayer and (sub-)ML PTCDA/Ag(111) [18, 78, 83]. Additionally, the line-shape of the C1s core level PES spectrum of a sub-ML SnPc on 1 ML PTCDA/Ag(111) can be successfully

reproduced with reference spectra of 1 ML PTCDA/Ag(111) and a SnPc multilayer [18]. Hence, C1s core level PES of SnPc molecules at the hetero-organic interface with 1 ML PTCDA/Ag(111) can be described with the same Hamiltonian and a similar set of parameters as the homo-molecular SnPc multilayer. In the following I will use the term multilayer-like for this property of a molecule in order to achieve a shorter formulation. All these experimental findings constitute the fulfillment of all requirements for a *fingerprint approach* analysis (see discussion of requirements in section 2.2) of the system SnPc/1 ML PTCDA/Ag(111). From the *fingerprint approach* analysis of the core-level PES spectra of this system in Ref. [18] the conclusion is drawn that SnPc molecules remain on top of 1 ML PTCDA/Ag(111). In order to be able to perform a *fingerprint approach* analysis of the system PTCDA on 1 ML SnPc/Ag(111) the fulfillment of one criterion still needs to be confirmed. This is the multilayer-like character of PTCDA molecules when they are at the hetero-molecular interface with 1 ML SnPc/Ag(111). This can be tested with the actual C1s core level PES data.

In Fig. 4.1 core level and valence PES data of the hetero-organic system of 0.65 ML PTCDA on 1 ML SnPc/Ag(111) is presented. The successful reproduction of the line-shape of the measured C1s PES spectrum by a linear combination of a 1 ML SnPc on Ag(111) and a PTCDA multilayer reference spectrum is demonstrated in Fig. 4.1(a). For this both reference spectra are scaled with a factor so that the sum of both (red line) matches the measured data (open circles). For the PTCDA multilayer reference spectrum an additional energy shift is applied. Such shifts of molecular energy levels of multilayer-like systems can be explained by the alignment of energetic levels to different vacuum levels [92–95]. In the PTCDA multilayer reference spectrum it is the vacuum level of 1 ML PTCDA/Ag(111) [18] to which the energy levels are aligned while in Fig. 4.1 it is the lower vacuum level of 1 ML SnPc/Ag(111) [83]. Hence a shift in the binding energy (E_B) of a PES spectrum of a molecule that exhibits multilayer-like character is of minor concern for the analysis with the *fingerprint approach*. Consequently, energy shifts of multilayer-like contributions in PES spectra will not be discussed in the rest of this chapter. In contrast an energy shift of a PES spectrum of a molecule which is not multilayer-like points towards a modification of the parameters in the *Molecular Gunnarsson-Schönhammer* Hamiltonian (see Eq. 2.9) since those PES spectra are unchanged by a mere variation of the vacuum level [18]. Such energy shifts can be compared to the variations of the line-shape of C1s core level PES spectra found for different Ag surfaces and different structural phases on the same Ag surface in Figs. 2.1 and 2.2. In the case of PTCDA/1 ML SnPc/Ag(111) in Fig. 4.1 the 1 ML SnPc/Ag(111) C1s PES reference spectrum is not shifted in energy with respect to the pure 1 ML SnPc/Ag(111) film. Furthermore, a significant variation of the line-shape of the SnPc contribution to the C1s PES spectrum in Fig. 4.1(a) with respect to the pure 1 ML SnPc/Ag(111) film can be excluded through the successful reproduction of the measured data with the 1 ML SnPc/Ag(111) reference. The same holds true for the PTCDA contribution which is equal to a PTCDA multilayer C1s reference spectrum. Hence PTCDA molecules are multilayer-like in the system PTCDA/1 ML SnPc/Ag(111). So all requirements for a significant *fingerprint approach* analysis are fulfilled for this system. This allows me

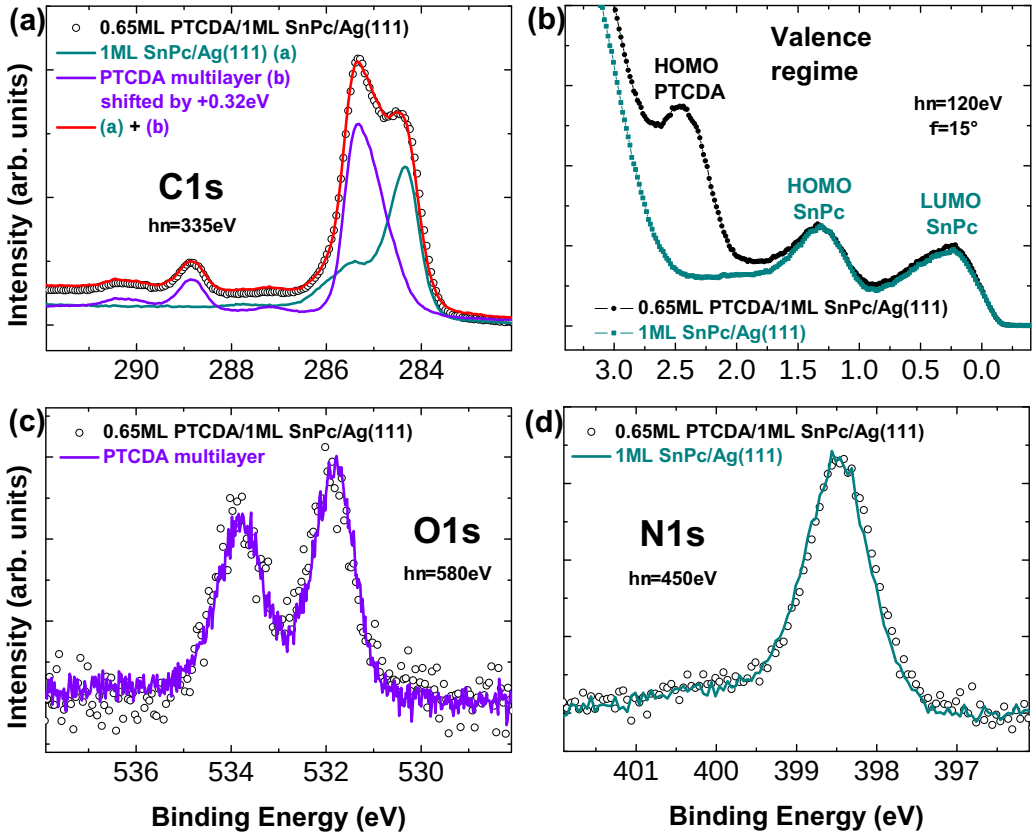

Figure 4.1: PES data of 0.65 ML PTCDA/1 ML SnPc/Ag(111). **(a)** C1s core level PES spectrum (open circles) together with scaled reference spectra of 1 ML SnPc/Ag(111) (cyan line) and a PTCDA multilayer (purple line). The red line is the sum of both reference spectra. **(b)** Valence PES data (black full circles) in comparison to a scaled 1 ML SnPc/Ag(111) reference spectrum (cyan full squares). **(c)** O1s core level PES spectrum (open circles) in comparison to a scaled PTCDA multilayer reference spectrum (purple line). **(d)** N1s core level PES spectrum (open circles) in comparison to a scaled 1 ML SnPc/Ag(111) reference spectrum (cyan line).

to conclude that the SnPc molecules are still in direct contact to the Ag(111) surface and hence in the first layer while PTCDA molecules are only adsorbed in higher layers. This conclusion is corroborated by the O1s and N1s core level PES spectra shown in Fig. 4.1(c) and (d), respectively. Hereby the equal line-shape (within measurement accuracy) of the O1s core level PES spectrum of the hetero-organic system (open circles) and the PTCDA multilayer reference spectrum (purple line) confirms the multilayer-like character of PTCDA since the O1s PES spectrum constitutes an exclusive signal of this molecule. The N1s core level PES spectrum on the other hand is an exclusive signal of the SnPc molecules. So the matching line-shape of the N1s core level PES spectrum of the hetero-organic system (open circles) and the 1 ML SnPc/Ag(111) N1s reference spectrum (cyan line) in Fig. 4.1(d) further confirms that the SnPc molecules are located in the first layer.

At this point I would like to discuss an alternative interpretation allowed by the *fingerprint approach* analysis. Although this interpretation is highly unlikely it demonstrates the limits of a pure *fingerprint approach* analysis. If PES of SnPc molecules in the second layer on top of PTCDA molecules could be described by the same Hamiltonian and a similar set of parameters as the system 1 ML SnPc/Ag(111) the PES data of the hetero-organic film in Fig 4.1 could also be reproduced by 1 ML SnPc/Ag(111) reference spectra. At the same time the contributions of the PTCDA molecules to the PES spectra of the hetero-organic film in Fig 4.1 would have to be multilayer-like although the PTCDA molecules are situated in the first layer. This scenario could be explained by some sort of intermolecular interaction between SnPc and PTCDA molecules. However, this alternative explanation can be excluded by the observed PES intensities. The attenuation of all core level PES signals originating from SnPc molecules with respect to the ones of the uncovered 1 ML SnPc/Ag(111) film shows that the PTCDA molecules must be adsorbed on top of the SnPc molecules. A decrease of the PES intensity stemming from the SnPc molecules due to self attenuation resulting from a Stranski-Krastanov growth mode can also be excluded since in this scenario SnPc molecules would be in a homo-molecular SnPc environment. Hence SnPc multilayer reference spectra would be necessary for a successful reproduction of the measured PES spectra. Additionally, the knowledge about the PES spectra of the system SnPc on 1 ML PTCDA/Ag(111) [17, 18], which has the discussed alternative layer order, immediately proofs this alternative layer order wrong. Anyway, it is important to keep in mind that the *fingerprint approach* analysis only allows statements about the Hamiltonian with which PES of a molecule can be described and the set of parameters included in this Hamiltonian. The layer order of the hetero-organic film is then derived on the basis of these statements in combination with relative and total PES intensities.

Some of the additional data in the small PTCDA coverage range ($\theta < 0.5$ ML) shows hints for PTCDA molecules in the first layer since features at the rising edge of some O1s and C1s PES spectra can be interpreted in this direction (see Fig. A2(c) and (d)). However, these hints are not unambiguous and could also be a consequence of the delicate background subtraction for small coverages (O1s) and a small error in the energy calibration (C1s). In DRS data a signal attributed to SnPc molecules in the second layer is observed when the first layer of SnPc is prepared by direct deposition [124]. Thus this preparation procedure allows PTCDA molecules to replace SnPc molecules from the first layer and force them into the second layer. For 1 ML SnPc/Ag(111) prepared by annealing of a SnPc multilayer this replacement is not observed in DRS [124]. Hence it seems to be the molecular density of the first SnPc layer which induces the observed difference. Similarly, a variation in the annealing procedure could result in a more or less densely covered 1 ML SnPc/Ag(111) so that on a minor fraction of the surface the replacement of SnPc molecules by PTCDA molecules is possible. These PES signals of PTCDA molecules in the first layer would then only be visible for small coverages since the growing PES signals of PTCDA molecules in higher layers would more and more dominate the PES spectra for larger PTCDA coverages. Anyway, the vast majority of PES spectra shows that SnPc molecules remain in the first layer and PTCDA molecules are

adsorbed in higher layers. With the PES spectra that show hints for PTCDA molecules in the first layer I can estimate a relative upper coverage limit of 20 % of 1 ML of PTCDA in this layer within the measured fraction of the surface. So the total amount of PTCDA molecules in the first layer can be estimated to be below a coverage of 0.1 ML of PTCDA.

After revealing the layer order of the system PTCDA on 1 ML SnPc/Ag(111) I investigate the PES spectrum of the valence regime. Due to the direct correspondence of core level and valence PES the assignment of the measured PES signals is based on the *fingerprint approach* analysis of the PES core level spectrum in Fig. 4.1(a). Fig. 4.1(b) displays the valence PES spectrum of 0.65 ML PTCDA on 1 ML SnPc/Ag(111) in comparison to the valence PES spectrum of 1 ML SnPc/Ag(111). From the *fingerprint approach* analysis of the PES core level spectra it follows that the valence PES signals of the SnPc molecules should be equal to the ones of 1 ML SnPc/Ag(111). Hence the two signals at lowest E_B can be assigned to the SnPc LUMO and the SnPc HOMO. The additional PES signal for the 0.65 ML PTCDA on 1 ML SnPc/Ag(111) spectrum at $E_B \approx 2.5$ eV grows with PTCDA coverage (see Fig. A2(b)). Furthermore, the *fingerprint approach* analysis of the PES core level spectra shows that no LUMO signal is expected for the PTCDA molecules. Thus I attribute this signal to the PTCDA HOMO. This PTCDA HOMO signal is situated at the steep rising edge of a peak that originates from several molecular orbitals of 1 ML SnPc/Ag(111). The deconvolution of such a PES spectrum is quite delicate since the two signals exhibit a large difference in PES intensity. So variations in the tailing edge of the PTCDA HOMO signal cannot be separated from small variations in the rising edge of the SnPc molecular orbital signal. Moreover, largely different PES intensities could lead to delicate subtraction artifacts in the resulting PES spectrum belonging to the less intense contribution. Consequently, the PTCDA contribution to the valence PES spectrum of this hetero-organic system cannot be significantly divided from signals that originate from SnPc molecules. In conclusion PTCDA on 1 ML SnPc/Ag(111) is not an appropriate system for further analysis with RPES.

CuPc/1 ML PTCDA/Ag(111)

The next system analyzed with the *fingerprint approach* and valence PES constitutes of a sub-ML of CuPc deposited onto a 1 ML PTCDA/Ag(111) film. For the system 1 ML PTCDA/Ag(111) a huge body of literature exists. For example Refs. [78–80, 128–132] give an impression how many experimental techniques have been used to investigate this metal-organic model system. In the discussion of the requirements for a significant *fingerprint approach* analysis in section 2.2 the examples of CuPc and PTCDA molecules on Ag(111) are included. The line-shapes of the C1s core level PES spectra of both molecules are found to be substantially different with respect to each other in the first layer on Ag(111) and in higher layers (see Figs. 2.1 and 2.2 and Ref. [78]). Moreover, it is found in Fig. 2.1 and in Ref. [78] that the C1s core level PES spectra of CuPc and PTCDA molecules exhibit a substantially different line-shape in the first layer on Ag(111) with respect to higher layers. Hence the only requirement left to

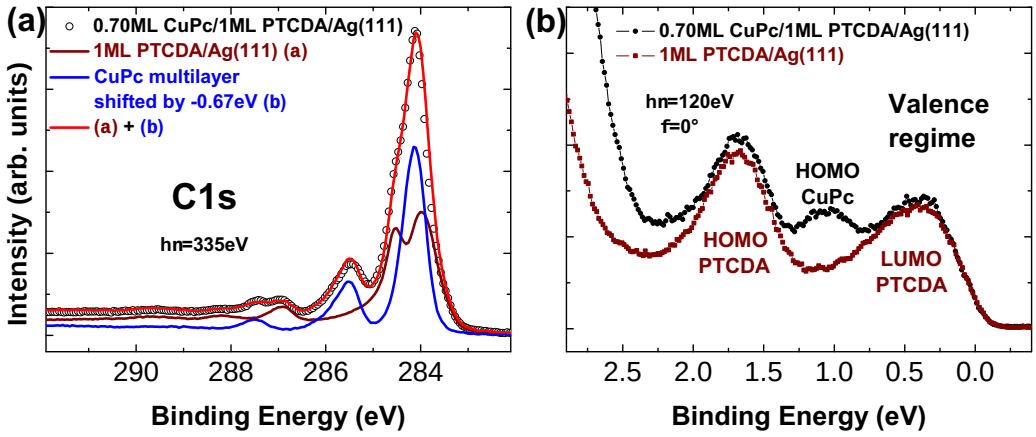

Figure 4.2: PES data of 0.70 ML CuPc/1 ML PTCDA/Ag(111). **(a)** C1s core level PES spectrum (open circles) together with scaled reference spectra of 1 ML PTCDA/Ag(111) (brown line) and a CuPc multilayer (blue line). The red line is the sum of both reference spectra. **(b)** Valence PES data (black full circles) in comparison to a scaled 1 ML PTCDA/Ag(111) reference spectrum (brown full squares).

be fulfilled for a significant *fingerprint approach* analysis of the system CuPc on 1 ML PTCDA/Ag(111) is the multilayer-like character of CuPc molecules at the hetero-organic interface with 1 ML PTCDA/Ag(111). In Ref. [20] chemical interaction at this hetero-organic interface is concluded from the data of different experimental techniques. This conclusion leads to the expectation of a variation of the line-shape of PES core level spectra of CuPc molecules at this hetero-organic interface with respect to a CuPc multilayer.

Analogous to Fig. 4.1(a) a linear combination of reference spectra is used in Fig. 4.2(a) to reproduce the measured C1s core level PES spectrum (open circles). Here a successful reproduction (red line) is performed with a 1 ML PTCDA/Ag(111) reference spectrum (brown line) and a CuPc multilayer reference spectrum (blue line). Since all features of the 0.70 ML CuPc/1 ML PTCDA/Ag(111) C1s PES spectrum (open circles) are equally present in the sum of the two reference spectra (red line) I can conclude that the PES contribution of the PTCDA molecules is well reproduced by a 1 ML PTCDA/Ag(111) reference spectrum. Additionally, the successful reproduction of the C1s core level PES spectrum in Fig. 4.2(a) shows that CuPc molecules at the hetero-organic interface with 1 ML PTCDA/Ag(111) are multilayer-like. Thus a significant *fingerprint approach* analysis of the system CuPc on 1 ML PTCDA/Ag(111) is possible. The energy shift applied to the CuPc multilayer reference spectrum can be explained analogous to the shift of the PTCDA multilayer reference spectrum of Fig. 4.1(a). Since the characteristic feature of a PTCDA multilayer C1s PES reference spectrum at $E_B \approx 289$ eV (see Fig. 4.1(a)) is not visible in Fig. 4.2(a) multilayer-like PTCDA molecules can be safely excluded. Moreover, the O1s core level PES spectrum (not shown) exhibits the same line-shape (within measurement accuracy) as a 1 ML PTCDA/Ag(111) reference spectrum and the

line-shape of the N1s core level PES spectrum (not shown) is equal to the CuPc multilayer reference spectrum. Hence the O1s and N1s core level PES spectra confirm the conclusion drawn from the analysis of the C1s core level PES spectrum. The expected variation of line-shapes of PES signals of the CuPc molecules at this hetero-organic interface with respect to a CuPc multilayer is not found. Apparently, the chemical interaction at this hetero-organic interface according to Ref. [20] has no detectable influence on the core level PES line-shape. So using the criterion of line-shapes of core level PES spectra the hetero-organic interface of CuPc/1 ML PTCDA/Ag(111) can be characterized as similar to CuPc on Au(111) and the homo-molecular CuPc interface (see Fig. 2.1). The core level PES intensities of the contributions of the PTCDA molecules to the PES spectra of the hetero-organic film exhibit the expected attenuation with respect to the 1 ML PTCDA/Ag(111) reference spectra. Consequently, these PES intensities in combination with the *fingerprint approach* analysis in Fig. 4.2(a) reveal that PTCDA molecules are in the first and CuPc molecules are in higher layers. Furthermore, the comparison of the deposited CuPc amount, estimated with the deposition rate, with the observed PES intensity stemming from CuPc molecules (C1s and N1s) points towards a wetting growth of CuPc. Such a conclusion solely based on PES intensities can exclude Volmer-Weber growth but in order to find out whether a third (and higher) layer growth in the order of 0.2 ML exists a comparison to other experimental techniques is necessary. From the data in Ref. [20] it can be reasoned that at 300 K the first layer of CuPc in fact grows in a wetting mode in the overall second layer on top of 1 ML PTCDA/Ag(111). Hence the requirements of a stable and well defined interface system are fulfilled by (sub-)ML CuPc/1 ML PTCDA/Ag(111).

The valence PES data illustrated in Fig. 4.2(b) reveals three separable peaks within the same PES intensity range. From the *fingerprint approach* analysis of Fig. 4.2(a) it is expected that the signals of the PTCDA molecules in the valence PES data are equal to the ones of 1 ML PTCDA/Ag(111). Moreover, the peak of the CuPc molecules with the lowest E_B in the valence PES spectrum must be the CuPc HOMO signal since the emergence of a CuPc LUMO signal can be excluded from the line-shape of the C1s core level PES spectrum in Fig. 4.2(a). Hence the peak at $E_B \approx 1$ eV in Fig. 4.2(b) is assigned to the CuPc HOMO which is in agreement with Ref. [20]. Moreover, the peak at lower E_B than the CuPc HOMO signal must be the PTCDA LUMO signal and the one at higher E_B the PTCDA HOMO signal (as indicated in Fig. 4.2(b)). In contrast to Ref. [20] an energy shift of the PTCDA LUMO signal in the PES spectrum of the hetero-organic system with respect to the PES spectrum of 1 ML PTCDA/Ag(111) in the order of 100 meV cannot be detected in Fig. 4.2(b). This can be explained by a difference in the photon energy ($h\nu$) of the valence PES spectrum of 0.70 ML CuPc/1 ML PTCDA/Ag(111) in Fig. 4.2(b) and the one in Ref. [20]. The larger $h\nu$ used in Fig. 4.2(b) results in a larger kinetic energy of the photoelectrons which leads to different scattering properties of these electrons with respect to the ones excited by He I light. The consequential difference in diffuse backscattering at the CuPc overlayer could lead to a different background of substrate s-p bands which might alter the apparent peak maximum of the LUMO signal (see Fig. A5). This scenario is in agreement with the observed variation of the relative intensity of the

HOMO and the LUMO signal in Ref. [20]. An energy shift of the observed magnitude due to backscattering in combination with a possible dispersion of the PTCDA LUMO signal (as for PTCDA/Ag(110) [133]) cannot be definitely excluded. If a dispersion of the same order of magnitude (approximately 200 meV) as for PTCDA/Ag(110) [133] was present in the system 1 ML PTCDA/Ag(111) the LUMO signal from a point in k-space where E_B exhibits a maximum could be backscattered into the k-space region probed in the measurement. In this scenario a difference between a measurement with $h\nu = 120$ eV and $h\nu =$ He I would be expected. However, the continuous energy shift with increasing CuPc coverage of the PTCDA LUMO in two different measurement geometries observed in Ref. [20] suggests that a dispersion related explanation is unlikely since this scenario would be a surprising coincidence. For a definite exclusion of this scenario detailed information about the k-space region from which the signal in the discussed energy distribution curve (EDC) stems is necessary. Anyway, the valence PES spectrum in Fig. 4.2(b) can allow a significant deconvolution of the PES signals from the PTCDA molecules and the CuPc molecules in RPES. For this a previous RPES study of the homo-molecular system 1 ML PTCDA/Ag(111) and at least one multilayer-like CuPc system will be necessary. This might of course reveal some unexpected difficulties but at this point the system sub-ML CuPc/1 ML PTCDA/Ag(111) is promising for an analysis with RPES. Consequently, this system will be investigated with this spectroscopic technique in subsection 5.4.2.

PTCDA/1 ML CuPc/Ag(111)

Continuing the search for further hetero-organic systems which are suited for the intended RPES analysis I switch the order of the preparations steps with respect to the previously discussed system CuPc on 1 ML PTCDA/Ag(111). So now a sub-ML PTCDA is deposited on top of 1 ML CuPc/Ag(111). For the system 1 ML CuPc/Ag(111) many similarities are found with respect to the system 1 ML SnPc/Ag(111). In valence PES spectra of a (sub-)ML CuPc/Ag(111) a LUMO signal is found in contrast to a CuPc multilayer (see Ref. [82] and Fig. 2.1). This strong change in the valence PES spectrum between (sub-)ML CuPc/Ag(111) and a CuPc multilayer manifests itself in strong changes of the line-shape of the corresponding core level PES spectra (see C1s spectra in Fig. 2.1 and N1s PES reference spectra in Fig. 4.3). Moreover, the phase diagrams of the growth of the first layer show similarities for sub-ML SnPc/Ag(111) [125] and sub-ML CuPc/Ag(111) [82]. At 300 K ordered structures start to form for coverages in the range of approximately 0.9 ML in both cases. For lower coverages gas-like phases are observed which points towards intermolecular repulsion.

Fig. 4.3 illustrates core level and valence PES data of 0.5 ML PTCDA deposited onto 1 ML CuPc/Ag(111). The reproduction of the measured C1s PES spectrum (open circles) with reference spectra (Fig. 4.3(a)) is successful. However, the reference spectra used in this case reveal a remarkable difference with respect to the two systems presented in Figs. 4.1 and 4.2. For the reproduction of the line-shape of the measured C1s core level PES spectrum (open circles) in Fig. 4.3(a) a 1 ML PTCDA/Ag(111) (brown

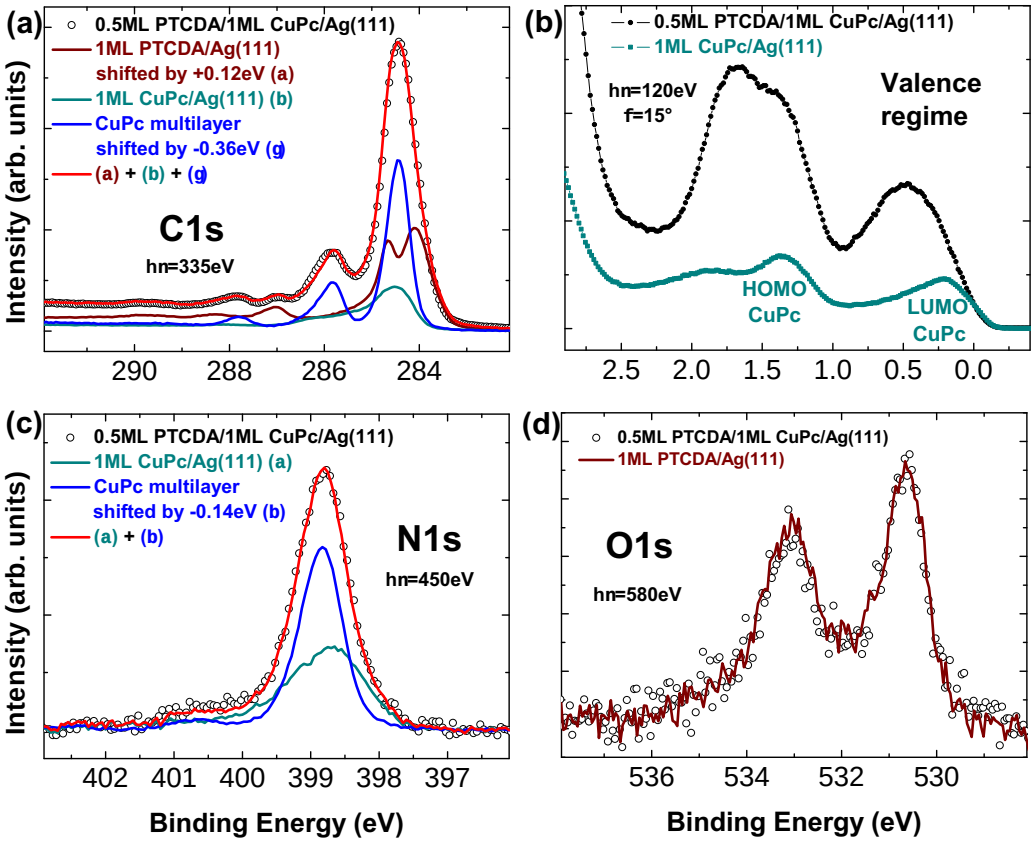

Figure 4.3: PES data of 0.5 ML PTCDA/1 ML CuPc/Ag(111). **(a)** C1s core level PES spectrum (open circles) together with scaled reference spectra of 1 ML PTCDA/Ag(111) (brown line), 1 ML CuPc/Ag(111) (cyan line) and a CuPc multilayer (blue line). **(b)** Valence PES data (black full circles) in comparison to a scaled 1 ML CuPc/Ag(111) reference spectrum (cyan full squares). **(c)** N1s core level PES spectrum (open circles) together with scaled reference spectra of 1 ML CuPc/Ag(111) (cyan line) and a CuPc multilayer (blue line). **(d)** O1s core level PES spectrum (open circles) in comparison to a scaled 1 ML PTCDA/Ag(111) reference spectrum (brown line). In each panel the red line is the sum of all reference spectra.

line) and a multilayer CuPc reference spectrum (blue line) have to be used in addition to a 1 ML CuPc/Ag(111) reference spectrum (cyan line). Hence PTCDA molecules can be described with the same Hamiltonian and a similar set of parameters as 1 ML PTCDA/Ag(111) although they are deposited in the second preparation step on top of 1 ML CuPc/Ag(111). The matching line-shape of the O1s core level PES spectra of 0.5 ML PTCDA/1 ML CuPc/Ag(111) (open circles) and the 1 ML PTCDA/Ag(111) reference spectrum (brown line) in Fig. 4.3(d) agrees with this finding. Interestingly, the C1s 1 ML PTCDA/Ag(111) reference spectrum needs to be shifted in E_B for a successful *fingerprint approach* analysis in Fig. 4.3(a) whereas E_B of the O1s 1 ML PTCDA/Ag(111) reference is unchanged in Fig. 4.3(d). The energy shift of the C1s 1 ML PTCDA/Ag(111) reference is significant since only a shifted 1 ML PTCDA/Ag(111) reference can properly reproduce the rising edge of the main peak and the peak at $E_B \approx 287$ eV. So there seems to be some difference in the set of parameters in the Hamiltonian of the PTCDA molecules with respect to 1 ML PTCDA/Ag(111). Similarly to the modifications in Fig. 2.2 this could be a consequence of a change in the adsorption geometry of PTCDA molecules on Ag(111). This change might be forced upon the PTCDA molecules by the presence of CuPc molecules (see discussion of energy shifts for lateral hetero-organic systems in subsection 4.2.1). PTCDA molecules which are multilayer-like can be excluded from the analysis of the line-shapes of the measured C1s and O1s PES spectra since no PTCDA multilayer reference spectrum is needed for a successful reproduction (in contrast to Fig. 4.1). Moreover, in Fig. 4.3(a) a multilayer-like CuPc contribution is found in addition to the 1 ML CuPc/Ag(111) signal. Thus some CuPc molecules are multilayer-like and others can be described by the same Hamiltonian and a similar set of parameters as 1 ML CuPc/Ag(111). The reproduction of the N1s PES spectrum of the hetero-organic film (open circles) with a CuPc multilayer (blue line) and a 1 ML CuPc/Ag(111) reference spectrum (cyan line) in Fig. 4.3(c) agrees with this finding. The observed contribution of multilayer-like CuPc molecules is quite unexpected since for the 1 ML CuPc/Ag(111) sample onto which PTCDA molecules are deposited such a contribution to the line-shape of the PES spectra (not shown) can be excluded. A *fingerprint approach* analysis of additional core level PES data for lower PTCDA coverages (not shown) is entirely analogue to Fig. 4.3.

The requirement that still needs to be fulfilled for a significant *fingerprint approach* of the system PTCDA/1 ML CuPc/Ag(111) is the multilayer-like character of PTCDA molecules at the hetero-organic interface with 1 ML CuPc/Ag(111). From the PES spectra in Fig. 4.3 this cannot be concluded since no multilayer-like contribution of PTCDA molecules is found. So in order to draw conclusions about the layer order of the system PTCDA/1 ML CuPc/Ag(111) from the *fingerprint approach* analysis multilayer-like PTCDA molecules need to be detected. At this point I search for a contribution to the line-shape of the PES spectra by multilayer-like PTCDA molecules in the PES data of a PTCDA/1 ML CuPc/Ag(111) sample with a higher PTCDA coverage. Fig. 4.4 displays the PES data of 0.8 ML PTCDA/1 ML CuPc/Ag(111). From the reproduction of the C1s (Fig. 4.4(a)) and the O1s (Fig. 4.4(d)) PES data a contribution of multilayer-like PTCDA molecules (purple lines) becomes obvious. Whether some of these multilayer-

like PTCDA molecules are situated at a hetero-molecular interface with CuPc molecules cannot be concluded. If this PTCDA-CuPc interface existed in this sample the third requirement for a significant *fingerprint approach* analysis would be fulfilled (see section 2.2). If such a hetero-molecular interface did not exist in this sample the third requirement would not have to be fulfilled. Hence I conclude that a significant *fingerprint approach* analysis of the system PTCDA/1 ML CuPc/Ag(111) is possible. Except for the contribution of multilayer-like PTCDA molecules the analysis of the core level PES data in Fig. 4.4 is analogue to Fig. 4.3. From the analysis of Figs. 4.4 and 4.3 in combination with the conclusions drawn from the system CuPc on 1 ML PTCDA/Ag(111) the layer order of the system PTCDA/1 ML CuPc/Ag(111) can be discussed. The most reasonable conclusion is that for PTCDA coverages up to 0.5 ML all PTCDA molecules are situated in the first layer while CuPc molecules are in the first and in higher layers. For larger PTCDA coverages both CuPc molecules and PTCDA molecules are present in the first and in higher layers. Consequently, approximately 0.5 ML of the deposited amount of PTCDA molecules diffuse into the first layer, replace some of the CuPc molecules in this first layer and force them into higher layers. Thus the notation PTCDA/1 ML CuPc/Ag(111) must not be interpreted as a description of the molecular order in the sample but rather seen as the documentation of the preparation of the sample. An alternative layer order than the one just discussed would require multilayer-like CuPc molecules in the first layer (see discussion of the previous systems). For this scenario electronic intermolecular interaction (e.g. hybridization) at the PTCDA-CuPc hetero-organic interface would be necessary. A significant influence on the core-level PES line-shape of such a possible intermolecular interaction has been excluded in the discussion of the PES data of the system CuPc/1 ML PTCDA/Ag(111). Thus it is extremely unlikely that such an interaction has a significant influence on the core-level PES line-shape of the same hetero-organic interface in the system PTCDA/1 ML CuPc/Ag(111). Additionally, the measured PES intensities do not agree with the scenario of CuPc molecules only in the first layer since the PES intensity stemming from multilayer-like CuPc molecules in the C1s and N1s PES spectra is too large. Furthermore, in the spot profile analysis low energy electron diffraction (LEED), valence PES and x-ray standing wave study of the same system in Ref. [134] all findings are also interpreted by a diffusion of PTCDA molecules into the first layer. Especially the disappearance of the diffraction spots of the characteristic CuPc LEED structure after the deposition of a small amount of PTCDA (approximately 0.1 ML) points towards the existence of PTCDA molecules in the first layer. Additionally, very recent scanning tunneling microscopy (STM) measurements of the same system find PTCDA molecules and CuPc molecules in the first layer [135]. This data unambiguously proofs an alternative layer order wrong.

In the case of a first layer with two different molecules quantitative statements with PES intensities are generally difficult. In order to draw conclusions from the attenuation of a particular PES core level signal it is necessary to know on top of which molecule in the first layer the molecules in higher layers are situated. CuPc and PTCDA molecules in higher layers could selectively adsorb on top of either of the two molecules in the first layer or be more or less homogeneously distributed over both. Furthermore, the growth

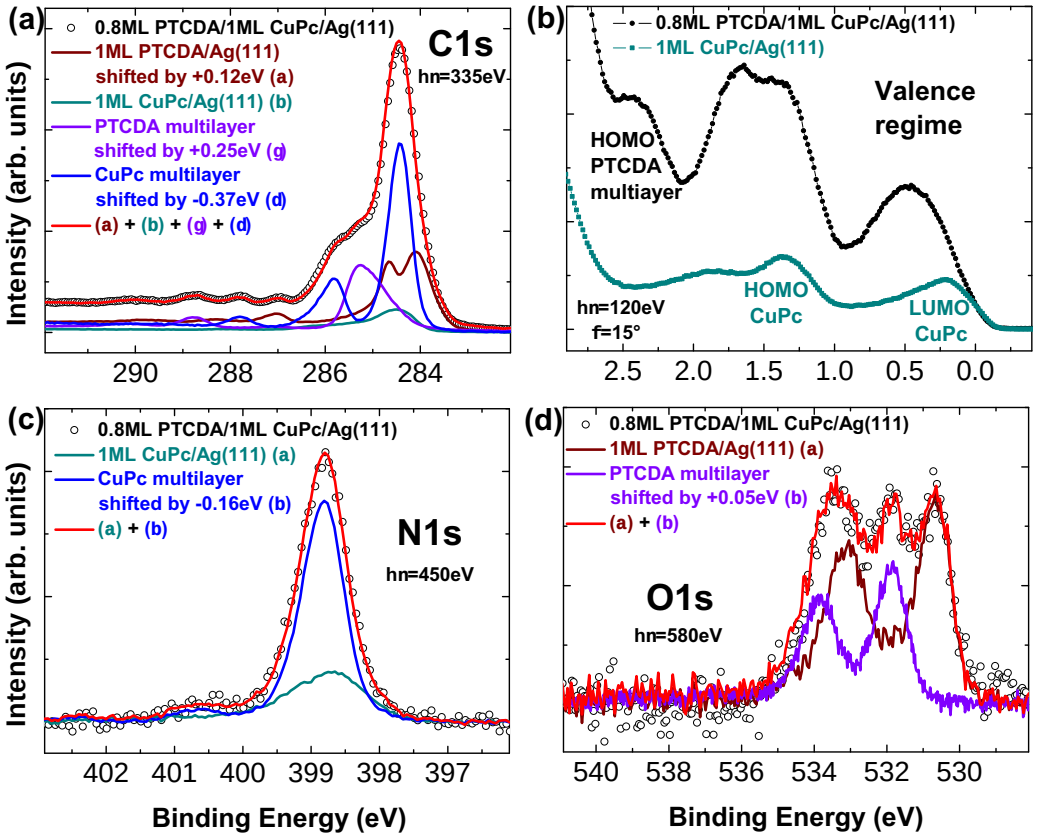

Figure 4.4: PES data of 0.8 ML PTCDA/1 ML CuPc/Ag(111). **(a)** C1s core level PES spectrum (open circles) together with scaled reference spectra of 1 ML PTCDA/Ag(111) (brown line), 1 ML CuPc/Ag(111) (cyan line), a PTCDA multilayer (purple line) and a CuPc multilayer (blue line). **(b)** Valence PES data (black full circles) in comparison to a scaled 1 ML CuPc/Ag(111) reference spectrum (cyan full squares). **(c)** N1s core level PES spectrum (open circles) together with scaled reference spectra of 1 ML CuPc/Ag(111) (cyan line) and a CuPc multilayer (blue line). **(d)** O1s core level PES spectrum (open circles) together with scaled reference spectra of 1 ML PTCDA/Ag(111) (brown line) and a PTCDA multilayer (purple line). In each panel the red line is the sum of all reference spectra.

mode of the higher layers is unknown. Hence the given total PTCDA coverages are estimated by the deposition rate and the visible PES intensity of all PTCDA signals. The latter correspond to a minimal coverage value which is only equal to the actual coverage in the case of no attenuation by an overlayer. Similarly the amount of PTCDA molecules in the first layer in the 0.8 ML PTCDA/1 ML CuPc/Ag(111) sample is estimated to be approximately 0.5 ML from the intensity of the 1 ML PTCDA/Ag(111) reference spectra used in the *fingerprint approach* analysis. Even though quantitative statements are difficult the *fingerprint approach* analysis of the system PTCDA/1 ML CuPc/Ag(111) allows significant qualitative statements. The separable signals in the E_B region of $E_B > 285$ eV of the C1s PES spectrum allow an unambiguous deconvolution of the measured PES data. Moreover, the agreement with the exclusive PES signals (O1s for PTCDA and N1s for CuPc) justifies the choice of reference spectra used to reproduce the C1s PES data. Hence for hetero-organic systems with metal-phthalocyanine and PTCDA molecules on Ag(111) a significant *fingerprint approach* analysis of the C1s core level PES spectra with three and even four components is possible.

An assignment of the signals in the valence PES spectra of the system PTCDA/1 ML CuPc/Ag(111) in Figs. 4.3(b) and 4.4(b) only through a comparison to the valence PES EDCs of the homo-molecular films is very difficult and quite speculative. The direct correspondence of valence PES and core level PES can be used to perform a rough assignment since for each contribution in the *fingerprint approach* analysis of the core level PES spectra a corresponding contribution must exist in the valence PES EDC. Consequently, the feature at $E_B \approx 0.5$ eV in Figs. 4.3(b) and 4.4(b) most probably consists of a CuPc LUMO signal and a PTCDA LUMO signal. The former should be similar to the CuPc LUMO signal of 1 ML CuPc/Ag(111) while the energy shifts applied to the C1s PES 1 ML PTCDA/Ag(111) reference spectra point towards a modification of the PTCDA LUMO signal with respect to 1 ML PTCDA/Ag(111). A detailed discussion of this possible modification in the valence regime will be given for the lateral hetero-organic systems in subsection 4.2.1. The double peak feature at $E_B \approx 1.5$ eV should consist of a CuPc HOMO signal from the first layer, a PTCDA HOMO signal from first layer and a CuPc HOMO signal from higher layers. Moreover, the additional feature at $E_B \approx 2.4$ eV in the valence PES spectrum in Fig. 4.4(b) with respect to Fig. 4.3(b) can be assigned to a PTCDA HOMO from higher layers. A comparison to the valence PES data of 0.65 ML PTCDA/1 ML SnPc/Ag(111) in Fig. 4.1(b) supports this assignment.

The instability of the system PTCDA/1 ML CuPc/Ag(111) at 300 K results in rather undefined hetero-molecular interfaces and multiple overlapping signals in the valence PES spectrum. Hence it is not an appropriate system for further analysis with RPES. However, the observed (partial) layer exchange introduces a new and interesting question about the origin of the found instability. Finding the reason for the layer exchange could exclude some hetero-organic systems from the search for well defined hetero-organic interfaces. These are of advantage for basic research questions since the well defined geometric structure of such model systems facilitates the interpretation of the data produced by complicated experimental techniques. Especially in the light of the findings

for the system PTCDA/1 ML SnPc/Ag(111) the instability of the system PTCDA/1 ML CuPc/Ag(111) is very surprising. For the latter system a partial layer exchange is energetically favorable at 300 K. For the former this is either not the case or an exchange is somewhat hindered. A lack of mobility for PTCDA molecules at 300 K can be excluded with the observed layer exchange for PTCDA/1 ML CuPc/Ag(111). A possible explanation for the observed difference of those two systems could be given by a difference in the adsorption energy per surface area between a CuPc and a SnPc molecule on Ag(111). If this quantity was smaller for a CuPc than for a PTCDA molecule and larger for a SnPc than for a PTCDA molecule the behavior of both systems with PTCDA molecules deposited on top could be explained. However, this explanation alone is in contrast to the observed stability of the system SnPc/1 ML PTCDA/Ag(111) [17, 18]. The fact that this system is stable might be related to the attractive intermolecular interaction of the PTCDA herringbone layer [79]. At this point it is apparent that more experimental information is needed for a discussion of this issue (see section 4.3). Taking additional effects, such as intermolecular forces, into account can certainly produce a working explanation but in order to reach a significant conclusion further information and more systems need to be included into the discussion (see section 4.3). The following search for additional hetero-organic systems with well defined interfaces could provide this additional information.

4.1.2 F4TCNQ and PTCDA molecules on Ag(110)

So far SnPc/1 ML PTCDA/Ag(111) and CuPc/1 ML PTCDA/Ag(111) have shown to provide structurally well defined and stable interfaces and exhibit separable signals in the valence PES spectrum. Since the electronic structure of the two different metal-phthalocyanines is very similar in the valence regime it can be expected that the RPES data of both of these interfaces will also be quite similar. In order to be able to compare interfaces with different electronic properties an additional and sufficiently different hetero-organic interface system is of interest. A parameter that might provide some previous knowledge on the electronic structure at a hetero-organic interface is the electron affinity of the involved components. This parameter is defined by the energetic difference of the LUMO and the vacuum level and is therefore a measure for the energy an electron gains when it is transfered onto the molecule. Thus it can be estimated that a molecule with a high electron affinity is more likely to receive an electron. In Ref. [95] electron affinities for many molecules are given and the molecule with the largest electron affinity therein is F4TCNQ. So I choose this molecule for the following investigations. Due to the huge amount of preliminary data the second molecule is chosen to be PTCDA. Since both of these molecules belong to the D_{2h} symmetry group the Ag(110) surface might be of advantage. The matching symmetry might lead to an ordered molecular orientation which facilitates obtaining additional information by ARPES measurements. This combination of molecules could also lead to valuable information for the discussion about the adsorption energy per surface area of π-conjugated molecules on metal substrates.

F4TCNQ/1 ML PTCDA/Ag(110)

For the first ML of PTCDA on Ag(110) two structural phases are possible. Direct deposition leads to the so-called brick-wall phase [80, 97, 99, 136–138] while annealing of a multilayer results in a herringbone phase [98, 99, 138]. In order to exclude an uncovered part of the Ag(110) surface I choose the later preparation procedure for the first layer of the hetero-organic interface system F4TCNQ on 1 ML PTCDA/Ag(111). In any case such an uncovered fraction of the Ag(110) surface would lead to a PES signal originating from molecules in the first layer which are deposited in the second preparation step and hence complicate the evaluation with the *fingerprint approach*. The herringbone ML PTCDA/Ag(110) will simply be called 1 ML PTCDA/Ag(110) in the following. As shown in Refs. [99, 138] and Fig. 2.2 a LUMO signal is visible in the valence PES spectrum of 1 ML PTCDA/Ag(110). The corresponding C1s core level PES spectrum shows a significant variation of its line-shape with respect to a PTCDA multilayer (see Fig. 2.2 and Ref. [78]). The system F4TCNQ/Ag(110) has, to my best knowledge, not been studied by valence PES prior to my work. However, valence PES measurements of F4TCNQ molecules on Ag(111) [139] show a LUMO signal and hence the same can be expected for F4TCNQ molecules on Ag(110). My valence PES measurements of the homo-molecular system (sub-)ML F4TCNQ/Ag(110) confirm this expectation (see Fig. 4.6(b) and Fig. A7). For an F4TCNQ multilayer no LUMO signal is observed in valence PES [140]. Similar to all other molecules investigated so far this difference in valence PES between an F4TCNQ multilayer and (sub-)ML F4TCNQ/Ag(110) manifests itself in substantially different line-shapes of the corresponding C1s core level PES spectra (see Fig. A6(a)). Furthermore, the line-shapes of the C1s core level PES spectra of an F4TCNQ multilayer and (sub-)ML F4TCNQ/Ag(110) are significantly different from a PTCDA multilayer and 1 ML PTCDA/Ag(110). Consequently, a significant *fingerprint approach* analysis of a hetero-organic system with F4TCNQ and PTCDA molecules on Ag(110) will be possible if both molecules are multilayer-like at the hetero-organic F4TCNQ-PTCDA interface.

Fig. 4.5 shows C1s core level and valence PES data of 0.5 ML F4TCNQ deposited on top of 1 ML PTCDA/Ag(110). The measured C1s core level PES spectrum (open circles) displayed in Fig. 4.5(a) is successfully reproduced with reference spectra of 1 ML PTCDA/Ag(110) (brown line), 1.0 ML F4TCNQ/Ag(110) (orange line) and a PTCDA multilayer (purple line). Hence all F4TCNQ molecules of this sample can be described with the same Hamiltonian and a similar set of parameters as 1.0 ML F4TCNQ/Ag(110). On the other hand there are two types of PTCDA molecules present in the 0.5 ML F4TCNQ/1 ML PTCDA/Ag(110) sample. Some PTCDA molecules are multilayer-like while others can be described with the same Hamiltonian and a similar set of parameters as 1 ML PTCDA/Ag(110). A *fingerprint approach* analysis of C1s data for a coverage of approximately 1.0 ML of F4TCNQ (see Fig. A6(b)) obtains a small additional multilayer-like F4TCNQ contribution in the successful reproduction of the measured C1s line-shape. Whether the multilayer-like contributions stem from molecules that are at a hetero-molecular interface cannot be concluded. The discussion of the fulfillment

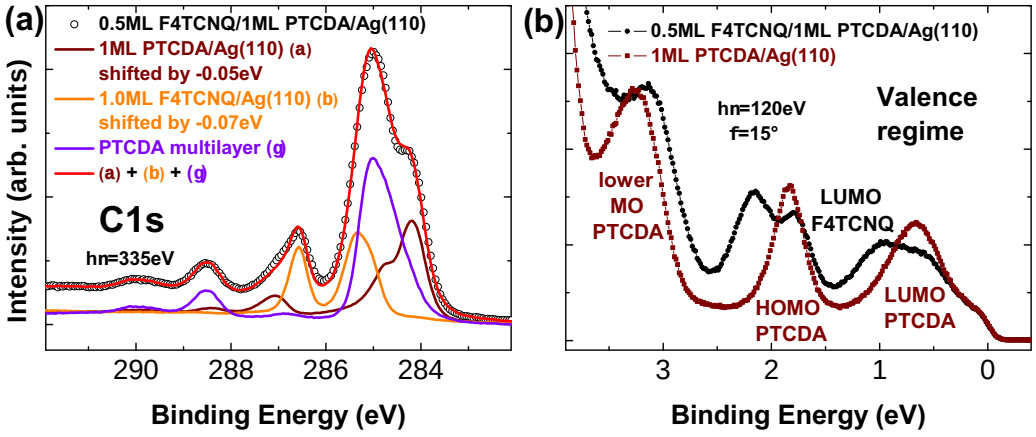

Figure 4.5: PES data of 0.5 ML F4TCNQ/1 ML PTCDA/Ag(110). **(a)** C1s core level PES spectrum (open circles) together with scaled reference spectra of 1 ML PTCDA/Ag(110) (brown line), 1.0 ML F4TCNQ/Ag(110) (orange line) and a PTCDA multilayer (purple line). The red line is the sum of all reference spectra. **(b)** Valence PES data (black full circles) in comparison to a scaled 1 ML PTCDA/Ag(110) reference spectrum (brown full squares).

of the third requirement for a significant *fingerprint approach* analysis (see section 2.2) is hence analogue to the system PTCDA on 1 ML CuPc/Ag(111). Either the third requirement is fulfilled or it does not need to be fulfilled. Consequently, for hetero-organic systems with F4TCNQ and PTCDA molecules on Ag(110) a significant *fingerprint approach* analysis is possible. The F4TCNQ coverage of both samples is again estimated by the deposition rate and the visible PES intensities (N1s and F1s). Furthermore, the line-shape analysis of the exclusive core level PES signals of F4TCNQ molecules (N1s and F1s, not shown) and the exclusive core level signal of PTCDA molecules (O1s, not shown) is in agreement with the findings for the corresponding C1s core level PES data. For both F4TCNQ/1 ML PTCDA/Ag(110) samples energy shifts with respect to the reference spectra of the homo-molecular ML samples on Ag(110) are observed. This points towards a modification of the parameters in the Hamiltonian of both molecules with respect to the pure 1.0 ML F4TCNQ/Ag(110) and 1 ML PTCDA/Ag(110) samples. For PTCDA molecules this modification could originate from structural changes as observed in Fig. 2.2. For F4TCNQ molecules different sub-ML coverages on Ag(110) do lead to an energy shift of all PES signals with respect to the 1.0 ML F4TCNQ/Ag(111) reference spectra (see Fig. A7). Consequently, either a structural modification or a change in the molecular environment can be given as a reason for the energy shift of the contribution of F4TCNQ molecules in the hetero-organic system F4TCNQ/1 ML PTCDA/Ag(110). The most reasonable conclusion from these findings is that F4TCNQ molecules diffuse into the first layer and force part of the PTCDA molecules into higher layers. An alternative layer order with multilayer-like PTCDA molecules in the first layer can again be excluded with an analysis of core level PES intensities.

The signals in the valence band PES data of Fig. 4.5(b) can be assigned to the particular molecules on the basis of the *fingerprint approach* analysis of the C1s PES spectrum in Fig. 4.5(a). For the PTCDA molecules in the first layer valence orbital signals similar to the valence PES spectrum of 1 ML PTCDA/Ag(110) (filled brown squares in Fig. 4.5(b)) are expected. F4TCNQ molecules in the first layer should exhibit valence orbital signals similar to the valence PES spectrum of 1.0 ML F4TCNQ/Ag(111) in Fig. 4.6(b). Additionally, a HOMO signal stemming from the PTCDA molecules in higher layers should also be present in the valence PES spectrum of 0.5 ML F4TCNQ/1 ML PTCDA/Ag(110) (filled black circles) in Fig. 4.5(b). Consequently, the signal at lowest E_B is assigned to the LUMO of PTCDA molecules in the first layer. The corresponding PTCDA HOMO signal should contribute to the double peak at $E_B \approx 2$ eV. The additional intensity found for the 0.5 ML F4TCNQ/1 ML PTCDA/Ag(110) spectrum in between the LUMO and the HOMO signal of PTCDA molecules in the first layer can be assigned to the F4TCNQ LUMO. Hence the double peak at $E_B \approx 2$ eV of the 0.5 ML F4TCNQ on 1 ML PTCDA/Ag(110) spectrum should include a contribution of the HOMO signal of F4TCNQ molecules in the first layer. Additionally, the HOMO signal of PTCDA molecules in the second layer is most probably incorporated in the signal at $E_B \approx 2$ eV. Similarly, signals of all three types of molecules contribute to the valence PES spectrum of 0.5 ML F4TCNQ/1 ML PTCDA/Ag(110) at $E_B > 2.5$ eV. Once again an assignment of the contributions to the valence PES spectrum is made possible by the knowledge of the contributions of the *fingerprint approach* analysis of the C1s PES data and the direct correspondence of core level and valence PES.

In conclusion the system F4TCNQ/1 ML PTCDA/Ag(110) is found to be instable and a layer exchange similar to PTCDA/1 ML CuPc/Ag(111) is found. So F4TCNQ on 1 ML PTCDA/Ag(110) does not exhibit a well defined hetero-organic interface. Furthermore, a significant deconvolution of the valence PES spectrum, that includes signals from both molecules in the first layer and at least the contribution of PTCDA molecules in higher layers, is very difficult due to the energetic overlap of multiple signals. Hence the system F4TCNQ/1 ML PTCDA/Ag(110) is inappropriate for a detailed analysis with RPES.

PTCDA/1.0 ML F4TCNQ/Ag(110)

Switching the order of the preparation steps with respect to the system F4TCNQ on 1 ML PTCDA/Ag(110) results in another system that might exhibit a well defined hetero-organic interface. Fig. 4.6 displays the PES data of the resulting 1.6 ML PTCDA/1.0 ML F4TCNQ/Ag(110) film. In Fig. 4.6(a) the successful reproduction of the measured C1s core level PES data is performed with a 1.0 ML F4TCNQ/Ag(110) (orange line) and a PTCDA multilayer (purple line) reference spectrum. Hence all PTCDA molecules are multilayer-like while all F4TCNQ molecules can be described with the same Hamiltonian and a similar set of parameters as 1.0 ML F4TCNQ/Ag(110). No hint for a modification of the parameter set with respect to a pure 1.0 ML F4TCNQ/Ag(110) sample is observed for the F4TCNQ molecules in the hetero-organic system PTCDA/1.0 ML

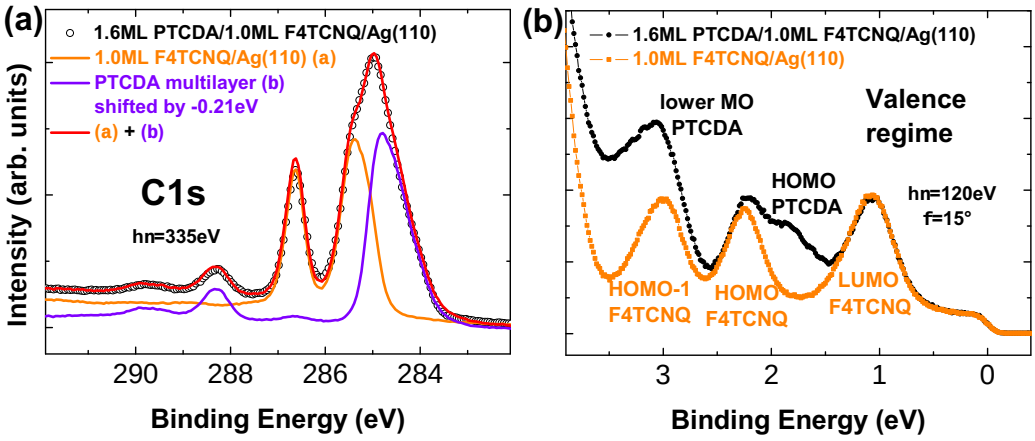

Figure 4.6: PES data of 1.6 ML PTCDA/1.0 ML F4TCNQ/Ag(110). **(a)** C1s core level PES spectrum (open circles) together with scaled reference spectra of 1.0 ML F4TCNQ/Ag(110) (orange line) and a PTCDA multilayer (purple line). The red line is the sum of the two reference spectra. **(b)** Valence PES data (black full circles) in comparison to a scaled 1.0 ML F4TCNQ/Ag(110) reference spectrum (orange full squares).

F4TCNQ/Ag(110). The data of the exclusive PES signals of both molecules (N1s, F1s for F4TCNQ and O1s for PTCDA, all not shown) agree with the *fingerprint approach* analysis of the C1s core level PES data. Consequently, it can be concluded that all F4TCNQ molecules remain in the first layer on the Ag(110) surface and that all deposited PTCDA molecules are situated in higher layers.

The valence PES data presented in Fig. 4.6(b) can be discussed with the result of the *fingerprint approach* analysis of the C1s core level PES data in Fig. 4.6(a). The signals stemming from the F4TCNQ molecules in the first layer should be equal to the ones of the 1.0 ML F4TCNQ/Ag(110) reference spectrum (orange full squares). The additional signals in the valence PES spectrum of the hetero-organic film (black full circles) are hence assigned to PTCDA molecules in higher layers (as indicated in Fig. 4.6(b)). A LUMO signal stemming from PTCDA molecules is not expected from the *fingerprint approach* analysis of the C1s core level PES data. Hence the signal with the lowest E_B originating from PTCDA molecules must be the PTCDA HOMO which is assigned to the additional intensity between the F4TCNQ LUMO and HOMO signal in the 1.6 ML PTCDA/1.0 ML F4TCNQ/Ag(110) spectrum (black full circles). Due to the energetic separation of the valence PES signals originating from the different molecules and their similar intensity a significant deconvolution of these signals in RPES could be possible.

The stability and the suitable valence PES spectrum of the hetero-organic system PTCDA on 1.0 ML F4TCNQ/Ag(110) are favorable for further analysis with RPES. However, a closer look at the PES intensities points towards Volmer-Weber growth of PTCDA molecules and thus an insufficiently defined hetero-organic interface. This conclusion stems from a comparison of the expected PES intensity and the visible PES intensity of

the PTCDA signals. The deposited amount of PTCDA is estimated with the deposition rate which suggests a coverage of 1.6 ML while only approximately 0.5 ML of PTCDA are visible in the C1s and the O1s core level PES data. The attenuation of the PES signals of the F4TCNQ molecules is in agreement with this finding. For further investigations, this growth behavior has to be taken into account.

In conclusion the findings in this subsection show that none of the hetero-organic systems consisting of PTCDA and F4TCNQ molecules on Ag(110) qualifies for a subsequent analysis with RPES. However, the behavior of these systems allows to push the discussion about the energy balance of the adsorption of a π-conjugated molecule on a metal forward. The fact that an F4TCNQ molecule is able to penetrate through a PTCDA herringbone layer shows that the attractive intermolecular interaction of this structure [79] can be overcome at 300 K. This finding leads to the question which role such a contribution of the intermolecular forces plays in the total energy balance of the hetero-molecular system. In section 4.3 a general discussion about the energy balance of the adsorption of π-conjugated molecules will be given which includes all experimental results of sections 4.1 and 4.2.

4.2 Stability of hetero-organic systems at elevated temperatures

The observed instability of the systems PTCDA on 1 ML CuPc/Ag(111) and F4TCNQ on 1 ML PTCDA/Ag(110) at 300 K together with the stability of the other systems cannot be explained on the basis of a single parameter. So far a difference in the adsorption energy per surface area is given as a possible reason for the found layer exchanges. For the hetero-organic systems consisting of CuPc, SnPc, and PTCDA molecules the stability of the system SnPc/1 ML PTCDA/Ag(111) hinders an explanation of the behavior of all these systems only with this parameter. Furthermore, the ability of F4TCNQ molecules to replace PTCDA molecules in the first layer on Ag(110) proofs that a possible energy barrier which could be due to attractive intermolecular forces [79] can be overcome at 300 K. Hence it is possible that SnPc molecules will penetrate through a PTCDA herringbone structure and diffuse into the first layer at elevated temperatures ($T > 300$ K) if the adsorption energy per surface area is indeed larger for a SnPc molecule than for a PTCDA molecule. The behavior of all other systems at elevated temperatures is equally interesting since this information might lead to a common explanation of all investigated systems. Thus in the following section all hetero-organic systems discussed in section 4.1 will be studied at elevated temperatures.

4.2.1 Metal-phthalocyanine and PTCDA molecules on Ag(111)

First the hetero-organic systems with all combinations of metal-phthalocyanine (SnPc or CuPc) and PTCDA molecules on Ag(111) will be measured before and after an annealing

procedure. For that all necessary PES signals of the sample are measured previous to the annealing procedure in order to fully characterize the initial state of the sample. Then the sample is heated with a rate of approximately 1 K/s until the desired final temperature is reached. The sample is then kept at this temperature for approximately 5 min so that there is enough time for the system to reach an equilibrium state and possible reordering processes can occur. Finally the result of the annealing procedure is measured with PES after the temperature of the sample has dropped close to 300 K.

SnPc and PTCDA molecules on Ag(111)

Annealing samples of 1.5–5 ML SnPc deposited on top of 1 ML PTCDA/Ag(111) up to temperatures of 420–470 K within the given procedure results in samples in which both SnPc and PTCDA molecules are situated in the first and in higher layers. This is concluded from the results of a *fingerprint approach* analysis of the C1s, N1s and O1s core level PES data. An example of a *fingerprint approach* analysis of the C1s and N1s core level PES spectra of a 1.5 ML SnPc/1 ML PTCDA/Ag(111) sample annealed to 430 K is presented in Fig. A3. For a successful reproduction of the measured C1s and N1s core level PES spectra of all measured spectra of all these samples a SnPc multilayer and a 1 ML SnPc/Ag(111) reference spectrum is required. Additionally, a PTCDA multilayer and a 1 ML PTCDA/Ag(111) reference are necessary to reproduce the measured C1s and O1s PES data of most of the spectra of the different samples. However, for some PES spectra of a sample with a final annealing temperature of approximately 470 K an almost vanishing PES intensity of the O1s spectrum is observed and no PTCDA reference spectrum is necessary to reproduce the line-shape of the C1s PES spectrum (see Fig. A4). The most reasonable explanation for these findings is that in the temperature range of 420–470 K SnPc molecules replace PTCDA molecules from the first layer and force them into higher layers. Additionally, it is quite likely that the desorption of PTCDA molecules from the sample starts around 470 K. An alternative explanation for the missing PTCDA contribution can be given by the formation of large pure SnPc domains. In any case the ability of SnPc molecules to penetrate into the 1 ML PTCDA/Ag(111) herringbone structure at elevated temperatures is unambiguously shown by a *fingerprint approach* analysis of the PES core level data. The missing information about the amount of desorbed molecules and the growth mode of the sample complicates a detailed characterization of the sample after the annealing procedure with final temperatures of 420–470 K. Hence an investigation of the sample after annealing it to a temperature at which all molecules not in direct contact to the Ag(111) substrate desorb is the next logical step. With a single ML on Ag(111) left the interpretation of the PES data is much simpler.

Fig. 4.7(a) illustrates C1s core level PES data of 1.5 ML SnPc on 1 ML PTCDA/Ag(111) before (top) and after (bottom) annealing the sample up to 570 K. The C1s PES spectrum measured before the annealing procedure (top of Fig. 4.7(a)) is successfully reproduced by a 1 ML PTCDA/Ag(111) (brown line) and a SnPc multilayer (blue line) reference spectrum. Following the line of arguments throughout section 4.1 the *fingerprint ap-*

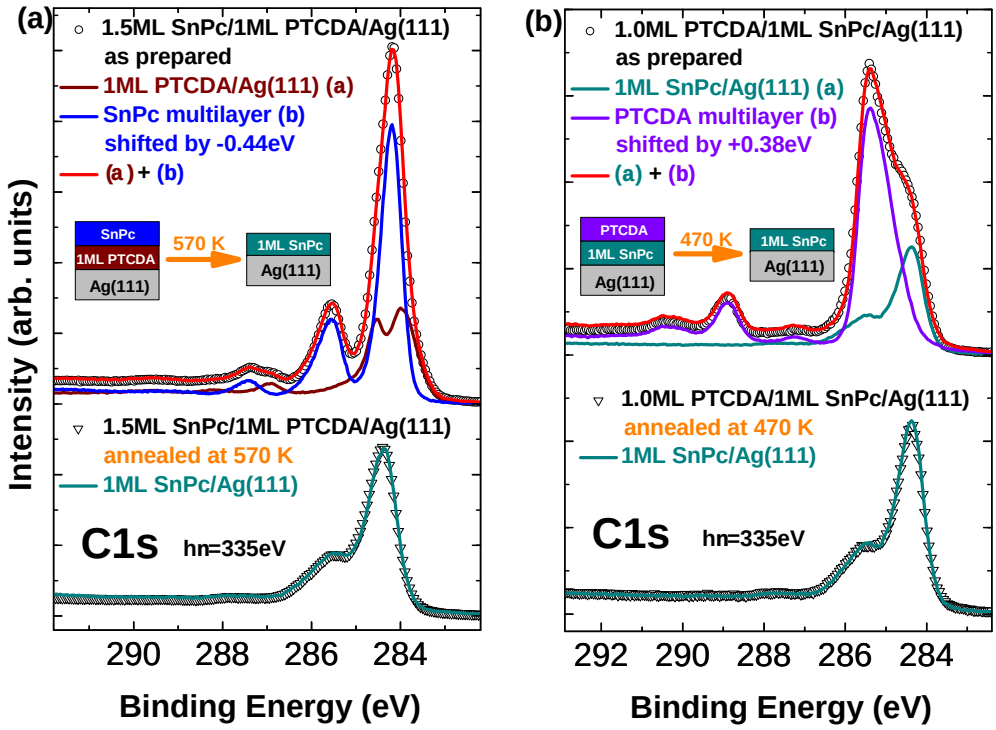

Figure 4.7: C1s PES data of 1.5 ML SnPc/1 ML PTCDA/Ag(111) **(a)** and 1.0 ML PTCDA/1 ML SnPc/Ag(111) **(b)** as prepared (top) and after the annealing procedure (bottom). **(a)** C1s PES spectrum of 1.5 ML SnPc/1 ML PTCDA/Ag(111) as prepared (open circles) together with scaled reference spectra of 1 ML PTCDA/Ag(111) (brown line) and a SnPc multilayer (blue line). **(b)** C1s PES spectrum of 1.0 ML PTCDA/1 ML SnPc/Ag(111) as prepared (open circles) together with scaled reference spectra of 1 ML SnPc/Ag(111) (cyan line) and a PTCDA multilayer (purple line). In the upper part of both panels the red line is the sum of the two reference spectra. At the bottom of each panel the C1s PES spectrum of the same sample after the annealing procedure (open triangles) in comparison to a 1 ML SnPc/Ag(111) reference spectrum (cyan line) is presented. The schematic pictures in the middle of both panels illustrate the sample before and after the annealing procedure.

proach analysis of this sample leads to the conclusion that all PTCDA molecules are in the first layer on Ag(111) while all SnPc molecules are situated in higher layers. PES intensities and line-shapes of N1s and O1s PES core level data (not shown) corroborate this conclusion. After the annealing procedure the line-shape of the measured C1s spectrum (bottom of Fig. 4.7(a)) is equal (within measurement accuracy) to a 1 ML SnPc/Ag(111) reference spectrum. Moreover, for the N1s core level and the valence PES spectrum (both not shown) matching line-shapes with respect to 1 ML SnPc/Ag(111) reference spectra are observed. Additionally, the measured O1s core level PES intensity is smaller than 10% of 1 ML PTCDA/Ag(111). Considering the uncertainties stemming from the normalization and the background subtraction a signal with such a small intensity has to be considered to be below the detection limit. These findings unabiguously proof that only SnPc moelcules situated directly on Ag(111) remain after annealing the sample up to 570 K. Hence PTCDA molecules in the first layer are fully replaced (coverage below the detection limit of 0.1 ML) by SnPc molcules at a temperature below the desorption temperature of SnPc molecules on 1 ML PTCDA/Ag(111). Furthermore, at a temperature of 570 K all molecules except the ones in the first layer are desorbed from the sample as it is the case for homo-molecular SnPc and PTCDA multilayers. LEED measurements [135, 141] and the detection of PTCDA moelcules with a mass spectrometer during the annealing procedure [141] confirm these conclusions. So it seems that the adsorption energy per surface area is indeed larger for a SnPc molecule than for a PTCDA molecule and that the energy barrier for the replacement of PTCDA molecules with SnPc molecules on Ag(111) can be overcome by a temperature in the range of approximately 420–470 K.

C1s core level PES data before and after annealing a sample of 1.0 ML PTCDA/1 ML SnPc/Ag(111) up to 470 K is presented in Fig. 4.7(b). The *fingerprint approach* analysis of the measured C1s PES data before the annealing procedure and the conclusions for the layer oder drawn from this analysis are analogue to Fig. 4.1(a). After the annealing procedure all PES signals (C1s, N1s, O1s and the valence region) are equal to 1 ML SnPc/Ag(111) reference spectra (Fig. 4.7(b) shows only the C1s core level PES spectra). Hence all PTCDA molecules are desorbed from 1 ML SnPc/Ag(111) at a temperature of 470 K. This further supports the interpretation of the PES data of the annealing experiments of SnPc on 1 ML PTCDA/Ag(111) for SnPc coverages above 1.5 ML and final temperatures of 420–470 K. So at this point a consistent picture for the explanation of the behavior of the hetero-organic systems with metal-phthalocyanine (SnPc or CuPc) and PTCDA molecules on Ag(111) can be drawn. For that an adsorption energy per surface area which is larger for a SnPc than for a PTCDA molecule and smaller for a CuPc than for a PTCDA molecule needs to be assumed. Additionally, an energy barrier for the exchange of PTCDA by SnPc molecules, that can be overcome at elevated temperatures, must exist. This explanation will be revised in the light of the findings of the annealing experiments performed with hetero-organic systems consisting of CuPc and PTCDA molecules on Ag(111).

At this point I investigate a variation of the SnPc coverage in the annealing experiment of the system SnPc on 1 ML PTCDA/Ag(111). As shown in Fig. 4.7(a) PTCDA molecules

are replaced by SnPc molecules at elevated temperatures. So a sample with an initial SnPc coverage in the sub-ML range should result in a sample with both molecules in the first (and only) layer after annealing it to 570 K. Annealing experiments confirm this expectation. Hereby the intensities of N1s and O1s PES spectra (not shown) compared to 1ML SnPc/Ag(111) and 1 ML PTCDA/Ag(111) reference spectra are used to determine the coverages of the particular molecules in the hetero-organic ML film. It is revealed that only a small amount of SnPc (approximately 0.1 ML or less) is desorbed and hence almost the total initial coverage of SnPc is still on the sample after the annealing procedure. A SnPc richer hetero-organic ML can be prepared by depositing additional SnPc molecules onto a hetero-organic ML and once again annealing the film to 570 K. Fig. 4.8(a) displays the C1s core level PES data of a hetero-organic ML of SnPc and PTCDA. Within a *fingerprint approach* analysis the measured spectrum is successfully reproduced by reference spectra of 1 ML SnPc/Ag(111) (cyan line) and 1 ML PTCDA/Ag(111) (brown line). The PES intensities of both contributions agree with the PES intensities of the corresponding exclusive PES signals (N1s for SnPc and O1s for PTCDA, both not shown). For the successful reproduction of the line-shape of the C1s core level PES spectrum in Fig. 4.8(a) both reference spectra need to be shifted in energy. This points towards a modification of the set of parameters in the Hamiltonian with which both molecules can be described. However, the fact that the measured C1s PES data can be reproduced with the pure ML reference spectra demonstrates that a strong modification, such as the difference between a molecule in a multilayer and directly on Ag(111), can be excluded. In contrast the changes with respect to the pure ML reference spectra observed in Fig. 4.8(a) can be compared to the changes observed in the PES spectra of PTCDA in different structural phases (see Fig. 2.2). Consequently, a possible explanation for the necessity of an energy shift in the *fingerprint approach* analysis in Fig. 4.8(a) is a modification of the structural order of both molecules. This could be realized by the formation of a mixed hetero-molecular ML.

In Fig. 4.8(b) the valence PES spectrum (filled black circles) corresponding to the C1s PES spectrum in Fig. 4.8(a) is displayed together with 1ML SnPc/Ag(111) (filled cyan triangles) and 1 ML PTCDA/Ag(111) (filled brown squares) reference spectra. A comparison of the line-shape of the LUMO signals of both reference spectra with the measured spectrum (filled black circles) shows that the valence region of the hetero-molecular ML cannot be explained by a simple superposition of the two valence PES reference spectra. Especially the additional PES intensity at the tailing edge of the peak at $E_B \approx$ 0.3 eV of the hetero-molecular ML (filled black circles) with respect to the LUMO signals of the homo-molecular reference spectra reveals the change which is expected from the direct correspondence of valence and core level PES. Thus the valence PES data supports the conclusions drawn from the *fingerprint approach* analysis of the C1s core level spectrum in Fig. 4.8(a). An alternative explanation for the observed change of the line-shape of the peak at $E_B \approx 0.3$ eV can be given with an energy dispersion of one or both of the LUMO signals in combination with a change in the orientation of the corresponding molecule. Whether the hetero-molecular ML exhibits such a dispersion is not known which prohibits the exclusion of this alternative explanation. In any case the signals in

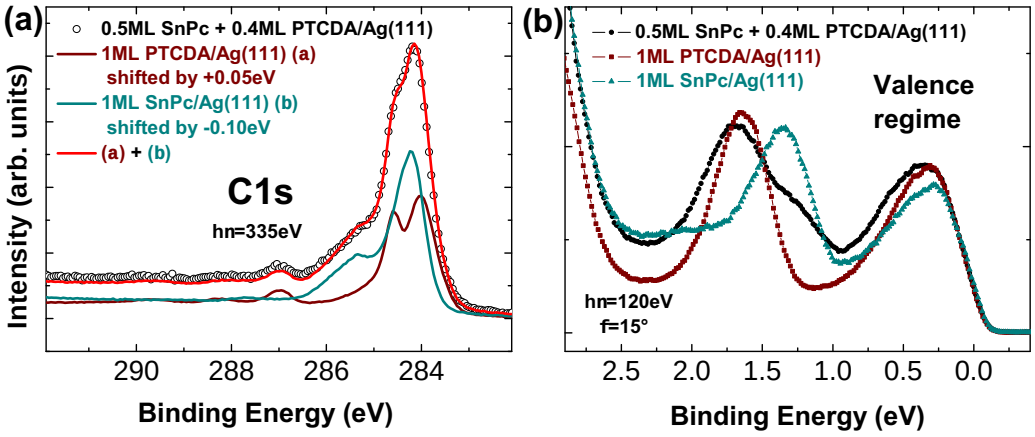

Figure 4.8: PES data of 0.5 ML SnPc + 0.4 ML PTCDA/Ag(111). **(a)** C1s PES spectrum (open circles) together with scaled reference spectra of 1 ML PTCDA/Ag(111) (brown line) and 1 ML SnPc/Ag(111) (cyan line). The red line denotes the sum of both reference spectra. **(b)** Valence PES spectrum (filled black circles) in comparison with reference spectra of 1 ML PTCDA/Ag(111) (filled brown squares) and 1 ML SnPc/Ag(111) (filled cyan triangles).

the valence PES spectrum in Fig. 4.8(b) can be assigned on the basis of the *fingerprint approach* analysis of the C1s PES spectrum. Hence, the peak at lowest E_B in Fig. 4.8(b) consists of the SnPc LUMO and the PTCDA LUMO signal. Moreover, the shoulder at $E_B \approx 1.2$ eV stems from the SnPc HOMO while the peak at $E_B \approx 1.7$ eV corresponds to the PTCDA HOMO signal.

Recent LEED investigations reveal that after the annealing procedure diffraction signals are found which differ from the characteristic signatures of the pure SnPc and PTCDA structures on Ag(111) [135]. The found signals further indicate that the new structure stems from a larger unit cell than the pure SnPc or PTCDA structures on Ag(111). This finding and the observations in the PES data of Fig. 4.8 suggest that the hetero-molecular ML does not consist of separated homo-molecular domains. In contrast a laterally ordered hetero-structure is formed, or in other words, a mixed hetero-molecular ML is produced with a lateral hetero-organic interface. Consequently, an additional system adequate for a detailed investigation with RPES is identified. The suitability of the mixed hetero-organic system SnPc + PTCDA on Ag(111) will be argued at the end of the investigation of the hetero-organic systems on Ag(111) at elevated temperatures.

CuPc and PTCDA molecules on Ag(111)

Annealing experiments of the system CuPc on 1 ML PTCDA/Ag(111) have been performed in Ref. [142] and will be briefly discussed in the following paragraph. The initial sample in this study is a 10 ML CuPc on 1 ML PTCDA/Ag(111) film for which a

Stranski-Krastanov growth is observed for the CuPc molecules. The annealing procedure is similar to the one described in the beginning of this subsection except for one major difference. In Ref. [142] the sample is kept at approximately 450 K for 15 min. Before and after this intermediate plateau the temperature is increased with a rate of 2 K/s up to a final temperature of 570 K. After this annealing procedure all PES core level signals show a CuPc to PTCDA ratio of approximately 4 to 1. Additionally, a LEED structure corresponding to a pure 0.9 ML CuPc/Ag(111) film is found. This points towards an incomplete exchange of PTCDA molecules by CuPc molecules which results in pure CuPc domains and most probably mixed hetero-organic domains of CuPc and PTCDA molecules (see discussion below). So at elevated temperatures CuPc molecules are able to penetrate into the 1 ML PTCDA/Ag(111) herringbone structure and partially replace PTCDA molecules in the first layer. Consequently, the assumption that a PTCDA molecule exhibits a larger adsorption energy per surface area than a CuPc molecule needs to be dropped. The difference of this observed behavior of CuPc with respect to SnPc molecules can be explained by the growth modes of both molecules on 1 ML PTCDA/Ag(111). SnPc molecules grow in a Frank-van-der-Merwe-like (layer-by-layer-like) mode while CuPc molecules grow in a Stranski-Krastanov mode (the first CuPc layer grows in a wetting mode [20]). So the incomplete exchange of PTCDA by CuPc molecules is most probably a consequence of missing CuPc molecules for the exchange since these are situated in higher layers or already desorbed from the sample. This explanation is in agreement with the finding of a smaller CuPc to PTCDA ratio after an annealing procedure without an intermediate plateau. Hence an annealing procedure with a smaller time interval at elevated temperatures (but below the desorption temperature of molecules not in direct contact to Ag(111)) goes along with a less complete exchange.

In Fig. 4.9 PES data of the sample analyzed in Fig. 4.4 is presented after an annealing procedure up to 570 K (as described in the beginning of this subsection). The line-shape of the measured C1s core level PES spectrum (open circles) displayed in Fig. 4.9(a) is almost equal to a 1 ML CuPc/Ag(111) reference spectrum (cyan line). Small differences are observed between the two spectra in Fig. 4.9(a) at the rising edge and at the tailing edge of the main peak at $E_B \approx 284.5$ eV. For the C1s core level PES spectrum measured on another spot of the same sample (Fig. 4.9(c)) the situation is different. Here a 1 ML CuPc/Ag(111) (cyan line) and a 1 ML PTCDA/Ag(111) (brown line) reference spectrum are necessary for an almost successful reproduction of the measured spectrum (open circles). At $E_B \approx 285.5$ eV a small deviation of the sum of the reference spectra (red line) and the measured C1s PES spectrum (open circles) is found which is similar but more pronounced with respect to the difference observed between the line-shapes of the two C1s PES spectra in Fig. 4.9(a). The peak at $E_B \approx 287$ eV in the C1s PES spectrum of 0.8 ML PTCDA/1 ML CuPc/Ag(111) annealed at 570 K in Fig. 4.9(c) can only be reproduced with a 1 ML PTCDA/Ag(111) reference spectrum. So the emergence of this peak in Fig. 4.9(c) justifies the different *fingerprint approach* analysis with respect to Fig. 4.9(a). Furthermore, the energy shift applied to the 1 ML PTCDA/Ag(111) reference spectrum is justified by the existence of this peak at $E_B \approx 287$ eV. Apparently the

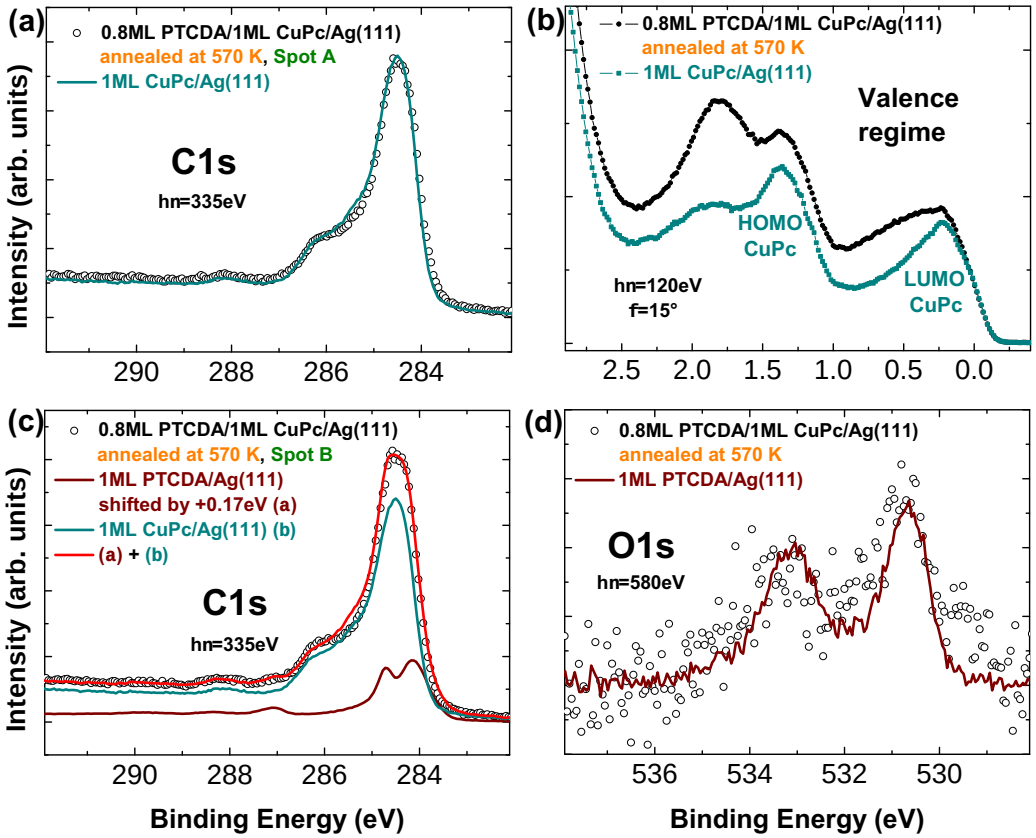

Figure 4.9: PES data of 0.8 ML PTCDA/1 ML CuPc/Ag(111) annealed at 570 K. **(a)** C1s PES spectrum (open circles) recorded on sample spot A together with a scaled reference spectrum of 1 ML CuPc/Ag(111) (cyan line). **(b)** Valence PES spectrum (filled black circles) in comparison to a 1 ML CuPc/Ag(111) reference spectrum (filled cyan squares). **(c)** C1s PES spectrum (open circles) recorded on sample spot B together with scaled reference spectra of 1 ML PTCDA/Ag(111) (brown line) and 1 ML CuPc/Ag(111) (cyan line). The red line denotes the sum of both reference spectra. **(d)** O1s PES spectrum (open circles) together with a scaled reference spectrum of 1 ML PTCDA/Ag(111) (brown line). The spectra in panels (b) and (c) originate from different sample spots that spot A and spot B.

sample is inhomogeneous on the scale of the beam spot (at least 50μm$\times 50\mu$m). The two selected spots presented in Fig. 4.9(a) and (c) are the extreme cases which means that all other measured C1s PES spectra of this sample are in between these two scenarios. So most probably this is also the case for the PES spectra presented in Fig. 4.9(b) and (d) which originate from different sample spots than Spot A and Spot B. For the corresponding samples annealed to 570 K with smaller PTCDA coverages deposited on top of 1 ML CuPc/Ag(111) less contribution from PTCDA molecules to the PES spectra is found in a *fingerprint approach* analysis (not shown). From the PTCDA contribution to the C1s PES spectrum and the PES intensity of the O1s spectrum (Fig. 4.9(d)) an upper limit of 0.1–0.2 ML can be given for the PTCDA coverage of these samples. A line-shape analysis of the O1s core level PES spectra (see for example Fig. 4.9(d)) is hindered by the low signal to noise ratio and the delicate background subtraction which both stem from the low PTCDA coverage. In conclusion the PES core level data in Fig. 4.9 shows that the layer exchange at 300 K observed for the system PTCDA on 1 ML CuPc/Ag(111) is reversed at elevated temperatures. So in agreement with Ref. [142] I can conclude that at elevated temperatures CuPc molecules replace PTCDA molecules in the first layer of an Ag(111) substrate. A further increase of the temperature up to 570 K leads to a desorption of PTCDA and CuPc molecules not in direct contact to the Ag(111) surface.

With the contributions identified from the *fingerprint approach* analysis of the core level PES signals in Fig. 4.9(a) and (c) the features in the valence PES spectrum in Fig. 4.9(b) can be identified. Thus PES signals similar to the 1 ML CuPc/Ag(111) spectrum (filled cyan triangles) are present in the valence PES spectrum of the 0.8 ML PTCDA on 1 ML CuPc/Ag(111) sample annealed to 570 K (filled black circles). The additional intensity in this spectrum with respect to the 1 ML CuPc/Ag(111) spectrum (filled cyan triangles) is assigned to PTCDA molecules on Ag(111). The peak at $E_B \approx 1.8$ eV corresponds to the PTCDA HOMO and the peak at $E_B \approx 0.3$ eV originates from the PTCDA LUMO (and the CuPc LUMO signal). Considering that only approximately 0.1 ML of PTCDA and roughly 0.8 ML of CuPc molecules are on the sample it is quite surprising that the features assigned to PTCDA molecules are as intense as observed. This fact can either be a consequence of the characteristic angular intensity variation of both molecules or originate from a large difference in the cross section of the molecular orbitals in valence PES. From ARPES measurements of both molecules it can be estimated that in valence PES the cross section of PTCDA molecules is roughly one order of magnitude larger than the one of CuPc molecules [143]. Hence the latter explanation is more reasonable although both effects might contribute to the observed difference in PES intensity. This yet unexplained difference in the cross section of molecular orbitals of different molecules in valence PES demonstrates the difficulty of drawing quantitative conclusions from valence PES data.

Analogous to the hetero-organic system SnPc on 1 ML PTCDA/Ag(111) annealing experiments are performed for the system CuPc on 1 ML PTCDA/Ag(111) with CuPc coverages below 1 ML. Similarly to the former system only approximately 0.1 ML of the initial coverage of CuPc is desorbed during the annealing procedure. Only for a coverage

of 0.9 ML of CuPc a desorption of approximately 0.2 ML is concluded from the analysis of the PES data before and after the annealing procedure. In Ref. [134] it is shown that the hetero-molecular ML which remains after annealing a sub-ML CuPc/1 ML PTCDA/Ag(111) film exhibits a long range lateral order and is a laterally mixed hetero-organic interface. In Fig. 4.10 the PES data of a sample prepared in this way is presented. The line-shape of the measured C1s core level PES spectrum (open circles) in Fig. 4.10(a) is not successfully reproduced at all E_B with reference spectra of 1 ML PTCDA/Ag(111) (brown line) and 1 ML CuPc/Ag(111) (cyan line). However, this combination of reference spectra for the *fingerprint approach* analysis results in the best possible reproduction of the measured line-shape of the C1s PES spectrum. Particularly all combinations including a reference spectrum of a CuPc or a PTCDA multilayer clearly fail to reproduce the line-shape of the measured C1s PES spectrum. Moreover, the best possible reproduction of the line-shape of the measured C1s PES spectrum of 0.6 ML CuPc + 0.3 ML PTCDA/Ag(111) requires energy shifts for the homo-molecular reference spectra. The deviation at $E_B \approx 285.5$ eV of the best possible reproduction with these homo-molecular reference spectra (red line) from the measured C1s PES spectrum (open circles) is similar but more pronounced in Fig. 4.10(a) with respect to Fig. 4.9(c). The inability to reproduce the C1s PES spectrum of CuPc + PTCDA/Ag(111) contradicts a hetero-molecular ML with two separated homo-molecular domains and hence points towards a mixed hetero-molecular ML. It is unclear whether both of the two contributions to the measured line-shape of the C1s PES spectrum of 0.6 ML CuPc + 0.3 ML PTCDA/Ag(111) differ from the homo-molecular reference spectra. Since the CuPc + PTCDA/Ag(111) sample of Fig. 4.10 is prepared in the same way as in Ref. [134] a structural difference between both molecules in the hetero-molecular ML and in the homo-molecular films on Ag(111) is expected. This should in principle effect the PES signals of both molecules. The line-shape of the exclusive PES signals (N1s for CuPc and O1s for PTCDA, both not shown) are both similar but not identical to the homo-molecular reference spectra on Ag(111). Hence it seems that both of the sets of parameters in the Hamiltonian which describes the two molecules are modified in the mixed hetero-molecular system with respect to the homo-molecular systems on Ag(111).

Although the *fingerprint approach* analysis of the C1s core level PES spectrum illustrated in Fig. 4.10(a) cannot fully reproduce the line-shape of the measured C1s PES spectrum of 0.6 ML CuPc + 0.3 ML PTCDA/Ag(111) it still can be used to exclude multilayer-like PTCDA and CuPc molecules in this system. Moreover, the difference between the line-shape of the measured C1s PES spectrum of 0.6 ML CuPc + 0.3 ML PTCDA/Ag(111) and the linear combination of the homo-molecular reference spectra on Ag(111) can be compared to the changes observed in the C1s PES spectra of PTCDA and CuPc molecules on Ag surfaces (see Figs. 2.1 and 2.2). Consequently, the corresponding valence PES spectrum (filled black circles) illustrated in Fig. 4.10(b) should include a HOMO and a LUMO signal from both molecules. Hence, the peak at $E_B \approx 0.5$ eV includes the CuPc LUMO signal and the PTCDA LUMO signal. The CuPc HOMO signal should be responsible for the PES intensity at the rising edge of the peak at $E_B \approx 1.7$ eV

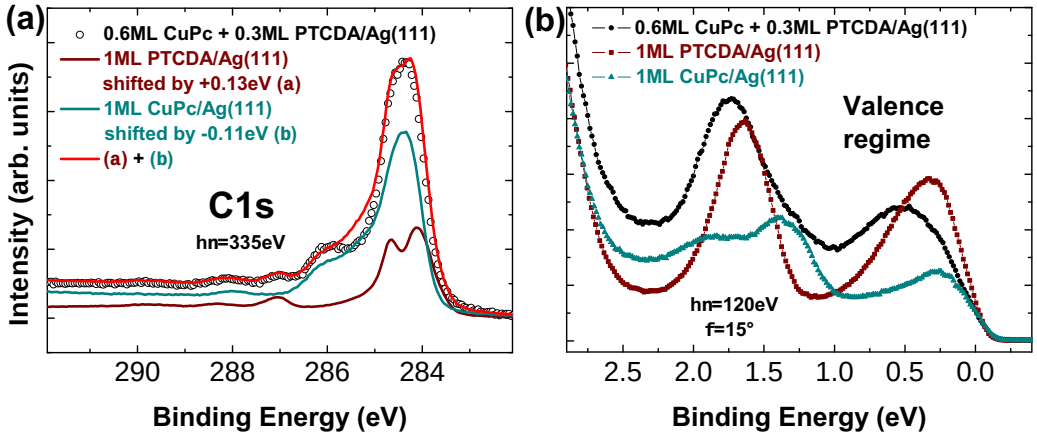

Figure 4.10: PES data of 0.6 ML CuPc + 0.3 ML PTCDA/Ag(111). **(a)** C1s PES spectrum (open circles) together with scaled reference spectra of 1 ML PTCDA/Ag(111) (brown line) and 1 ML CuPc/Ag(111) (cyan line). The red line denotes the sum of both reference spectra. **(b)** Valence PES spectrum (filled black circles) in comparison with reference spectra of 1 ML PTCDA/Ag(111) (filled brown squares) and 1 ML CuPc/Ag(111) (filled cyan triangles).

while this peak itself stems from the PTCDA HOMO. From the discussion of the PES intensities of the valence PES spectrum in Fig. 4.9(b) larger PES intensities are expected for the molecular orbital signals of the PTCDA molecules. This explains why the valence PES spectrum in Fig. 4.10(b) is dominated by the PTCDA HOMO and LUMO signals.

This assignment of the signals in the valence PES spectrum of the system CuPc + PTCDA/Ag(111) disagrees with the assignment performed in Ref. [30]. Therein a vanishing contribution by a CuPc LUMO signal is reported. This disagreement can be explained on the basis of the difference in the cross section of the PTCDA LUMO and the CuPc LUMO signal in valence PES. The latter can be estimated to be one order of magnitude smaller than the former [143]. Moreover, the sample analyzed in Ref. [30] exhibits a 2 to 1 ratio of PTCDA molecules to CuPc molecules in the mixed ML in addition to pure PTCDA domains. The LUMO signal of the latter is slightly more intense in valence PES than the LUMO signal of the PTCDA molecules in the mixed ML [30]. Consequently, a total PTCDA to CuPc ratio of at least 4 to 1 and a PTCDA to CuPc cross section ratio of approximately 10 to 1 lead to the expectation of a PTCDA LUMO to CuPc LUMO intensity ratio in valence PES of approximately 40 to 1. Furthermore, the theoretical angular intensity distribution of the CuPc LUMO in the structure of the sample investigated in Ref. [30] overlaps with the theoretical angular intensity distributions of both PTCDA LUMO contributions. Hence there is no point in k-space where the expected CuPc LUMO signal contributes exclusively to the ARPES data. In conclusion, the absence of a CuPc LUMO signal in the analysis of Ref. [30] does not necessarily mean that there is no CuPc LUMO signal that contributes to the valence PES spectrum. In contrast

it could simply be a consequence of the fact that this signal is below the detection limit of the applied analysis method. For the 0.6 ML CuPc + 0.3 ML PTCDA/Ag(111) sample corresponding to the PES data in Fig. 4.10 no LEED data exists. Hence an alternative explanation for the disagreement between the assignment of the signals in the valence PES spectrum in Fig. 4.10(b) and the one in Ref. [30] can be given by considering that the geometric structure of both samples is different (although both are prepared by annealing a sub-ML CuPc/1 ML PTCDA/Ag(111) film). If that was the case a comparison of the valence PES data of these samples could be inappropriate.

The *fingerprint approach* analysis in combination with structural data [134, 135] shows that annealing the system of a sub-ML of a metal-phthalocyanine (SnPc or CuPc) on 1 ML PTCDA/Ag(111) constitutes a way to prepare lateral hetero-organic interfaces. Hence the systems CuPc + PTCDA/Ag(111) and SnPc + PTCDA/Ag(111) are both suitable for a subsequent analysis with RPES. For the latter system only preliminary structural data is available [135] while for the system CuPc + PTCDA/Ag(111) an extensive structural characterization exists [134]. Hence I choose the system CuPc + PTCDA/Ag(111) for my detailed analysis with RPES in subsection 5.4.1. Additionally, a comparison of this lateral hetero-organic interface with the vertical hetero-organic interface CuPc/1 ML PTCDA/Ag(111) appears to be straightforward and might lead to valuable information since both consist of the same molecules.

4.2.2 F4TCNQ and PTCDA molecules on Ag(110)

For the hetero-organic system of F4TCNQ on 1ML PTCDA/Ag(110) it was found that at 300 K F4TCNQ molecules replace PTCDA molecules in the first layer and force them into higher layers. Motivated by the unexpected temperature dependent behavior of hetero-organic systems consisting of metal-phthalocyanine (SnPc or CuPc) and PTCDA molecules on Ag(111) annealing experiments are also performed for the hetero-organic system consisting of F4TCNQ and PTCDA molecules on Ag(110).

In Fig. 4.11 the PES data of a 1.0 ML F4TCNQ/1 ML PTCDA/Ag(110) sample annealed up to 520 K is presented. The measured C1s core level PES spectrum (filled black circles) displayed in Fig. 4.11(a) is almost equal to the scaled 1.0 ML F4TCNQ/Ag(110) spectrum (filled orange squares). A subtraction of the latter from the former (filled gray triangles) identifies the difference of the two spectra as a broad peak at $E_B \approx 285$ eV. Moreover, Fig. 4.11(b) reveals that all features of the valence PES spectrum of 1.0 ML F4TCNQ/1 ML PTCDA/Ag(110) annealed up to 520 K (filled black circles) are equal to the 1.0 ML F4TCNQ/Ag(110) reference spectrum (filled orange squares). Merely a variation of relative PES intensity of the signals stemming from the molecular orbitals of F4TCNQ molecules and the metal s-p bands is observed as a difference between the two spectra in Fig. 4.11(b). Furthermore, the line-shape of the N1s (open circles in Fig. 4.11(c)) and F1s (open circles in Fig. 4.11(d)) spectra is found to be equal (within measurement accuracy) to the line-shape of the corresponding 1.0 ML F4TCNQ/Ag(110) reference spectrum (orange line). Additionally, the line-shape of the O1s core level PES

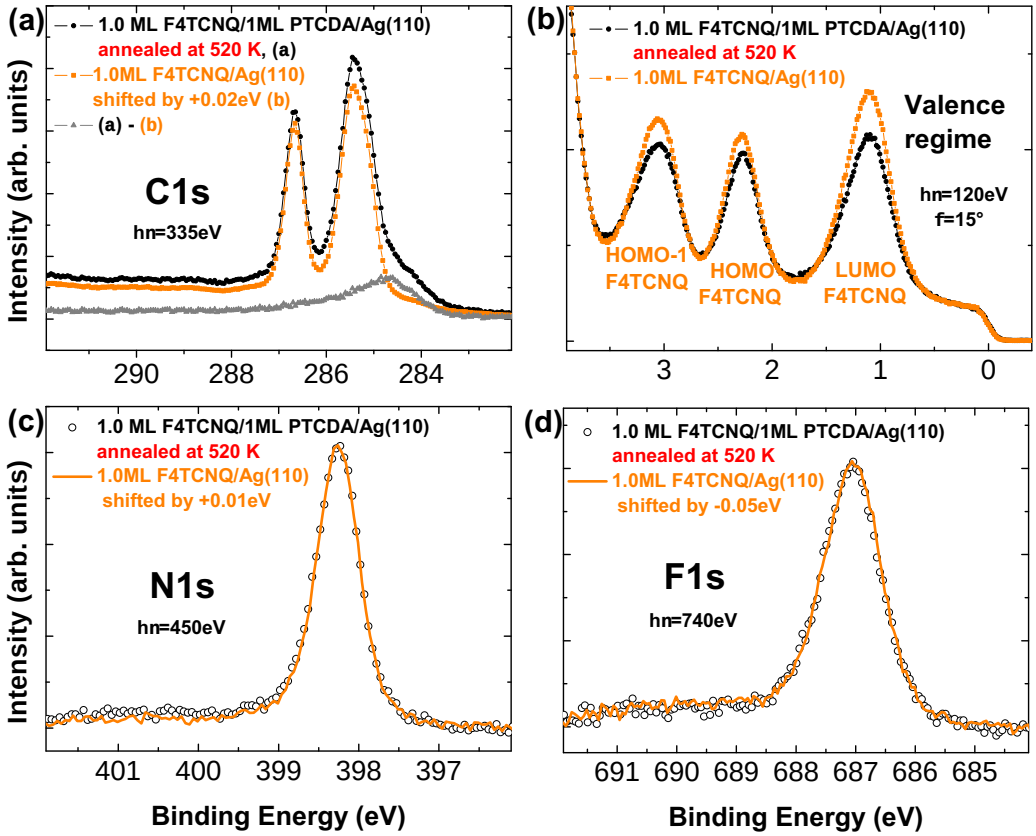

Figure 4.11: PES data of 1.0 ML F4TCNQ/1 ML PTCDA/Ag(110) annealed at 520 K. **(a)** C1s PES spectrum (filled black circles) together with a scaled reference spectrum of 1.0 ML F4TCNQ/Ag(110) (filled orange squares). The difference of these two spectra is illustrated by the filled gray triangles **(b)** Valence PES spectrum (filled black circles) in comparison to a 1.0 ML F4TCNQ/Ag(110) reference spectrum (filled orange squares). **(c)** N1s PES spectrum (open circles) together with a scaled reference spectrum of 1.0 ML F4TCNQ/Ag(110) (orange line). **(d)** F1s PES spectrum (open circles) together with a scaled reference spectrum of 1.0 ML F4TCNQ/Ag(110) (orange line).

spectrum (not shown) is not evaluable due to its low PES intensity. Based on this PES intensity the PTCDA coverage can be estimated to be below 0.1 ML and thus below the detection limit. All these findings lead to the conclusion that after the annealing procedure only F4TCNQ molecules remain on the sample. The additional signal in the C1s core level PES spectrum (filled gray triangles) and the decreased intensity of all F4TCNQ originated signals with respect to the 1.0 ML F4TCNQ/Ag(110) reference spectra point towards a partial decomposition of the F4TCNQ molecules at elevated temperatures. Hence it is most probably a PES signal stemming from amorphous carbon (filled gray triangles in Fig. 4.11(a)) that contributes to the C1s core level PES spectrum in addition to F4TCNQ molecules. Furthermore, this contribution of amorphous carbon varies for different spots on the same sample. Consequently, the observed coverage dependent energy shifts of all PES signals of F4TCNQ molecules in the sub-ML range (see Fig. A7)

together with this sample inhomogeneity explains the small relative energy shifts of the different core level PES signals in Fig. 4.11. Annealing a sample of PTCDA on 1.0ML F4TCNQ/Ag(110) to 520 K results in very similar PES spectra as the ones illustrated in Fig. 4.11.

The partial decomposition of F4TCNQ molecules at a temperature below the temperature needed to desorb PTCDA molecules which are not in direct contact to the Ag(110) surface hinders a selective preparation of a lateral hetero-organic interface with a combination of these molecules. Furthermore, in subsection 4.1.2 it is shown that a vertical hetero-organic interface with these molecules is not appropriate for a subsequent investigation with RPES. So neither a vertical nor a lateral hetero-organic interface can be prepared in the desired way with a combination of F4TCNQ and PTCDA molecules on Ag(110).

4.3 Summary and discussion

The results of the *fingerprint approach* analysis of the hetero-organic systems on Ag(111) at 300 K and at elevated temperatures are summarized in Fig. 4.12. It is shown that the system CuPc on 1 ML PTCDA/Ag(111) is stable at 300 K and that after annealing the sample to 570 K CuPc molecules are present in the first layer. Hence a temperature induced layer exchange occurs which results in a sample with CuPc and PTCDA coverages that depend on the initial CuPc coverage. For CuPc coverages below 1.0 ML a laterally ordered mixed hetero-organic ML [134] is produced. An initial CuPc amount of 10 ML results in pure CuPc domains [142] and approximately 0.1–0.2 ML of PTCDA molecules which are most probably in a mixed lateral hetero-organic structure together with CuPc molecules. The incomplete exchange can be explained by a lack of CuPc molecules on some sample spots due to the Stranski-Krastanov growth mode. Consequently, at elevated temperatures homo-molecular CuPc domains are energetically favored on Ag(111) with respect to homo-molecular PTCDA domains and all possible mixed hetero-molecular domains of CuPc and PTCDA molecules. Both the vertical hetero-molecular interface of CuPc/1 ML PTCDA/Ag(111) and the lateral hetero-molecular interface of CuPc + PTCDA/Ag(111) are identified as proper systems for further analysis with RPES. This will be performed in section 5.4. The fact that both systems consist of the same molecules should facilitate a comparison of certain aspects in the discussion of the RPES data. In Refs. [17, 18] it is shown that the system SnPc/1 ML PTCDA/Ag(111) fulfills the requirements for an analysis with RPES. All other systems investigated in this chapter are found to be inappropriate for such a detailed investigation.

The behavior of the system SnPc on 1 ML PTCDA/Ag(111) is quite similar to the system CuPc on 1 ML PTCDA/Ag(111). The main difference is that the Frank-van-der-Merwe-like growth of SnPc molecules on 1 ML PTCDA/Ag(111) allows a complete exchange of PTCDA molecules by SnPc molecules in the first layer on Ag(111) at elevated temperatures. For this complete exchange a SnPc coverage of 1.5 ML is sufficient. Thus homo-

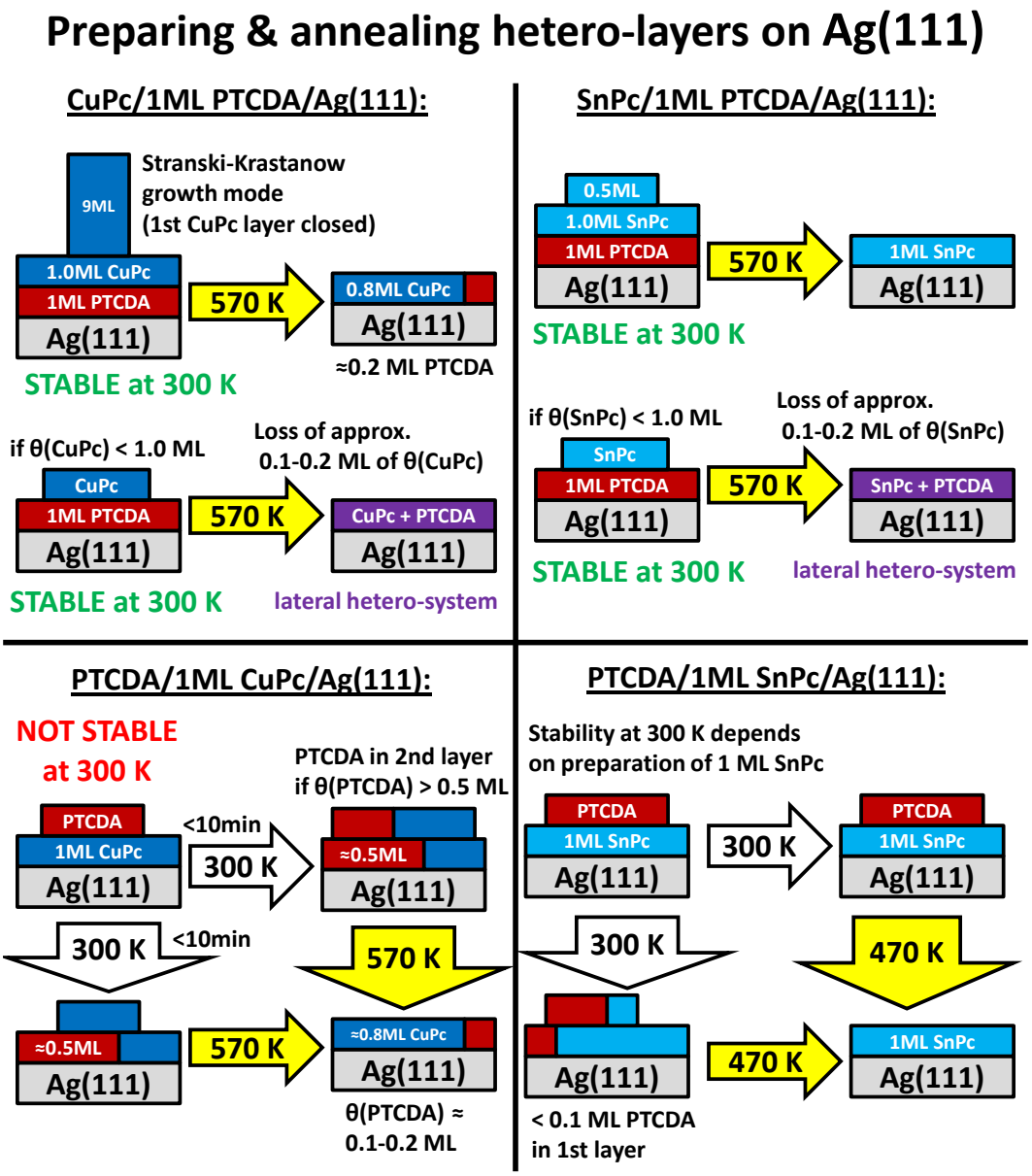

Figure 4.12: Schematic illustration of the behavior of all investigated hetero-organic systems with different coverages (θ) on Ag(111) at 300 K and at elevated temperatures. The used colors denote the particular molecules CuPc (dark blue), SnPc (light blue) and PTCDA (red). The purple color is only used for long range ordered lateral hetero-molecular structures.

molecular SnPc domains are energetically favored at elevated temperatures with respect to pure PTCDA domains and hetero-molecular domains of PTCDA and SnPc molecules on Ag(111). In contrast to the observed similarities of SnPc and CuPc molecules on top of 1 ML PTCDA/Ag(111) unexpected differences are found for the reversed layer sequence. Depositing PTCDA molecules on top of 1 ML SnPc/Ag(111) is found to result in a stable system when the 1 ML SnPc/Ag(111) film is prepared by annealing a SnPc multilayer. In the case of the system PTCDA on 1 ML CuPc/Ag(111) a partial layer exchange is observed even though the 1 ML CuPc/Ag(111) film is prepared in the same way as the 1 ML SnPc/Ag(111) film. Hence at 300 K PTCDA molecules diffuse into the first layer and force part of the CuPc molecules previously situated in the first layer into higher layers. The resulting first layer is found to be a mix of both molecules without long range order [135]. At elevated temperatures this layer exchange is reversed as expected from the finding of the annealing experiments of the system CuPc on 1 ML PTCDA/Ag(111). Consequently, in the case of CuPc and PTCDA molecules on Ag(111) a mix of both molecules is energetically favored at 300 K while in the case of SnPc and PTCDA molecules on Ag(111) the homo-molecular SnPc film is energetically favored for all investigated temperatures.

The study of hetero-organic systems of F4TCNQ and PTCDA molecules on Ag(110) is summarized in Fig. 4.13. In the system F4TCNQ on 1 ML PTCDA/Ag(110) it is observed that at 300 K F4TCNQ molecules diffuse into the first layer of PTCDA molecules in a herringbone phase. A reversed order in the preparation steps results in a stable system with PTCDA molecules situated only above the first layer and in a Volmer-Weber growth mode. After annealing both of these films up to 520 K no significant amount of PTCDA molecules can be found. Hence at all investigated temperatures F4TCNQ molecules are energetically favored over PTCDA molecules on Ag(110). Since a partial decomposition of F4TCNQ molecules occurs upon annealing the sample up to a temperature at which PTCDA molecules not in direct contact to the Ag(110) surface desorb the preparation of a mixed ML in this way is hindered.

For a complete thermodynamic treatment of the hetero-organic systems investigated in this chapter the total free energy of the system would have to be considered. This quantity includes an entropy and an enthalpy term (see Refs. [32, 144] for a more detailed discussion). Without the latter term the system in thermodynamic equilibrium would maximize its entropy and favor a mixed phase. However, there are several molecule-metal and molecule-molecule interactions which can be of importance for a hetero-molecular system on a metal substrate and thus contribute to its enthalpy term. Since these terms themselves are not fully understood it is unclear what role entropy plays in these systems (for a discussion of entropy in a phase transition of a molecule-metal interface see Ref. [86]). At this point a discussion of the terms contributing to the enthalpy of a hetero-molecular system on a metal surface can be given. Furthermore, a possible consistent explanation of all studied systems can be presented on the basis of some assumptions and ignoring the entropy term. The situation for the hetero-organic systems consisting of F4TCNQ and PTCDA molecules on Ag(110) is simpler than for the systems composed of metal-phthalocyanine (SnPc or CuPc) and PTCDA molecules on Ag(111). So I will start the

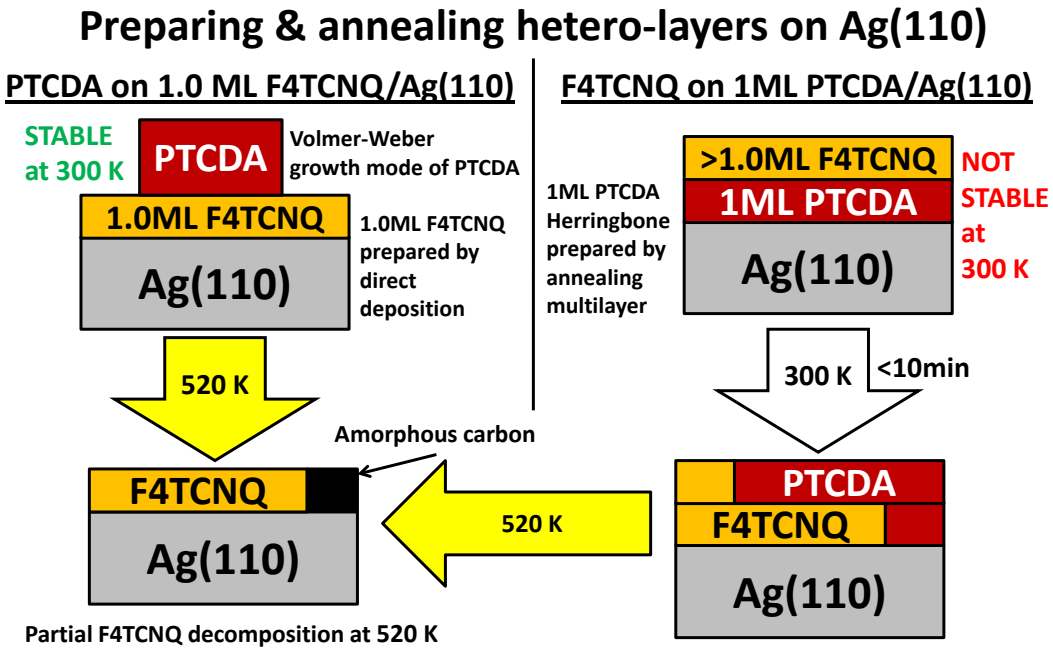

Figure 4.13: Schematic illustration of the behavior of hetero-organic systems consisting of PTCDA and F4TNCQ molecules on Ag(110) at 300 K and at elevated temperatures. The used colors denote the particular molecules PTCDA (red) and F4TCNQ (orange).

discussion with the former systems. With the assumption that an F4TCNQ molecule gains more energy per surface area than a PTCDA molecule upon the adsorption on Ag(110) ($E_{ad/s}$(F4TCNQ/Ag(110)) $> E_{ad/s}$(PTCDA/Ag(110))) the behavior illustrated in Fig. 4.13 is explained. Hence a single parameter ($E_{ad/s}$) is enough to explain the behavior of these systems.

For a consistent explanation of the behavior of the hetero-organic systems containing metal-phthalocyanine (SnPc or CuPc) and PTCDA molecules on Ag(111) additional parameters are required. The behavior displayed in Fig. 4.12 requires a larger adsorption energy per surface area for a SnPc molecule on Ag(111) with respect to a PTCDA molecule ($E_{ad/s}$(CuPc/Ag(111)) $> E_{ad/s}$(PTCDA/Ag(111))) since after the annealing procedure SnPc molecules are situated in the first layer. The same holds true for a comparison of the adsorption energy per surface area for a CuPc and a PTCDA molecule ($E_{ad/s}$(SnPc/Ag(111)) $> E_{ad/s}$(PTCDA/Ag(111))). Moreover, the diffusion of PTCDA molecules into the first layer of CuPc molecules on Ag(111) at 300 K points towards an energy gain at 300 K that must either be negligible or absent at elevated temperatures. A possible explanation for this can be given by considering the contribution of intermolecular interaction. At 300 K a mix of PTCDA and CuPc molecules could be energetically more favorable than a pure CuPc film on Ag(111) because of the reported intermolecular repulsion in the latter system [82]. Investigations of the former system argue with an intermolecular attraction in between CuPc and PTCDA molecules [134]. Hence a partial energy gain is expected by the exchange of CuPc molecules with

PTCDA molecules in the first layer on Ag(111) when both molecules form a mixed ML after the partial layer exchange. The disappearing CuPc diffraction spots in LEED [134] and very recent STM data [135] of this system together with my *fingerprint approach* analysis of C1s core level PES data point towards such a CuPc + PTCDA mix without long range order in the first layer on Ag(111). So the schematic picture of the system PTCDA on 1 ML CuPc/Ag(111) (lower left in Fig. 4.12) must not be interpreted as separated homo-molecular domains in the first layer. Not using the same way of presentation as for the laterally ordered mixed ML (purple layer) should demonstrate the difference in long range order with respect to this system. Anyway, this energy gain due to the difference in intermolecular interaction possibly is the reason for the total energy gain through the partial layer exchange of this system at 300 K. At elevated temperatures an increased mobility of the molecules or the excitation of rotations and vibrations might hinder the formation of a structure with attractive intermolecular interaction which eliminates the corresponding energy gain. However, this explanation also demands a partial energy gain through the exchange of SnPc molecules by PTCDA molecules since for SnPc on Ag(111) also a repulsive intermolecular interaction is found [125] and an attractive intermolecular interaction between SnPc and PTCDA molecules can be expected. Whether there is a fundamental difference between the lateral hetero-organic system of SnPc + PTCDA molecules on Ag(111) with respect to the corresponding systems of CuPc + PTCDA molecules is unknown. However, the revelation of such a fundamental difference would be quite surprising considering the similarities in the phase diagrams of SnPc [125] and CuPc molecules [82] on Ag(111). The assumption of a similar intermolecular interaction between SnPc and PTCDA molecules and CuPc and PTCDA molecules could be retained if the adsorption energy per surface area differed for CuPc and SnPc molecules on Ag(111). With the assumption of a larger adsorption energy per surface area on Ag(111) for a SnPc molecule than for a CuPc molecule and a larger adsorption energy per surface area for both of these molecules with respect to a PTCDA molecule ($E_{ad/s}$(SnPc/Ag(111)) $> E_{ad/s}$(CuPc/Ag(111)) $> E_{ad/s}$(PTCDA/Ag(111))) a working scenario can be constructed. So at elevated temperatures, when the intermolecular interactions could be negligible, both SnPc and CuPc molecules would be energetically favored over PTCDA molecules. At 300 K on the other hand the magnitude of the adsorption energy per surface area of a SnPc and a CuPc molecule on Ag(111) could decide whether an exchange with PTCDA molecules happens or not. In this situation the energy loss due to the exchange of SnPc molecules with PTCDA molecules might not be overcome by the expected energy gain through the intermolecular attraction of both molecules while for a combination of CuPc and PTCDA molecules it could. Explaining the stability of the systems SnPc/1 ML PTCDA/Ag(111) and CuPc/1 ML PTCDA/Ag(111) requires an additional assumption. Based on the assumptions made so far a mixed ML should form for both of these systems at 300 K unless the intermolecular interaction within the PTCDA herringbone structure leads to an energy gain that is larger than the energy gain of the mixed ML and the difference in the adsorption energies per surface area. Considering that at elevated temperatures all energetic contributions by intermolecular interaction are eliminated explains the observed layer exchanges at elevated temperatures of the systems SnPc/1 ML PTCDA/Ag(111) and CuPc/1 ML

PTCDA/Ag(111). If all these assumptions were appropriate the behavior of the systems of SnPc and CuPc molecules in combination with PTCDA molecules on Ag(111) could be consistently explained.

In this case the questions about the difference in the adsorption energy per surface area for SnPc, CuPc, and PTCDA molecules on Ag(111) still needs to be answered. It could be due to differences in the energy gain through electrostatic interaction, fluctuating dipole interaction, and covalent chemical bonding of a single molecule to the Ag(111) surface. Furthermore, an energy cost due to intramolecular Coulomb repulsion could be important. The terms $U_{m,m'}$ in the *Molecular Gunnarsson-Schönhammer* Hamiltonian (Eq. 2.9) demand an energy cost as a consequence of CT from the metal into the molecule in the ground state. For CuPc [145] and PTCDA [146] molecules on Ag(111) adsorption energies as a function of the vertical distance to the surface are calculated. From these curves the adsorption energy of a PTCDA molecule $E_{ad}(\text{PTCDA}) \approx 2.7$ eV and a CuPc molecule $E_{ad}(\text{CuPc}) \approx 4.0$ eV can be extracted. For the system 1 ML PTCDA/Ag(111) the unit cell (length of basis vectors: $a = 19.0$ Å, $b = 12.6$ Å; angle: $\gamma = 89^\circ$ [97]) includes two molecules in the area of 239 Å^2. Hence I obtain for the adsorption energy per surface area $E_{ad/s}(\text{PTCDA/Ag(111)}) \approx 23$ meV/Å^2 in the herringbone structure on Ag(111). The unit cell of 1 ML CuPc/Ag(111) includes one molecule and has an area of 192 Å [82] which results in an adsorption energy per surface area $E_{ad/s}(\text{CuPc}) \approx 21$ meV/Å^2. So according to these calculations a PTCDA molecule is energetically favored over a CuPc molecule on Ag(111) which is in contrast to the assumption made above. To what extend the used areas a molecule occupies on the surface are appropriate for the actually realized structures after the layer exchange cannot be argued. Furthermore, it is unclear whether all necessary contributions to the adsorption energy, especially an energy cost due to intramolecular Coulomb repulsion, are included in the calculations in Refs. [145, 146]. Measurements for the adsorption energies exist for PTCDA molecules on an Au(111) surface [147, 148]. Since the bonding of SnPc, CuPc, and PTCDA molecules to the Au(111) surface is believed to be fundamentally different than the bonding of these molecules to an Ag(111) surface a comparison of both is not useful.

Even if the assumed adsorption energies per surface area on Ag(111) and the discussed intermolecular interactions had the proper order and magnitude it would still be unclear whether these parameters are appropriate to describe the experimental findings. The *fingerprint approach* analysis in sections 4.1 and 4.2 and the structural investigations of Refs. [134, 135] reveal that in both mixed lateral hetero-molecular ML systems (SnPc + PTCDA/Ag(111) and CuPc + PTCDA/Ag(111)) the geometric structure is modified with respect to the pure ML films on Ag(111). Hence the adsorption sites on the surface should be changed as a consequence of the intermolecular interaction. In other words both molecules align with respect to each other and the surface in order to reach a potential minimum which most probably leads to different adsorption sites with respect to the pure ML films. If the bonding to the substrate significantly depends on the adsorption site the energy gain upon adsorption and the intermolecular interaction will be coupled to each other. So strictly speaking a separated consideration of the terms from these

contributions to the enthalpy term might not be possible. Furthermore, it is not the mere adsorption energy of a molecule on the metal surface which is required for the explanation of the experimental results of the layer exchanges of some and the stability of other systems. The energetic difference of molecule A on top of molecule B on Ag(111) with respect to molecule B on top of molecule A on Ag(111) is the decisive parameter. It is not clear whether there is a significant difference in the adsorption energies of molecule A on top of molecule B with respect to the reversed layer order. Possibly even the lateral intermolecular interaction in the higher layers needs to be taken into account for a successful description of the enthalpy term. Additional annealing experiments of hetero-organic systems also report a temperature induced layer inversion [19, 149]. In both of these experiments a hetero-organic film is prepared below 300 K and annealing to higher temperatures (still below 300 K) leads to a layer inversion. The reason why one molecule is energetically favored with respect to the other molecule of these hetero-organic systems is not discussed in these studies.

In conclusion a possible consistent explanation of the observed behavior for the hetero-organic systems on Ag(111) displayed in Fig. 4.12 can be given on the basis of some assumptions. However, this explanation is a constructed scenario for the observed experimental results and hence does not allow any significant conclusions. The discussion of possible contributions to the enthalpy term given above identifies multiple effects which could be important while a contribution of an entropy term is not considered. In order to understand the found temperature dependent layer exchanges more information on the lateral order of the system SnPc + PTCDA/Ag(111) is necessary. Additionally, values of adsorption energies of SnPc, CuPc, and PTCDA molecules on Ag(111) and intermolecular interaction terms, which are independently determined in an experiment, might lead to a satisfying conclusion. If the investigation of additional hetero-organic systems is helpful to reach a significant and consistent explanation will become clear after these are performed. The partially unexpected behavior of the systems investigated in this chapter demonstrates that predictions for hetero-organic systems are very difficult. However, solving the riddle of the temperature dependent stability and instability of hetero-organic systems will certainly push the understanding of molecule-metal and molecule-molecule interaction to the next level.

5 Resonant photoelectron spectroscopy applied to π-conjugated molecules: from homo to hetero-molecular systems

Resonant photoelectron spectroscopy (RPES) is a powerful technique which allows to study dynamical processes at interfaces [9]. In a simplified picture the lifetime of the core excited intermediate state can be seen as an internal clock that serves as a reference for an investigation of charge transfer (CT) times. In order to be able to analyze dynamical CT across an interface a well defined interface is required. In the previous chapter two appropriate hetero-molecular systems with such an interface have been identified. These are a vertical and a lateral hetero-organic interface of CuPc and PTCDA molecules on Ag(111). Both will be studied in section 5.4 at the end of this chapter and a discussion of CT properties of both will be given on the basis of the results of the previous investigations. The quantitative extraction of CT times from RPES data with the core-hole-clock technique [9] requires the extraction of photoelectron spectroscopy (PES) intensities of a signal corresponding to CT and another one corresponding to no CT. For the signal associated with CT the total energy (including the photon) is not conserved due to energy dissipation through the transfered electron. The signal of this autoionization channel hence has the characteristic of a regular Auger decay and disperses linearly with the photon energy ($h\nu$) on a binding energy (E_B) scale. For the signal associated with no CT the excited electron is still present and the energy of the total RPES process is conserved. Hence with changing $h\nu$ this signal stays at constant E_B. These two different possibilities for the $h\nu$ dependence of E_B of a signal in RPES lead to two different types of spectroscopies. The investigation of the $h\nu$ dependence of a constant E_B interval is called constant initial state (CIS) spectroscopy while the study of the $h\nu$ dependence of a constant kinetic energy (E_K) interval is termed constant final state (CFS) spectroscopy. The electronic structure of atoms can result in RPES data for which the two types of signals just discussed (constant E_B and constant E_K) can be separated and their relative PES intensities can be significantly extracted from the RPES data [11–13]. Alternatively, a CT time evaluation of atoms and small molecules can be performed with a deconvolution of the RPES data into a CT part and a part without CT by using RPES measurements in the gas phase [10, 55]. These gas phase RPES spectra obviously do not contain any CT features since the atoms and molecules are isolated in the gas phase.

The electronic structure of π-conjugated molecules is much more complicated with respect to atoms and small molecules. Many molecular orbitals are energetically close to each other which results in RPES spectra in which multiple signals can overlap energetically. Thus the autoionization signals of interest (with and without CT) are energetically not separable from each other. Furthermore, gas phase RPES measurements are experimentally quite demanding due to the larger sublimation temperatures of π-conjugated molecules. Hence an analogue evaluation as for atoms and small molecules is not possible. The CT time evaluation of π-conjugated molecules so far reported in literature [150–157] relies on different approaches. Assuming that in a multilayer film molecules are not significantly coupled to each other, CT on the time scale of the core hole lifetime is negligible. Hence a decrease of a constant E_B signal from the multilayer film to the submonolayer (sub-ML) or monolayer (ML) film can be interpreted as CT. This approach requires a normalization of the multilayer data with respect to the (sub-)ML data. If the signal of interest overlaps with substrate signals a subtraction of these from the RPES data will be necessary for a comparison. Both the normalization and the subtraction of substrate signals in the valence regime are problematic for the systems investigated in this thesis. As discussed in section 3.3 the normalization of a 1D valence PES energy distribution curve (EDC) with respect to another one originating from a different sample is very difficult. The same holds true for the EDCs in RPES. Hence a normalization of the RPES EDCs of the bare substrate with respect to the corresponding EDCs of the substrate with the adsorbed molecule is very delicate. So a subtraction of the former from the latter is dangerous and can lead to artifacts. Especially at E_B of the intense substrate signals (Ag4d and Au5d) subtraction artifacts (for example negative intensity) can be produced which hinders quantitative and even qualitative statements about PES intensities in this region. However, at lower E_B than the intense substrate signals (Ag4d and Au5d) the small intensity and the featureless line-shape of the RPES EDCs of the bare substrate allow a comparison of line-shapes of signals from the adsorbate after a subtraction of the EDC of the bare substrate. The normalization of RPES data in the $h\nu$ direction as discussed in section 3.3 is even more complicated. Dividing the PES map by the measured beamline flux curve (see Fig. 3.2) does for example not take into account the background produced by higher order light [119]. This makes a quantitative evaluation of PES intensities highly questionable. Furthermore, the normalization of a CIS spectrum of a (sub-)ML sample with respect to a multilayer sample would not be possible even if the normalization in $h\nu$ direction was perfectly performed. Due to the fact that there is no $h\nu$ value at which the intensity of a CIS spectrum is independent of the molecular overlayer a proper normalization is very difficult.

Despite these difficulties I will be able to present qualitative statements about dynamical CT for π-conjugated molecules on metal substrates. The identification of signals in the RPES data which are related to dynamical CT constitutes the basis for my CT analysis with RPES. Hence I can state whether CT on the time scale of the core hole lifetime is possible or not by the presence or absence of the identified CT related signals in the RPES data. This can be seen as a qualitative core-hole clock investigation but since this term is usually associated with a quantitative determination of CT times I

will not use it in the following. The study of a large RPES data set is the cornerstone of the identification of CT related signals. Comparing RPES data of homo-molecular multilayer samples and homo-molecular (sub-)ML samples with each other and gas phase data of small molecules will reveal CT related signals. First of all multilayer samples of NTCDA and coronene molecules are analyzed. A general investigation of this data includes a discussion of all possible signals that contribute to the PES map as well as their PES intensity and energy position as a function of $h\nu$. Thereby signals are identified which are energetically separated on the E_B axis from all other signals. These frontier molecular orbital signals are then inspected more closely and their $h\nu$ dependent line-shape evolution is discussed in comparison to small molecules in the gas phase. Moreover, the influence of the adsorption on metal substrates is investigated by comparing the $h\nu$ dependent line-shape evolution of molecular orbital signals of multilayer films with the corresponding RPES data of (sub-)ML films. This comparison is only performed for molecule-metal interface systems without a signal from the lowest unoccupied molecular orbital (LUMO) in direct valence PES since the $h\nu$ dependent line-shape evolution of molecular orbital signals in systems with a LUMO signal in direct valence PES turns out to be not comparable with the one of multilayer films. In the investigated region of the PES maps a CT state is found for the coronene/Ag(111) interface and explained on the basis of the theoretical concepts introduced in section 2.3. This motivates a search for similar features in the same region of the PES map for the systems with a LUMO signal in direct valence PES. The RPES data of these systems is discussed with an emphasis on the particular special case found in the different investigated systems. This discussion leads to a search for CT related constant E_K features at larger $h\nu$ which are observed for many (sub-)ML samples. Only for the systems without a LUMO signal in direct valence PES an explanation for these constant E_K features can be given. At the end of this chapter the knowledge gained by the RPES investigations of homo-molecular systems is applied to the hetero-molecular systems which have been identified to be suitable for such an investigation in chapter 4. First the lateral hetero-organic system CuPc + PTCDA/Ag(111) and then the vertical hetero-organic system CuPc/1 ML PTCDA/Ag(111) is investigated with RPES. The CT related features which are detected in the former system are very similar to the corresponding features observed for the homo-molecular CuPc and PTCDA ML films on Ag(111). Hence no feature related to CT across the lateral hetero-organic interface on the time scale of the core hole lifetime can be revealed for the system CuPc + PTCDA/Ag(111). In the RPES data of the system CuPc/1 ML PTCDA/Ag(111) none of the CT related features identified in the homo-molecular metal-organic interface systems can be found. Hence either CT on the time scale of the core hole lifetime does not occur across the vertical hetero-organic CuPc-PTCDA interface in this system or this interface cannot be compared to homo-molecular metal-organic interfaces.

5.1 Photon energy dependent intensity variations

As a starting point for RPES investigations of π-conjugated molecules a large region of $h\nu$ and E_B is measured and discussed. The $h\nu$ region of interest includes the intense π-resonances. Here the electron is resonantly excited into a previously unoccupied molecular orbital with mainly π-character. Moreover, the measurement should include a region of $h\nu$ which is clearly larger than the ionization potential of all different core level species of the investigated system. A comparison of this $h\nu$ region with the region of the π-resonances can reveal differences within the particular RPES processes. Additionally, recording an $h\nu$ region of 1–2 eV below the π-resonances is desired for the confirmation of proper normalization in the $h\nu$ direction (see section 3.3). A flat plateau below the first π-resonance in a CFS or CIS spectrum points towards a negligible energy mismatch of the PES map and the beamline flux curve and hence a proper normalization of the former. In the E_B direction the signals of interest are autoionization signals which involve the molecular orbitals of the adsorbed molecule. In combination with the identified $h\nu$ region of approximately 282–295 eV the E_B region of approximately -2–23 eV is selected for the initial RPES measurements.

Overview PES maps of multilayer films in this $h\nu$ and E_B range are investigated first. In the RPES data of these films molecule-metal interface CT features are not present since the PES signals stemming from this interface are almost completely attenuated by the overlayers. Hence the observed features must be related to molecular properties alone. A model system which is extensively studied by near edge x-ray absorption fine structure (NEXAFS) spectroscopy is the NTCDA molecule [60, 61, 67, 86, 114, 158–161]. The NEXAFS data of this molecule exhibits energetically well separated resonances with electronic transitions that correspond to different carbon species. At the same time its smaller size with respect to the PTCDA and the phthalocyanine molecule (see Fig. 3.1) should result in less complicated core level spectra. Hence this molecule is chosen for the investigation of $h\nu$ dependent intensity variations on the large scale. A second system that is well suited for this study is the coronene molecule. Its simple pure hydrocarbon composition (see Fig. 3.1) and the fact that high quality off-resonant valence PES data exists [59, 121] should facilitate the interpretation of the RPES data.

First a general discussion of the contributions to a PES overview map is given for the example of an NTCDA multilayer. Then the observation of the $h\nu$ dependent intensity variation of molecular orbital signals in RPES is discussed on the basis of a simple approach. Therein the relative intensities observed in RPES are explained by the local character of the electronic transition in the particular NEXAFS resonance and the relative real space probability density of the particular molecular orbital. For an NTCDA multilayer the relative probability densities of the molecular orbitals that contribute to the particular CIS spectrum are estimated with the RPES data and the electronic transitions obtained by calculations of the NEXAFS spectrum. After that the limits of this simple approach are identified in the discussion of the observed relative $h\nu$ dependent intensity variation of molecular orbital signals of a coronene multilayer. It is shown that

differences in relative intensities by orders of magnitude can be explained in this simple approach while statements about differences within the same order of magnitude are troublesome.

5.1.1 NTCDA

NTCDA is a well characterized model system which has been investigated extensively by PES [81, 85, 158, 159, 162] and NEXAFS spectroscopy [60, 61, 67, 86, 114, 158–161]. RPES measurements of an ML film have also been performed [81]. NEXAFS measurements reveal that a multilayer film grows flat lying and Frank-van-der-Merwe-like on Ag(111) when it is deposited at 100 K [61, 114, 161]. Above approximately 160 K a reordering occurs in which the molecules stand up and reorder into a Stranski-Krastanow growth mode [61, 114, 158, 161]. For the investigation of NTCDA molecules isolated from the metal substrate the flat lying Frank-van-der-Merwe-like growth mode is required. Hence the preparation and RPES measurement of the NTCDA multilayer on Ag(111), which results in the RPES data illustrated in Fig. 5.1, are performed at 100 K.

Fig. 5.1(a) displays a PES overview map in the $h\nu$ and E_B region discussed in the introductory part of this section. The RPES process can lead to one-hole final states and two-hole final states. The latter can further be divided into two-hole-one-electron and bare two-hole final states. In a two step picture of RPES an electron is excited from a core level into a previously unoccupied orbital in the first step. In the second step this excited state decays via autoionization. If the electron excited in the first step takes part in this decay a one-hole final state will be produced which is the same electronic final state as in direct valence PES. In all other cases different two-hole final states are produced with the additional excited electron or without it. The latter case is a consequence of delocalization of the electron (for example by CT). So in the PES overview map one-hole final states are present at the same E_B position as the signals from molecular orbitals in direct valence PES at all $h\nu$. Their intensity depends on the magnitudes of the probabilities for the particular excitation and decay processes. Hence at different $h\nu$ the same molecular orbital one-hole final state signal can exhibit different PES intensities. All two-hole final states also undergo an $h\nu$ dependent PES intensity variation. They can also remain at constant E_B when no energy dissipation mechanism, like for example CT, occurs. If this happens during the RPES process a two-hole final state equal to a regular Auger will be produced which disperses linearly to larger E_B with increasing $h\nu$.

In addition to the PES signals from the adsorbed molecule a direct PES contribution from the substrate is present in the PES overview map. In the case of an Ag(111) substrate these are the intense Ag4d bands in between $E_B \approx 4-8$ eV. At lower E_B the much less intense s-p bands from the Ag(111) substrate are present. For the NTCDA multilayer film in Fig. 5.1 these substrate signals are significantly attenuated but for $h\nu$ smaller than the first NEXAFS resonance their contribution is visible together with the contribution of the

direct PES signal of the molecular orbitals. Since the monochromator also transmits light of higher order signals which stem from direct PES with $n \times h\nu$ ($n \in \mathbb{N}$) are also present in the RPES data. The signal at $E_B \approx 2$ eV and $h\nu \approx 285.5$ eV in Fig. 5.1(a) which disperses to lower E_B with increasing $h\nu$ is the second order carbon contribution. It is produced by direct PES with $2 \times h\nu$ and hence does not exhibit the same intensity variation as the first order signals (see the beamline flux curves in Fig. 3.2). Consequently, this second order signal is more intense in the $h\nu$ region of low intensity in the beamline flux curve after the normalization procedure. Furthermore, background intensity produced by higher order light is present at all parts of the PES overview map. The E_B and $h\nu$ variation of this background signal is actually unknown but a rather moderate variation can be estimated. Similar to the second order C1s signal this background intensity is also more intense in the $h\nu$ region of low intensity in the beamline flux curve after the normalization procedure. Whenever these higher order signals overlap with the discussed first order signals special care needs to be taken in order to exclude a significant influence of the higher order contributions.

Transforming the PES overview map in Fig. 5.1(a) onto an E_K scale ($E_B = h\nu - E_K$) an integration over a constant E_K interval, or in other words CFS spectroscopy, is possible. On an E_B scale such a constant E_K interval disperses like the black parallelogram in Fig. 5.1(a). The spectrum which is the result of the integration of the area inside this black parallelogram is displayed with filled black diamonds in Fig. 5.1(b). The investigation of a large RPES data set shows that such a CFS NEXAFS spectrum is very similar to the corresponding partial electron yield NEXAFS spectrum. An integration over a constant E_B interval (CIS spectroscopy) in the large E_B region of the PES overview map differs from the latter for large $h\nu$. This can be explained by the fact that for $h\nu$ larger than the core level ionization potential the mayor part of the signals in the PES overview map disperse with constant E_K. The CFS NEXAFS spectrum can be used to identify the NEXAFS resonances. Using a signal inside the PES map has the advantage that a comparison to other signals in this map (for example CIS spectra) is independent of the normalization procedure and the energy calibration. A comparison of signals in the PES map with the partial electron yield NEXAFS spectrum might be influenced by an energy calibration mismatch and normalization artifacts. The CFS NEXAFS spectrum can also serve as a reference for a comparison of intensities (see Fig. 5.1(c)) but since different resonantly enhanced molecular orbital signals could contribute to the CFS NEXAFS spectrum for different $h\nu$ quantitative statements are troublesome. However, for a rough identification of the absorption cross section the CFS NEXAFS spectrum is an appropriate signal.

The direct valence PES spectrum (see Fig. A8(a)) reveals that the PES signals from the molecular orbitals cannot be separated for an NTCDA multilayer on Ag(111). Hence the CIS spectra extracted from Fig. 5.1(a) by integration of the hatched areas in E_B direction and displayed in Fig. 5.1(c) consist of a group of molecular orbital signals. This does not have an influence on the conclusion drawn from the comparison of the CIS 1 with the CIS 2 spectrum. These two CIS spectra are set to 0 at the lowest $h\nu$ and are normalized at NEXAFS resonance A for a comparison of their relative intensities in Fig. 5.1(c).

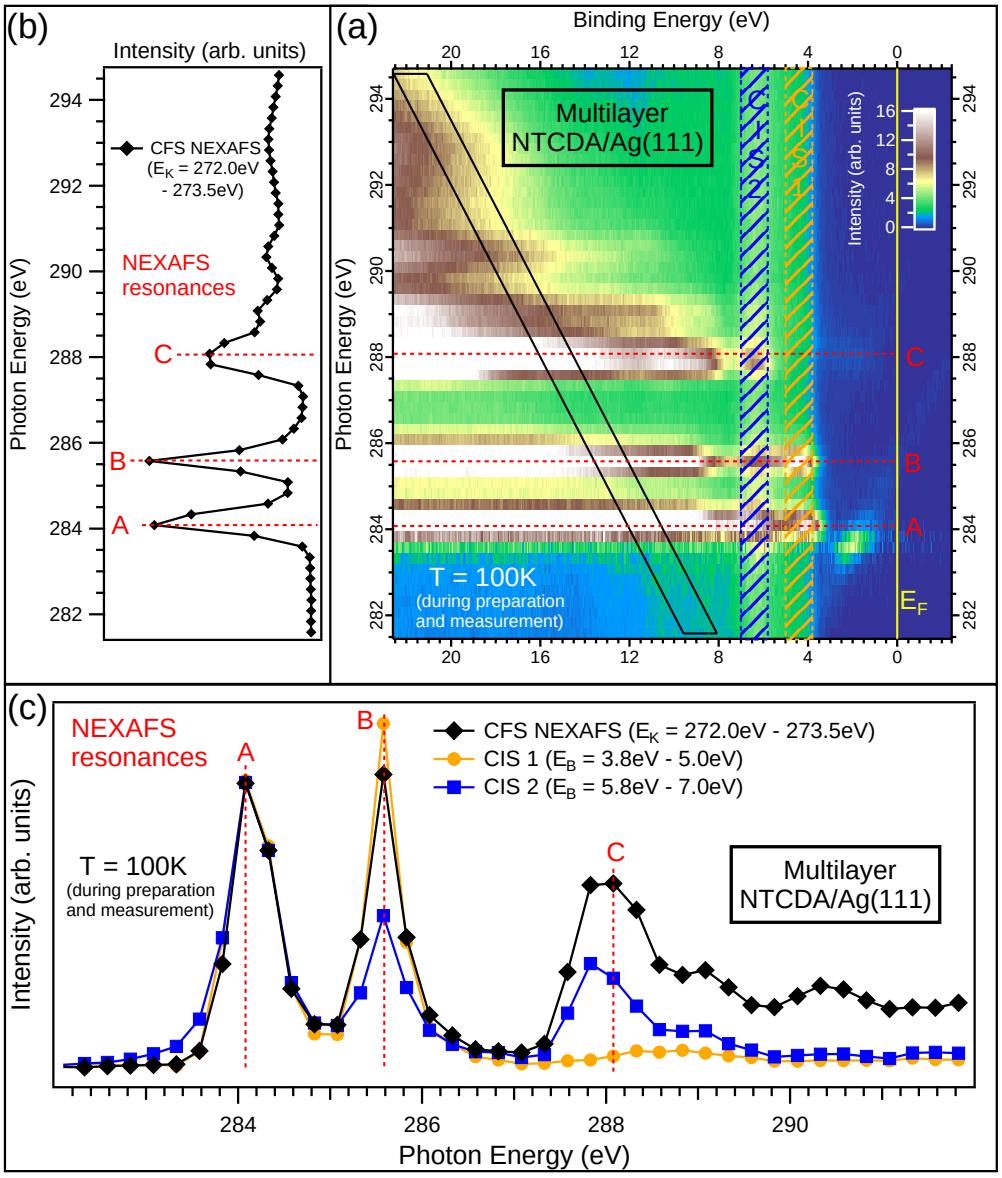

Figure 5.1: RPES data at the carbon K-edge of a multilayer of NTCDA/Ag(111) prepared and measured at 100 K. **(a)** PES overview map with an $h\nu$ increment of 250 meV and an E_B increment of 50 meV. The red dashed horizontal lines denote the NEXAFS resonances identified by the CFS NEXAFS spectrum in panel (b). The black parallelogram marks the area from which this CFS NEXAFS spectrum originates. The CIS spectra displayed in panel (c) originate from the orange and blue hatched areas. The yellow vertical line represents E_F. The signal at $E_B \approx 2$ eV and $h\nu \approx 285.5$ eV is the second order carbon contribution. **(b)** CFS NEXAFS spectrum used for the identification of the NEXAFS resonances A–C. **(c)** CIS 1 spectrum (filled orange circles) and CIS 2 (filled blue squares) spectrum compared to each other and to the CFS NEXAFS spectrum (filled black diamonds). At the lowest $h\nu$ all spectra are set to 0 and at NEXAFS resonance A all spectra are normalized.

It is observed that both groups of molecular orbital signals exhibit a unique $h\nu$ dependent intensity variation with respect to each other and the CFS NEXAFS spectrum. In a simplified model this can be seen as a consequence of the localized character of the electronic transitions in NEXAFS spectroscopy and the real space probability density of the molecular orbitals. The combination of both leads to different excitation and decay probabilities and hence to unique $h\nu$ dependent PES intensities in the $h\nu$ region of the NEXAFS resonances. From the knowledge about the electronic transitions which contribute to the NEXAFS spectrum the real space probability density of the molecular orbitals can be estimated. A comparison of the CIS 1 spectrum with the CIS 2 spectrum allows me to make statements about relative intensities. So the statements about real space probability densities are also restricted to a comparison of relative real space probability densities. For example it is obvious from Fig. 5.1(c) that the intensity of the CIS 1 spectrum (filled orange circles) in NEXAFS resonance C with respect to NEXAFS resonance A is smaller than for the CIS 2 spectrum (filled blue squares). For NTCDA molecules the electronic transitions which contribute to NEXAFS resonance C mainly include the carbon species which is bound to the oxygen atoms [161]. So the molecular orbitals that contribute to the CIS 1 spectrum have less real space probability density at this carbon species with respect to the orbitals that contribute to the CIS 2 spectrum, both in comparison to the real space probability densities at the carbon species contributing to NEXAFS resonance A. In this NEXAFS resonance electronic transitions including the carbon species bound to oxygen do not contribute [161]. The fact that the CFS NEXAFS spectrum exhibits intensities that are in the same order of magnitude for NEXAFS resonance A and C allows me to exclude that the observed relative intensity variation of the CIS spectra in NEXAFS resonance C is a consequence of the x-ray absorption probability alone. Hence the discussed difference in real space probability densities should be the dominant effect. All other intensity variations of CIS spectra extracted from the RPES data of the NTCDA multilayer can be discussed analogously. However, the electronic transitions contributing to the resonances of interest in the NEXAFS spectrum need to be known and contributions that include different carbon species need to be energetically separable. A similar investigation of intensities of CIS spectra from RPES data of an ML of NTCDA/Ag(111) can be found in Ref. [81]. The differences in the molecular orbital signals in direct valence PES of the NTCDA multilayer with respect to the ML on Ag(111) (see Fig. A8) demonstrates that a significant comparison of the RPES data of both systems is very difficult.

5.1.2 Coronene

The valence electronic structure of an ML of coronene/Ag(111) has been studied with ARPES and compared to density functional theory (DFT) calculations [59, 121]. Hence the correctness of the order of the frontier molecular orbitals in DFT calculations is experimentally verified and calculated real space probability densities can be related to some of the molecular orbital signals in PES. Furthermore, calculations of NEXAFS spectroscopy exist which assign specific electronic transitions to the observed NEXAFS

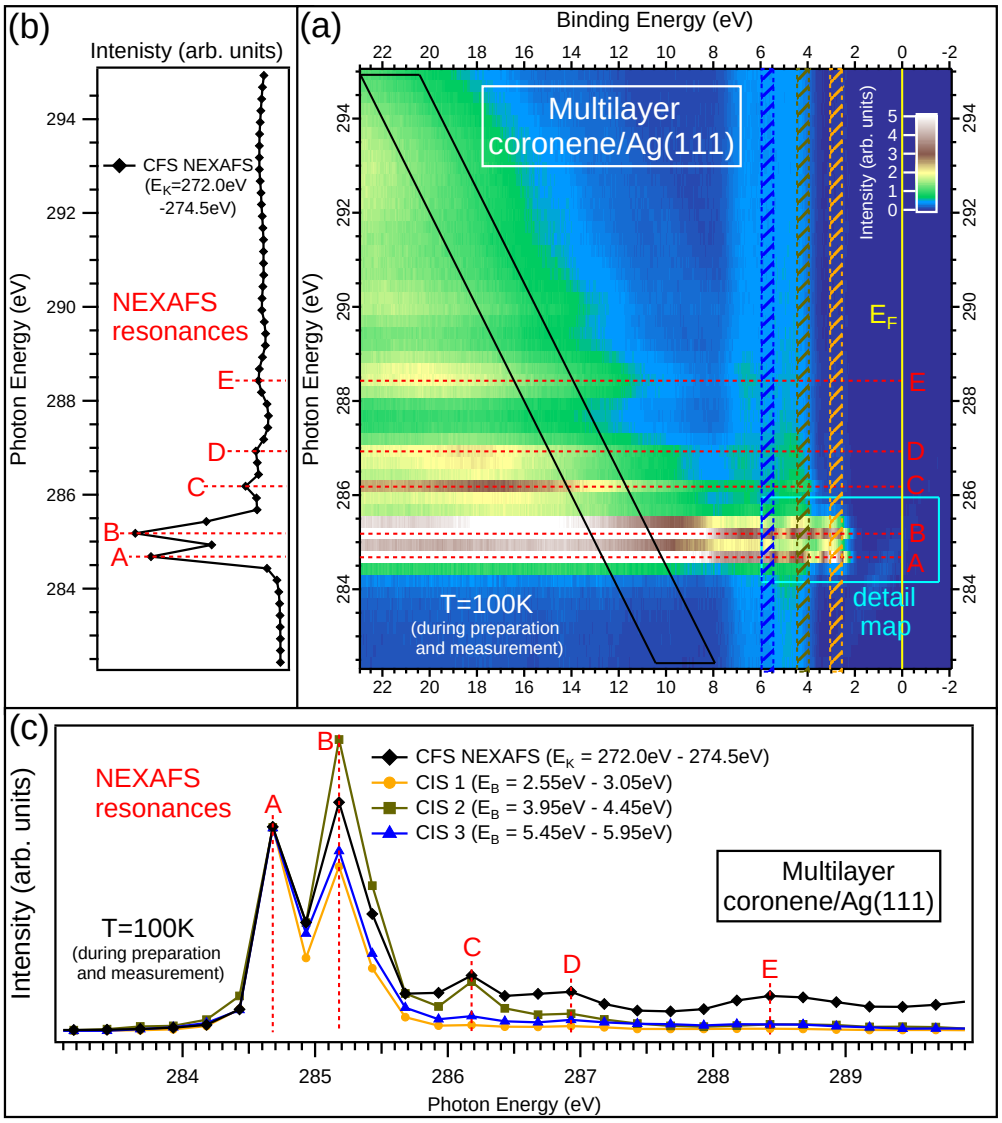

Figure 5.2: RPES data at the carbon K-edge of a multilayer of coronene/Ag(111) prepared and measured at 100 K. **(a)** PES overview map with an $h\nu$ increment of 250 meV and an E_B increment of 50 meV. The red dashed horizontal lines denote the NEXAFS resonances identified by the CFS NEXAFS spectrum in panel (b). The black parallelogram marks the area from which this CFS NEXAFS spectrum originates. The CIS spectra displayed in panel (c) originate from the orange, olive and blue hatched areas. The yellow vertical line represents E_F. The cyan box denotes the area of the PES detail map shown in Fig. 5.3(a). The signal at $E_B \approx 1$ eV and $h\nu \approx 284$ eV is the second order carbon contribution. **(b)** CFS NEXAFS spectrum used for the identification of the NEXAFS resonances A–E. **(c)** CIS 1 spectrum (filled orange circles), CIS 2 spectrum (filled olive squares) and CIS 3 spectrum (filled blue triangles) compared to each other and to the CFS NEXAFS spectrum (filled black diamonds). At the lowest $h\nu$ all spectra are set to 0 and at NEXAFS resonance A all spectra are normalized.

resonances [163]. So in principle the $h\nu$ dependent relative intensity variation of CIS spectra in RPES should be predictable by the relative real space probability densities of the molecular orbitals at the particular carbon species at which the electronic transition in NEXAFS spectroscopy is localized. In Fig. 5.2 RPES data of a coronene multilayer is presented analogously to Fig. 5.1. Since at room temperature a closed film cannot be grown both the preparation and the measurement are performed at 100 K. In the PES overview map (Fig. 5.2(a)) three separable molecular orbital signals are identified and for each one a CIS spectrum is extracted from the RPES data by integration over the indicated E_B region. These CIS spectra are displayed in Fig. 5.2(c). The comparison of the three CIS spectra reveals the special character of the relative intensity variation of the CIS 2 spectrum. In NEXAFS resonance C it is the only CIS spectrum that shows a significant increase in intensity with respect to NEXAFS resonance A. Furthermore, the global intensity maximum of the CIS 2 spectrum is observed in NEXAFS resonance B which also differs from the observed relative intensity variation of the CIS 1 and the CIS 3 spectrum.

A comparison to the ARPES investigation in Refs. [59, 121] suggests that the highest occupied molecular orbital (HOMO, called MO1 in Refs. [59, 121]) contributes to the CIS 1 spectrum while the CIS 2 spectrum consists of a contribution from the HOMO-1 (called MO2 in Refs. [59, 121]). The assignment of the molecular orbital(s) which contribute to the CIS 3 spectrum is difficult. The energetic separation of the molecular orbitals in DFT calculations does not match the found E_B differences in the RPES data [143]. Moreover, at E_B larger than the signal of the HOMO-1 a comparison of DFT calculations with ARPES data is prohibited by the overlap of molecular orbital signals with the intense Ag4d bands [59, 121]. Hence I will only discuss the comparison of the CIS 1 with the CIS 2 spectrum and merely state at this point that the observed $h\nu$ dependent intensity variation of the CIS 3 spectrum is similar to the one of the CIS 1 spectrum. So the real space probability density of the molecular orbitals which contribute to these CIS spectra should also be similar. The NEXAFS calculation in Ref. [163] assigns an electronic transition localized at the carbon species of the inner benzene ring of coronene (see Fig. 3.1 and Fig. A9) to NEXAFS resonance C. According to these calculations an electronic transition localized at the carbon species bound to hydrogen contributes to NEXAFS resonance A. The calculated real space probability density of the frontier molecular orbitals of coronene (see Fig. A9) suggests a higher real space probability density of the HOMO-1 at the carbon species of the inner benzene ring with respect to the HOMO while the real space probability density of both molecular orbitals is similar at the carbon species bound to hydrogen. Consequently, the larger relative intensity of the CIS 2 spectrum (filled olive squares) in NEXAFS resonance C with respect to the CIS 1 spectrum (filled orange circles) observed in Fig. 5.2(c) can be explained with a higher relative real space probability density of the contributing molecular orbital at the carbon species of the responsible electronic transition in the NEXAFS spectrum.

The discussion of the difference in the observed relative intensities of the CIS 1 and the CIS 2 spectra in the NEXAFS resonances A and B is based on the PES detail map presented in Fig. 5.3(a). The large $h\nu$ increment (250 meV) of the PES overview map

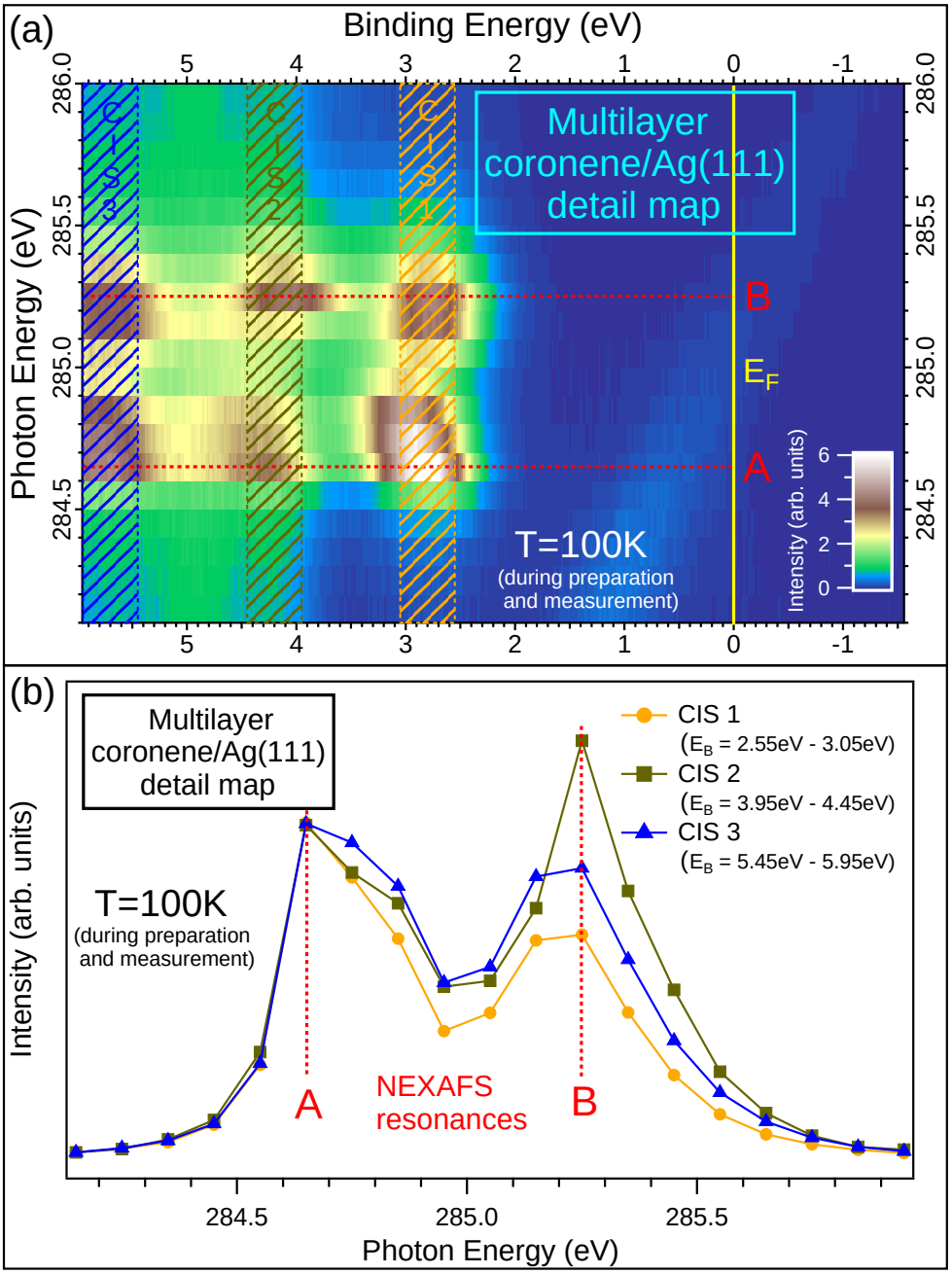

Figure 5.3: RPES data at the carbon K-edge of a multilayer of coronene/Ag(111) prepared and measured at 100 K. **(a)** PES detail map with an $h\nu$ increment of 100 meV and an E_B increment of 15 meV. The red dashed horizontal lines denote the NEXAFS resonances. The CIS spectra displayed in panel (c) originate from the orange, olive and blue hatched areas. The yellow vertical line represents E_F. The signal at $E_B \approx 1$ eV and $h\nu \approx 284$ eV is the second order carbon contribution. **(b)** CIS 1 spectrum (filled orange circles), CIS 2 spectrum (filled olive squares) and CIS 3 spectrum (filled blue triangles) compared to each other. At the lowest $h\nu$ all spectra are set to 0 and at NEXAFS resonance A all spectra are normalized.

(Fig. 5.2(a)) in comparison to the energetically close lying NEXAFS resonances A and B complicates a comparison of the intensities of the CIS spectra. So in the region of interest a PES detail map is recorded with a smaller $h\nu$ increment (100 meV) in a subsequent measurement. The integration over the same E_B interval as in the PES overview map results in the CIS spectra displayed in Fig. 5.3(b). Here a larger relative intensity of the CIS 2 spectrum in NEXAFS resonance B with respect to the CIS 1 spectrum is clearly observed. According to Ref. [163] the two electronic transitions that contribute to NEXAFS resonance B are localized at both carbon species bound to carbon. Thus the $h\nu$ dependent relative intensity variation in Fig. 5.3(b) could be explained by a larger relative real space probability density at the carbon bound carbon species for the HOMO-1 with respect to the HOMO. This is not observed in the calculated real space probability densities (see Fig. A9). Therefore it is questionable whether the simple approach of the consideration of the localization of the electronic transition(s) in NEXAFS spectroscopy and the real space probability density of the contributing molecular orbital(s) is able to predict differences within the same order of magnitude. The difference between the relative intensities of the CIS 1 and the CIS 2 spectrum in NEXAFS resonance B is roughly a factor of two. Such a difference can originate from many other effects. In contrast the difference observed in Fig. 5.2(c) for these CIS spectra in the NEXAFS resonance C is much larger. For the CIS 1 spectrum there is practically no increase in intensity in NEXAFS resonance C while the intensity of the CIS 2 spectrum is clearly enhanced. The magnitude of this difference in relative PES intensities could very well be several orders of magnitude. Hence the predictability of the PES intensities of the CIS spectra in NEXAFS resonance C in the discussed way is reasonable. The inability to successfully predict the behavior observed in NEXAFS resonance B on the other hand demonstrates the limit of the applied simple approach.

Whether the calculated ground state density of states of single particle molecular orbitals calculated in DFT can be utilized for this simple approach to explain relative intensities in RPES is unclear. The agreement of these calculations and the angular intensity distribution presented in Refs. [59, 121] cannot be used as a justification for such simplifications. In contrast to direct valence PES core excited states are involved in the RPES process so a simplification for the former might not be appropriate for the latter. An alternative explanation for the intensity variation within this $h\nu$ range can for example be given by vibrational modes coupled to the electronic transition. A detailed discussion of this issue is given in subsection 5.2.1.

A closer look at the PES detail map of Fig. 5.3(a) reveals an effect that could also influence the $h\nu$ dependent intensity variations of CIS spectra. The apparent peak maximum of all molecular orbital signals changes with $h\nu$ which results in a fraction of the intensity of these signals that is shifted out of the hatched area used for the integration. However, for the CIS 1 and the CIS 2 spectrum this effect is similarly present. A detailed investigation of this $h\nu$ dependent line-shape evolution in RPES will be given in the following section.

5.2 Photon energy dependent line-shape evolution of molecular orbital signals

The RPES study of $h\nu$ dependent intensity variations on the large $h\nu$ scale of the previous section revealed molecular signals which are energetically separable for a coronene multilayer. A detailed investigation of these frontier molecular orbital signals might lead to information that can be used for an analysis of dynamical CT. If these signals can be deconvoluted into a contribution which can be associated with CT and one without CT a quantitative CT investigation will be possible. The observed $h\nu$ dependent line-shape evolution in Fig. 5.3(a) could be a consequence of a contribution by a signal that disperses linearly to larger E_B with increasing $h\nu$ (constant E_K feature) and another signal that remains at constant E_B. The existence of a constant E_K feature in the RPES data of an organic multilayer sample would point towards intermolecular CT on the time scale of the core hole lifetime. This would be in strict contrast to the commonly used assumption that hybridization in a homo-molecular multilayer is negligible. However, in the special case of the transient phase in an NTCDA multilayer the existence of such an intermolecular interaction can be concluded from NEXAFS data [61, 161]. Hence this is generally also possible for other systems.

In the following the $h\nu$ dependent line-shape evolution of molecular orbital signals will be investigated in detail. First the continuous behavior of this effect is revealed for the CuPc HOMO signal and discussed in comparison to small molecules in the gas phase. It is found that the observed behavior of CuPc can be explained by an $h\nu$ dependent change in the relative intensity distribution within final state vibrational levels. The comparison of a CuPc multilayer with a SnPc multilayer shows a characteristic $h\nu$ dependent line-shape evolution of the HOMO signals of both molecules. Thereby the character of the involved potential energy surfaces is identified as the origin of the difference between the RPES data of these two molecules. The discontinuous $h\nu$ dependent line-shape evolution of the frontier molecular orbital signals of a coronene multilayer is then related to the discussion of the RPES data of CuPc and SnPc multilayer samples. Either the existence of multiple electronic transitions or the coupling of multiple vibrational modes is presented as an explanation for the RPES data of a coronene multilayer. In the second part of this section the influence of the adsorption on metal substrates on the $h\nu$ dependent line-shape evolution of molecular orbital signals is investigated. While no influence is found for SnPc molecules on Au(111) a quenching of the distribution of intensity into the high E_B part of the HOMO signal is observed for CuPc molecules on Au(111). For the coronene/Ag(111) interface a resonance specific influence of the adsorption is revealed with an increased intensity distribution into the high E_B part of the HOMO signal only in one NEXAFS resonance. The found variation of the $h\nu$ dependent line-shape evolution of molecular orbital signals in these systems is explained within the same set of parameters as the effect itself. Hence an influence by the adsorption on the character of the potential energy surfaces involved in the RPES process is identified as the most reasonable explanation for the observed differences of the metal-organic interfaces with respect to the corresponding multilayer samples. Finally, alternative explanations based

on molecule-metal interface CT on the time scale of the core hole lifetime are discussed for all investigated metal-organic interface systems.

5.2.1 Multilayer films

For π-conjugated molecules the effect of an $h\nu$ dependent line-shape evolution of molecular orbital signals in RPES has previously been reported in literature [123, 164] and is explained through electron vibration coupling. In Ref. [164] multilayers of C60 are investigated. A comparison of vibrational properties of the ball shaped C60 with the (almost) flat molecules investigated in this work appears difficult. The study of a SnPc multilayer and SnPc molecules on 1 ML PTCDA/Ag(111) in Ref. [123] on the other hand is definitely relevant for my work. In this study the $h\nu$ dependent line-shape evolution of the SnPc HOMO signal is explained by detuning of $h\nu$ from the electronic transition in NEXAFS spectroscopy. Such an influence on the vibrational progression of molecular orbital signals in RPES is observed for CO molecules [165]. The molecular orbital signal corresponding to large detuning has to be less intense than the one corresponding to vanishing detuning. In Ref. [123] the exact opposite is observed. Thus this effect can be excluded as a possible explanation for the $h\nu$ dependent line-shape evolution of the SnPc HOMO signal in Ref. [123].

I will start my investigation with the similar system of a CuPc multilayer. A comparison of the observations for CuPc and SnPc molecules is a promising approach in order to find an explanation for the $h\nu$ dependent line-shape evolution. In a first step RPES data is recorded for a CuPc multilayer on the large $h\nu$ scale in order to identify a region in the map in which an appropriate intensity enhancement for a significant line-shape analysis exists. In the second step this region is investigated in a subsequent RPES measurement with smaller $h\nu$ and E_B increments and higher E_K resolution. Especially the smaller $h\nu$ increment is important since it can be used to discuss the possibility of the contribution by several electronic transitions in the $h\nu$ region of interest.

In Fig. 5.4 the RPES data of a CuPc multilayer at the carbon K-edge is presented. In the PES overview map (Fig. 5.4(a)) the same contributions as discussed for the NTCDA multilayer in subsection 5.1.1 are present. In the case of a CuPc multilayer prepared at 300 K a stronger contribution of the Ag4d bands is observed due to the Stranski-Krastanow growth mode of the film. The NEXAFS resonances are identified with the CFS NEXAFS spectrum which is extracted from the black parallelogram in Fig. 5.4(a) and presented in Fig. 5.4(b). In the PES overview map a considerable increase of the intensity of the HOMO signal at $E_B \approx 2$ eV is observed in NEXAFS resonance B. Hence the region around this signal, which is bounded by the cyan box, is recorded in a subsequent measurement. The resulting PES detail map is presented in Fig. 5.4(c). Therein a continuous intensity variation of the HOMO signal becomes obvious. Approximately 100 meV below the maximum of the NEXAFS resonance B (red dashed line) the intensity of the HOMO signal increases and then decreases monotonically after the maximum. The first question which needs to be answered in order to discuss the observed $h\nu$ depen-

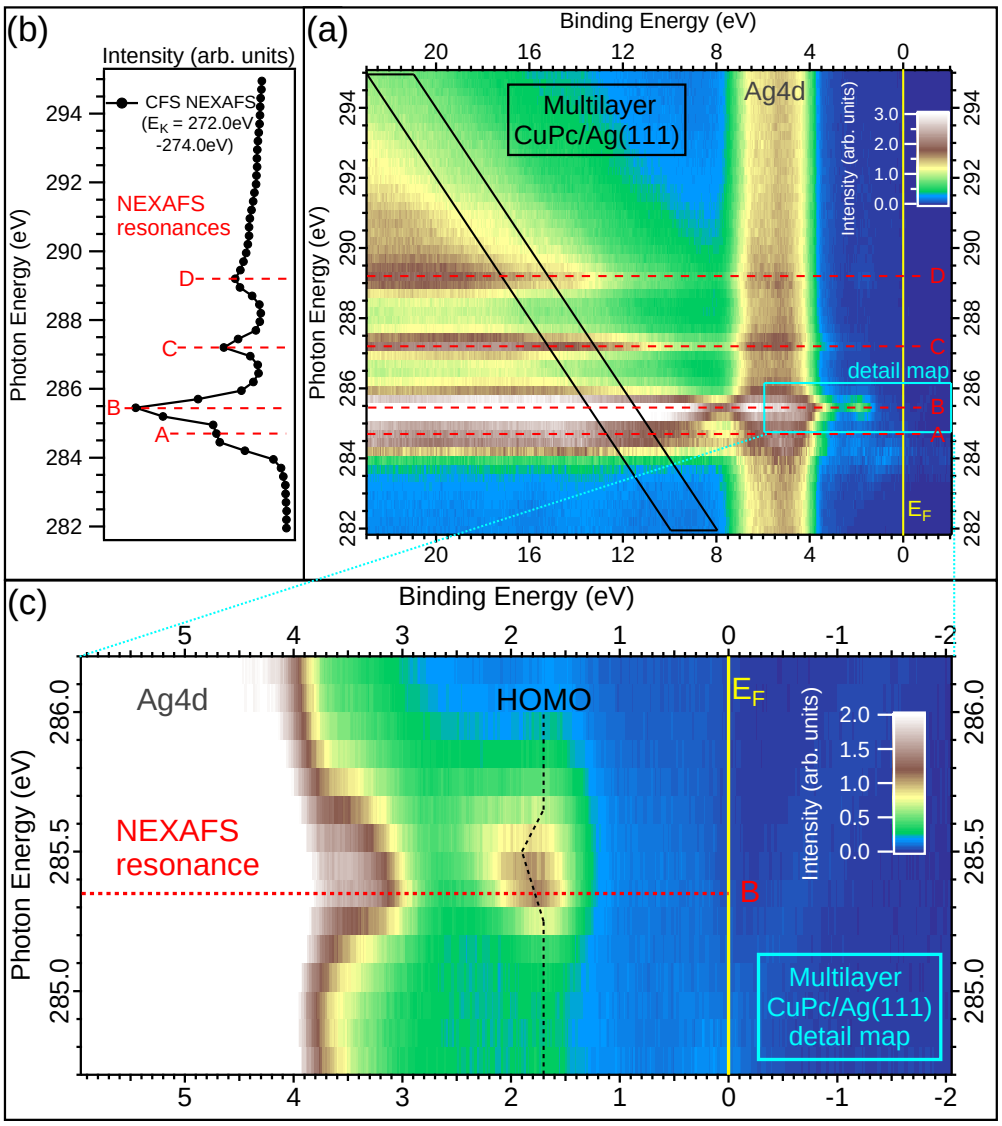

Figure 5.4: RPES data at the carbon K-edge of a multilayer of CuPc/Ag(111). **(a)** PES overview map with an $h\nu$ increment of 250 meV and an E_B increment of 50 meV. The red dashed horizontal lines denote the NEXAFS resonances. The black parallelogram marks the area from which this CFS NEXAFS spectrum originates. The yellow vertical line represents E_F. The cyan box denotes the area of the PES detail map shown in panel (c). The signal at $E_B \approx 1$ eV and $h\nu \approx 284$ eV is the second order carbon contribution. **(b)** CFS NEXAFS spectrum used for the identification of the NEXAFS resonances A–D. **(c)** PES detail map with an $h\nu$ increment of 100 meV and an E_B increment of 15 meV. The dashed black line is a guide to the eye which roughly represents the peak maximum of the HOMO signal.

dent intensity and line-shape evolution is how many and which electronic transitions are responsible for the emergence of the CuPc HOMO signal in this $h\nu$ region. In three different theoretical studies three different assignments of electronic transitions in NEXAFS resonance B of a CuPc molecule are reported [166–168]. Hence no definite conclusion can be drawn from these theoretical studies. Considering the continuous intensity variation of the HOMO signal it is either one single or multiple energetically very close lying electronic transitions in NEXAFS resonance B which then decay into a final state with a single hole in the HOMO. Several significantly separated electronic transitions should lead to several intensity maxima if all of them exhibit a measurable decay probability into the HOMO one-hole final state. Hence the following discussion will be based on one effective electronic excitation and deexcitation process which is responsible for the observed $h\nu$ dependence of the intensity of the HOMO signal.

For the discussion of the $h\nu$ dependent line-shape evolution of the CuPc HOMO signal the RPES data is presented in an EDC waterfall plot in Fig. 5.5(a). In the PES detail map a variation of E_B of the HOMO peak maximum with changing $h\nu$ is visible (black dashed line in Fig. 5.4(c)). However, small changes of the line-shape of the HOMO signal can only be observed in EDCs. The $h\nu$ dependent line-shape evolution of the CuPc HOMO signal in Fig. 5.5(a) can be characterized as a gradual redistribution of relative intensity into the high E_B part of HOMO signal. Thus the peak maximum first shifts towards higher E_B with increasing $h\nu$. Then the line-shape of the peak gets more and more asymmetric until it splits into two separate peaks in the three uppermost EDCs in Fig. 5.5(a). For the multilayer CuPc/Ag(111) the $h\nu$ dependent line-shape evolution of the HOMO signal is equal (within measurement accuracy) for the 300 K (filled black circles) and the 100 K (open green circles) data (see Fig. 5.5(a)). Hereby the spectra at the same position within NEXAFS resonance B are compared to each other. This means that the two EDCs at the resonance maximum are compared to each other and so on. In Fig. 5.5(a) a shift in $h\nu$ direction of 100 meV and a shift in E_B direction of 70 meV is observed between the 100 K and the 300 K EDCs. An error in the energy calibration can be excluded as a reason for these shifts since the off-resonant valence PES spectra ($h\nu = 120$ eV in Fig. A10) show the same difference in E_B for the CuPc HOMO signal. As mentioned in section 3.2 the CuPc film grows in a Frank-van-der-Merwe-like mode at 100K while it grows in a Stranski-Krastanow mode at 300 K. This difference in growth modes apparently leads to energetic shifts in the electronic transitions in NEXAFS spectroscopy and in the E_B position of the HOMO signal in RPES and direct valence PES. However, it has no influence on the mechanism responsible for the $h\nu$ dependent line-shape evolution of the HOMO signal. A direct comparison of the RPES data of the multilayer CuPc/Ag(111) (Fig. 5.5(a)) with the RPES data of the multilayer CuPc/Au(111) (green open circles in Fig. 5.5(b)) shows an equal $h\nu$ dependent line-shape evolution of the HOMO signals of all three films.

The observed $h\nu$ dependent line-shape evolution of molecular orbital signals can be discussed in comparison to small molecules in the gas phase [62, 63, 69, 70] (CO, N_2, O_2, and OCS). For these an $h\nu$ dependent excitation of vibrations coupled to the electronic transitions in the RPES process is observed and theoretically calculated (see subsection

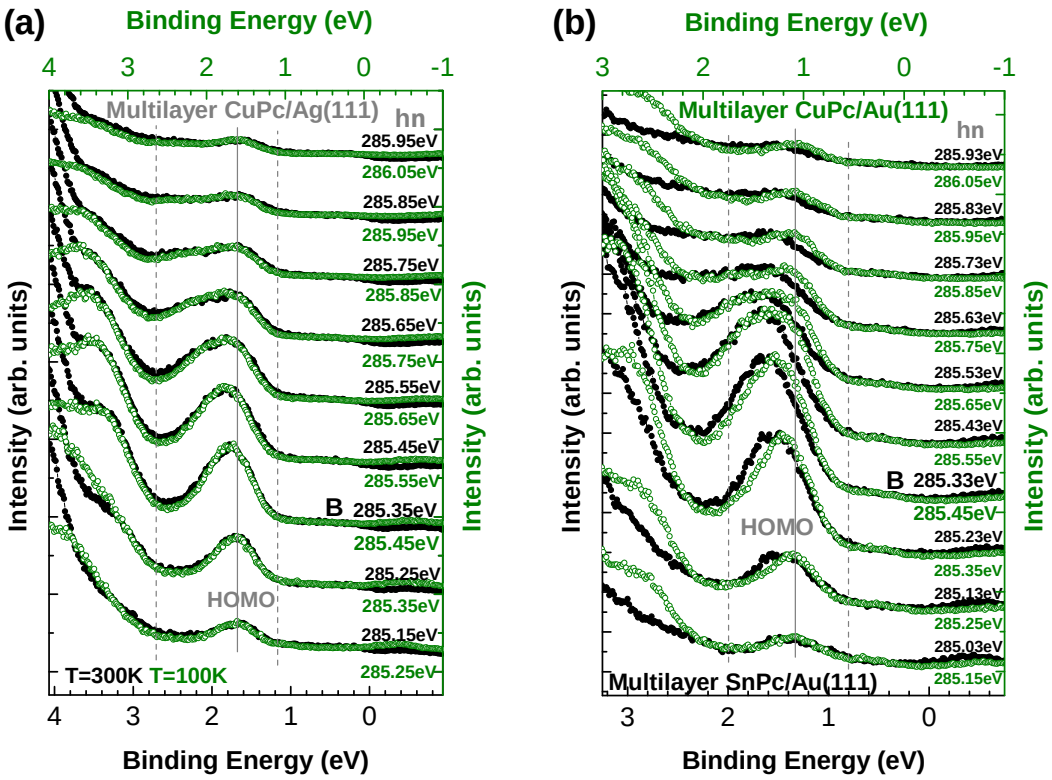

Figure 5.5: RPES data at the carbon K-edge of multilayer films of CuPc and SnPc molecules presented as EDCs in waterfall plots. The EDCs of equivalent $h\nu$ positions within the NEXAFS resonance B (resonance maximum denoted by the capital B) are compared to each other. The black axes (E_B and intensity) correspond to the black EDCs and the green axes to the green EDCs. The gray vertical dashed lines denote the E_B region in which the line-shapes are compared and the gray solid line marks E_B of the HOMO signal in direct valence PES. **(a)** Comparison of multilayer CuPc/Ag(111) at 300 K (filled black circles) and at 100 K (open green circles). The green E_B axis is shifted by -70 meV with respect to the black one. The intensities of the $T = 300$ K EDCs are unchanged while for each of the $T = 100$ K EDCs an offset was added for a matching pre-peak plateau (differently attenuated substrate signal) and a scaling factor for best comparability of the line-shape of the HOMO signal is applied. **(b)** Comparison of a multilayer of CuPc/Au(111) with a multilayer of SnPc/Au(111). The green E_B axis was shifted by -250 meV with respect to the black one. The intensities of the SnPc EDCs are unchanged while each of the CuPc EDCs is scaled for best comparability of the line-shape of the HOMO signal.

2.1.4). I choose the CO molecule for the discussion since this is the simplest system with a single and well separated electronic transition in NEXAFS spectroscopy and a single vibrational mode. In the electronic transition in NEXAFS spectroscopy a particular vibrational level ν_n of the intermediate state potential energy surface V_n is excited. The excitation of the this ν_n depends on $h\nu$ and the intensity of this transition is governed by its Franck-Condon factor. This electronic and vibrational intermediate state decays into an electronic and vibrational final state via autoionization. Depending on the excited ν_n different relative intensities are produced for the final state vibrational levels ν_f of the final state potential energy surface V_f. Again these intensities are governed by the Franck-Condon factors. For the CO molecule it is found that the higher the ν_n of the excitation into the V_n is the more relative intensity is observed in higher vibrational final state levels ν_f of the molecular orbital signals (see Fig. A11). The simple electronic and vibrational structure of the CO molecule allows to observe the different vibrational levels separately. If single final state vibrational levels overlap this effect will lead to a distribution of relative intensity into the high E_B part of the molecular orbital signal for larger $h\nu$. This is exactly the situation found for the CuPc HOMO signal in Fig. 5.5(a). Hence I conclude that the observed $h\nu$ dependent line-shape evolution can be explained by this electron vibration coupling effect.

For the CO molecule it is further found that the effect of lifetime vibrational interference is larger for higher ν_n [62, 69] (see Fig. A11(c) and (d)). In order to identify the importance of this effect for π-conjugated molecules actual calculations of the RPES process that include the multidimensional potential energy surfaces for the many vibrational modes are necessary. This is to my best knowledge not possible at this point. It can only be mentioned here that a change of the lifetime broadening of the vibrational levels can alter the $h\nu$ dependent line-shape evolution of molecular orbital signals. For O_2 molecules a much larger influence of this effect is observed with respect to N_2 and CO molecules (carbon K-edge measurements) [69]. This can be explained by the larger core hole lifetime of the O1s level and the resulting larger energetic overlap of the neighboring vibrational levels ν_n.

In Fig. 5.5(b) the $h\nu$ dependent line-shape evolution of the HOMO signal of a multilayer of CuPc/Au(111) (open green circles) and a multilayer of SnPc/Au(111) (full black circles) is presented. In the EDC of the lowest $h\nu$ the line-shape of both HOMO signals is equal (within measurement accuracy). At higher $h\nu$ the HOMO signals of both molecules evolve differently despite the similar electronic structure of both molecules. Especially the electron density distribution of the HOMO of CuPc is basically equal to the one of SnPc since the center metal atom does not contribute to it [125, 169]. Hence the different geometric structure of both molecules constitutes the basis for the most reasonable explanation of the observed difference. A deviation in the vibrational properties of the flat CuPc molecule with respect to the bent SnPc molecule (see Fig 3.1) is not surprising. Hence different potential energy surfaces are involved in the RPES process that leads to the HOMO one-hole final state. This results in a different $h\nu$ dependent line-shape evolution of the HOMO signal for both molecules. The explanation of the findings

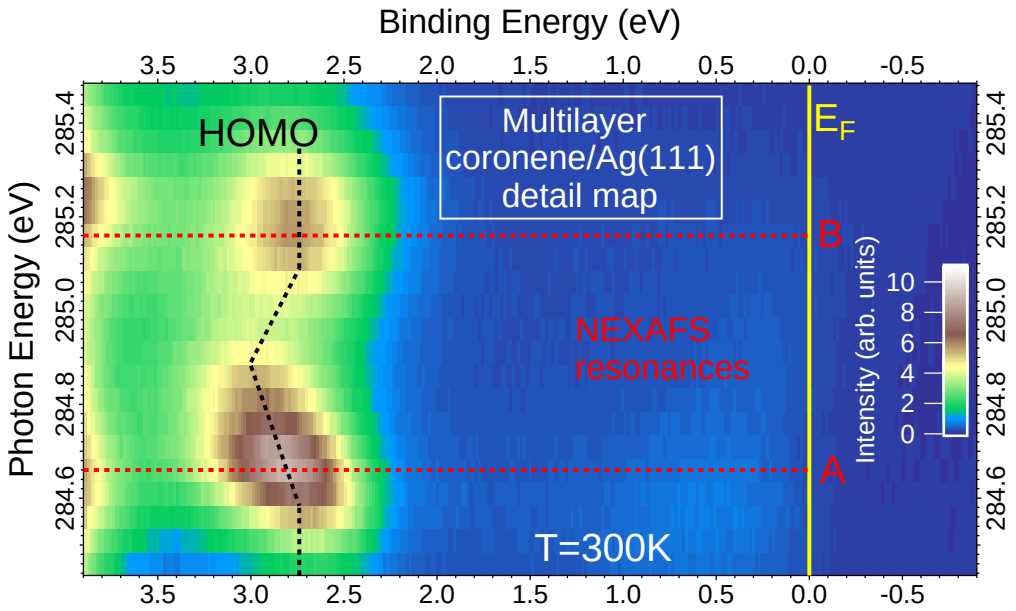

Figure 5.6: PES detail map of a multilayer coronene/Ag(111) at the carbon K-edge with an $h\nu$ increment of 50 meV and an E_B increment of 15 meV. The red dashed lines denote the NEXAFS resonance maxima A and B. The dashed black line is a guide to the eye which roughly represents the peak maximum of the HOMO signal.

of Fig. 5.5(b) agrees with the conclusion that the $h\nu$ dependent line-shape evolution is an effect of electron vibration coupling.

Comparing the $h\nu$ dependent intensity variation of a coronene multilayer in Fig. 5.3(a) with the one of a CuPc multilayer in Fig. 5.4(c) an obvious difference is observed. For the coronene multilayer the $h\nu$ dependent intensity is not continuous. This can be explained by the contribution of more than one electronic transition in this $h\nu$ region (see subsection 5.1.2). An alternative explanation can be given by the coupling of multiple vibrational modes to one electronic transition and to each other as it is for example the case for an H_2CO molecule [170]. Both situations are possible for the coronene molecule. NEXAFS calculations of a coronene molecule find one electronic transition in NEXAFS resonance A and another two in NEXAFS resonance B [163]. Moreover, the existence of multiple vibrational modes is obvious for a molecule of this size. Which of these vibrational modes couples strong enough to the electronic transitions in NEXAFS spectroscopy cannot be concluded without calculations that take molecular vibrations into account. These do, to my best knowledge, not exist at this point. The unknown origin for the $h\nu$ dependent intensity variation of a coronene multilayer has no consequence for the discussion of the $h\nu$ dependent line-shape evolution. In both cases a larger $h\nu$ leads to the excitation of higher ν_n and hence the same mechanism for the $h\nu$ dependent line-shape evolution of the molecular orbital signals. RPES investigations of small molecules reveal a discontinuous $h\nu$ dependent line-shape evolution of the molecular orbital signals for an H_2CO molecule [171] and an NO [172] molecule. The NEXAFS spectrum of the former has just been discussed. In the NEXAFS spectrum of the latter multiple electronic

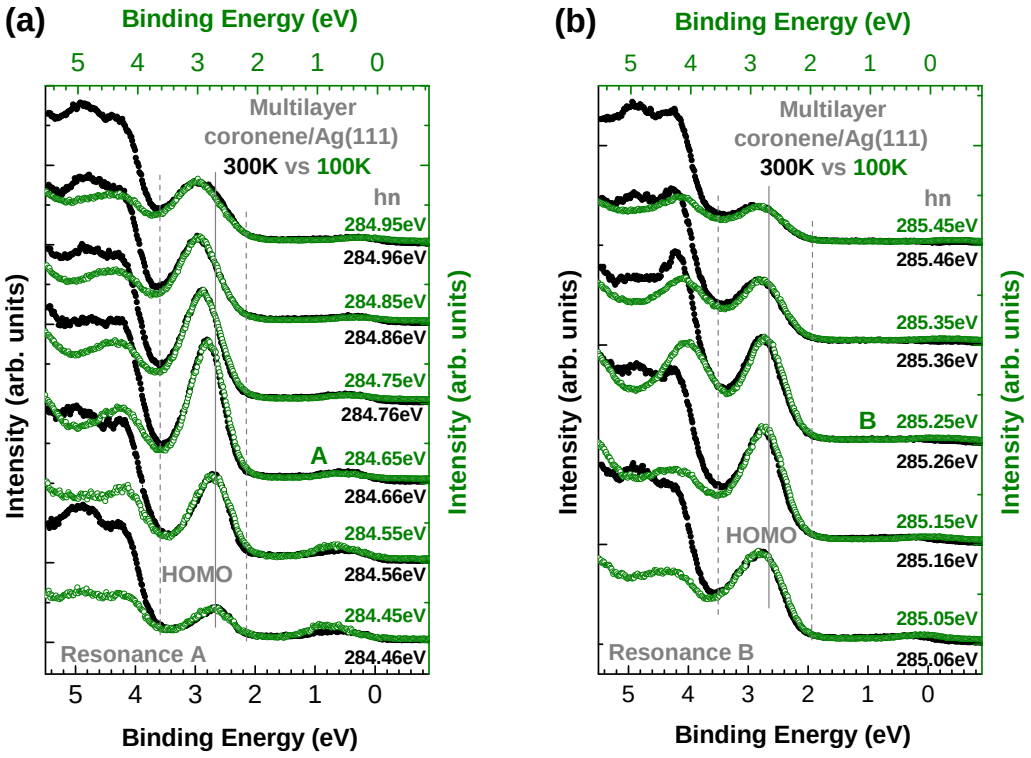

Figure 5.7: RPES data at the carbon K-edge of a multilayer of coronene/Ag(111) presented as EDCs in waterfall plots. The EDCs of equivalent $h\nu$ positions within the NEXAFS resonance (resonance maxima denoted by the capital letters) are compared to each other. The black axes (E_B and intensity) correspond to the black EDCs and the green axes to the green EDCs. The green E_B axis is shifted by 40 meV with respect to the black one. The intensities of the $T = 300$ K EDCs are unchanged while for each of the $T = 100$ K EDCs an offset is added for a matching pre-peak plateau (differently attenuated substrate signal) and a scaling factor for best comparability of the line-shape of the HOMO signal is applied. The gray vertical dashed lines denote the E_B region in which the line-shapes are compared and the gray solid line marks E_B of the HOMO signal in direct valence PES. **(a)** Comparison of two multilayer samples of coronene/Ag(111) at 300 K (filled black circles) and 100 K (open green circles) around NEXAFS resonance A. **(b)** Analogue comparison to panel (b) around NEXAFS resonance B.

transitions are present with the single vibrational mode of the NO molecule coupling to them. Hence from the comparison to small molecules a discontinuous $h\nu$ dependent line-shape evolution is expected for the molecular orbital signals. From Fig. 5.3(a) this behavior can be suspected. For a more detailed observation a smaller $h\nu$ increment is helpful. With that the continuous behavior within the NEXAFS resonances A and B can also be checked.

In Fig. 5.6 a PES detail map of a coronene multilayer is presented with an $h\nu$ increment of 50 meV. From this data the overall discontinuous intensity variation and the continuous intensity variation within the NEXAFS resonances A and B becomes obvious. Furthermore, the $h\nu$ dependent line-shape evolution of the HOMO signal also appears continuous within each of these two NEXFAS resonances. This can be concluded by the E_B variation of the peak maximum which is roughly represented by the black dashed line. For a detailed investigation of the line-shape of the HOMO signal the RPES data is again presented in an EDC waterfall plot in Fig. 5.7. Therein the observations of the PES detail map (Fig. 5.6) are confirmed. The $h\nu$ dependent line-shape evolution of the coronene HOMO signal in NEXAFS resonance A can be explained analogous to the CuPc and the SnPc HOMO signal. In between the NEXAFS resonances A and B the $h\nu$ dependent line-shape evolution of the HOMO signal is most probably a consequence of the overlap of the decreasing HOMO signal within NEXAFS resonance A and the increasing HOMO signal within NEXAFS resonance B. So the line-shape produced by the excitation of high ν_n in NEXAFS resonance A more and more transforms into the line-shape produced by the excitation of low ν_n in NEXAFS resonance B. This results in the shift of the maximum of the HOMO signal to lower E_B. Within NEXAFS resonance B less distribution of relative intensity into the large E_B region of the HOMO signal for larger $h\nu$ is observed with respect to NEXAFS resonance A. This can be explained by a difference in the intermediate state potential energy surface V_n. The observed difference between NEXAFS resonance A and B is similar for all visible molecular orbital signals in Fig. 5.3(a). This NEXAFS resonance specific behavior fits well with the assignment of V_n as the responsible origin since this quantity certainly is determined by the excitation. Additionally, the parallel $h\nu$ dependent line-shape evolution of the different molecular orbital signals points towards similar final state potential energy surfaces V_f. This is not surprising for different molecular orbitals that all exhibit mainly π-character.

The multilayer coronene/Ag(111) grown at 300 K shows Stranski-Krastanow growth while at 100 K a Frank-van-der-Merwe-like growth is found (see section 3.2). As observed for a CuPc multilayer in Fig. 5.5(a) this difference in the growth mode does not lead to a significant alteration of the $h\nu$ dependent line-shape evolution of the HOMO signal in the coronene multilayer data in Fig. 5.7. In conclusion the $h\nu$ dependent line-shape evolution of the molecular orbital signals of a coronene multilayer is in agreement with the discussed mechanism for a CuPc and a SnPc multilayer. Hence this effect can be explained by an $h\nu$ dependent variation of the relative intensity distribution among the final state vibrational levels ν_f for all these systems. In the following section the influence of the adsorption on a metal surface on this effect will be inves-

tigated for metal-organic interface systems without a LUMO signal in direct valence PES.

5.2.2 Influence of the adsorption on a metal surface

In the previous subsection the $h\nu$ dependent line-shape evolution of molecular orbital signals has been discussed in comparison to small molecules in the gas phase. Hence the observed effect has been related to properties of isolated molecules. A comparison of this effect for a multilayer sample with a sample of a sub-ML of the same molecule adsorbed on a metal substrate might reveal an influence of dynamical molecule-metal interface CT. In this case the distribution of additional relative intensity into the high E_B part of the molecular orbital signal is expected for the sub-ML film due to an additional or increased contribution by a constant E_K feature. At this point only metal-organic interface systems without a LUMO signal in direct valence PES are investigated since it will turn out in subsection 5.3.2 that RPES data of metal-organic interface systems with a LUMO signal in direct valence PES can hardly be compared to RPES data of multilayer samples.

EDC waterfall plots of RPES data of sub-ML samples of SnPc and CuPc molecules adsorbed on Au(111) in comparison to the corresponding multilayer RPES data are presented in Fig. 5.8. In Fig. 5.8(a) it is found that the $h\nu$ dependent line-shape evolution of the SnPc HOMO signal around NEXAFS resonance B is equal for a sub-ML on Au(111) and a multilayer film. For $E_B > 2$ eV a comparison of each of the two data sets in Fig. 5.8 is hindered by the different contribution of the Au5d signal. This signal is subtracted for the sub-ML films but due to possible subtraction artifacts no information can be extracted from the region with $E_B > 2$ eV. Within the dashed vertical lines no difference of the line-shape evolution (beyond measurement accuracy) of the SnPc HOMO signal can be found for the sub-ML on Au(111) with respect to the multilayer sample. Hence the most reasonable explanation is that the adsorption on Au(111) has no significant influence on the potential energy surfaces involved in the RPES process leading to the HOMO one-hole final state. Furthermore, no additional signatures that might be related to CT at the SnPc/Au(111) interface can be found in this region of the PES map (not shown). So if a constant E_K feature contributed to the observed $h\nu$ dependent line-shape evolution it would have to be equal for both SnPc films in Fig. 5.8(a). An alternative explanation with two contrary effects that cancel each other out is unlikely.

The comparison of the $h\nu$ dependent line-shape evolution of the CuPc HOMO signal for a multilayer and a sub-ML on Au(111) is shown in Fig. 5.8(b). Except for the EDC at lowest $h\nu$ a clear difference in the line-shape of the CuPc HOMO signal is observed. In the evolution of the line-shape of the CuPc HOMO signal less distribution of relative intensity into the high E_B part with increasing $h\nu$ is found for the sub-ML on Au(111) with respect to the multilayer film. So the influence of the adsorption on Au(111) on the line-shape evolution of the HOMO signal differs between CuPc and SnPc molecules. Apparently the potential energy surfaces of a CuPc molecule are more sensitive to the ad-

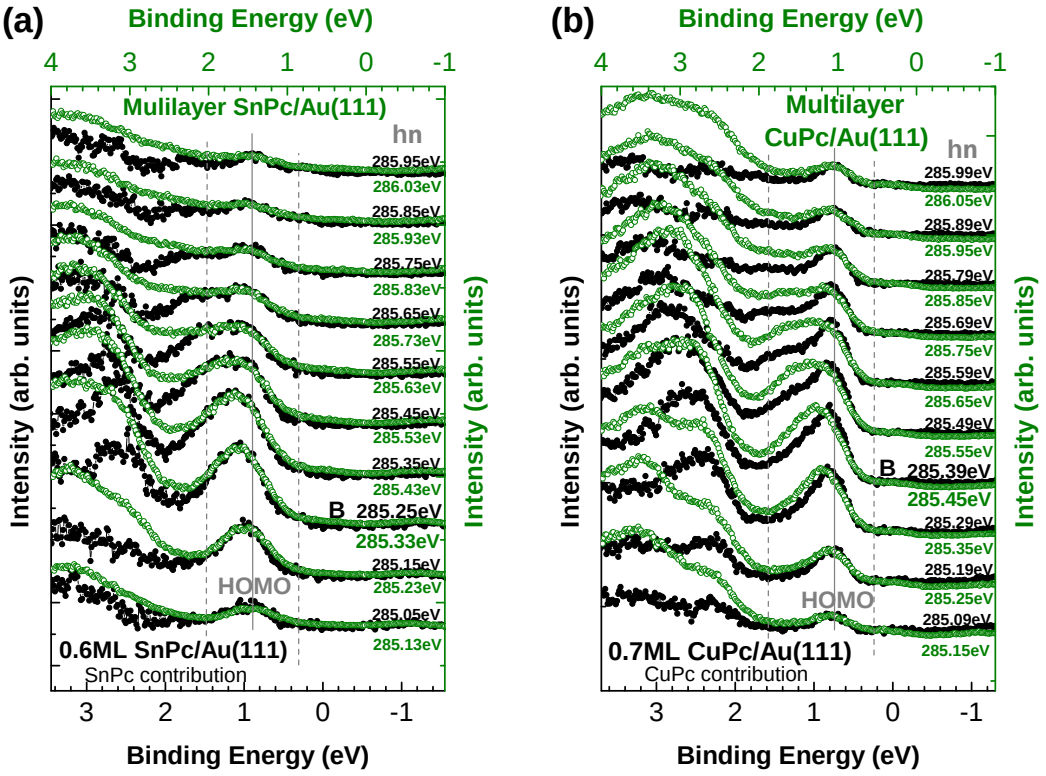

Figure 5.8: RPES data at the carbon K-edge of sub-ML of CuPc and SnPc molecules on Au(111) in comparison to the RPES data of the corresponding multilayer film presented as EDCs in waterfall plots. The EDCs of equivalent $h\nu$ positions within the NEXAFS resonance (resonance maxima denoted by the capital B) are compared to each other. The black axes (E_B and intensity) correspond to the black EDCs and the green axes to the green EDCs. For the sub-ML EDCs the scaled Au(111) substrate EDCs at equal $h\nu$ are subtracted and the intensities are unchanged. The gray vertical dashed lines denote the E_B region in which the line-shapes are compared and the gray solid line marks E_B of the HOMO signal in direct valence PES. **(a)** Comparison of 0.6 ML SnPc/Au(111) (filled black circles) with a multilayer SnPc/Au(111) (open green circles). The green E_B axis is shifted by 550 meV with respect to the black one. Each of the multilayer SnPc/Au(111) EDCs is scaled for best comparability of the line-shape of the HOMO signal. **(b)** Comparison of 0.7 ML CuPc/Au(111) (filled black circles) with a multilayer CuPc/Au(111) (open green circles). The green E_B axis is shifted by 300 meV with respect to the black one. To each of the multilayer CuPc/Au(111) EDCs an offset is added for a matching pre-peak plateau (clean Au(111) subtracted only for the 0.7 ML CuPc EDCs) and a scaling factor for best comparability of the line-shape of the HOMO signal is applied.

sorption on Au(111) than the ones of a SnPc molecule. To interpret this change between a CuPc multilayer and a sub-ML of CuPc on Au(111) as an influence of interface CT would lead to the conclusion that molecule-metal CT is quenched at the CuPc/Au(111) interface with respect to intermolecular CT in the CuPc multilayer film. This scenario appears unlikely.

In Fig. 5.9 the $h\nu$ dependent line-shape evolution of the coronene HOMO signal is compared for a sub-ML on Ag(111) and a multilayer. The EDC at lowest $h\nu$ is broader in the case of the multilayer. This is most probably due to increased inhomogeneity in the multilayer with respect to the sub-ML film. At higher $h\nu$ in the region around NEXAFS resonance A (Fig. 5.9(a)) the $h\nu$ dependent line-shape evolution of the HOMO signal is equal (within measurement accuracy) for both films. Hence the influence of the inhomogeneous broadening is overcome by the magnitude of this effect. In contrast to this finding in NEXAFS resonance A there is an increased distribution of relative intensity into the high E_B part of the coronene HOMO signal for the sub-ML film in NEXAFS resonance B. From the different behavior of the multilayer films in both NEXAFS resonances (see Fig. 5.7) a difference in the intermediate state potential energy surface V_n has been concluded. The difference in the influence of the adsorption on Ag(111) in Fig. 5.9 points towards a more sensitive V_n in NEXAFS resonance B. If this change by the adsorption on Ag(111) was interpreted as a consequence of molecule-metal interface CT a difference in the excited previously unoccupied molecular orbital in the two NEXAFS resonances would have to be responsible. How realistic this scenario is for a coronene molecule on Ag(111) cannot be concluded without calculations. However, the finding of a CT related state in both NEXAFS resonances in subsection 5.3.1 contradicts this scenario.

Comparing the differences in the $h\nu$ dependent line-shape evolution of molecular orbital signals in the molecule-metal interface systems without a LUMO signal in direct valence PES with respect to the corresponding multilayer samples for all molecules investigated in this subsection a significant influence of CT is unlikely. The fact that no influence is found for SnPc molecules on Au(111) and a quenching of CT would have to be concluded for CuPc molecules upon adsorption on Au(111) also makes an interpretation based on CT for the influence of the adsorption of coronene molecules on Ag(111) very questionable. On the other hand an interpretation with an influence on the potential energy surfaces by the adsorption allows me to explain the RPES data of multilayer and sub-ML samples in this section within the same effect and thus a common set of parameters. This contains all parameters which are necessary to characterize the potential energy surfaces included in the RPES process that leads to the particular final state. A consistent explanation for such a large data set is more reasonable than considering multiple effects that are only important for some systems.

The changes upon adsorption might also be related to lifetime vibrational interference since the adsorption on a metal surface is able to alter the lifetime broadening of valence orbital signals [59, 173]. Hence an influence on the core hole lifetime upon adsorption is generally also possible. However, the different influence of the adsorption on Ag(111) on different chemical C1s species in a coronene molecule requires a proper explana-

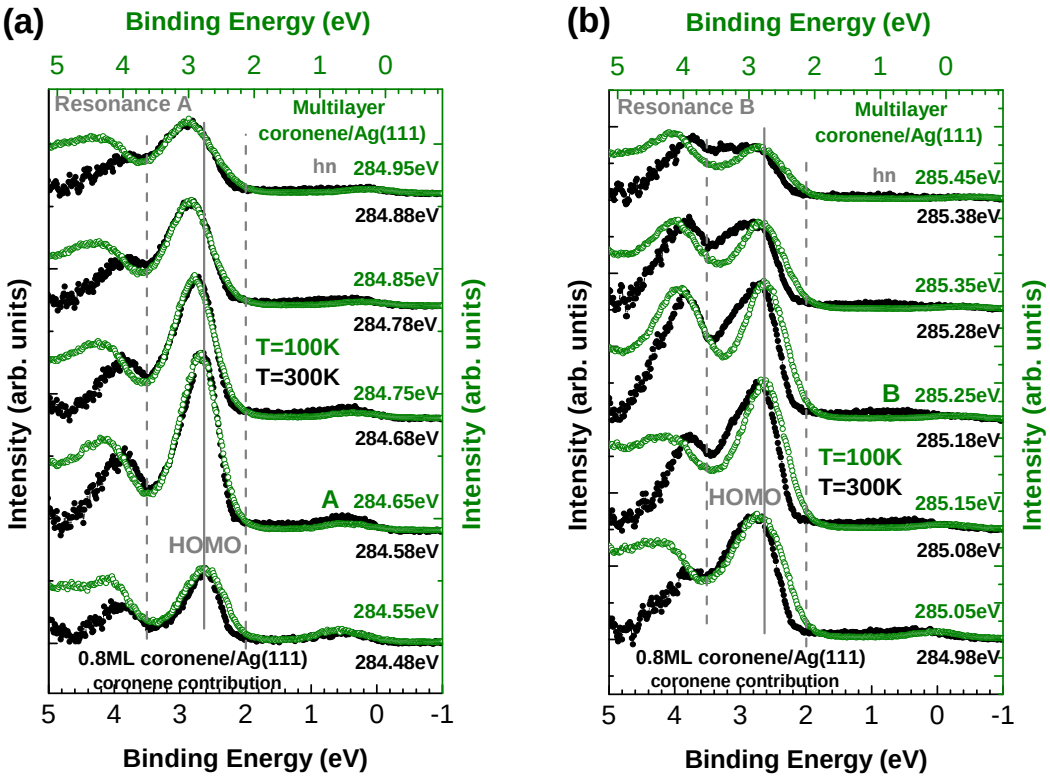

Figure 5.9: RPES data at the carbon K-edge of 0.8ML coronene/Ag(111) at 300 K (filled black circles) in comparison to multilayer coronene/Ag(111) at 100 K (open green circles) presented as EDCs in waterfall plots. The EDCs of equivalent $h\nu$ positions within the NEXAFS resonance (resonance maxima denoted by the capital letters) are compared to each other. The black axes (E_B and intensity) correspond to the black EDCs and the green axes to the green EDCs. The green E_B axis is shifted by 130 meV with respect to the black one. For the 0.8 ML coronene/Ag(111) EDCs scaled Ag(111) substrate EDCs at equal $h\nu$ are subtracted and the intensities are unchanged. Each of the multilayer coronene/Ag(111) EDCs is scaled for best comparability of the line-shape of the HOMO signal. The gray vertical dashed lines denote the E_B region in which the line-shapes are compared and the gray solid line marks E_B of the HOMO signal in direct valence PES. **(a)** $h\nu$ region of NEXAFS resonance A. **(b)** $h\nu$ region of NEXAFS resonance B.

tion. In any case calculations that are able to include the effect of lifetime vibrational interference would be necessary in order to justify an explanation of the data with this effect.

5.3 Revelation of charge transfer related features

Up to this point no features in the RPES data have been found which can be associated with dynamical CT across the molecule-metal interface. Differences with respect to the multilayer data have been observed for the $h\nu$ dependent line-shape evolution of molecular orbital signals in the RPES data of molecule-metal interface systems without a LUMO signal in direct valence PES. However, these differences have been explained by an influence of the molecule-metal interface on the potential energy surfaces involved in the RPES process. This explanation is favored since it allows to discuss a large data set with a single effect and within a common set of parameters. In the following I will look for features in the RPES data of metal-organic interfaces that are absent in multilayer samples. Such features are promising hints for a mechanism that includes molecule-metal interface CT in the generation of these final states in RPES since an involvement of metal states in the mechanism responsible for these features is quite likely.

In the first part of this section a metal-organic interface feature is found in the low E_B region of the PES detail map of a sub-ML of coronene on Ag(111). In a quantitative consistency check within the *Molecular Cluster Model* this feature is assigned to a satellite of the HOMO signal. Then the *Molecular Cluster Model* approach is translated into a multichannel model in which the involvement of interface CT in the mechanism responsible for the satellite feature is identified. Hence this feature is termed CT state. The emergence of such a CT state in an interface system without a LUMO signal in direct valence PES then motivates the search for similar features in the RPES data of interface systems with a LUMO signal in direct valence PES. An assignment of final states to the observed features, as for the CT state of coronene/Ag(111), is hindered by the overall broad line-shape in the E_B region of the frontier molecular orbital signals in these systems. Through the comparison to the line-shape of the CT state the relation of this broad line-shape to molecule-metal interface CT is discussed. Additionally, hints for possibly CT related constant E_K features are found for the interface systems with a LUMO signal in direct valence PES which leads to a closer investigation of the RPES data at larger $h\nu$. At these $h\nu$ constant E_K features are revealed for molecule-metal interface systems with and without a LUMO signal in direct valence PES. For the latter systems the assignment of the responsible mechanism is quantitatively confirmed by calculating the measured E_K of these constant E_K features on the basis of the assigned mechanism and some simplifying assumptions. The involvement of interface CT in the mechanism that produces the constant E_K features identifies these signals as an indicator for interface CT. Hence in this section three criteria for a qualitative CT analysis are identified. The emergence of a CT state, the observation of the characteristic broad line-shape of molecular orbital signals, and the appearance of constant E_K features in the high $h\nu$ region can be used

to confirm interface CT on the time scale of the core hole lifetime. According to these criteria the hetero-organic interface systems will be investigated with RPES in section 5.4.

5.3.1 The charge transfer state at the coronene/Ag(111) interface

The $h\nu$ dependent line-shape evolution of the coronene HOMO signal for a sub-ML of coronene/Ag(111) has been investigated in subsection 5.2.2. In the RPES data of this system a feature can be found that is absent in the multilayer data (Fig. 5.3(a)). In the EDC water fall plot of Fig. 5.9 and the PES detail map presented in Fig. 5.10(a) this additional feature is hardly visible. Only a closer investigation through an intensity zoom by a factor of 10 in the E_B range illustrated in Fig. 5.10(b) is able to reveal this feature at $E_B \approx 0.5$ eV. A comparison to the PES detail map of clean Ag(111) (Fig. 5.10(d)) shows that this low E_B feature is absent for the clean substrate. Even though the limits of the color code are set for a change of colors in the same range as in Fig. 5.10(b) no similar feature can be observed. The found change from yellow to brown in the lower $h\nu$ region of the map is quite noisy and most probably due to an upscaling of the diffuse PES background through the normalization procedure (see section 3.3). The CIS spectra extracted from the PES detail map of clean Ag(111) in the same E_B region as the hatched areas in Fig. 5.10(a) are presented with open symbols in Fig. 5.10(c). These CIS spectra corroborate the finding from the substrate PES detail map in Fig. 5.10(d) since they do not show an $h\nu$ dependence anyhow close to the one observed for the CIS spectra of 0.8 ML coronene/Ag(111) (filled symbols in Fig. 5.10(c)). Hence I can conclude that the low E_B feature originates from the metal-organic interface.

The two CIS spectra of the 0.8 ML coronene/Ag(111) film (filled symbols in Fig. 5.10(c)) show a very similar $h\nu$ dependent intensity variation. This means that the HOMO one-hole final state and the low E_B feature are most probably closely connected. The quite constant E_B position of the low E_B feature further points towards an energy conserving RPES process that leads to a one-hole final state which is responsible for this feature. So the low E_B feature could be produced by an excitation s in the sense of Eq. 2.5 of the HOMO one-hole final state and hence could be a HOMO signal satellite. Since this feature only exist at the metal-organic interface metal states must be involved in this excitation process. Interestingly this feature is not visible in direct valence PES at any point of the measured k-space [59, 121] (for exemplary EDCs of the data cube of Refs. [121] and [59] see Fig. A12). From this data the intensity of the low E_B feature can be estimated to be below 1% of the intensity of the HOMO signal in direct valence PES [143]. From the CIS spectra in Fig. 5.10(c) an intensity of the low E_B feature of approximately 5% of the intensity of the HOMO signal is found for RPES. Thus the low E_B feature is resonantly enhanced with respect to the HOMO signal.

As discussed in the introductory part of section 2.3 the *Molecular Cluster Model* constitutes a possible way to calculate satellite excitations. In the following treatment, which

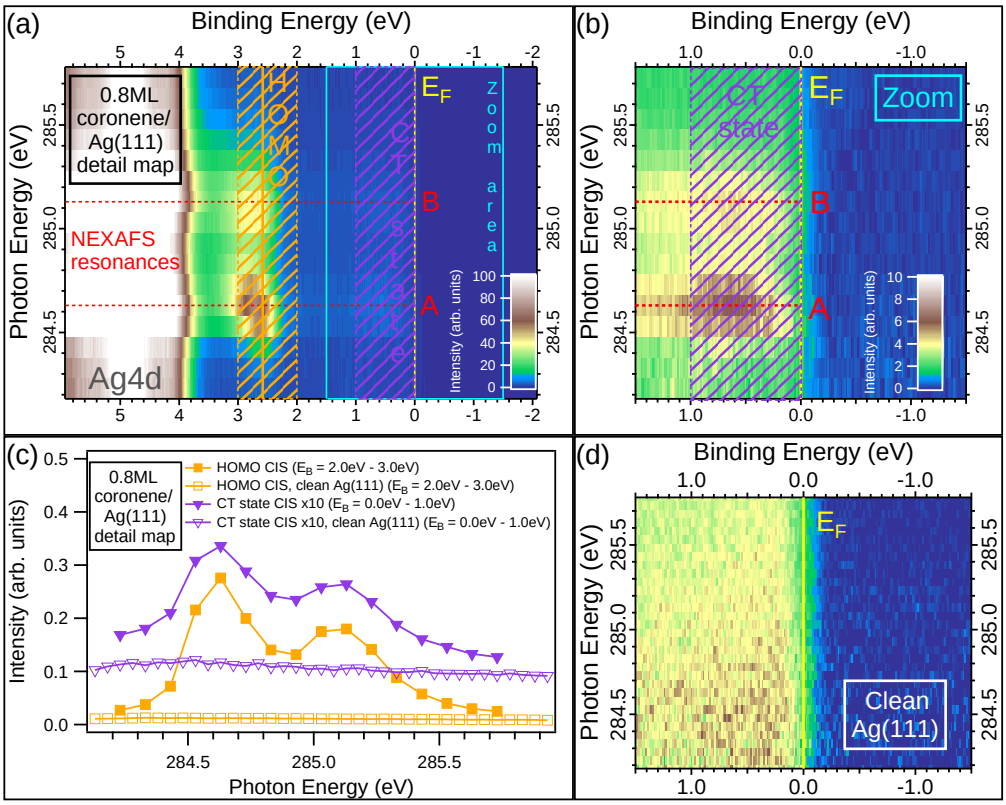

Figure 5.10: RPES data at the carbon K-edge of 0.8 ML coronene/Ag(111). **(a)** PES detail map with an $h\nu$ increment of 100 meV and an E_B increment of 15 meV. The red dashed horizontal lines denote the NEXAFS resonances. The hatched areas mark the E_B region from which the CIS spectra presented in panel (c) originate. The yellow vertical line represents E_F. The cyan box denotes the area of the PES detail map zoom shown in panel (b). The second order carbon contribution has been subtracted from this PES detail map. **(b)** PES detail map with a zoom of the intensity color code by a factor of 10. **(c)** CIS spectra extracted from panel (a) (filled symbols) in comparison to corresponding CIS spectra of the clean Ag(111) substrate (open symbols). The CIS spectra of the E_B region of the CT state (purple triangles) are multiplied by a factor of 10. **(d)** PES detail map of the clean Ag(111) substrate with an $h\nu$ increment of 50 meV and an E_B increment of 15 meV in the same area as the PES detail map zoom shown in panel (b). The color code is chosen to observe similar variations of colors as in panel (b).

has been introduced in section 2.3, this is explicitly demonstrated for PES, RPES and NEXAFS. Within this formalism I will test whether the low E_B feature can be explained by a HOMO signal satellite or not. For that I try to reproduce the experimentally obtained quantities with *Molecular Cluster Model* calculations with a physically reasonable set of parameters. The ability to obtain the measured quantities by these calculations serves as a quantitative consistency check for the assignment of the low E_B feature. From the direct valence PES data [59, 121] and the RPES data in Fig. 5.10 the following quantities can be extracted

$$\begin{aligned} \Delta E_{VPES,F,exp} = \Delta E_{RPES,F,exp} &= 2.1 \text{ eV} \\ IR_{VPES,exp} &< 0.01 \\ IR_{RPES,exp} &= 0.05 \end{aligned} \tag{5.1}$$

Hereby the subscript *exp* is used to state that these values are determined by experiments. The theoretical value of the energetic separation of the final states in direct valence PES ($\Delta E_{VPES,F,theo}$) and RPES ($\Delta E_{RPES,F,theo}$) is calculated with Eq. 2.24. For the calculation of the intensity ratio in valence PES ($IR_{VPES,theo}$) Eq. 2.27 is used in combination with Eq. 2.17 and Eqs. 2.22 and 2.23. In the case of RPES the intensity ratio $IR_{RPES,theo}$ is calculated with Eqs. 2.34, 2.35, and 2.36 in combination with Eq. 2.17 and Eqs. 2.22 and 2.33. In order to reproduce the measured quantities in Eq. 5.1 values for the *Molecular Cluster Model* parameters need to be inserted into these equations. For PES and RPES these are the differences of the single particle energies $\varepsilon_H - \varepsilon_M$ and $\varepsilon_L - \varepsilon_M$, the Coulomb parameters $U_{H,H}$ and $U_{H,L}$, the hopping matrix elements $V_{H,M}$ and $V_{L,M}$, and the autoionization weighting factor γ. Hence, seven more or less free parameters need to be chosen for the reproduction of three experimentally determined quantities. It is obvious that simplifying assumptions are necessary at this point for a more significant theoretical treatment of the system coronene/Ag(111). Thus I set the hopping matrix elements equal and connect the Coulomb parameters with γ. The latter simplification can be justified by the fact that the difference of the Coulomb parameters stems from the involvement of two equal molecular orbitals in $U_{H,H}$ and two different molecular orbitals in $U_{H,L}$. The same difference constitutes the justification for the introduction of γ which serves as a weighting factor for autoionization decays that include two different or two equal molecular orbitals. It is reasonable to assume that an overlap matrix element with two equal molecular orbitals is larger than the corresponding matrix element with two different ones (see subsection 2.3.6). With these simplifications I select parameters with which the experimentally determined values in Eq. 5.1 can be reproduced. It is important to emphasize at this point that the following choice of parameters is a possible way for a quantitative consistency check for the assignment of the the final states. It is not a significant extraction of quantitative values for the *Molecular Clus-*

ter Model parameters of the system coronene/Ag(111). The mentioned parameters are chosen as

$$\begin{aligned} \varepsilon_H - \varepsilon_M &= -2.6 \text{ eV} \\ \varepsilon_L - \varepsilon_M &= 0.7 \text{ eV} \\ V_{H,M} = V_{L,M} &= 0.1 \text{ eV} \\ U_{H,H} &= 4.7 \text{ eV} \\ U_{H,L} &= \frac{U_{H,H}}{\gamma} \\ \gamma &= 6 \end{aligned} \tag{5.2}$$

Hereby ε_H was set to be energetically below ε_M while ε_L is taken to be above ε_M. So the hopping of an electron from the state M to the state H (without considering the Coulomb parameters) leads to a gain in energy while the hopping from the state M to the state L costs energy. Inserting these parameters into the above summarized equations of the *Molecular Cluster Model* leads to the following theoretical values

$$\begin{aligned} \Delta E_{VPES,F,theo} = \Delta E_{RPES,F,theo} &= 2.1 \text{ eV} \\ IR_{VPES,theo} &= 0.000012 \\ IR_{RPES,theo} &= 0.046 \end{aligned} \tag{5.3}$$

This agreement between calculations and experiment shows that the *Molecular Cluster Model* is able to reproduce the experimentally found situation within reasonable assumptions and a physically possible choice of parameters. Through this the final states measured in RPES can be assigned. The HOMO signal is the state

$$\left|\Psi_{RPES,F,0}\right\rangle = \alpha_{RPES,F,0}\left|C^2H^1L^0M^n\right\rangle + \beta_{RPES,F,0}\left|C^2H^2L^0M^{n-1}\right\rangle \tag{5.4}$$

with the prefactors

$$\alpha^2_{RPES,F,0} = 0.998 \quad \text{and} \quad \beta^2_{RPES,F,0} = 0.002 \tag{5.5}$$

The low E_B feature is the HOMO signal satellite which is the state

$$\left|\Psi_{RPES,F,1}\right\rangle = \alpha_{RPES,F,1}\left|C^2H^1L^0M^n\right\rangle + \beta_{RPES,F,1}\left|C^2H^2L^0M^{n-1}\right\rangle \tag{5.6}$$

with the prefactors

$$\alpha^2_{RPES,F,1} = 0.002 \quad \text{and} \quad \beta^2_{RPES,F,1} = 0.998 \tag{5.7}$$

Hence both final states are a quantum mechanical superposition of the basis states without CT ($\left|C^2H^1L^0M^n\right\rangle$) and with CT ($\left|C^2H^2L^0M^{n-1}\right\rangle$) but the HOMO signal exhibits almost only the character of the state without CT while the HOMO signal satellite has almost entirely the character of the state with CT. Consequently, the HOMO signal satellite will be called CT state in the following.

Considering the mechanism which leads to the CT state it can also be interpreted as resonantly enhanced PES from the LUMO. The final state of the CT state has mainly the character of the basis state $\left|C^2H^2L^0M^{n-1}\right\rangle$. Since the PES process is described by the annihilation of one electron in the formalism of the *Molecular Cluster Model* this state can only be reached from the basis state $\left|C^2H^2L^1M^{n-1}\right\rangle$ in the initial state. Going directly from the state $\left|C^2H^2L^1M^{n-1}\right\rangle$ to the state $\left|C^2H^2L^0M^{n-1}\right\rangle$ is valence PES from the LUMO. The mechanism through an intermediate state with the same initial and final states leads to the resonant enhancement.

For a significant determination of *Molecular Cluster Model* parameters of a coronene molecule on Ag(111) more quantitative experimental information (e.g. intensity ratios and energetic separations of additional pairs of a main line and its satellite) would be necessary. Additionally, the *Molecular Cluster Model* parameters could be directly calculated and compared to the used set of parameters. This is beyond the scope of this work. Anyway, there is still some additional information in the RPES data that has not been used yet. From the CIS spectra of the HOMO signal and the CT state in Fig. 5.10 it is found that the $h\nu$ dependent intensity variation of both signals is very similar. Consequently, the energetic separation of the two final states of NEXAFS spectroscopy ($\Delta E_{NEX,F}$) must be very small since these two states are the intermediate states Z of the two different channels leading to the HOMO signal and the CT state. This quantity can be calculated with Eq. 2.15 in combination with Eq. 2.31. The theoretical intensity ratio in NEXAFS ($IR_{NEX,theo}$) can be calculated with Eq. 2.27 in combination with Eqs. 2.17, 2.22, and 2.31. For that the additional *Molecular Cluster Model* parameters $U_{L,L}$ and $U_{C,L}$ need to be chosen. Following the simplifications of Eq. 5.2 all Coulomb parameters with two equal molecular orbitals are taken to be of the same magnitude. Moreover, for the Cluster Model parameters in Ref. [105] the Coulomb parameter including a core level orbital is always larger than the corresponding Coulomb parameter with two valence orbitals (U_{dd} and U_{cd} in Table 7.1 in Ref. [105]). Hence the additional *Molecular Cluster Model* parameters are chosen as

$$\begin{aligned} U_{L,L} = U_{H,H} &= 4.7 \text{ eV} \\ U_{C,L} &= 7 \text{ eV} \end{aligned} \tag{5.8}$$

This results in

$$\begin{aligned} \Delta E_{NEX,F,theo} &= 0.20 \text{ eV} \\ IR_{NEX,theo} &= 1.2 \end{aligned} \tag{5.9}$$

The small theoretical energetic separation $\Delta E_{NEX,F,theo}$ of the two NEXAFS final states is in acceptable agreement with the situation of almost equal $h\nu$ of the maxima in the CIS spectra in Fig. 5.10(c). The theoretical intensity ratio $IR_{NEX,theo}$ of the NEXAFS final states cannot be verified or excluded by the NEXAFS data. The high resolution partial electron yield NEXAFS spectrum in this $h\nu$ range is displayed in Fig. 5.11(b). It could consist of many electronic transitions broadened by the excited molecular vibrations coupled to them. Hence two contributions for each electronic transition of roughly the same

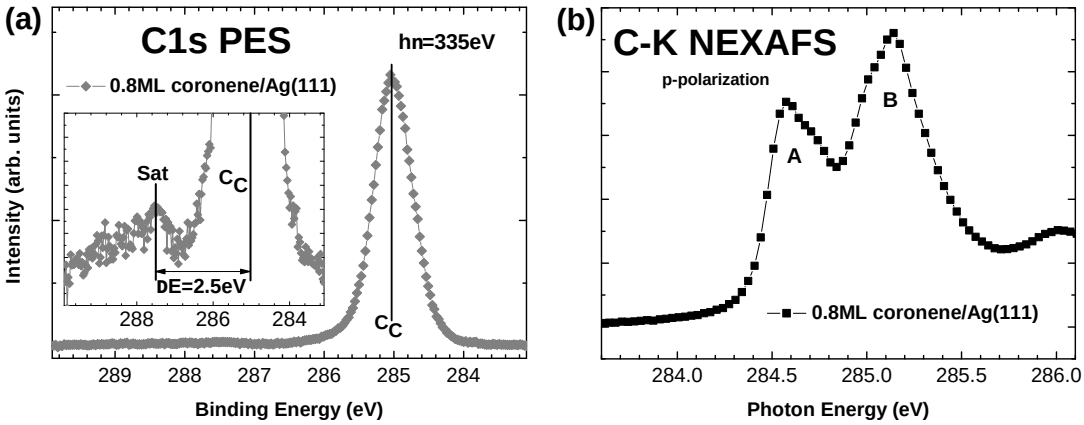

Figure 5.11: C1s core level PES and carbon K-edge NEXAFS data of 0.8 ML coronene/Ag(111). **(a)** C1s core level PES spectrum. The inset shows the spectrum scaled up in order to visualize the only visible satellite (Sat). **(b)** High resolution carbon K-edge partial electron yield NEXAFS spectrum in the $h\nu$ region of the NEXAFS resonances A and B.

magnitude are possible. An additional consistency check with the now complete set of *Molecular Cluster Model* parameters can be performed with the core level PES data. With the full parameter set the intensity ratio IR_{CPES} is calculated with Eq. 2.27 in combination with Eqs. 2.17, 2.22 and 2.29 to be

$$IR_{CPES,theo} = 235 \tag{5.10}$$

This means that the satellite is the only visible peak since this ratio is too large to observe the main peak. The C1s spectrum displayed in Fig. 5.11(a) does show one large peak and a satellite but this satellite is also visible in the multilayer data. Hence it cannot stem from a process including CT from the metal. The most reasonable explanation for this satellite in the multilayer and sub-ML data is an intramolecular shake-up excitation [108]. Such an excitation is not included in the chosen basis states and consequently no statement can be made about its intensity and energetic separation with respect to the main peak.

The additional information of the high resolution partial electron yield NEXAFS spectrum and the C1s core level PES spectrum is not of quantitative nature. Separable pairs of main peak and satellite in both spectra would be much more valuable information for testing the applicability of the *Molecular Cluster Model* to coronene/Ag(111). Furthermore, the restrictions for the choice of *Molecular Cluster Model* parameters would be much more strict and the chosen values that reproduce all data quantitatively correct could be regarded as significant. Hence, the applicability of the *Molecular Cluster Model* to coronene/Ag(111) is justified rather qualitatively. The assignment of a particular final state to the CT state is checked for consistency in a quantitative way but with

the large number of free parameters the significance of this approach remains questionable.

Describing the RPES process within the *Molecular Cluster Model* leads to a quite difficult interpretation of CT. The established model interprets CT as a process that can or cannot happen on the time scale of the core hole lifetime [9]. In the *Molecular Cluster Model* CT partially occurs in the ground state and from there different final states can be reached with certain probabilities that depend on the *Molecular Cluster Model* parameters. Each of the involved states is a quantum mechanical superposition of a basis state with CT from the metal ligand to a molecular orbital and one without. In the case of the final states of RPES given above one of the two parts hardly contributes due to its very small prefactor. Hence this negligible part can be dropped and the physics of the quantum mechanical superposition can be covered by considering several decay channels. Such a multichannel model is not quantitatively but qualitatively equal to the *Molecular Cluster Model*. Its advantage is that it is didactically superior to the rather complicated mathematical formalism presented in section 2.3.

In this multichannel model the CT state can be assigned through a simplified two step picture (named steps (a) and (b)) that describes coherent and energy conserving processes in separated channels (termed channels (I) and (II)). The difference between those two channels is given by including or excluding CT in the process leading to the intermediate state. Keeping the notation for the states and starting with the basis state without CT as a ground state the channel leading to the enhanced HOMO signal (denoted as channel (I)) can be written in the following way

$$\begin{aligned} &\text{(Ia)} \quad \left|C^2H^2L^0M^n\right\rangle + h\nu \xrightarrow[noCT]{NEXAFS} \left|C^1H^2L^1M^n\right\rangle \\ &\text{(Ib)} \quad \left|C^1H^2L^1M^n\right\rangle \xrightarrow{AI} \left|C^2H^1L^0M^n\right\rangle + e^- \end{aligned} \tag{5.11}$$

Hereby the text above the arrow denotes the process (autoionization (AI) or NEXAFS) that occurs in the particular step. Below the arrow it is explicitly stated whether CT takes place in the described step or not. In the same way I can write down an alternative channel (denoted as channel II) which includes CT in an intermediate state

$$\begin{aligned} &\text{(IIa)} \quad \left|C^2H^2L^0M^n\right\rangle + h\nu \xrightarrow[CT]{NEXAFS} \left|C^1H^2L^2M^{n-1}\right\rangle \\ &\text{(IIb1)} \quad \left|C^1H^2L^2M^{n-1}\right\rangle \xrightarrow{AI} \left|C^2H^1L^1M^{n-1}\right\rangle + e^- \\ &\text{(IIb2)} \quad \left|C^1H^2L^2M^{n-1}\right\rangle \xrightarrow{AI} \left|C^2H^2L^0M^{n-1}\right\rangle + e^- \end{aligned} \tag{5.12}$$

This channel can lead to two different final states ((1) and (2)) through autoionization (AI) which both could lead to the CT state in RPES. In this multichannel model the observed relative resonant enhancement of the CT state with respect to the HOMO signal can be used to decide which of these final states corresponds to the CT state. The probability for the responsible step must be larger than the one for step (Ib) since this leads to the HOMO signal. In step (IIb1) the same orbitals (C, H and L) are included in the

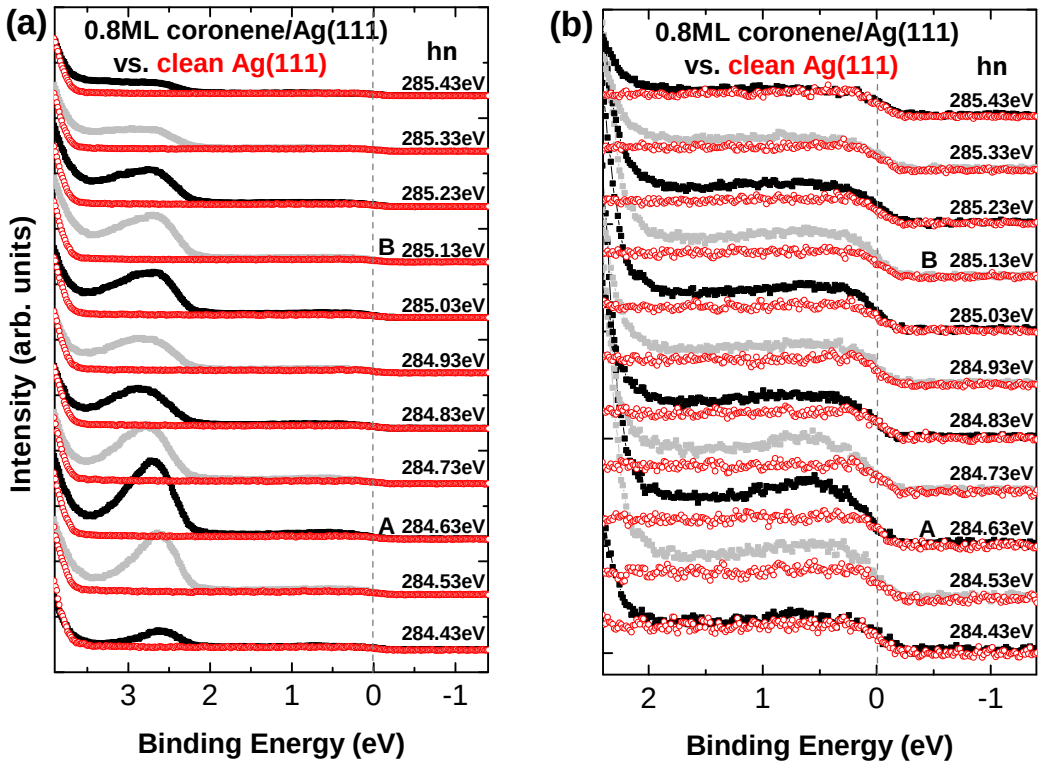

Figure 5.12: RPES data at the carbon K-edge of 0.8 ML coronene/Ag(111) compared to clean Ag(111) at the same $h\nu$ presented in EDC waterfall plots. The second order carbon contribution has been subtracted from these EDCs. Both sets of EDCs are normalized. The EDCs of the clean Ag(111) are multiplied by one common factor for matching EDCs at $h\nu = 285.43$ eV. **(a)** EDCs of the PES detail map shown in Fig. 5.10. **(b)** Same EDCs as in panel (a) scaled up for a comparison of the CT state with the clean Ag(111).

autoionization decay as in step (Ib). Hence an increased probability of step (IIb1) with respect to step (Ib) is unlikely. On the other hand in step (IIb2) the state L is included twice in the autoionization decay which justifies the assumption of an increased probability with respect to step (Ib). With the same line of arguments the weighting factor γ is introduced in the *Molecular Cluster Model*. Consequently, the observed relative resonant enhancement of the CT state allows me to assign the final state $\left|C^2H^2L^0M^{n-1}\right\rangle$ to this signal.

At this point it is interesting to analyze the CT state in more detail. Since this state is produced through molecule-metal interface CT electronic interaction at this interface is involved in the responsible mechanism. Hence the line-shape of this state should also exhibit spectroscopic signs for electronic interaction. As usual the analysis of the line-shape of a signal in RPES is performed with an EDC waterfall plot. In Fig. 5.12(a) the coronene/Ag(111) EDCs are compared to the EDCs of the clean Ag(111) substrate at the same $h\nu$ on the intensity scale of the HOMO signal. On this scale there is hardly any deviation visible between the clean Ag(111) and the coronene/Ag(111) film in the

E_B region around 0.5 eV. Enhancing the intensity scale in this E_B region in Fig. 5.12(b) reveals an obvious difference. It is important to note at this point that the second order C1s contribution has been subtracted from the coronene/Ag(111) EDCs (see section 3.3). Furthermore, the clean Ag(111) ECDs are normalized with the same procedure as the coronene/Ag(111) EDCs. After that all clean Ag(111) EDCs have been scaled with a common factor so that the EDCs of the clean Ag(111) and the 0.8 ML coronene/Ag(111) film match at $h\nu = 285.43$ eV. Thus the additional intensity found for the coronene/Ag(111) EDCs in fact stems from the metal organic interface. Around the resonance maximum of NEXAFS resonance A the CT state exhibits a peak-like character but this peak is situated on top of a broad intensity background. At different $h\nu$ only this broad line-shape is observed. For all other molecular orbital signals of metal-organic interfaces without a LUMO signal in direct valence PES this has not been observed. Especially the comparison of the line-shapes of the CT state with the coronene HOMO signal reveals the different character of the former. Relating this so far unique line-shape to the electronic interaction involved in the mechanism that leads to the CT state appears reasonable. The fact that the CT state is produced in a coherent and energy conserving process suggests that the character of the origin of the transfered electron might be visible in the line-shape of the CT state. So a possible explanation for the broad line-shape of the CT state is that the intensity distribution over a broad E_B range of the Ag(111) s-p bands is imprinted in the line-shape of this state. This means that the transfer of an electron from the energetically broad s-p band results in an energetic broadening of the observed CT state. Since in this explanation M in (IIa) of Eq. 5.12 does not have a discrete ε_M it would be in contrast to the assumptions made in the *Molecular Cluster Model* in which the metal ligand electrons are treated to be of such a discrete energy ε_M. Thus the quantitative values used for the *Molecular Cluster Model* parameters must be interpreted carefully. The possible explanation of the line-shape of the CT state demonstrates the limits of the assumptions of the *Molecular Cluster Model*. However, this model serves as an important attempt for a comprehensive understanding of PES, NEXAFS and RPES on a well defined mathematical basis even though not all of its assumption may be fully justified.

In conclusion the low E_B feature is assigned to the final state $\left|C^2H^2L^0M^{n-1}\right\rangle$ by the multichannel model. In the *Molecular Cluster Model* the assigned final state exhibits mainly this same character. In both formalisms CT from the metal state M to the molecular orbital L is involved in the mechanism that produces this molecule-metal interface feature. Hence this low E_B feature is termed CT state. So according to the established model [9] CT on the timescale of the core hole lifetime is possible for the interface system coronene/Ag(111). The fact that in direct valence PES no LUMO signal is observed for this molecule-metal interface system demonstrates the possibility of interface CT in RPES for these systems. Thus CT features could also be present for the other interface systems without a LUMO signal in direct valence PES. In the region of the PES detail map an interface originated feature, such as the CT state, is not observed for SnPc/Au(111) and CuPc/Au(111) but in different regions of the PES overview map CT related features could be present. However, in interface systems with a LUMO sig-

nal in direct valence PES CT related features in RPES, similar to the one found for coronene/Ag(111), are expected since these systems show a molecule-metal interface CT originated feature (the LUMO signal) already in direct valence PES. The observed line-shape of the CT state demonstrates the involvement of electronic interaction which is expected to be increased in the interface systems with a LUMO signal in direct valence PES. So the E_B region of the frontier molecular orbitals of these systems will be investigated by RPES in the following subsection.

5.3.2 Charge transfer signatures in the valence region

In Ref. [174] the interface system 1 ML SnPc/Ag(111), for which a LUMO signal is detected in direct valence PES [83], is investigated with RPES. In comparison to the direct valence PES spectrum additional features are observed in the RPES EDCs. Due to the relatively large $h\nu$ increment of 250 meV the $h\nu$ dependence of the E_B position of these additional features cannot be extracted from this RPES data. Generally a broad line-shape is observed for the molecular orbital signals of 1 ML SnPc/Ag(111) in RPES which for some $h\nu$ resemble a step-function. Compared to the line-shape of the CT state of coronene/Ag(111) this finding could be discussed with an increased visibility of the energetically broad character of the Ag(111) s-p bands that is imprinted in the line-shape of the molecular orbital signals in the RPES data of 1 ML SnPc/Ag(111). However, in order to be able to draw a conclusion the comparison to RPES data of other interface systems with a LUMO signal in direct valence PES is necessary. Furthermore, a smaller $h\nu$ increment could permit an investigation of the $h\nu$ dependence of the E_B position of signals which are absent in the corresponding direct valence PES spectrum. Additionally, the comparison of multiple interface systems with a LUMO signal in direct valence PES with each other also allows a systematic search for any sort of differences in RPES with respect to direct valence PES.

In Fig. 5.13 the RPES data of an ML NTCDA/Ag(111) is presented in EDC waterfall plots in the $h\nu$ region around NEXAFS resonance B (Fig. 5.13(a)) and NEXAFS resonance C (Fig. 5.13(b)). The CFS NEXAFS spectrum which shows the $h\nu$ regions corresponding to these NEXAFS resonances is displayed in Fig. 5.14(a). Although differently localized electronic transitions are assigned to these two NEXAFS resonances (see for example Ref. [161]) the overall behavior of the molecular orbital signals is found to be quite similar. In both NEXAFS resonances the HOMO and the LUMO signal are resonantly enhanced and a broad line-shape is found for both. In NEXAFS resonance C the enhancement of the LUMO signal with respect to the HOMO signal is less pronounced. Hence the local character of the electronic transition in NEXAFS spectroscopy and its consequences for the intensity of molecular orbital signals in RPES (see Ref. [81] and discussion in subsection 5.1.1) is qualitatively retained at the molecule-metal interface with a LUMO signal in direct valence PES. The comparison of the RPES EDCs with the direct valence PES data ($h\nu = 120$ eV) reveals additional intensity between the E_B positions of the HOMO and the LUMO signal for the RPES EDCs. Since there is no molecular orbital that lies energetically between the HOMO and the LUMO a feature

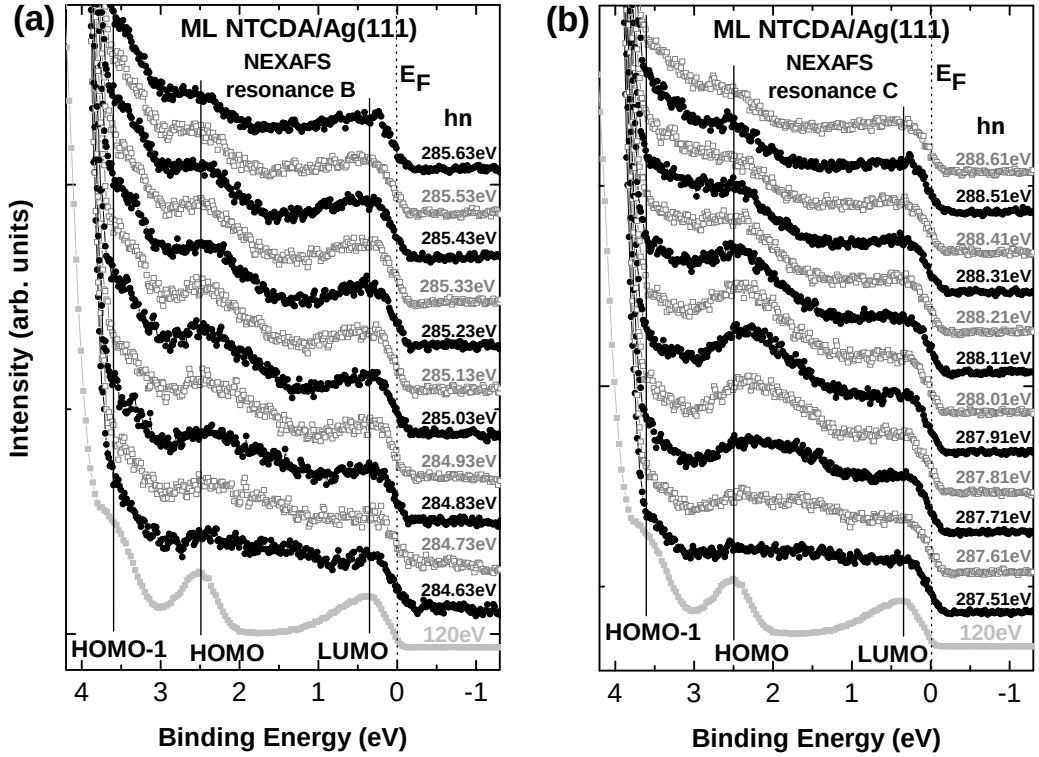

Figure 5.13: RPES data at the carbon K-edge of an ML NTCDA/Ag(111) in comparison to direct valence PES data at $h\nu = 120$ eV. The presented EDCs stem from the PES detail maps shown on an E_K scale in Fig. 5.14(b) and (c). The vertical lines denote the E_B positions of the molecular orbital signals in direct valence PES. The dashed vertical line represents E_F. **(a)** EDCs in the $h\nu$ region around NEXAFS resonance B. **(b)** EDCs in the $h\nu$ region around NEXAFS resonance C. For a CFS NEXAFS spectrum defining those resonances see Fig. 5.14(a).

found at this E_B position cannot stem from a resonantly enhanced molecular orbital one-hole final state. In order to produce such a feature some mechanism of energy dissipation must be involved. The onset of the intensity between the HOMO and the LUMO signal disperses roughly linear to higher E_B with increasing $h\nu$ in both resonances. Within the $h\nu$ region around NEXAFS resonance C in the EDC at $h\nu = 287.61$ eV a broad peak structure can be found at $E_B \approx 1.5$ eV. At higher $h\nu$ this feature cannot be separated from the HOMO signal. These experimental findings point towards a feature that disperses with constant E_K between the E_B position of the HOMO and the LUMO signal.

Investigating the same data in a PES detail map on an E_K scale ($E_K = h\nu - E_B$) facilitates the detection of a constant E_K feature. In Fig. 5.14(b) and (c) a change in the color code from green to yellow can be found which roughly remains at constant E_K. This possible onset of a constant E_K feature is marked by the red dashed line. In both PES detail maps the energy position of the HOMO signal is indicated by the blue dashed line. With

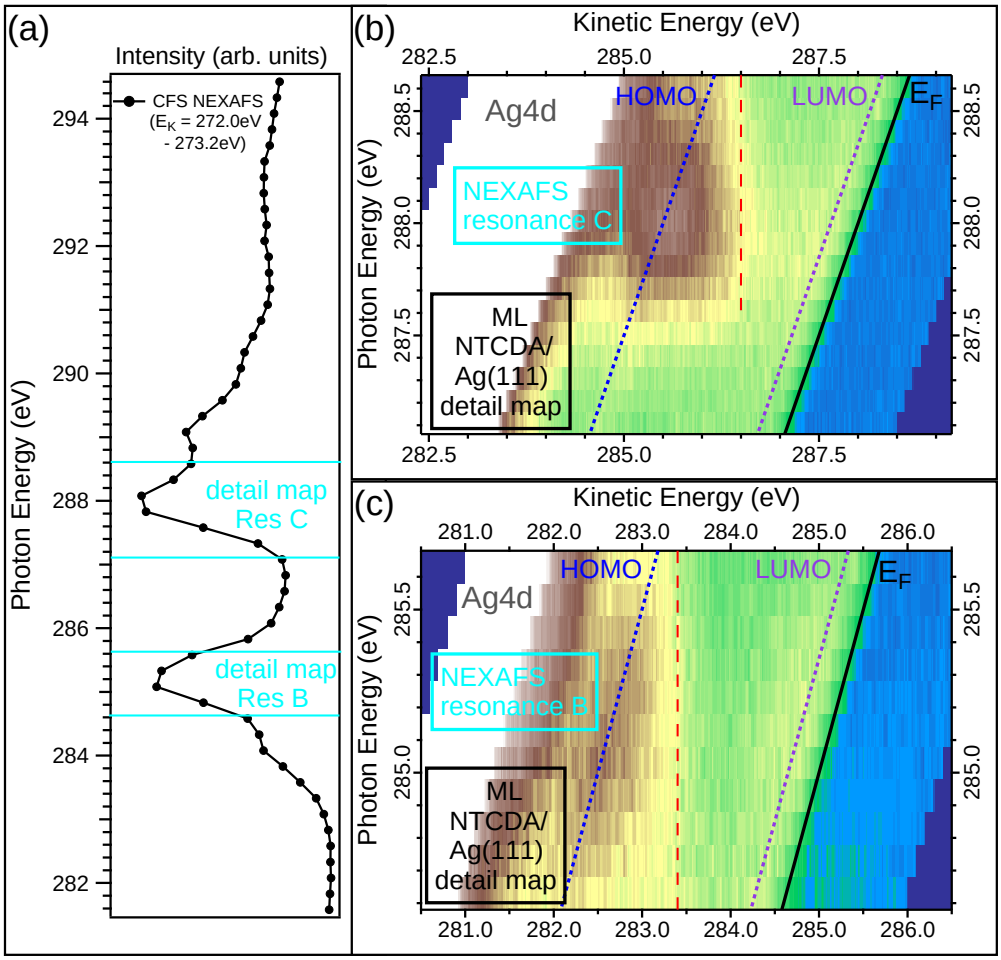

Figure 5.14: RPES data at the carbon K-edge of an ML NTCDA/Ag(111). **(a)** CFS NEXAFS spectrum extracted from a PES overview map with an $h\nu$ increment of 250 meV. The cyan lines denote the $h\nu$ region of the PES detail maps presented in panels (b) and (c). The assignment of the NEXAFS resonances follows the RPES data of the NTCDA multilayer in Fig. 5.1. **(b)** PES detail map with an $h\nu$ increment of 100 meV and an E_B increment of 15 meV in the $h\nu$ region around NEXAFS resonance B. The red dashed vertical line denotes a possible onset of a constant E_K feature. The black line represents E_F. The dashed blue and purple lines mark the E_B position in direct valence PES of the HOMO and the LUMO signal, respectively. **(c)** Analogue PES detail map in the $h\nu$ region around NEXAFS resonance C.

increasing $h\nu$ this signal shifts closer to the possible onset of a constant E_K feature so that both gradually merge with each other. This energetic overlap of the signals makes the detection of the constant E_K feature difficult but the $h\nu$ dependent line-shape evolution of the EDCs in Fig. 5.13 together with the apparent onset at constant E_K in the PES maps provides adequate evidence for its existence.

A possible explanation for a constant E_K feature between the HOMO and the LUMO signal can be given by an Auger-like autoionization decay. Since $h\nu$ is way below the core level ionization potential in both PES detail maps such a non energy conserving process most probably involves CT from the molecule to the metal. In contrast to the CT state in coronene/Ag(111) the electron is transfered from a molecular orbital into the metal substrate. Thereby it has to be delocalized into the metal and not transfered into the ligand state M since it must not influence E_K of the emitted electron produced by autoionization which leads to the constant E_K feature. In the notation used in the previous subsection a possible mechanism leading to such a constant E_K feature can be presented. Considering a ground state for a ML NTCDA/Ag(111) that exhibits mainly the character of the state $\left|C^2H^2L^1M^{n-1}\right\rangle$ the final state of the LUMO signal in direct valence PES is $\left|C^2H^2L^0M^{n-1}\right\rangle$. Analogously the final state of the HOMO signal in direct valence PES is $\left|C^2H^1L^1M^{n-1}\right\rangle$. The final states in RPES for the HOMO and the LUMO signal are the same ones. A constant E_K feature that is situated energetically between those two final states could for example be the final state $\left|C^2H^2L^0M^{n-2}\right\rangle$ which could be produced through autoionization from the intermediate state $\left|C^1H^2L^2M^{n-2}\right\rangle$. In a process that needs to include the delocalization of the excited electron into the metal substrate such an intermediate state could be produced either by assuming a ground state $\left|C^2H^2L^2M^{n-2}\right\rangle$ or starting from the ground state $\left|C^2H^2L^1M^{n-1}\right\rangle$ and including CT from the state M to L in the process.

The fact that not even the occupancy of the LUMO in the ground state is known for an ML NTCDA/Ag(111) demonstrates the speculative character of this possible explanation. Moreover, the consequence of an apparent partial LUMO filling in direct valence PES for the RPES process is unknown. A direct comparison of a system for which the LUMO signal in direct valence PES is entirely below the Fermi energy (E_F) with a system for which this signal is cut by E_F should lead to some valuable information for the understanding of RPES applied to such molecule-metal interfaces. The direct valence PES data illustrated in Fig. 2.2(b) reveals that PTCDA molecules adsorbed on different Ag surfaces can be employed for such a comparison. By selecting 1 ML PTCDA/Ag(111) and the 1 ML herringbone PTCDA/Ag(110) for an RPES study two systems with the same molecule and roughly the same geometric structure are compared to each other. At the same time the former system exhibits a LUMO signal which is cut by E_F while the LUMO signal of the latter is situated entirely below E_F. So the combination of these two systems is ideal for the desired comparison.

For this comparison of the behavior of the frontier molecular orbital signals in $h\nu$ regions around NEXAFS resonances cutouts of PES overview maps of 1 ML PTCDA/Ag(111)

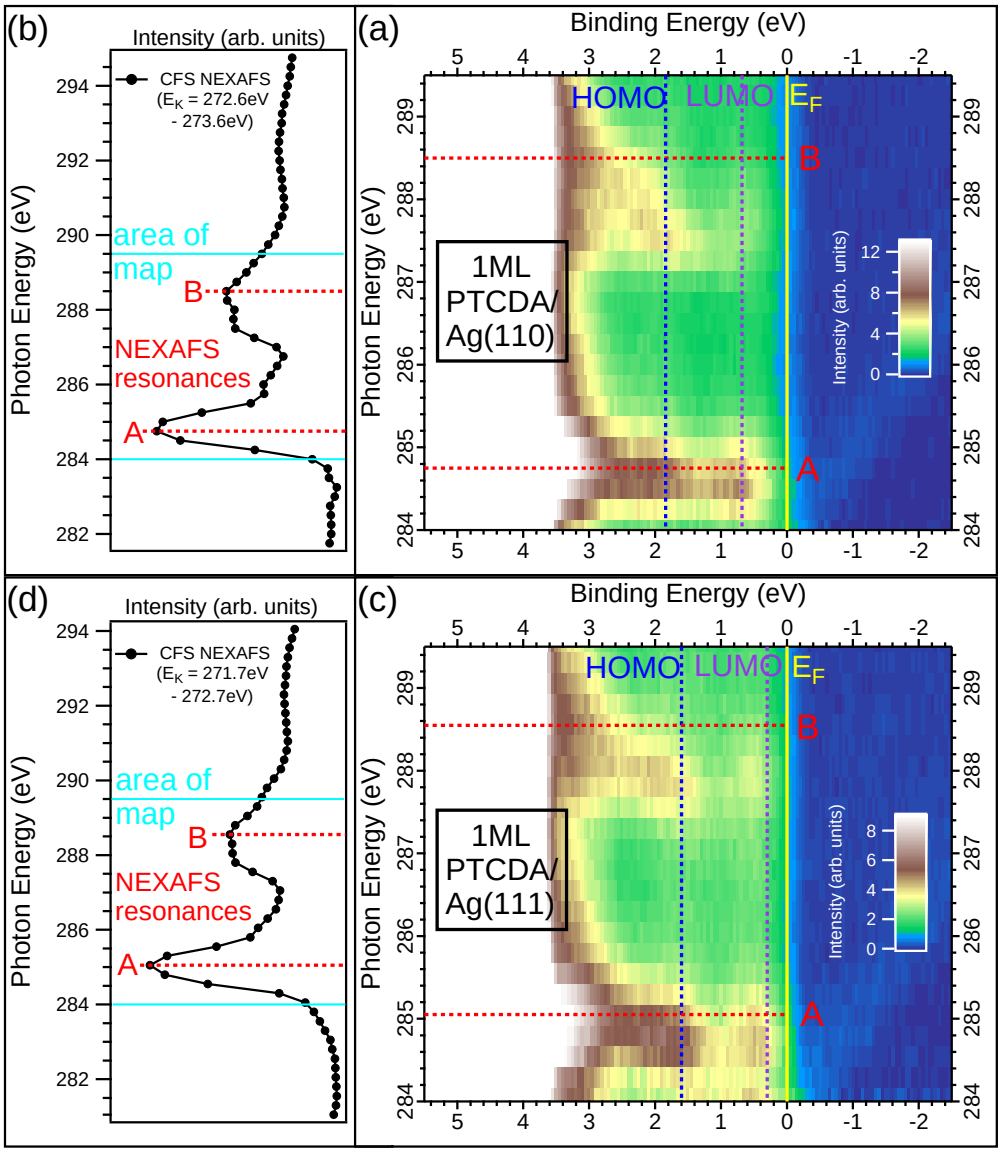

Figure 5.15: RPES data at the carbon K-edge of 1 ML PTCDA/Ag(110) compared to 1 ML PTCDA/Ag(111). **(a)** Cutout of a PES overview map of 1 ML PTCDA/Ag(110) with an $h\nu$ increment of 250 meV and an E_B increment of 50 meV. The red dashed horizontal lines denote the NEXAFS resonances A and B which are identified in the CFS NEXAFS spectrum in panel (b). The vertical dashed blue and purple lines represent the HOMO and the LUMO, respectively. The vertical yellow line denotes E_F. **(b)** CFS NEXAFS spectrum extracted from the PES overview map of which a cutout is presented in panel (a). The cyan lines mark the area of the cutout displayed in panel (a). **(c)** Cutout of a PES overview map of 1 ML PTCDA/Ag(111) analogue to panel (a). **(d)** CFS NEXAFS spectrum extracted from the PES overview map of which a cutout is presented in panel (c). The cyan lines mark the area of the cutout displayed in panel (c).

and the 1 ML herringbone PTCDA/Ag(110) are presented together in Fig. 5.15. On the left hand side the CFS NEXAFS spectra of the total measured $h\nu$ region are illustrated for both systems. The presented $h\nu$ region is marked by the cyan lines. In the RPES data of 1 ML PTCDA/Ag(110) no fundamental differences are observed with respect to the corresponding data of 1 ML PTCDA/Ag(111). If the apparent partial filling of the LUMO signal in direct valence PES had been connected to the mechanism which is responsible for the broad line-shape of molecular orbital signals in RPES obvious differences in the RPES data of these two systems would have been observed. Hence the existence and not the apparent partial filling of the LUMO signal in direct PES goes together with the observed broad line-shape of molecular orbital signals in RPES.

In both cutouts of the PES overview maps (Fig. 5.15(a) and (c)) the constant color code of large E_B regions shows the broad line-shape of the HOMO and the LUMO signal. This means that at some $h\nu$ no actual peaks are visible due to resonantly enhanced PES intensity between the molecular orbital signals. This PES intensity could stem from the same sort of constant E_K feature which has been discussed for the ML NTCDA/Ag(111) RPES data in Figs. 5.13 and 5.14. The only significant difference found between the RPES data of the systems 1 ML PTCDA/Ag(111) and 1 ML PTCDA/Ag(110) is a variation of the relative intensity enhancement of the LUMO signal with respect to the HOMO signal. For 1 ML PTCDA/Ag(110) the LUMO signal is more enhanced in NEXAFS resonance A with respect to the HOMO signal than for 1 ML PTCDA/Ag(111). In NEXAFS resonance B the situation is reversed and the larger enhancement of the LUMO signal with respect to the HOMO signal is observed for 1 ML PTCDA/Ag(111). Such differences in the RPES data of the same molecule demonstrate that there is an influence of the molecule-metal interface on the NEXAFS and autoionization matrix elements. In the example of Fig. 5.15 this influence leads to a relative intensity variation within the same order of magnitude.

A more detailed investigation of the line-shape of the frontier molecular orbital signals of 1 ML PTCDA/Ag(110) is again performed by analyzing EDC waterfall plots with smaller $h\nu$ increments in the $h\nu$ region around both NEXAFS resonances. In Fig. 5.16 it becomes obvious that not only at the E_B positions of the molecular orbital signals the PES intensity is enhanced but practically in the total E_B region displayed. Especially between the HOMO signal and the signal of the lower molecular orbitals (see Ref. [162] for contributions to this signal) this intensity enhancement is observed. In both NEXAFS resonances a line-shape is found that reminds of a step-function for the EDCs with larger $h\nu$ and the onset of this step-function coincides with the onset of the HOMO signal in direct valence PES. With increasing $h\nu$ this line-shape transforms into a linearly increasing PES intensity without any peak-like structure in NEXAFS resonance B. This line-shape of the frontier molecular orbital signals in RPES shows some similarities to the system 1 ML SnPc/Ag(111) [174]. A comparison of the RPES data of these two systems with the RPES data of the system 1 ML CuPc/Ag(111) is the next logical step. Due to the similar electronic structure of 1 ML SnPc/Ag(111) and 1 ML CuPc/Ag(111) similarities in the RPES data of these two systems are expected.

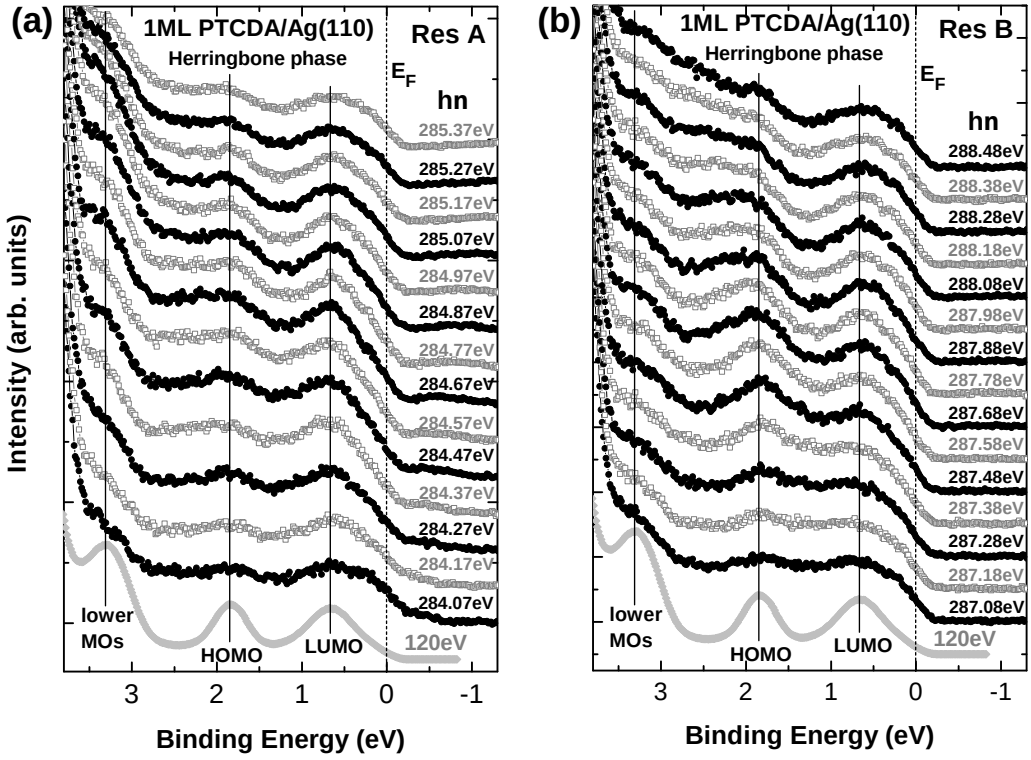

Figure 5.16: RPES data at the carbon K-edge of a 1 ML herringbone PTCDA/Ag(110) in comparison to direct valence PES data at $h\nu = 120$ eV. The vertical lines denote the E_B positions of the molecular orbital signals in direct valence PES. The dashed vertical line represents E_F. **(a)** EDCs in the $h\nu$ region around NEXAFS resonance A. **(b)** EDCs in the $h\nu$ region around NEXAFS resonance B. For a CFS NEXAFS spectrum defining those resonances see Fig. 5.15(b).

The CFS NEXAFS spectrum extracted from the PES overview map of the system 1 ML CuPc/Ag(111) is presented in Fig. 5.17(a). In the $h\nu$ region of the broad main intensity maximum the PES detail map is recorded (denoted by cyan lines) and illustrated in Fig. 5.17(b). From the color code of this PES detail map it becomes obvious that the main signal is situated at an E_B position at which no molecular orbital signal is found in direct valence PES (see dashed vertical lines). The region of the map in which the most prominent intensity enhancement is found is marked by the black box and displayed in an EDC waterfall plot in Fig. 5.17(c). Therein the main feature of the PES detail map is identified as a broad peak around $E_B \approx 2.2$ eV. For the EDCs in which this feature is present its E_B position is found to be roughly constant with a variation of $h\nu$ while the width of the peak changes discontinuously. The fact that in direct valence PES (lowermost EDC with $h\nu = 120$ eV) no feature can be observed at this E_B position is in contrast to the roughly constant E_B in RPES since this points towards a molecular one-hole final state (constant E_B feature). The direct valence PES data in Refs. [82] and [122] measured with $h\nu =$ He I find the HOMO-1 at this E_B position. So in principle the main

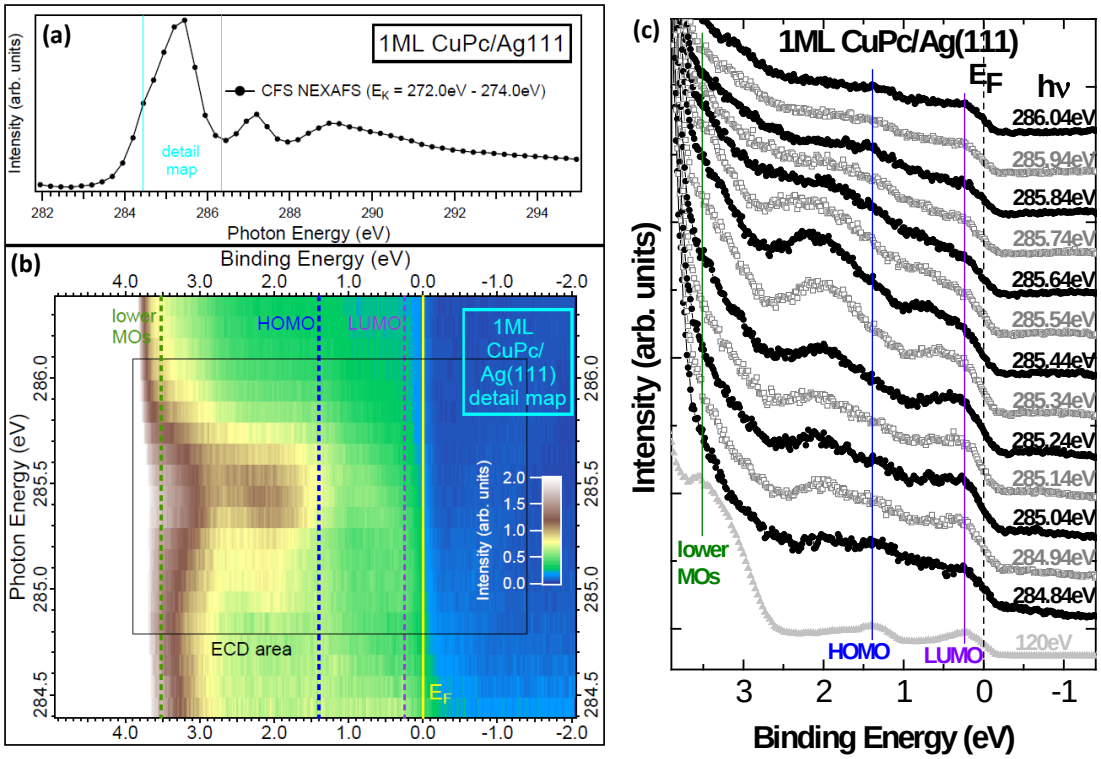

Figure 5.17: RPES data at the carbon K-edge of a 1 ML CuPc/Ag(111). **(a)** CFS NEXAFS spectrum extracted from a PES overview map with an $h\nu$ increment of 250 meV. The cyan lines mark the $h\nu$ region of the PES detail map illustrated in panel (b). **(b)** PES detail map with an $h\nu$ increment of 100 meV and an E_B increment of 15 meV. The vertical dashed olive, blue and purple lines represent the E_B position in direct valence PES of the lower molecular orbitals (MOs), the HOMO and the LUMO signal, respectively. The yellow vertical line represents E_F. The black box denotes the area of the PES detail map from which the EDCs presented in panel (c) originate. **(c)** EDCs in the marked $h\nu$ and E_B region in panel (b) in comparison to direct valence PES data at $h\nu = 120$ eV. The vertical lines denote the E_B positions of the molecular orbital signals in direct valence PES. The dashed vertical line represents E_F.

feature in the EDC waterfall plot at $E_B \approx 2.2$ eV could stem from the HOMO-1. Since neither for the CuPc multilayer (see Fig. 5.5) nor for the sub-ML CuPc on Au(111) (see Fig. 5.8) a resonant enhancement of the HOMO-1 signal is observed this assignment would require a large alteration of the NEXAFS and autoionization matrix elements by the molecule-metal interface of 1 ML CuPc/Ag(111). Further considering that at the E_B position of the HOMO and the LUMO signal hardly any peak structure is visible while at $h\nu = 285.44$ eV a clear peak between the E_B position of those two signals emerges suggests that the assignment of any feature in this RPES data is quite speculative. In the large E_B areas in which only a linearly increasing PES intensity is found due to the intensity enhancement at basically all E_B positions this is not possible anyway. In the two topmost EDCs the step-function like line-shape previously found in the RPES data of the other molecule-metal interface systems with a LUMO signal in direct valence PES appears again. So for 1 ML CuPc/Ag(111) several differences of the line-shape of the frontier molecular orbital signals are found in RPES with respect to direct valence PES. These variations are similar to the findings for the other molecule-metal interface systems with a LUMO signal in direct valence PES. However, the magnitude of the change between the direct valence PES and RPES data appears to be largest for the system 1 ML CuPc/Ag(111).

In conclusion the RPES data in the E_B region of the frontier molecular orbital signals of all molecule-metal interface systems with a LUMO signal in direct valence PES is fundamentally different with respect to the corresponding data of the molecule-metal interface systems without a LUMO signal in direct valence PES. In the latter systems the main features are observed as peaks situated roughly at the E_B position of the molecular orbital signals in direct valence PES. Furthermore, the $h\nu$ dependent line-shape evolution of the molecular orbital signals in RPES of these molecule-metal interface systems can be compared to the corresponding multilayer data. Both of these findings are not observed for the molecule-metal interface systems with a LUMO signal in direct valence PES. These have in common that a broad line-shape is detected for the molecular orbital signals in RPES. Compared to the line-shape of the CT state in coronene/Ag(111) (see Fig. 5.12) an increased broadening is observed which in some EDCs results in a step-function like line-shape or a linearly increasing intensity without any peak features. A possible explanation for this finding is that the energetically broad character of substrate s-p bands is imprinted onto all molecular orbital signals by CT from these metal s-p bands (see discussion in subsection 5.3.1). In addition to resonantly enhanced molecular orbital signals novel features are present in the RPES data of all molecule-metal systems with a LUMO signal in direct valence PES. Since these features are absent for the corresponding multilayer data they can be associated with CT at the molecule-metal interface. An assignment of final states to these features (as for the CT state in subsection 5.3.1) is not possible since too many energetically overlapping features are present in the investigated E_B region. This most probably originates from the fact that both constant E_K and constant E_B features contribute in this E_B region. Moreover, both of these differently dispersing features can exhibit a unique intensity variation with $h\nu$ (see section 5.1) and are most probably broadened due to electron vibration coupling (see section 5.2). Hence

a significant deconvolution of the EDCs at this $h\nu$ is very difficult. However, at larger $h\nu$ the constant E_K features might be separable from molecular orbital one-hole finial state signals (constant E_B features) so this $h\nu$ region is investigated in the following subsection.

5.3.3 Constant kinetic energy features

The possible contribution of constant E_K features in the E_B region of the frontier molecular orbital signals in the molecule-metal interface systems with a LUMO signal in direct valence PES, discussed in the previous subsection, motivates a search for such features at higher $h\nu$ in the PES overview map. At these $h\nu$ the intense frontier molecular orbital signals would not overlap with the constant E_K features due to the linear dispersion to higher E_B with increasing $h\nu$ of the latter. Mainly less intense and energetically broad molecular orbital signals are situated in the E_B region higher than the intense Ag4d and Au5d substrate signals (see for example Fig. A8(b) and Fig. A15(a)). If those molecular orbitals do not exhibit a significant increase in intensity for large $h\nu$ and the constant E_K features are simultaneously intense enough I will be able to extract their E_K from the RPES data. With that the origin of the identified constant E_K features can be discussed.

In order to identify constant E_K features in the PES overview map it is transformed onto an E_K scale ($E_K = h\nu - E_B$). In regions where hints for constant E_K features emerge an integration over the $h\nu$ direction is performed. The $h\nu$ interval of this integration is chosen so that a crossing with the intense Ag4d and Au5d signals is avoided because in this situation a constant E_K feature would only be a tiny feature on top of a huge substrate signal. An integration over the $h\nu$ direction of a PES map on the E_K scale leads to an accumulation of PES intensity stemming from features at constant E_K while features at constant E_B add up linearly shifted and smear out. Thus finding a peak feature in the resulting $h\nu$ integrated EDC constitutes the detection of a constant E_K feature. In each of the following figures the area of integration and presentation of the $h\nu$ integrated EDC is marked by a blue dashed box in the PES overview map (middle panel). The resulting $h\nu$ integrated EDC is presented on the right hand side while the CFS NEXAFS spectrum is displayed on the left hand side of the PES overview map.

In this way the RPES data of an ML NTCDA/Ag(111) and 1 ML CuPc/Ag(111) is presented in Fig. 5.18. For both systems constant E_K features are observed in the particular $h\nu$ integrated EDC on the right hand side. In the $h\nu$ integrated EDC of an ML NTCDA/Ag(111) in Fig. 5.18(c) one single constant E_K feature is found at a very similar E_K as in the RPES data of 1 ML NTCDA/Ag(111) in Ref. [81]. For 1 ML CuPc/Ag(111) two constant E_K features are identified in the $h\nu$ integrated EDC in Fig. 5.18(f). In both cases the constant E_K features stick out of a several tenths of eV broad dome which mainly consists of KVV Auger decays and otherwise exhibits much broader features. The extracted E_K of these constant E_K features does not match the E_B region of the frontier molecular orbital signals at the $h\nu$ of NEXAFS resonances B and C for the

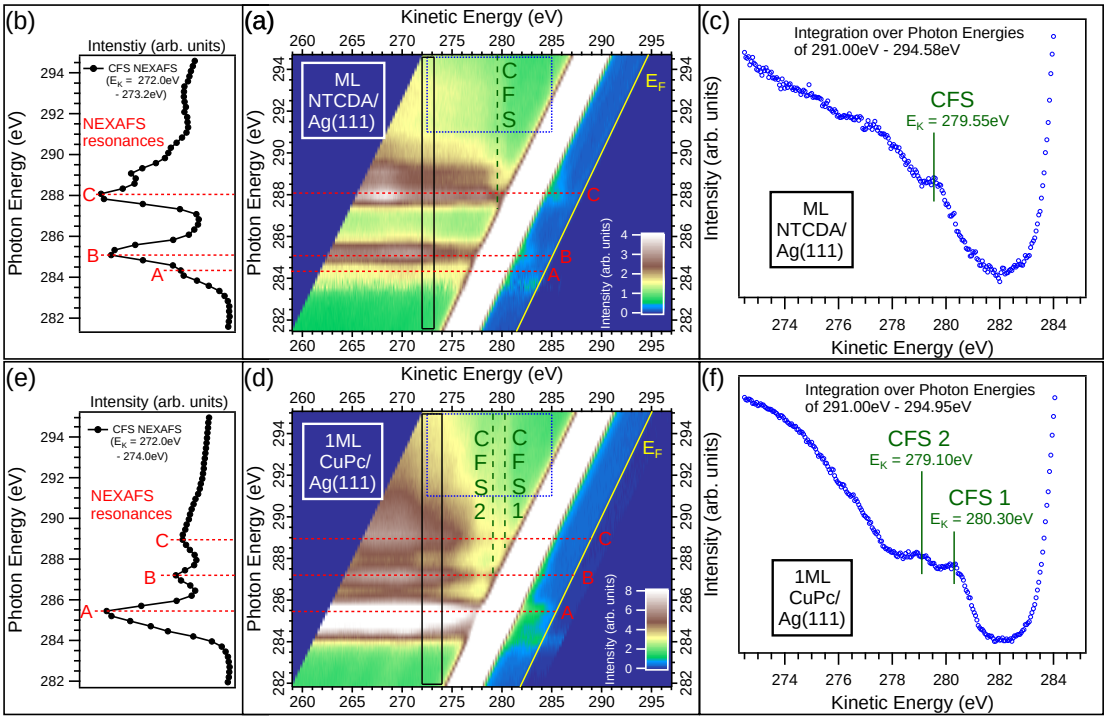

Figure 5.18: RPES data at the carbon K-edge of an ML NTCDA/Ag(111) and 1 ML CuPc/Ag(111). **(a)** PES overview map of an ML NTCDA/Ag(111) with an $h\nu$ increment of 250 meV and an E_K increment of 50 meV presented on an E_K scale. The red dashed horizontal lines denote the NEXAFS resonances which are identified in the CFS NEXAFS spectrum in panel (b). The black box marks the region from which the CFS NEXAFS spectrum is obtained by an integration over E_K. The blue dashed box illustrates the area from which the $h\nu$ integrated EDC originates and the E_K region in which it is presented in panel (c). The olive dashed vertical lines denote the constant E_K feature identified in panel (c). The yellow line represents E_F. **(b)** CFS NEXAFS spectrum of an ML NTCDA/Ag(111) extracted from the black box in the PES overview map in panel (a). **(c)** $h\nu$ integrated EDC of an ML NTCDA/Ag(111) obtained by integration over $h\nu$ in the area of the blue dashed box in the PES overview map in panel (a). The identified constant E_K feature is marked with an olive line. **(d)** PES overview map of 1 ML CuPc/Ag(111) analog to panel (a). **(e)** CFS NEXAFS spectrum of 1 ML CuPc/Ag(111) analog to panel (b). **(f)** $h\nu$ integrated EDC of 1 ML CuPc/Ag(111) analog to panel (c).

ML NTCDA/Ag(111) and the NEXAFS resonance A for 1 ML CuPc/Ag(111). Consequently, these constant E_K features are not the ones expected from the investigation of the line-shapes of the frontier molecular orbital signals in Figs. 5.13 and 5.14 for the ML NTCDA/Ag(111) and Fig. 5.17 for 1 ML CuPc/Ag(111). At the expected E_K no significant constant E_K features can be found in the PES overview map or single EDCs at higher $h\nu$ (above approximately 290 eV). So either they are not present at all or not observable at these high $h\nu$ because of a small PES intensity which might be due to a decreased cross section of the responsible RPES (or Auger) process.

For the system 1 ML SnPc/Ag(111) investigated in Ref. [174] the same situation is found as for 1 ML CuPc/Ag(111). Two constant E_K features are visible in the PES overview map which are situated at equal E_K as the ones in Fig. 5.18(f). For the other investigated molecule-metal interface systems with a LUMO signal in direct valence PES (1 ML PTCDA/Ag(111) and 1 ML PTCDA/Ag(110)) the RPES data is inconclusive. In the $h\nu$ integrated EDCs possible constant E_K features are present but these are significantly broader than the ones found for the systems in Fig. 5.18. This could be a consequence of multiple energetically overlapping constant E_K features. Anyway, since no significant evaluation of this data is possible it will not be considered in the following discussion. The observation of constant E_K features in some of the molecule-metal interface systems with a LUMO signal in direct valence PES introduces the question about a possible connection of the emergence of this LUMO signal and these constant E_K features. An analogue investigation of molecule-metal interface systems without a LUMO signal in direct valence PES can certainly clarify this issue.

The search for constant E_K features in the RPES data of several molecule-metal interface systems without a LUMO signal in direct valence PES is presented in Figs. 5.19 and 5.20. For the system 0.8 ML coronene/Ag(111) in Fig. 5.19(c), for 0.7 ML CuPc/Au(111) in Fig. 5.20(c), and for 0.6 ML SnPc/Au(111) in Fig. 5.20(f) two constant E_K features are found. Hence the existence of a LUMO signal in direct valence PES and the corresponding ground state, that most probably exhibits a significant contribution of the basis state $\left|C^2H^2L^1M^{n-1}\right\rangle$, is not mandatory for the emergence of these constant E_K features. The very similar spectroscopic signature of the constant E_K features in both types of molecule-metal interface systems points into the direction that the same mechanism is responsible for the production of these features in both types of systems. Additionally, these constant E_K features are absent in the RPES data of all corresponding multilayer films (see Figs. A13 and A14). Similar constant E_K features have previously been reported in Refs. [154, 175] exclusively for (sub-)ML samples. Thus all these constant E_K features stem from the molecule-metal interface. Consequently, a substrate state must be involved in the mechanism that leads to the constant E_K features. For the interface systems with a LUMO signal in direct valence PES the significant contribution of the basis state $\left|C^2H^2L^1M^{n-1}\right\rangle$ to the ground state could serve as the required state which is exclusive for the molecule-metal interface.

Considering the E_K values of the constant E_K features a clear difference can be observed between the two different types of molecule-metal interface systems. For SnPc and CuPc molecules a direct comparison of the E_K values on Au(111) and Ag(111) is possible.

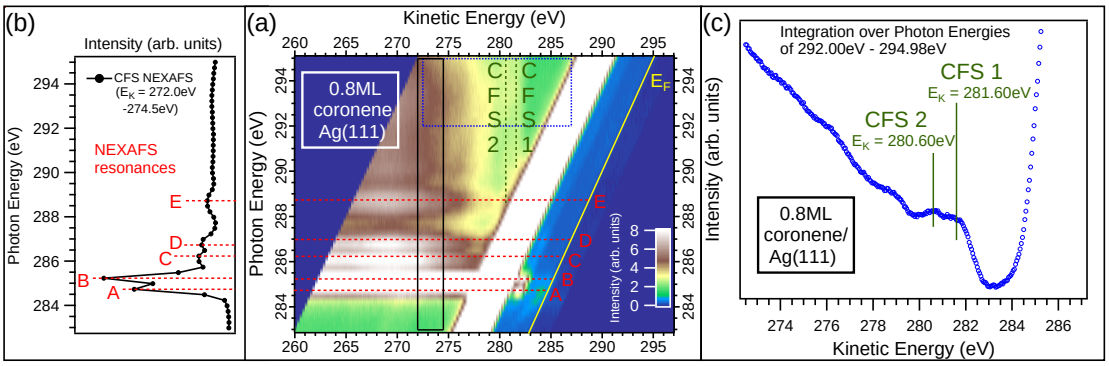

Figure 5.19: RPES data at the carbon K-edge of 0.8 ML coronene/Ag(111). **(a)** PES overview map with an $h\nu$ increment of 250 meV and an E_K increment of 50 meV presented on an E_K scale. The red dashed horizontal lines denote the NEXAFS resonances which are identified in the CFS NEXAFS spectrum in panel (b). The black box marks the region from which the CFS NEXAFS spectrum is obtained by an integration over E_K. The blue dashed box illustrates the area from which the $h\nu$ integrated EDC originates and the E_K region in which it is presented in panel (c). The olive dashed vertical lines denote the constant E_K features identified in panel (c). The yellow line represents E_F. **(b)** CFS NEXAFS spectrum extracted from the black box in the PES overview map in panel (a). **(c)** $h\nu$ integrated EDC obtained by integration over $h\nu$ in the area of the blue dashed box in the PES overview map in panel (a). The identified constant E_K features are marked with olive lines.

It reveals a difference in E_K of approximately 4 eV with the lower E_K values for the Ag(111) systems. For a general comparison of E_K values the most reasonable reference is the largest possible E_K of a regular Auger decay $E_K(Auger_{max})$. For a ground state with an unoccupied LUMO ($\left|C^2H^2L^0M^n\right\rangle$) this E_K can be estimated with the difference of E_B of the chemical species of the core level exhibiting the largest E_B (called C_{max}) and twice the E_B of the HOMO signal (called H_0). Expressing this in a mathematical form results in $E_K(Auger_{max}) = E_B(C_{max}) - 2 \times E_B(H_0)$. Thereby all electronic correlations are neglected. It turns out that for all interface systems without a LUMO signal in direct valence PES the constant E_K feature CFS 1 exhibits a larger E_K than this estimated value of $E_K(Auger_{max})$. For the interface systems with a LUMO signal in direct valence PES E_K of the constant E_K features is smaller than this $E_K(Auger_{max})$ and hence also smaller than the E_K of the Auger decay including the LUMO instead of the HOMO. Hence only for the interface systems without a LUMO signal in direct valence PES a true restriction for the states involved in the responsible process for the constant E_K features evolves from the observed E_K. This is the involvement of a state with a lower E_B than the HOMO signal.

Following the constant E_K features in the PES overview maps of the interface systems with a LUMO signal in direct valence PES to lower $h\nu$ ends in a region of the map where the intense Ag4d signals hinder any significant observation. For the interface systems without a LUMO signal in direct valence PES the same approach ends in the

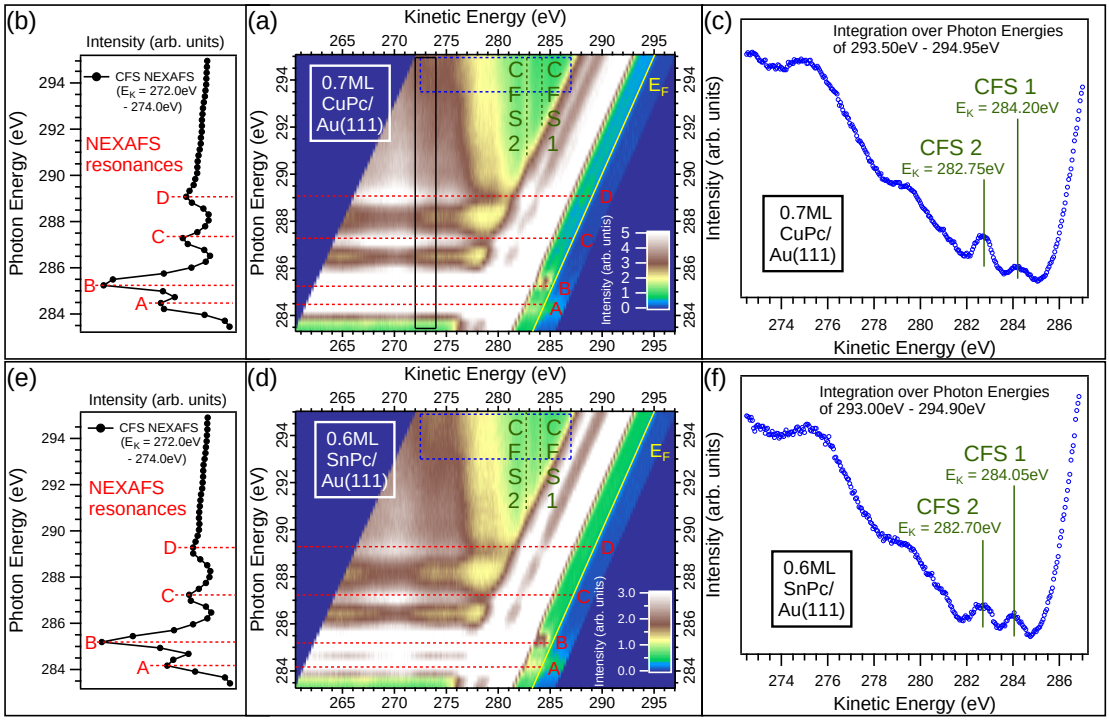

Figure 5.20: RPES data at the carbon K-edge of 0.7 ML CuPc/Au(111) and 0.6 ML SnPc/Au(111). **(a)** PES overview map of 0.7 ML CuPc/Au(111) with an $h\nu$ increment of 250 meV and an E_K increment of 50 meV presented on an E_K scale. The red dashed horizontal lines denote the NEXAFS resonances which are identified in the CFS NEXAFS spectrum in panel (b). The black box marks the region from which the CFS NEXAFS spectrum is obtained by an integration over E_K. The blue dashed box illustrates the area from which the $h\nu$ integrated EDC originates and the E_K region in which it is presented in panel (c). The olive dashed vertical lines denote the constant E_K features identified in panel (c). The yellow line represents E_F. **(b)** CFS NEXAFS spectrum of 0.7 ML CuPc/Au(111) extracted from the black box in the PES overview map in panel (a). **(c)** $h\nu$ integrated EDC of 0.7 ML CuPc/Au(111) obtained by integration over $h\nu$ in the area of the blue dashed box in the PES overview map in panel (a). The identified constant E_K features are marked with olive lines. **(d)** PES overview map of 0.6 ML SnPc/Au(111) analog to panel (a). **(e)** CFS NEXAFS spectrum of 0.6 ML SnPc/Au(111) analog to panel (b). **(f)** $h\nu$ integrated EDC of 0.6 ML SnPc/Au(111) analog to panel (c).

region of the PES detail map which is extensively investigated for all these systems in subsection 5.2.2. The overlap of the constant E_K feature CFS 2 with either the Ag4d or Au5d signals does not allow any statement of its existence in the $h\nu$ region of the NEXAFS resonances. This is similar to the situation in the interface systems with a LUMO signal in direct valence PES. In contrast the larger E_K of the constant E_K feature CFS 1 permits a discussion of the existence of this feature for $h\nu$ smaller than the core level ionization potential.

Since for a sub-ML SnPc/Au(111) the same $h\nu$ dependent line-shape evolution of the HOMO signal is observed as for a SnPc multilayer (see Fig. 5.8(a)) a significant contribution of the constant E_K feature CFS 1 in NEXAFS resonance B can be excluded. For a sub-ML CuPc/Au(111) less intensity is observed with respect to a CuPc multilayer at the E_B position of a possible contribution of the constant E_K feature CFS 1 (see Fig. 5.8(b)). Hence for a sub-ML CuPc/Au(111) this interface feature cannot be detected in NEXAFS resonance B. In the case of a sub-ML coronene/Ag(111) a significant contribution of the constant E_K feature CFS 1 in NEXAFS resonance A is excluded in the same way as for a sub-ML SnPc/Au(111) (see Fig. 5.9(a)) while in NEXAFS resonance B (see Fig. 5.9(b)) E_K of the constant E_K feature CFS 1 does not match the high E_B part of the HOMO signal. So the observed difference of the $h\nu$ dependent line-shape evolution of the HOMO signal of the sub-ML coronene/Ag(111) with respect to the coronene multilayer sample cannot be a consequence of the existence of the constant E_K feature CFS 1 in NEXAFS resonance B. To conclude this discussion I can state that there is no evidence for a contribution of any constant E_K feature for an $h\nu$ smaller than the core level ionization potential in any of the investigated systems. So the discussion of the origin of the constant E_K features only makes sense for an $h\nu$ larger than the core level ionization potential. Hence the required mechanism of energy dissipation in the process responsible for the constant E_K features is the emission of a photoelectron into vacuum.

As discussed above for the interface systems without a LUMO signal in direct valence PES there are additional restrictions which can be used to identify the process responsible for the observed constant E_K features. A process that leads to a molecule-metal interface feature with such a large E_K must involve a metal state and a molecular state with lower E_B than the HOMO signal. For the interface systems with a LUMO signal in direct valence PES such restrictions cannot be extracted from the RPES data. Hence in the following I will first present a possible mechanism for the interface systems without a LUMO signal in direct valence PES that fulfills the found requirements. Then simplifying assumptions are introduced with which I can quantitatively check whether the presented mechanism can be responsible for the observed constant E_K features. At the end this mechanism will be discussed in relation to the interface systems with a LUMO signal in direct valence PES. In the nomenclature used in subsection 5.3.1 a non energy

conserving two-step process (steps (a) and (b)) with core level PES in the first and an Auger decay in the second step can be given as

$$\begin{aligned} &\text{(a)} \quad \left|C_i^2 H_j^2 L_0^0 M^n\right\rangle + h\nu \xrightarrow[CT]{PES} \left|C_i^1 H_j^2 L_0^1 M^{n-1}\right\rangle + e^- \\ &\text{(b)} \quad \left|C_i^1 H_j^2 L_0^1 M^{n-1}\right\rangle \xrightarrow{Auger} \left|C_i^2 H_j^1 L_0^0 M^{n-1}\right\rangle + e^- \end{aligned} \tag{5.13}$$

Hereby C_i denotes the C1s core level of the carbon species i, H_j the occupied molecular orbital j and L_0 the LUMO. Moreover, only the basis state which is assumed to be the dominating contribution to the particular state is considered for the description of the states involved in the RPES process. Including CT from M to L fulfills the above given requirements of the involvement of a substrate state and a molecular state with a lower E_B than the HOMO signal. E_K of the electron emitted in step (b) can be calculated by taking the difference of the energy of the state $\left|C_i^1 H_j^2 L_0^1 M^{n-1}\right\rangle$ and the state $\left|C_i^2 H_j^1 L_0^0 M^{n-1}\right\rangle$. Hence by measuring the energy of these two states E_K of the constant E_K features can be determined. This is in fact possible on the basis of the following assumptions

$$\begin{aligned} &(1) \quad \left|C_i^1 H_j^2 L_0^1 M^{n-1}\right\rangle \approx \left|C_i^1 H_j^2 L_0^1\right\rangle \cdot \left|M^{n-1}\right\rangle \\ &(2) \quad \left|C_i^2 H_j^1 L_0^0 M^{n-1}\right\rangle \approx \left|C_i^2 H_j^1 L_0^0\right\rangle \cdot \left|M^{n-1}\right\rangle \\ &(3) \quad \text{NEXAFS} \;\widehat{=}\; \left|C_i^2 H_j^2 L_0^0\right\rangle + h\nu \rightarrow \left|C_i^1 H_j^2 L_0^1\right\rangle \\ &(4) \quad \text{valence PES} \;\widehat{=}\; \left|C_i^2 H_j^2 L_0^0\right\rangle + h\nu \rightarrow \left|C_i^2 H_j^1 L_0^0\right\rangle + e^- \end{aligned} \tag{5.14}$$

In assumptions (1) and (2) the states are factorized into a metal part and a molecular part which means that small hopping matrix elements $V_{H,M}$ and $V_{L,M}$ are assumed. This is somewhat problematic since at the same time $V_{L,M}$ must be large enough to enable CT in step (a). However, even if the probability for CT is small compared to the probability for no CT the signals produced by the latter processes will be situated at a smaller E_K. Hence their larger intensity does not hinder the observation of the signals that originate from the processes with CT. The interpretation of the process in assumption (3) as a NEXAFS spectroscopy experiment and the process in assumption (4) as a direct valence PES experiment ignores any excitations including states of the metal substrate. Hence these assumptions also rely on small hopping matrix elements $V_{H,M}$ and $V_{L,M}$. Applying the assumptions (1) and (2) of Eq. 5.14 to step (b) in Eq. 5.13 the energy of the state $\left|M^{n-1}\right\rangle$ cancels out in the energy balance of the process and E_K of the emitted electron is simply a difference of the states $\left|C_i^1 H_j^2 L_0^1\right\rangle$ and $\left|C_i^2 H_j^1 L_0^0\right\rangle$. With assumptions (3) and (4) the energy of these two states can be directly measured by a NEXAFS and a valence PES experiment. So on the basis of step (b) in Eq. 5.13 and assumptions (1) – (4) in Eq. 5.14 E_K of the constant E_K feature m ($E_{K,theo}$(CFS m)) can be calculated as the difference of two experimentally determined quantities with

$$E_{K,theo}(\text{CFS } m) = h\nu(\left|C_i^1 H_j^2 L_0^1\right\rangle) - E_B(\left|C_i^2 H_j^1 L_0^0\right\rangle) \tag{5.15}$$

Hereby the subscript *theo* denotes that this is a theoretical value in contrast to the value extracted directly from the RPES experiment $E_{K,exp}(\text{CFS } m)$. Moreover, the notation $h\nu(\left|C_i^1 H_j^2 L_0^1\right\rangle)$ stands for $h\nu$ necessary for the production of the final state $\left|C_i^1 H_j^2 L_0^1\right\rangle$ and the notation $E_B(\left|C_i^2 H_j^1 L_0^0\right\rangle)$ represents E_B of the state $\left|C_i^2 H_j^1 L_0^0\right\rangle$. For the explicit mechanism leading to the constant E_K feature with index $m = 1{,}2$ a different combination of states (chemical species C_i and occupied molecular orbital H_j) can be involved.

From the discussion about the excitation of vibrations in the beginning of subsection 2.1.4 and the references given there it becomes obvious that electron vibration coupling needs to be considered in order to extract the energies of the states in Eq. 5.15 from the NEXAFS and direct valence PES data. In the NEXAFS data the adiabatic transition (no vibration excited) can be estimated with the onset of the particular peak feature. Should the determination of this onset be hindered by energetically overlapping peak features additional assumptions are necessary. These will be given explicitly below for each of the quantitatively investigated systems. The estimated error for the extracted energy will depend on the particular assumption. In the direct valence PES data the final state without the excitation of a vibration can be estimated with the intensity maximum of the particular peak. From a single mode analysis [59] the possible error made by this approximation is estimated to be less than 100 meV.

The determination of the NEXAFS onset of the system coronene/Ag(111) is shown in Fig. 5.21(a). From the NEXAFS calculations in Ref. [163] it follows that this onset corresponds to the chemical carbon species bound to hydrogen C_H. The two NEXAFS onsets corresponding to the carbon species bound to carbon C_C should be situated somewhere between NEXAFS resonances A and B [163] and cannot be determined experimentally. However, it is not clear which of these carbon species is actually included in the Auger decay of step (b) in Eq. 5.13. If more than one of these decay channels lead to a feature that is intense enough to be detected this should result in a single broad constant E_K feature instead of the emergence of multiple constant E_K features. Hence I use the NEXAFS onset obtained in Fig. 5.21(a) for all carbon species of the coronene molecule and call all of them C_C in the assignment of the contributing states. Thus the observation of two constant E_K features in the system coronene/Ag(111) is explained with the contribution of two different H_j in the Auger decay. So the constant E_K feature CFS 1 is produced by the decay of the state $\left|C_C^1 H_0^2 L_0^1\right\rangle$ into the state $\left|C_C^2 H_0^1 L_0^0\right\rangle$ and the constant E_K feature CFS 2 is assigned to the decay of the state $\left|C_C^1 H_{-1}^2 L_0^1\right\rangle$ into the state $\left|C_C^2 H_{-1}^1 L_0^0\right\rangle$. E_B of the HOMO signal (H_0 corresponding to the state $\left|C_C^2 H_0^1 L_0^0\right\rangle$) and the HOMO-1 signal (H_{-1} corresponding to the state $\left|C_C^2 H_{-1}^1 L_0^0\right\rangle$) are determined in Fig. A15(b). For the HOMO signal I obtain $E_B(\left|C_C^2 H_0^1 L_0^0\right\rangle) = 2.58$ eV and for the HOMO-1 signal $E_B(\left|C_C^2 H_{-1}^1 L_0^0\right\rangle) = 3.77$ eV is found. Inserting these values and $h\nu$ of the NEXAFS onset determined in Fig. 5.21(a) into Eq. 5.15 leads to $E_{K,theo}(\text{CFS } 1) = (281.74 \pm 0.20)$ eV and $E_{K,theo}(\text{CFS } 2) = (280.55 \pm 0.20)$ eV. These values are in agreement with the experimentally found values $E_{K,exp}(\text{CFS } 1) = (281.60 \pm 0.15)$ eV and $E_{K,exp}(\text{CFS } 2) = (280.60 \pm 0.15)$ eV. Hereby the errors of the experimentally determined

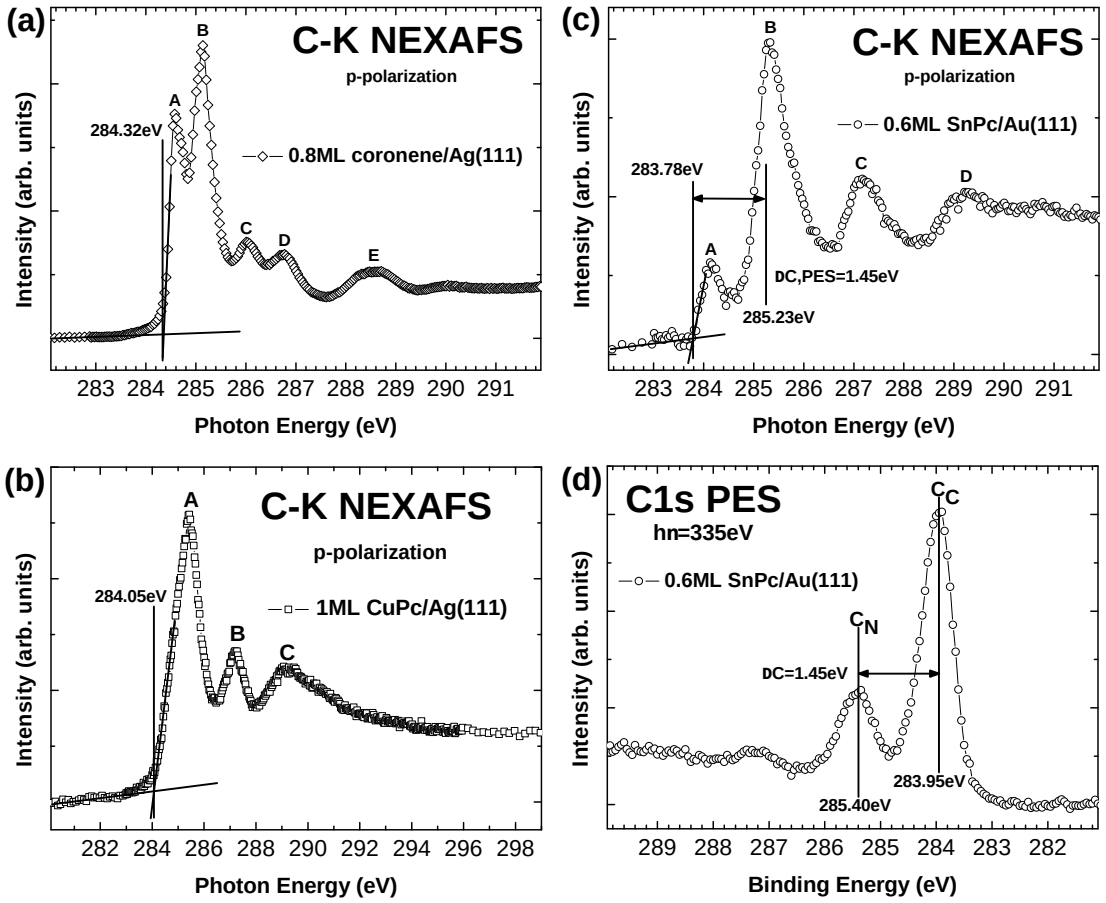

Figure 5.21: Carbon K-edge NEXAFS and C1s core level PES data for the determination of the NEXAFS onsets used for the calculations of E_K of the constant E_K features. The thick black lines demonstrate the determination of the NEXAFS onsets and the energetic separation of the different C1s species. The capital letters in panels (a) – (c) denote the NEXAFS resonances and in panel (d) the different carbon species (C_C and C_N). **(a)** NEXAFS spectrum of 0.8 ML coronene/Ag(111). **(b)** NEXAFS spectrum of 1 ML CuPc/Ag(111). **(c)** NEXAFS spectrum of 0.6 ML SnPc/Au(111). **(d)** C1s core level PES spectrum of 0.6 ML SnPc/Au(111).

values stem from the reading accuracy in the $h\nu$ integrated EDC in Fig. 5.19(c) while the errors of the theoretical values are estimated from the uncertainty of the determination of the adiabatic transitions in the NEXAFS and the PES spectrum. From the agreement of the theoretical and the experimental values I can conclude that the assignment of the Auger decays for the constant E_K features seem to be correct and that the applied assumptions seem to be justified for the system coronene/Ag(111).

Analogously the values $E_{K,theo}(\text{CFS } 1)$ and $E_{K,theo}(\text{CFS } 2)$ can be determined for the system SnPc/Au(111). For this system two different carbon species are considered since in the C1s core level PES spectrum (Fig. 5.21(d)) two separated peaks can be identified. The one representing all carbon atoms that are bound only to carbon and hydrogen atoms is termed C_C and the one standing for all carbon atoms that are bound to a nitrogen atom are called C_N. Consequently, the onset of NEXAFS resonance A in Fig. 5.21(c) corresponds to the carbon species C_C. The NEXAFS onset of the C_N carbon species is situated at higher $h\nu$ and cannot be directly extracted from the NEXAFS spectrum in Fig. 5.21(c). However, with the energetic separation of the two different carbon species in the core level PES spectrum (see Fig. 5.21(d)) the NEXAFS onset of the C_N carbon species can be estimated (see Fig. 5.21(c)). Ignoring the difference of energetic separations of the final states of core level PES and NEXAFS spectroscopy corresponds to the assumption that the reaction of the molecular orbitals on a core hole at different sites on the molecule is equal. This crude approximation will be considered in the error of the theoretical values $E_{K,theo}(\text{CFS } m)$ of the system SnPc/Au(111). From the EDC at lowest $h\nu$ in Fig. 5.8(a) I obtain $E_B(\left|C_i^2 H_0^1 L_0^0\right\rangle) = 0.89$ eV for the HOMO of 0.6 ML SnPc/Au(111). Additionally, the RPES data of this system does not show any resonantly enhanced PES intensity for the HOMO-1 signal. Hence the decays from the states $\left|C_i^1 H_{-1}^2 L_0^1\right\rangle$ to the state $\left|C_i^2 H_{-1}^1 L_0^0\right\rangle$ do not lead to a detectable PES intensity. Consequently, a detectable constant E_K feature which stems from a process that includes the HOMO-1 can be excluded. So the two constant E_K features observed for SnPc/Au(111) must stem from the involvement of the different carbon species C_C and C_N. Thus I assign the decay from the state $\left|C_N^1 H_0^2 L_0^1\right\rangle$ into the state $\left|C_N^2 H_0^1 L_0^0\right\rangle$ to constant E_K feature CFS 1 and the constant E_K feature CFS 2 is identified as the decay of the state $\left|C_C^1 H_0^2 L_0^1\right\rangle$ into the state $\left|C_C^2 H_0^1 L_0^0\right\rangle$. For these decays the values of $E_{K,theo}(\text{CFS } m)$ are obtained by inserting the two $h\nu$ determined in Fig. 5.21(c) and the above given E_B of the HOMO signal into Eq. 5.15. This results in $E_{K,theo}(\text{CFS } 1) = (284.34 \pm 0.30)$ eV and $E_{K,theo}(\text{CFS } 2) = (282.89 \pm 0.20)$ eV. These theoretical values agree with the experimental values $E_{K,exp}(\text{CFS } 1) = (284.05 \pm 0.10)$ eV and $E_{K,exp}(\text{CFS } 2) = (282.70 \pm 0.10)$ eV which are extracted from the $h\nu$ integrated EDC in Fig. 5.20(f). Hence the assignment of the Auger decays seems to be correct and the applied assumptions seem to be justified for the system SnPc/Au(111). The discussion for the system CuPc/Au(111) is analogue.

Considering molecular orbitals H_j with larger E_B for step (b) in Eq. 5.13 suggests the emergence of many more constant E_K features at lower E_K. These are not observed in the above presented RPES data. This can be explained by the fact that molecular orbitals with larger E_B are usually energetically closer to each other than the frontier molecular

orbitals. For the system coronene/Ag(111) a discussion in terms of quantum confinement within a circular area is explicitly given in Ref. [121] and a smaller energy separation is found for the energetically lower lying states. For SnPc/Au(111) the situation of the energetic separation of molecular orbitals should be quite similar. Hence these constant E_K features would lead to broad structures in the $h\nu$ integrated EDCs if all of these constant E_K features were similar in intensity. An alternative explanation for the absence of additional constant E_K features can be given by a small probability for the Auger decays that include molecular orbitals with larger E_B.

Transforming the mechanism identified for the molecule-metal interface systems without a LUMO signal in direct valence PES into a possible mechanism for the interface systems with a LUMO signal in direct valence PES can be achieved by starting form a ground state with a singly occupied LUMO. Hence the analogue two step process to Eq. 5.13 for the interface systems with a LUMO signal in direct valence PES (steps (ã) and ($\tilde{\text{b}}$)) is

$$\begin{aligned} &(\tilde{\text{a}}) \quad \left|C_i^2 H_j^2 L_0^1 M^{n-1}\right\rangle + h\nu \xrightarrow[CT]{PES} \left|C_i^1 H_j^2 L_0^2 M^{n-2}\right\rangle + e^- \\ &(\tilde{\text{b}}) \quad \left|C_i^1 H_j^2 L_0^2 M^{n-2}\right\rangle \xrightarrow{Auger} \left|C_i^2 H_j^1 L_0^1 M^{n-2}\right\rangle + e^- \end{aligned} \tag{5.16}$$

A factorization of the wave functions and the interpretation of the NEXAFS and valence PES experiments analogue to Eq. 5.14 results in an equation analogue to Eq. 5.15. So the difference of the NEXAFS onset in Fig. 5.21(b) and E_B of the HOMO signal in the EDC recorded with $h\nu = 120$ eV in Fig. 5.17(c) should result in E_K of the constant E_K feature CFS 2 of 1 ML CuPc/Ag(111) in Fig. 5.18(f). The fact that the E_K value calculated in this way is 3.6 eV larger than the value extracted from the experiment shows that either the assignment of the Auger decay is incorrect or at least one of the assumptions is inappropriate. Since all these assumptions are based on small hopping matrix elements between molecular states and metal states the failure of this approach for the interface systems with a LUMO signal in direct valence PES is not too surprising. Especially interesting at this point is that the calculated E_K value is too large. Including the LUMO twice in an Auger decay similar to step ($\tilde{\text{b}}$) of Eq. 5.16 results in a larger E_K. Thus this difference of the interface systems with a LUMO signal in direct valence PES with respect to the interface systems without a LUMO signal in direct valence PES cannot explain the observed lower E_K of the constant E_K features of 1 ML CuPc/Ag(111). For 1 ML SnPc/Ag(111) and ML NTCDA/Ag(111) the same or similarly low E_K values are found for the constant E_K features in the RPES data which makes the discussion of these E_K values analogue to the discussion of the E_K values of 1 ML CuPc/Ag(111). A reasonable explanation of the observed difference in $E_{K,exp}(\text{CFS } m)$ between CuPc molecules on Au(111) and on Ag(111) with an energetic shift cannot be given. So I will consider that the constant E_K features might be of different origin in both types of molecule-metal interface systems despite the similar spectroscopic signature.

An alternative explanation for the constant E_K features of 1 ML CuPc/Ag(111) could be given by an Auger decay that includes the LUMO and a molecular orbital H_{-x} with

$E_B \approx 5$ eV. Hence a decay of the state $\left|C_i^1 H_{-x}^2 L_0^1 M^{n-1}\right\rangle$ into the state $\left|C_i^2 H_{-x}^1 L_0^0 M^{n-1}\right\rangle$ would lead to the constant E_K feature with the observed E_K. However, this decay is also possible for the system CuPc/Au(111) but is not observed in Fig. 5.20(c). So if this decay was responsible for the constant E_K features of 1 ML CuPc/Ag(111) its probability would have to be strongly decreased in the system CuPc/Au(111). At the same time the fact that the Auger decays identified for the constant E_K features of CuPc/Au(111) are absent in the RPES data of 1 ML CuPc/Ag(111) must be explained in the same way. The scenario of an interface interaction induced modification of Auger matrix elements that makes the constant E_K features visible for CuPc/Au(111) vanish for CuPc/Ag(111) and simultaneously leads to new constant E_K features for CuPc/Ag(111) which are absent for CuPc/Au(111) is extremely unrealistic. Consequently, I exclude the $C_i L_0 H_{-x}$-Auger decay as a possible explanation for the constant E_K features in the RPES data of the interface systems with a LUMO signal in direct valence PES.

In conclusion there must be a fundamental difference between the interface systems with and those without a LUMO signal in direct valence PES concerning the mechanism responsible for the constant E_K features. For the line-shape of the frontier molecular orbital signals in RPES investigated in subsections 5.2.2 and 5.3.2 a similarly fundamental difference is observed. From the strong variation of the line-shape of the C1s core level PES spectrum between a CuPc-metal interface system with and one without a LUMO signal in direct valence PES (see Fig. 2.1(a)) it becomes already obvious that large differences for the same molecule can be induced through the adsorption on a different metal. For a dynamical CT analysis it is a minor setback that the mechanism responsible for the constant E_K features cannot be identified for the interface systems with a LUMO signal in direct valence PES. With the existence or absence of this feature only a qualitative dynamical CT analysis is possible. The general possibility of CT at the molecule-metal interface of these systems is already obvious from the existence of the LUMO signal in direct valence PES. Hence the successful assignment of a particular Auger decay that includes CT to the constant E_K features of these systems would not have led to entirely new information. For the molecule-metal interface systems without a LUMO signal in direct valence PES on the other hand the above given quantitative confirmation of the assignment of the responsible mechanism for the constant E_K features opens up a new possibility to characterize CT at these interfaces. The association of the constant E_K features with interface CT allows the confirmation of CT on the timescale of the core hole lifetime whenever these features are observed.

5.4 Application to hetero-organic interface systems

In the previous section three criteria are identified for a qualitative dynamical CT analysis. For the system coronene/Ag(111) a CT state is identified in subsection 5.3.1 through the revelation of the mechanism that leads to this signal in the RPES data. So observing

a similar feature in the RPES data of a hetero-organic interface system and finding the responsible mechanism, which includes interface CT, is the first possible way to confirm hetero-organic interface CT on the time scale of the core hole lifetime. Hence the RPES data of the hetero-organic interface systems will be scanned for such a feature. The second criterion is the observation of a characteristic broad line-shape of the frontier molecular orbital signals. This spectroscopic signature is related to interface CT by the possible explanation given in the discussion of the line-shape of the CT state in subsection 5.3.1. There the broad line-shape is explained through the energetically broad character of substrate s-p bands that is imprinted onto the molecular orbital signals by CT from these substrate states to a molecular orbital in the RPES process. In other words, CT from a broad E_B range (M in (IIa) of Eq. 5.12 does not have a discrete ε_M) results in a molecular orbital signal broadened in energy over this energetic range. This broad line-shape is found only for the CT state in coronene/Ag(111) and to a larger extend for the molecular orbital signals of interface systems with a LUMO signal in direct valence PES (see subsection 5.3.2). Hence it might be exclusive to systems with a LUMO signal either in direct valence PES and in RPES or only in the latter. The constant E_K features observed in subsection 5.3.3 on the other hand could only be significantly related to interface CT for the interface systems without a LUMO signal in direct valence PES. For these systems a mechanism that includes interface CT is proposed to be responsible for the constant E_K features. Successful calculations of the measured E_K values of the constant E_K features based on this mechanism quantitatively confirm this assignment. Since for the interface systems with a LUMO signal in direct valence PES this cannot be achieved a confirmation of interface CT through the detection of constant E_K features is not possible for these systems. Consequently, before the analysis of the RPES data of the particular hetero-molecular interface it must be known which of its constituents exhibits a LUMO signal and which one does not. Through this characterization of the particular molecule it becomes clear which conclusion can be drawn from which CT criterion. Then the knowledge gained in the investigation of the homo-molecular interface systems of both categories can be applied to the corresponding hetero-organic system.

In the following the RPES data of the lateral hetero-organic system CuPc + PTCDA on Ag(111) and the vertical hetero-organic system CuPc/1ML PTCDA/Ag(111) will be inspected for the above discussed features related to dynamical CT. For the system CuPc + PTCDA on Ag(111) a constant E_K feature is found and assigned to CuPc molecules by a comparison to the corresponding 1 ML CuPc/Ag(111) RPES data. Furthermore, the characteristic broad line-shape observed for the interface systems with a LUMO signal appears in the E_B region of the frontier molecular orbitals in the RPES data of CuPc + PTCDA/Ag(111). Both of these findings identify that the two vertical molecule-Ag(111) interfaces are dominating the behavior of the molecules in this system rather than the lateral CuPc-PTCDA interface. So a statement about hetero-molecular interface CT cannot be given. In the second part of this section the RPES data of the vertical hetero-organic interface of the system CuPc/1ML PTCDA/Ag(111) is scanned for the identified CT criteria. Neither a CT state nor a constant E_K feature can be observed in

the RPES data of CuPc/1ML PTCDA/Ag(111). Furthermore, the characteristic broad line-shape of frontier molecular orbital signals is not observed for the CuPc HOMO signal. Hence hetero-molecular interface CT at the vertical CuPc-PTCDA interface cannot be revealed. The comparison of the lateral and the vertical hetero-organic interface systems consisting of CuPc and PTCDA molecules is used to discuss the exclusion of dynamical interface CT for the latter system. It is concluded that strong evidence is found to exclude the existence of such a mechanism for the hetero-organic interface in the system CuPc/1ML PTCDA/Ag(111) but that a definite statement is not possible.

5.4.1 Lateral hetero-organic interface: CuPc + PTCDA/Ag(111)

The core level PES data of the lateral hetero-organic interface CuPc + PTCDA/Ag(111) is investigated with the *fingerprint approach* in Fig. 4.10(a). It is shown that both molecules exhibit a LUMO signal in direct valence PES (see Fig. 4.10(b)) by identifying very similar core level line-shapes as in the corresponding homo-molecular films on Ag(111). The modification with respect to homo-molecular films on Ag(111) is characterized to be similar to the modifications found for CuPc and PTCDA molecules on different Ag surfaces or in different structural phases on the same Ag surface. So in PES the bonding of each molecule to the Ag(111) surface dominates the physics of this hetero-organic system. However, the RPES data of this system will be closely investigated for possible consequences of the modified bonding situation.

The discussion of the RPES data of the interface systems with a LUMO signal in direct valence PES in subsection 5.3.2 revealed that an assignment of final states to the observed features is not possible. Hence the same most probably applies for CuPc + PTCDA/Ag(111) since it is a hetero-organic system with two molecules that both exhibit a LUMO signal in direct valence PES. In any case a comparison of this hetero-organic system to the homo-molecular interface systems with and without a LUMO signal in direct valence PES can be performed. So even if an explicit explanation of the measured RPES data is not possible for CuPc + PTCDA/Ag(111) a discussion with respect to the RPES data of homo-molecular interfaces will be.

In Fig. 5.22 the RPES data of 0.6 ML CuPc + 0.3 ML PTCDA/Ag(111) is presented. The PES overview map (Fig. 5.22(a)) is displayed on an E_K scale in order to facilitate the detection of constant E_K features. From the region denoted by the blue dashed box an $h\nu$ integrated EDC is extracted and illustrated as open blue circles in Fig. 5.22(c) together with the corresponding spectrum of the system 1 ML CuPc/Ag(111) (open green squares). The direct comparison of these two $h\nu$ integrated EDCs shows that for 0.6 ML CuPc + 0.3 ML PTCDA/Ag(111) very similar constant E_K features are found as for 1 ML CuPc/Ag(111). Especially the detection of the constant E_K feature CFS 2 at a very similar energy as in the RPES data of 1 ML CuPc/Ag(111) is unambiguous so I conclude that this constant E_K feature stems from the CuPc molecule. This finding demonstrates

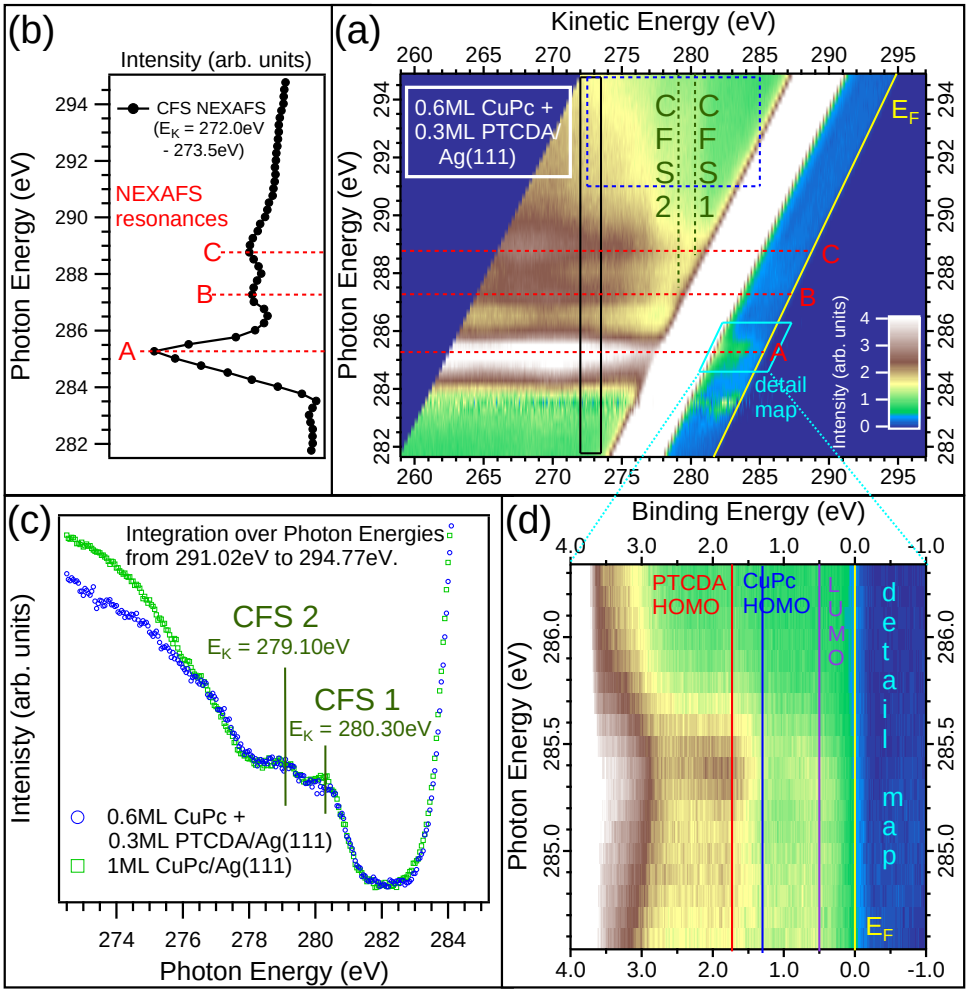

Figure 5.22: RPES data at the carbon K-edge of 0.6 ML CuPc + 0.3 ML PTCDA/Ag(111). **(a)** PES overview map with an $h\nu$ increment of 250 meV and an E_K increment of 50 meV presented on an E_K scale. The red dashed horizontal lines denote the NEXAFS resonances which are identified in the CFS NEXAFS spectrum in panel (b). The black box marks the region from which the CFS NEXAFS spectrum is obtained by an integration over E_K. The blue dashed box illustrates the area from which the $h\nu$ integrated EDC originates and the E_K region in which it is presented in panel (c). The olive dashed vertical lines denote the constant E_K features of 1 ML CuPc/Ag(111) illustrated in panel (c). The cyan parallelogram marks the region of the PES detail map shown in panel (d). The yellow line represents E_F. **(b)** CFS NEXAFS spectrum extracted from the black box in the PES overview map in panel (a). **(c)** $h\nu$ integrated EDC of 0.6 ML CuPc + 0.3 ML PTCDA/Ag(111) (open blue circles) obtained by integration over $h\nu$ in the area of the blue dashed box in the PES overview map in panel (a). The constant E_K features identified for the $h\nu$ integrated EDC of 1 ML CuPc/Ag(111) (open green squares, see Fig. 5.18 for origin of spectrum) are marked with olive lines. **(d)** PES detail map with an $h\nu$ increment of 100 meV and an E_B increment of 15 meV presented on an E_B scale. The colored vertical lines represent the E_B positions of the particular molecular orbital signals in direct valence PES (see also Fig. 5.23).

that the energetic overlap with features corresponding to PTCDA molecules in this E_K region does not hinder the detection of a constant E_K feature that originates from CuPc molecules. Hence the assignment of constant E_K features to a particular molecule seems possible for this hetero-organic systems by a comparison to the RPES data of the corresponding homo-molecular film.

In the PES overview map (Fig. 5.22(a)) a significant resonant enhancement of the frontier molecular orbital signals is observed at $h\nu$ of NEXAFS resonance A. Comparing the CFS NEXAFS spectrum of 0.6 ML CuPc + 0.3 ML PTCDA/Ag(111) in Fig. 5.22(b) with the CFS NEXAFS spectra of 1 ML CuPc/Ag(111) in Fig. 5.18(e) and the one of 1 ML PTCDA/Ag(111) in Fig. 5.15(d) it can be concluded that NEXAFS resonance A of the hetero-organic film consists of NEXAFS resonances from both molecules. Hence the observed resonantly enhanced PES intensity in the E_B region of the frontier molecular orbital signals should include signals from both molecules. A closer investigation of the region of the PES overview map marked by the cyan parallelogram can be performed with the PES detail map presented in Fig. 5.22(d). Therein the main feature is observed at $E_B \approx 2$ eV and $h\nu \approx 285.2 - 285.6$ eV. This E_B roughly coincides with the E_B of the PTCDA HOMO signal in direct valence PES (see EDC at $h\nu = 120$ eV in Fig. 5.23) so the assignment of this main feature to the resonantly enhanced PTCDA HOMO signal appears straightforward. Considering the energetic separation of the CuPc HOMO signal in direct valence PES and this main feature it could also stem from CuPc molecules since in the 1 ML CuPc/Ag(111) RPES data (see Fig. 5.17(b)) the main feature is found at an E_B position with a similar energetic separation from the CuPc HOMO signal. Both of these scenarios are reasonable which demonstrates that in this hetero-organic interface system with two molecules that both exhibit a LUMO signal in direct valence PES even the assignment of features to one of the two molecules is difficult. The most important finding from this PES detail map is that no distinct peak feature is visible. Such a feature would be for example similar to the HOMO signal of the CuPc multilayer in Fig. 5.4(c). Hence an increase of intensity by at least an order of magnitude within some 100 meV of $h\nu$ together with a gradual distribution of intensity to higher E_B with increasing $h\nu$ should be observed. This is not the case in Fig. 5.22(d).

For a detailed discussion of the line-shape of the frontier molecular orbital signals 1D EDCs are investigated. So the $h\nu$ region of significant resonant intensity enhancement in the 2D PES map illustrated in Fig. 5.22(d) is presented in an EDC waterfall plot in Fig. 5.23. The absence of distinct peak features with the expected $h\nu$ dependent line-shape evolution and intensity variation discussed for Fig. 5.22(d) is confirmed by this EDC waterfall plot. In Fig. 5.23 resonantly enhanced PES intensity is found at all E_B positions. Moreover, an overall broad line-shape is observed that for some EDCs exhibits a step-function-like line-shape which is quite similar to to line-shape in the E_B region of the frontier molecular orbital signals in subsection 5.3.2.

All the experimental findings of the RPES data illustrated in Figs. 5.22 and 5.23 can be summarized in one conclusion. The existence of a LUMO signal in direct valence PES of both molecules which was concluded from the *fingerprint approach* analysis in Fig. 4.10(a) is confirmed by the RPES data. The identification of at least one constant

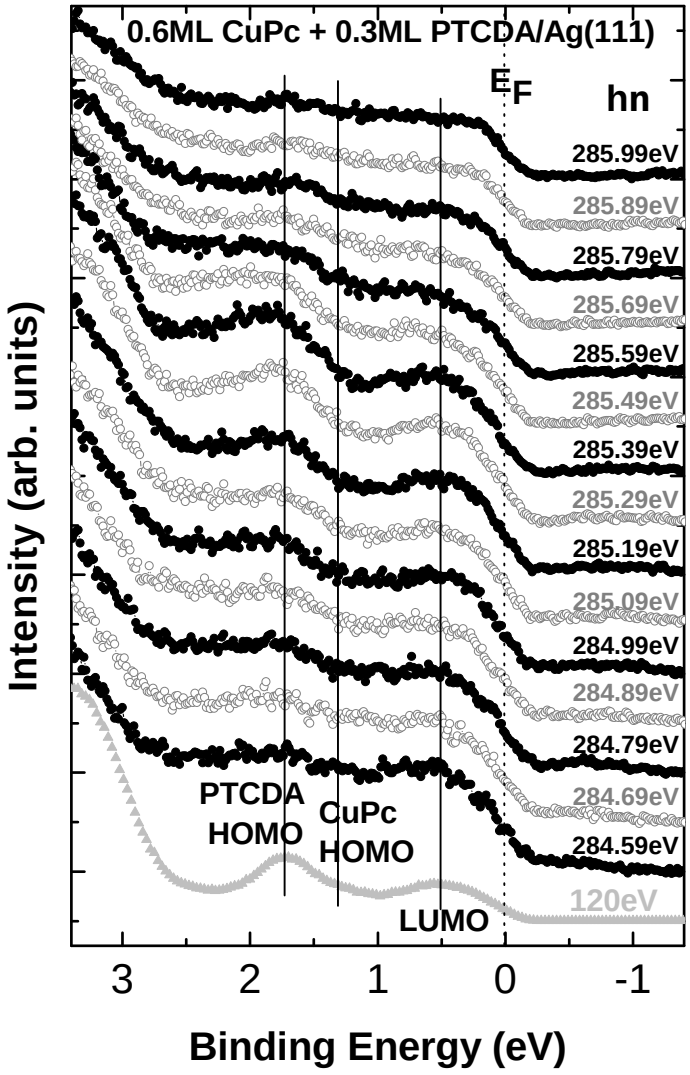

Figure 5.23: EDC waterfall plot of the carbon K-edge RPES data of 0.6 ML CuPc + 0.3 ML PTCDA/Ag(111) in comparison to direct valence PES data at $h\nu = 120$ eV. The presented EDCs stem from the PES detail map shown in Fig. 5.22(d). The vertical lines denote the E_B positions of the molecular orbital signals in direct PES. The dashed vertical line represents E_F.

E_K feature at a very similar E_K as for 1 ML CuPc/Ag(111) shows that CuPc molecules in this lateral hetero-organic film are similar to CuPc molecules in the system 1 ML CuPc/Ag(111). If multilayer-like CuPc molecules were present in the system CuPc + PTCDA/Ag(111) this constant E_K feature would most probably exhibit an E_K closer to the constant E_K features found for CuPc molecules on Au(111). Furthermore, the line-shape of the frontier molecular orbital signals shows the characteristic signatures observed in subsection 5.3.2 for the homo-molecular interface systems with a LUMO signal in direct valence PES. Additionally, the fact that no signature similar to the line-shape of the homo-molecular systems without a LUMO signal in direct valence PES (see section 5.2) is found demonstrates that none of the two molecules belongs to this category. Consequently, the RPES data confirms the conclusion of the *fingerprint approach* analysis that a LUMO signal stemming from each of the two molecules must exist in direct valence PES. Hence molecule-metal CT is possible for both molecules since the detection of a LUMO signal is interpreted as a consequence of molecule-metal interface CT and a ground state with a significant contribution of a basis state with an occupied LUMO. Since no significant changes with respect to the homo-molecular systems 1 ML CuPc/Ag(111) and 1 ML PTCDA/Ag(111) (or 1 ML PTCDA/Ag(110)) are found in the RPES data of the hetero-organic interface of CuPc + PTCDA/Ag(111) the intermolecular interaction at this interface seems to have no significant influence on the RPES process. The bonding of each molecule to the Ag(111) surface appears to dominate the physics of this system which makes a statement about intermolecular CT at this lateral hetero-organic interface very difficult.

5.4.2 Vertical hetero-organic interface: CuPc/1ML PTCDA/Ag(111)

The core level PES data of the system CuPc/1 ML PTCDA/Ag(111) is analyzed with the *fingerprint approach* in Fig. 4.2(a). There the contribution of PTCDA molecules to the C1s core level PES spectrum of the hetero-organic system is found to be unchanged with respect to 1 ML PTCDA/Ag(111). Furthermore, the contribution of CuPc molecules to this C1s PES spectrum is identified to be equal to the CuPc multilayer reference spectrum. Hence CuPc molecules are multilayer-like and consequently no CuPc LUMO signal is present in direct valence PES. A recent differential reflectance spectroscopy investigation of CuPc molecules deposited onto 1 ML PTCDA/Ag(111) finds a CuPc signal that is interpreted as CuPc monomers which points towards optically decoupled CuPc molecules [135]. This corroborates the conclusion drawn from the *fingerprint approach* analysis in Fig. 4.2(a). PTCDA molecules on the other hand do exhibit a LUMO signal in direct valence PES in the system CuPc/1 ML PTCDA/Ag(111). However, a change of E_B of the LUMO signal of PTCDA molecules in this hetero-organic system with respect to the system 1 ML PTCDA/Ag(111) is reported in Ref. [20]. Whether the apparent variation of E_B of the LUMO signal observed in Ref. [20] stems from an actual change of E_B or is a consequence of a modification of backscattering (see discussion of Fig. 4.2(b) in section 4.1.1 and Fig. A5) is of minor interest for the interpretation of the RPES data.

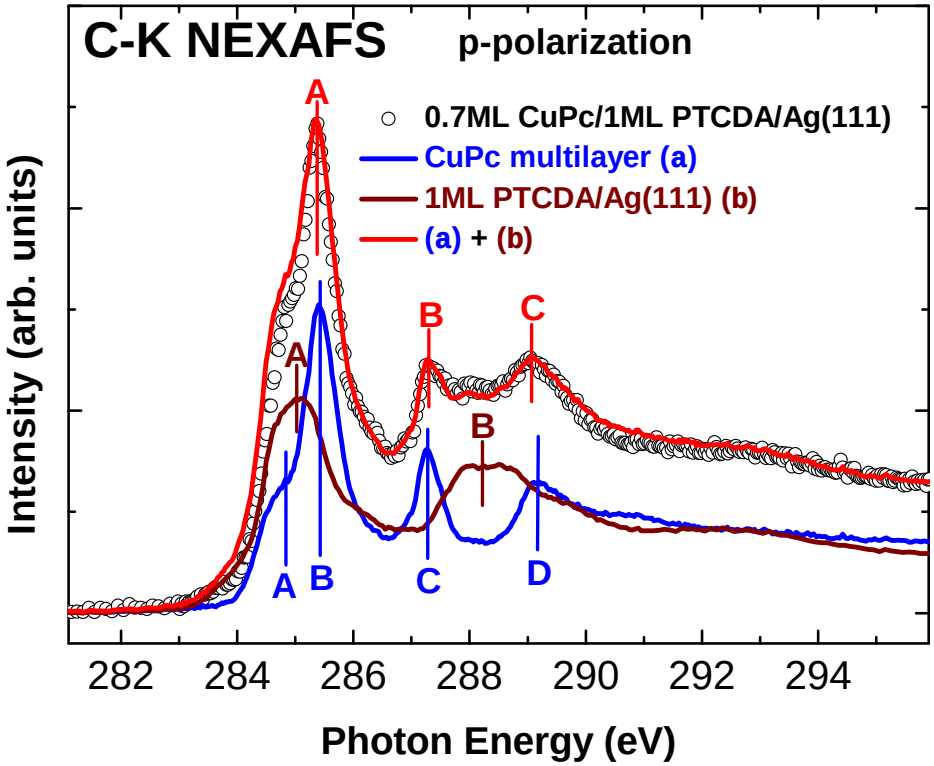

Figure 5.24: Carbon K-edge NEXAFS data of 0.7 ML CuPc/1 ML PTCDA/Ag(111) (open circles) together with scaled reference spectra of 1 ML PTCDA/Ag(111) (brown line) and a CuPc multilayer (blue line). The red line is the sum of both reference spectra. The capital letters denote the NEXAFS resonances of the NEXAFS spectrum of the corresponding color.

The comparison of the systems 1 ML PTCDA/Ag(111) and 1 ML PTCDA/Ag(110) in Fig. 5.15 reveals that a difference in the E_B position (or the apparent filling) of the LUMO signal in direct valence PES does not lead to significant changes of CT related features in the corresponding RPES data. Hence the relevant fact for an RPES investigation of the system CuPc/1 ML PTCDA/Ag(111) is that PTCDA molecules do exhibit a LUMO signal in direct valence PES while CuPc molecules do not. Consequently, the CT investigation with RPES at the vertical CuPc-PTCDA interface can be based on the search for the features related to dynamical CT which are found for the metal-organic interface systems without a LUMO signal in direct valence PES. CT on the time scale of the core hole lifetime across the PTCDA-CuPc interface is expected to go along with the emergence of these CT related features originating from CuPc molecules.

A very similar situation as for the system CuPc/1 ML PTCDA/Ag(111) is found for the vertical hetero-organic interface system SnPc/1 ML PTCDA/Ag(111) in Ref. [18]. SnPc molecules do not exhibit a LUMO signal in direct valence PES while PTCDA molecules do. Furthermore, in the RPES data of this system a difference in the $h\nu$ dependent

line-shape evolution of the SnPc HOMO signal with respect to the SnPc multilayer is reported in Ref. [123]. With increasing $h\nu$ more intensity distribution into the high E_B part of the SnPc HOMO signal is found for the hetero-organic interface with respect to the SnPc multilayer. Moreover, no constant E_K features are reported for the system SnPc/1 ML PTCDA/Ag(111) [174]. In the light of the following investigation of the RPES data of the system CuPc/1 ML PTCDA/Ag(111) these observations will be discussed.

Before I concentrate on the RPES data the carbon K-edge NEXAFS spectrum of the system 0.7 ML CuPc/1 ML PTCDA/Ag(111) is analyzed by the *fingerprint approach* in order to assign the measured NEXAFS resonances to a particular molecule. In Fig. 5.24 the measured data (open circles) is successfully reproduced in almost the entire energy region by reference spectra of 1 ML PTCDA/Ag(111) and a CuPc multilayer. Solely in the rising edge of NEXAFS resonance A of the hetero-organic film (red capital A) at $h\nu = 284 - 285$ eV a difference between the sum of the reference spectra (red line) and the measured spectrum remains. This is the $h\nu$ region of the intensity minimum of the beamline flux curve (see July 2011 spectrum in Fig. 3.2). So extracting a quantitative statement from this $h\nu$ region is very difficult. Even though the *fingerprint approach* analysis is not able to quantitatively reproduce the measured data at all $h\nu$ it is capable of properly producing all features. Hence an assignment of these particular features of the vertical hetero-organic film to the corresponding molecule is possible. For the CuPc multilayer and CuPc on Au(111) resonant enhancement of the HOMO signal is found in NEXAFS resonance B (see Fig. 5.4(c) and Fig. 5.8(b)). In the NEXAFS spectrum of the hetero-organic film in Fig. 5.24 this NEXAFS resonance B of the contribution of the CuPc molecules (blue capital B) corresponds to the maximum of NEXAFS resonance A (red capital A). So at this $h\nu$ a resonant enhancement of the CuPc HOMO signal in the hetero-organic film is expected.

In the PES overview map illustrated in Fig. 5.25(a) the NEXAFS resonances are identified with the CFS NEXAFS spectrum presented in Fig. 5.25(b). This CFS NEXAFS spectrum exhibits all the main features of the partial electron yield NEXAFS spectrum analyzed in Fig. 5.24. Hence applying the assignment of the NEXAFS resonances of the particular reference spectra in Fig. 5.24 to the CFS NEXAFS spectrum in Fig. 5.25(b) is straightforward. At $h\nu$ of the intensity maximum of NEXAFS resonance A indeed resonant enhancement is found in the E_B region of the frontier molecular orbital signals in the PES overview map (Fig. 5.25(a)). The region of the cyan parallelogram is thus investigated more closely with the PES detail map presented in Fig. 5.25(d). Therein a distinct peak feature is observed at the E_B position of the CuPc HOMO signal in direct valence PES (blue vertical line). The intensity variation of this distinct peak feature with $h\nu$ is similar to the one found for the CuPc multilayer in Fig. 5.4(c). Furthermore, a similar intensity distribution into the high E_B part of this CuPc HOMO signal with increasing $h\nu$ is visible in the PES detail maps of these two systems (see Figs. 5.4(c) and 5.25(c)). Thus a comparative discussion in relation to the CuPc multilayer of the line-shape of the CuPc HOMO signal in the 0.7 ML CuPc/1 ML PTCDA/Ag(111) RPES data (as for CuPc/Au(111) in Fig. 5.8(b)) is justified by the observed similarities in these PES detail

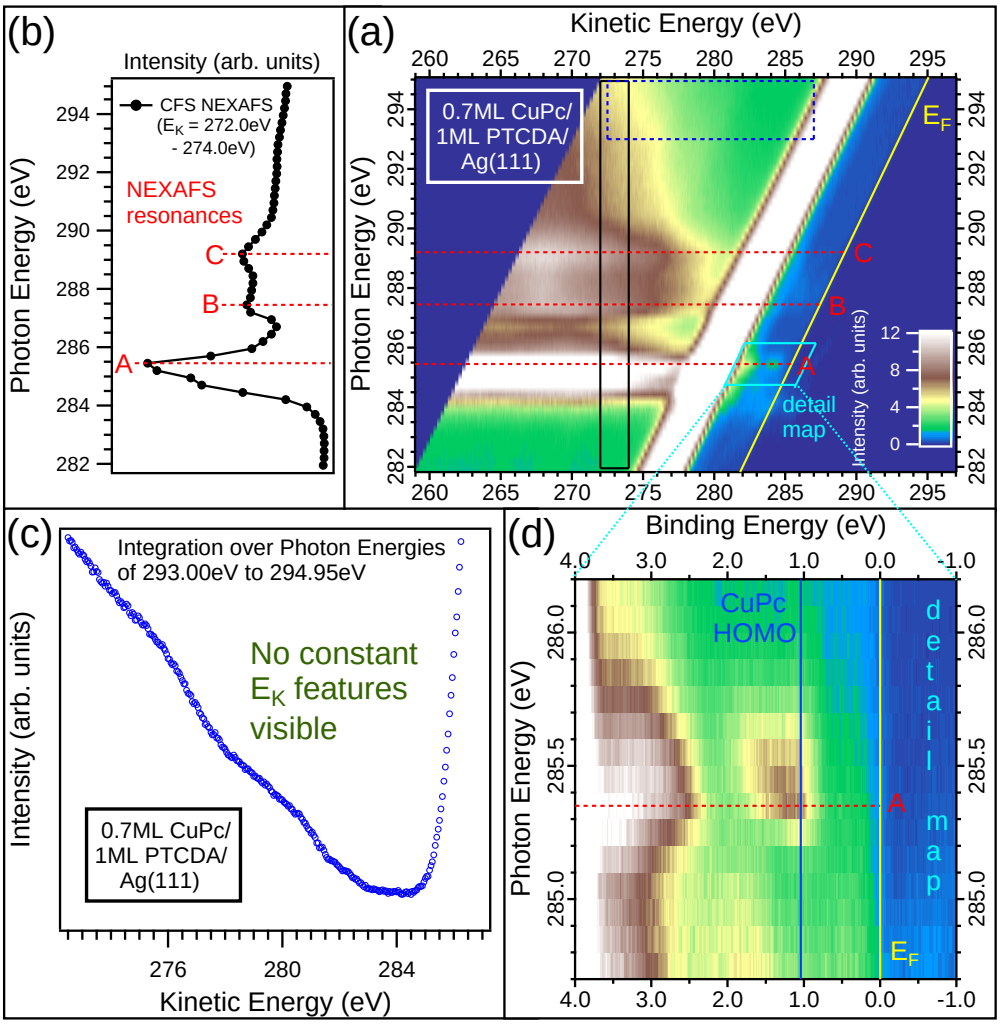

Figure 5.25: RPES data at the carbon K-edge of 0.7 ML CuPc/1 ML PTCDA/Ag(111). **(a)** PES overview map with an $h\nu$ increment of 250 meV and an E_K increment of 50 meV presented on an E_K scale. The red dashed horizontal lines denote the NEXAFS resonances which are identified in the CFS NEXAFS spectrum in panel (b). The black box marks the region from which the CFS NEXAFS spectrum is obtained by an integration over E_K. The blue dashed box illustrates the area from which the $h\nu$ integrated EDC originates and the E_K region in which it is presented in panel (c). The cyan parallelogram denotes the region of the PES detail map shown in panel (d). The yellow line represents E_F. **(b)** CFS NEXAFS spectrum extracted from the black box in the PES overview map in panel (a). **(c)** $h\nu$ integrated EDC obtained by integration over $h\nu$ in the area of the blue dashed box in the PES overview map in panel (a). **(d)** PES detail map with an $h\nu$ increment of 100 meV and an E_B increment of 15 meV presented on an E_B scale. The blue vertical line represents the E_B position of the CuPc HOMO signal in direct valence PES (see also Fig. 5.26).

maps. For that the 1 ML PTCDA/Ag(111) contribution is subtracted from the 0.7 ML CuPc/1 ML PTCDA/Ag(111) data with EDCs at the same $h\nu$ taken from Ref. [176]. Since the 1 ML PTCDA/Ag(111) EDCs do not exhibit any distinct peak features and the overall intensity variation with $h\nu$ is of a small magnitude compared to the CuPc HOMO signal no subtraction artifacts are produced on the intensity scale of the $h\nu$ dependent line-shape evolution of the CuPc HOMO signal.

The comparison of the $h\nu$ dependent line-shape evolution of the CuPc HOMO signal of the CuPc multilayer and the 0.7 ML CuPc/1 ML PTCDA/Ag(111) film is presented in Fig. 5.26. The EDCs at the lowest $h\nu$ are almost equal but at higher $h\nu$ more intensity is distributed into the high E_B part of the HOMO signal for the EDCs of the 0.7 ML CuPc/1 ML PTCDA/Ag(111) film. So the $h\nu$ dependent line-shape evolution of the CuPc HOMO signal in the system CuPc/1 ML PTCDA/Ag(111) is very similar to the one of the SnPc HOMO signal in the system SnPc/1 ML PTCDA/Ag(111) in Ref. [123]. In the light of the investigations of the $h\nu$ dependent line-shape evolution of molecular orbital signals of the interface systems without a LUMO signal in direct valence PES (see section 5.2) the most reasonable explanation for the difference observed in Fig. 5.26 is a modification of the potential energy surfaces involved in the RPES process. The same holds true for the deviation of the line-shape evolution of the SnPc HOMO of the system SnPc/1 ML PTCDA/Ag(111) from the one of a SnPc multilayer revealed in Ref. [123]. Hence the difference between the CuPc multilayer and CuPc molecules on top of 1 ML PTCDA/Ag(111) is identified to be a consequence of a modification of electron vibration coupling. Hence the $h\nu$ dependent line-shape evolution of the molecular orbital signals of all systems without a LUMO signal in direct valence PES can be explained by the same effect.

In Fig. 5.26 no broad line-shape as for the molecular orbital signals of the interface systems with a LUMO signal in direct valence PES in subsection 5.3.2 and the CT state in subsection 5.3.1 can be found for the CuPc HOMO signal. Moreover, no feature is observed in the RPES data of 0.7 ML CuPc/1 ML PTCDA/Ag(111) that can be assigned to a CT state. Considering that the PES intensity of the CT state observed for the system coronene/Ag(111) is found to be approximately 5% of the HOMO signal suggests that the existence of a similarly intense CT state in the RPES data of 0.7 ML CuPc/1 ML PTCDA/Ag(111) cannot be excluded either. Furthermore, in the $h\nu$ integrated EDC of 0.7 ML CuPc/1 ML PTCDA/Ag(111) in Fig. 5.25(c) no hint for a constant E_K feature is found as for the system SnPc/1 ML PTCDA/Ag(111) [174]. In the case of a hetero-organic film the absence of these constant E_K features could also be a consequence of an overlap with signals stemming from the PTCDA molecules in the first layer. So possible constant E_K features originating from the CuPc molecules could be below the detection limit in the RPES data of 0.7 ML CuPc/1 ML PTCDA/Ag(111). A comparison to the RPES data of the system 0.6 ML CuPc + 0.3 ML PTCDA/Ag(111) can be used to estimate whether constant E_K features should be detectable in the RPES data of 0.7 ML CuPc/1 ML PTCDA/Ag(111) or not. The observation of at least one constant E_K feature for this lateral hetero-organic interface system (Fig. 5.22(c)) shows that constant E_K features of 0.6 ML CuPc with a LUMO signal in direct valence PES are

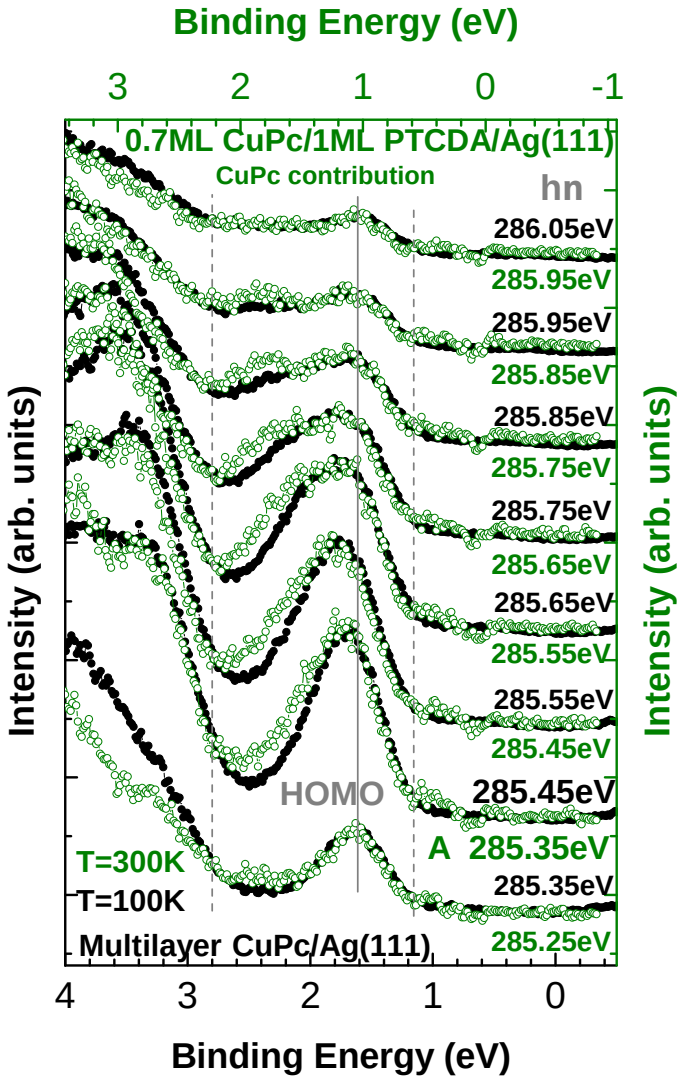

Figure 5.26: RPES data at the carbon K-edge of 0.7 ML CuPc/1 ML PTCDA/Ag(111) (open green circles) in comparison to RPES data of a CuPc multilayer prepared and measured at $T = 100$ K (filled black circles) presented as EDCs in a waterfall plot. The EDCs of equivalent $h\nu$ positions within the NEXAFS resonance (resonance maximum denoted by the larger $h\nu$ values and capital A) are compared to each other. The black axes (E_B and intensity) correspond to the black EDCs and the green axes to the green EDCs. The green E_B axis is shifted by -570 meV with respect to the black one. For the 0.7 ML CuPc/1 ML PTCDA/Ag(111) EDCs scaled 1 ML PTCDA/Ag(111) EDCs at equal $h\nu$ (from Ref. [176]) are subtracted and each EDC is scaled for best comparability of the line-shape of the HOMO signal. The gray vertical dashed lines denote the E_B region in which the line-shapes are compared and the gray solid line marks E_B of the HOMO signal in direct valence PES (see Fig. 4.2(b)). The presented EDCs stem from the PES detail map shown in Fig. 5.25(d).

detectable. Hence the signals of 0.3 ML PTCDA molecules with a LUMO signal in direct valence PES do not hinder the detection of these features. Additionally, it needs to be considered that the constant E_K features of 0.7 ML CuPc without a LUMO signal in direct valence PES are found to be more intense (especially CFS 2 in the RPES data of CuPc/Au(111), see Fig. 5.20(c)) than for 1 ML CuPc with a LUMO in direct valence PES (RPES data of 1 ML CuPc/Ag(111), see Fig. 5.18(f)). So if CuPc molecules on top of 1 ML PTCDA/Ag(111) can be considered equal to CuPc molecules on Au(111) concerning the issue of the production of constant E_K features I expect that constant E_K features will in principle be detectable for 0.7 ML CuPc/1 ML PTCDA/Ag(111). In this case the absence of constant E_K features in the $h\nu$ integrated EDC in Fig. 5.25(c) can be seen as strong evidence for the statement that hetero-molecular interface CT does not occur on the time scale of the core hole lifetime for this system.

However, the question of the comparability of PES and RPES of a π-conjugated molecule on an Au(111) surface with the same molecule on 1 ML PTCDA/Ag(111) leads to a discussion of its own. Considering the line-shape of the CuPc contribution to C1s core level PES spectra (see Figs. 2.1(a) and 4.2(a)) CuPc molecules in the systems CuPc/Au(111) and CuPc/1 ML PTCDA/Ag(111) can be regarded as equal (within measurement accuracy) to each other. This equality in core level PES spectra constitutes an unchanged reaction of the molecular orbitals on the creation of a core hole. That is only one requirement for the comparability concerning the issue of the production of constant E_K features. The central point in the responsible mechanism for these features (see Eq. 5.13) is CT from the state M of the metal ligand to the state L of the molecule. For the system CuPc/1 ML PTCDA/Ag(111) the PTCDA molecules have to play the role of the metal ligand. Consequently, the LUMO of PTCDA molecules on Ag(111) needs to be comparable to the Au(111) s-p bands in order to enable the comparison of the production of constant E_K features in the systems CuPc/Au(111) and CuPc/1 ML PTCDA/Ag(111). Then the probability for CT from the LUMO of PTCDA molecules to the LUMO of CuPc molecules can be related to the probability of CT from the Au(111) s-p bands to the LUMO of CuPc molecules and a statement about CT at the vertical PTCDA-CuPc interface is possible. Whether the LUMO of PTCDA molecules on Ag(111) can play a similar role as the Au(111) s-p bands in this mechanism cannot be argued at this point.

As discussed in subsection 5.2.2 an alternative explanation for the additional intensity in the high E_B part of the CuPc HOMO signal in the system CuPc/1 ML PTCDA/Ag(111) can be given by a CT related constant E_K feature. At higher $h\nu$ this feature would not overlap with the HOMO signal due to its linear dispersion on an E_B scale. Hence it should be detectable in the PES overview map at larger $h\nu$ unless its PES intensity is below the detection limit. In the expected E_K region of the $h\nu$ integrated EDC in Fig. 5.25(c) no such constant E_K feature is found. Additionally, in the systems for which constant E_K features are found a contribution of these features to the investigated frontier molecular orbitals in the intense NEXAFS resonances can be excluded (see discussion in subsection 5.3.3). Hence an interpretation of the additional intensity in the high E_B part of the CuPc HOMO signal as a CT related constant E_K feature lacks any experimen-

tal justification. Consequently, this alternative explanation is considered to be unlikely. Thus I can conclude that there is no evidence for hetero-organic interface CT in the RPES data of the system CuPc/1 ML PTCDA/Ag(111). The same holds true for the system SnPc/1 ML PTCDA/Ag(111). If these system were comparable to the systems CuPc/Au(111) and SnPc/Au(111) concerning the issue of the production of constant E_K features I would be able to exclude CT on the time scale of the core hole lifetime at the PTCDA-CuPc and the PTCDA-SnPc interface in these vertical hetero-molecular systems.

5.5 Summary and conclusion

In order to be able to perform a dynamical CT investigation with RPES of the hetero-molecular interface systems, which are found to be appropriate for such a study in chapter 4, the detection of CT related signals is necessary. For that a basic understanding of the RPES process of homo-molecular systems consisting of the same or similar molecules is required. The most reasonable starting point for acquiring the required understanding is a large $h\nu$ and E_B scale RPES investigation of molecules that are isolated from a metal surface. This RPES data of multilayer samples can be scanned for signals that are energetically separable and intense enough to allow a more detailed analysis. A comparison of these features found in multilayer samples with the corresponding features in the RPES data of molecule-metal interface systems can be discussed in terms of molecule-metal interface CT. Moreover, signals which are exclusively detected in the RPES data of molecule-metal interface systems further constitute a promising basis for a CT investigation with RPES. The knowledge gained by these investigations of homo-molecular systems can then be applied to hetero-molecular interface systems to achieve the goal of a dynamical CT investigation with RPES of such an interface.

In section 5.1 an RPES study of multilayer samples of the model molecules NTCDA and coronene is performed on the large $h\nu$ and E_B scale for the purpose of gaining a basic understanding of the RPES process of π-conjugated molecules. The observed $h\nu$ dependent intensity variation of the molecular orbital signals is discussed within a simplified description of the RPES process. For an NTCDA multilayer the unique $h\nu$ dependent intensity variation of different groups of molecular orbital signals is explained with the local character of the electronic transitions in the particular NEXAFS resonance and the real space probability density of the molecular orbitals that contribute to the particular CIS spectrum. On the basis of this simplified description the measured $h\nu$ dependent intensity variation and the knowledge about the localization of electronic transitions are used for a rough determination of the real space probability density of the contributing molecular orbitals. With an evaluation of the RPES data of a coronene multilayer the limits of this simplified explanation are revealed. It is shown that with the knowledge about the localization of the electronic transition in the particular NEXAFS resonance and the real space probability density of the particular molecular orbital the measured

$h\nu$ dependent relative intensity variations can be successfully predicted when these constitute differences by orders of magnitude. On the other hand differences within the same order of magnitude cannot be predicted within this simplified explanation of the $h\nu$ dependent intensity variation.

The RPES investigation on the large $h\nu$ and E_B scale in section 5.1 reveals energetically separated signals with a sufficient resonant enhancement of PES intensity for a more detailed analysis. The $h\nu$ dependence of the line-shape of these resonantly enhanced frontier molecular orbital signals is studied extensively in section 5.2. Through the comparison to RPES investigations of small molecules in the gas phase the observed $h\nu$ dependent line-shape evolution of molecular orbital signals is explained by electron vibration coupling. Explicitly the explanation of this $h\nu$ dependence is based on the excitation of different vibrational levels of the intermediate state potential energy surface and the consequential characteristic intensity distribution among the vibrational levels of the final state potential energy surface. This explanation is applicable to a large data set consisting of multilayer films and molecule-metal interface systems without a LUMO signal in direct valence PES. In contrast the RPES data presented in subsection 5.3.2 demonstrates that the $h\nu$ dependent line-shape evolution of molecular orbital signals of molecule-metal interface systems with a LUMO signal in direct valence PES shows hardly any resemblance to the one of the systems analyzed in section 5.2. An alternative explanation of the $h\nu$ dependent line-shape evolution of molecular orbital signals of systems without a LUMO signal in direct valence PES on the basis of a CT related constant E_K feature in addition to a constant E_B feature is concluded to be unlikely. This conclusion originates from the comparison of the RPES data of the multilayer and the molecule-metal interface films. Hence the observed modification of molecular orbital signals at molecule-metal interfaces with respect to the multilayer films found in section 5.2 cannot be used for a CT investigation.

The observation of features in the RPES data of molecule-metal interface systems that are absent in the RPES data of the corresponding multilayer sample enables the revelation of features related to dynamical CT in section 5.3. Therein three such CT related features are identified in the RPES data of homo-molecular molecule-metal interface systems. The first of these CT related features is the CT state of the system coronene/Ag(111) which is detected through relative resonant enhancement with respect to the HOMO signal. The assignment of an explicit final state to this CT state is confirmed by a quantitative consistency check within the *Molecular Cluster Model*. Then the translation of the responsible process in the *Molecular Cluster Model* into a qualitatively equal process in a multichannel model enables the presentation of this CT state in the established picture of CT in an intermediate state which can or cannot occur on the time scale of the core hole lifetime. In contrast to the CT state in the system coronene/Ag(111) an explicit assignment of final states to features in the E_B region of molecular orbital signals at $h\nu$ of the intense NEXAFS resonances is very difficult for the systems with a LUMO signal in direct valence PES. In the RPES data of these systems a broad line-shape without any peak features for some $h\nu$ hinders such an assignment. This broad line-shape constitutes the second CT related feature since a possible explanation for this observation is based

on CT from the energetically broad substrate s-p bands to the molecular orbitals. It is argued that the energetically broad character of substrate s-p bands is imprinted onto molecular orbital signals by interface CT. Furthermore, hints for CT related constant E_K features in the E_B region of the molecular orbital signals of molecule-metal interface systems with a LUMO signal in direct valence PES motivates a search for such features at larger $h\nu$. For both types of molecule-metal interface systems such constant E_K features are observed at large $h\nu$ but these are not situated at the expected E_K position. Only for the molecule-metal interface systems without a LUMO signal in direct valence PES the mechanism responsible for these constant E_K features is identified by a successful calculation of the measured E_K which is based on the proposed mechanism and explicitly stated simplifying assumptions. The fact that molecule-metal interface CT is included in the responsible mechanism identifies the constant E_K features as the third CT related feature which is revealed in section 5.3.

In section 5.4 the knowledge gained by the RPES investigations of homo-molecular systems in the previous sections is applied to hetero-molecular interfaces. A dynamical CT investigation of these systems relies on a search for the three CT related features in the RPES data of hetero-organic interface systems. Constant E_K features very similar to the ones observed for the system 1 ML CuPc/Ag(111) are detected for the lateral hetero-organic interface system CuPc + PTCDA/Ag(111). Moreover, in the RPES data of this system a similar broad line-shape as for the homo-molecular molecule-metal interface systems with a LUMO signal in direct valence PES is observed in the E_B region of the molecular orbital signals. Additionally, no feature related to CT across the lateral hetero-organic interface is detected in this RPES data. These experimental findings lead to the conclusion that in the system CuPc + PTCDA/Ag(111) the bonding of each molecule to the Ag(111) surface seems to dominate the physical properties relevant for RPES. In the RPES data of the vertical hetero-organic system CuPc/1 ML PTCDA/Ag(111) none of the three CT related features is observed. The $h\nu$ dependent line-shape evolution of the CuPc HOMO signal of this system can be compared to the one of a CuPc multilayer film. Moreover, the involvement of a constant E_K feature in the observed difference of this effect between these two systems is found to be unlikely which contradicts a relation of this difference to interface CT. The absence of constant E_K features at large $h\nu$ in the RPES data of the system CuPc/1 ML PTCDA/Ag(111) is discussed in comparison to the systems CuPc + PTCDA/Ag(111) and CuPc/Au(111). From this discussion it is concluded that if CT occurred on the time scale of the core hole lifetime constant E_K features should be detectable. However the conclusion that CT on this time scale can be excluded from the absence of such constant E_K features requires the comparability of the CuPc-PTCDA interface in the system CuPc/1 ML PTCDA/Ag(111) with the CuPc-Au(111) interface. Hence CT across this vertical hetero-molecular CuPc-PTCDA interface can neither be confirmed nor be definitely excluded.

6 Discussion and outlook

The conclusions which can be drawn from this work rely on both molecular and solid state physics concepts. An interpretation of the high resolution core level photoelectron spectroscopy (PES) and resonant photoelectron spectroscopy (RPES) data from a single viewpoint might have led to a simpler overall picture but at the same time could have favored some quite questionable statements. It is the solid state physics concept based *Molecular Gunnarsson-Schönhammer* theory which established the connection of core level and valence PES and introduced the direct correspondence of the spectra measured with both techniques. With that the contributions to complicated valence PES spectra of hetero-molecular films, that showed hardly any resemblance to the homo-molecular spectra, could be revealed through the *fingerprint approach* analysis of core level PES data. A direct assignment of signals to such spectra would have been quite speculative and probably would have allowed a variety of different conclusions. The same applies for the investigation of the layer order of the hetero-organic systems. The unexpected instability of some of the systems investigated in chapter 4 is unambiguously shown by the reproduction of the core level PES data within the *fingerprint approach* analysis. For that the solid state physics originated *Molecular Gunnarsson-Schönhammer* theory provides the proper theoretical justification and motivates the necessary discussion of possible alternative explanations. Excluding these with a consideration of the measured PES intensities allowed to draw a consistent picture on a solid foundation. A pure molecular picture would have lacked an established theoretical background which might have opened the door for some intuitive but at the same time false interpretation of the data. Consequently, the identification of two hetero-molecular interface systems in chapter 4 that are appropriate for a subsequent RPES analysis in chapter 5 depended on solid state physics concepts and would probably not have been possible without applying these.

The explanation of the photon energy ($h\nu$) dependent line-shape evolution of molecular orbital signals in section 5.2 on the other hand takes advantage of an established molecular physics concept. The fact that this effect has been successfully calculated for small molecules in the gas phase [62, 63, 69] (CO, N_2, and O_2) permitted the comparison to the π-conjugated molecules investigated in this work. Especially the detection of additional intensity in the high binding energy (E_B) part of the signal of the highest occupied molecular orbital (HOMO) of CuPc in the system CuPc on one monolayer (ML) of PTCDA on Ag(111) with respect to the CuPc multilayer data (see subsection 5.4.2) offered a tempting alternative explanation. Explaining this observation with charge transfer (CT) across the hetero-molecular interface constitutes a spectacular experimental finding. However, being aware of the possibilities of modifications of the line-shape

of a molecular orbital signal within an electron vibration coupling based explanation questions the former scenario. At the end the consideration of all measured systems could be used to identify the latter explanation as the favorable one since for the former unlikely scenarios would have been required. Furthermore, the effect of the interface originated modification of the $h\nu$ dependent line-shape evolution of molecular orbital signals can be used as a very sensitive probe for interface interaction since it is able to find differences within the systems without a signal of the lowest unoccupied molecular orbital (LUMO) in direct valence PES. These behave otherwise quite similar in electron spectroscopic techniques. The comparison of multilayer films and submonolayer (sub-ML) films, which is usually hindered by the inhomogeneous broadening of the molecular orbital signals of the former, becomes possible through this effect in RPES. Since molecular vibrations are closely connected to the reorganization energy accompanied by CT processes [57, 58] this comparison enables further application relevant studies with RPES.

Moreover, the consideration of the *Molecular Cluster Model* for the explanation of the CT state in subsection 5.3.1 opens up new ways to investigate molecule-metal interface CT. Hereby, the perspective of a solid state physics concept automatically included many body physics though the picture of states which are quantum mechanical superpositions of the selected basis states. This elegantly avoided the necessity to utilize a single particle picture on which for example many core-hole clock investigations are based. Whether such a single particle picture is justified is usually not discussed in the literature of RPES applied to molecule-metal interfaces. The attempt to calculate the kinetic energy (E_K) of the constant E_K features in subsection 5.3.3 on the basis of a particular decay process and explicitly defined simplifications permits such a discussion of the applicability of a certain type of a single particle picture. Therein it is the size of the hopping matrix element between molecular and metal states that appears to be the decisive parameter. For the systems without a LUMO signal in direct valence PES the applied simplifications were justified by the agreement between calculations and measurements. Consequently, it can be concluded that the single particle picture which neglects a significant hybridization of molecular and metal states can be applied to these systems. The failure of analogous calculations to obtain the E_K values measured for the molecule-metal interface systems with a LUMO signal in direct valence PES on the other hand suggests that for these systems such simplifications are not appropriate. An analysis based on the *Molecular Cluster Model* should in fact be able to allow statements about CT at such metal-organic interfaces but for that a significant extraction of intensities of energetically separable features would be necessary. For the RPES data presented in subsection 5.3.2 this could not be achieved.

In the final RPES investigation of a lateral and a vertical hetero-organic interface with CuPc and PTCDA molecules on Ag(111) in section 5.4 the conclusions previously drawn from the *fingerprint approach* analysis of core level PES data of these systems were confirmed by the RPES data. For CuPc + PTCDA/Ag(111) the main result from both techniques was that the molecule-metal interaction dominates the physics of this system. Moreover, both techniques came to the conclusion that at the CuPc-PTCDA interface

of the system CuPc/1 ML PTCDA/Ag(111) no significant hybridization takes place. A very similar agreement of the interpretation of RPES and core level PES data has been found for the comparison of the systems without and those with a LUMO signal in direct valence PES. Fundamental differences between these two classes of systems in the line-shape of homo-molecular core level PES spectra, the E_B region of the frontier molecular orbital signals in RPES, and the energetic position of the constant E_K features are observed in both techniques. The consideration of smaller deviations, however, identified RPES as the more sensitive technique. Therein the emergence of the CT state, the constant E_K features as well as the $h\nu$ dependent line-shape evolution of molecular orbital signals were found to differ for some molecular multilayer samples with respect to a sub-ML film of the corresponding molecule-metal system without a LUMO signal in direct valence PES. In core level PES no difference could be revealed for this comparison.

Throughout this work it has been clearly demonstrated that a comparative data discussion can be a successful way of data analysis. Especially for systems for which actual calculations of the experimental techniques are not available this approach is a promising method. To my best knowledge neither core level PES nor RPES have been calculated for the π-conjugated molecules investigated in this work. Furthermore, a significant reproduction of the data of these techniques with fitting routines utilizing Gaussian, Lorenzian, or Voigt peak functions requires knowledge about the number and relative intensities of the contributions to the spectra. Considering the possibility of excitations of satellites due to the interaction with the substrate (as in Ref. [84]) such a fitting routine analysis remains questionable for core level PES and RPES of complicated molecule-metal interface systems (for example PTCDA/Ag(111)). In contrast, the reproduction of a core level PES spectrum of a hetero-organic film with homo-molecular reference spectra, as in the *fingerprint approach* analysis of chapter 4, does only require significantly different line-shapes of the used reference spectra. This was the case for all systems investigated in chapter 4. Similarly, a comparative discussion of complicated systems with simple systems (CO, N_2, and O_2), for which calculations exist [62, 63, 69], was identified to be a successful approach. With that a reasonable explanation for the effect of the $h\nu$ dependent line-shape evolution of molecular orbital signals in section 5.2 was found. However, also the limits of such a comparative data analysis have become clear in this thesis. Whenever the *fingerprint approach* analysis reveals a deviation of the measured data from the combination of the reference spectra it is usually unclear which of the contributions is altered with respect to the corresponding reference spectrum. Furthermore, only a possible explanation for the origin of the observed deviation can be given. Hence the partially unsuccessful reproduction of the core level PES data of the system CuPc + PTCDA/Ag(111) leaves some questions unanswered. The same is true for the line-shape of the E_B region of the frontier molecular orbital signals in the RPES data of the molecule-metal interface systems with a LUMO signal in direct valence PES in subsection 5.3.2. To my best knowledge no comparable system can be found in literature for these observations. Merely a comparison within this category of systems is possible for the mentioned effect. The cornerstone for a comparative data analysis is

the comprehensive discussion of a large data set. For a single system a possible explanation for an observed effect through the comparison to a previously investigated system is in most cases easily found. Finding a common explanation for a large data set, on the other hand, is much more difficult and hence way more significant. Hence the analysis of a single system in this way is dangerous and must be interpreted very carefully.

A possible way to push the understanding of RPES applied to π-conjugated molecules forward is to perform RPES experiments with todays state of the art experimental equipment on simpler molecule-metal interface systems (for example CO, N_2 or O_2 on single crystal metal surfaces). This would enable a comparative discussion with the molecule-metal interface systems investigated in this work. For example issues like interface CT, $h\nu$ dependent intensity variations, and the modification of an $h\nu$ dependent lineshape evolution by a surface could be studied in more detail. Furthermore, such simpler molecule-metal interface systems should be a proper starting point to establish calculations of core level PES and RPES. From there analogous calculations of more complicated systems might be achieved as soon as a fundamental understanding of the theoretical techniques is gained. This would allow a direct comparison of experiment and theory from which way deeper insight into the experimental technique and the investigated systems can be expected. For core level PES calculations of metal-organic interfaces with π-conjugated molecules the Gunnarsson-Schönhammer theory [71, 72] could be a proper theoretical basis. RPES calculation might be successfully performed by a combination of model Hamiltonian techniques and density functional theory (DFT) methods. Hereby the parameters of the model Hamiltonian could be calculated with DFT calculations. Additionally, single particle molecular orbitals could be inserted into the Fano formula [42–45]. An additional RPES experiment that might lead to new interesting information is resonant ARPES. With a measurement of the angular intensity distribution of the resonantly enhanced molecular orbital signals the question whether these should be seen as resonant Auger signals or resonant PES signals could be answered. In the latter case the same angular intensity distribution as obtained in direct ARPES measurements can be expected. So far this question still is a matter of the different viewpoints of molecular and solid state physics concepts.

7 Summary / Zusammenfassung

Summary

This thesis consists of two parts of original experimental work, its evaluation, and interpretation. Its final goal is to investigate dynamical charge transfer (CT) at a hetero-molecular interface with resonant photoelectron spectroscopy (RPES). In order to achieve this goal preliminary studies have been necessary. First two hetero-molecular interfaces that exhibit adequate structural properties as well as an appropriate photoelectron spectroscopy (PES) spectrum of the valence regime have been identified. The desired CT analysis with RPES of these hetero-molecular systems is then conducted on the basis of the knowledge gained by previous RPES studies of homo-molecular systems.

The characterization of hetero-molecular films on single crystal Ag surfaces in the first part of this thesis is performed with high resolution core level PES and valence PES. The reproduction of the core level PES data with reference spectra of homo-molecular films allows me to determine which molecule is in direct contact to the Ag surface and which one is situated in higher layers (not the first one). Due to the direct correspondence of core level and valence PES the assignment of features in the spectra of the latter technique can be achieved with the identification of the contributions extracted from the evaluation of the data of the former technique. It is found that the systems PTCDA on one monolayer (ML) of SnPc on Ag(111) and CuPc/1 ML PTCDA/Ag(111) are stable at 300 K which means that no significant layer exchange occurs for these systems. In contrast a vertical exchange of CuPc and PTCDA molecules is observed for PTCDA deposited on top of 1 ML CuPc/Ag(111). Up to a coverage of approximately 0.5 ML of PTCDA molecules these diffuse into the first layer, replace CuPc molecules, and consequently force them into higher layers. Above a coverage of approximately 0.5 ML of PTCDA molecules these are also found in higher layers. The search for a promising system for the intended RPES study then leads to an investigation of hetero-molecular films with a combination of F4TCNQ and PTCDA molecules on Ag(110) within the same approach. Depositing F4TCNQ molecules onto a 1 ML PTCDA/Ag(110) film in the herringbone phase at 300 K results in an instable hetero-organic system which undergoes a layer exchange. Hereby PTCDA molecules in the first layer are replaced by F4TCNQ molecules similar to the behavior of the system PTCDA/1 ML CuPc/Ag(111). Switching the order of the preparation steps leads to a stable film of PTCDA/1.0 ML F4TCNQ/Ag(110) at 300 K. Among the stable hetero-molecular films only the system CuPc/1 ML PTCDA/Ag(111) exhibits the required wetting growth of the first two lay-

ers at 300 K and a valence PES spectrum with energetically separable molecular orbital signals in the same intensity range. Thus this system is identified to be appropriate for a detailed analysis with RPES.

The unexpected findings of vertical exchanges in the hetero-molecular films at 300 K motivate a study of the behavior at elevated temperatures for all systems investigated before. Therein it is revealed that annealing 1.5 ML SnPc/1 ML PTCDA/Ag(111) and 1.0 ML PTCDA/1 ML SnPc/Ag(111) to a temperature above the desorption temperature of molecules not in direct contact to the Ag(111) surface results in a 1 ML SnPc/Ag(111) film in both cases. Hence at elevated temperatures (approximately above 420 K) SnPc molecules replace PTCDA molecules in the first layer on Ag(111). At higher temperatures (approximately above 470 K) PTCDA molecules and SnPc molecules situated above the first layer then desorb from the 1 ML SnPc/Ag(111) sample. Annealing all hetero-molecular films with CuPc and PTCDA molecules on Ag(111) to 570 K leads to a sample with CuPc and PTCDA molecules in the first and only layer. Depending on the initial CuPc coverage different ratios of both molecules are obtained. With a CuPc coverage of exactly 1 ML, or above, films with PTCDA coverages of approximately 0.1–0.2 ML are produced. So at elevated temperatures CuPc molecules replace PTCDA molecules in the first layer of the system CuPc/1 ML PTCDA/Ag(111). Analogously the layer exchange at 300 K for the system PTCDA/1 ML CuPc/Ag(111) is reversed at elevated temperatures. In the case of SnPc and CuPc coverages below 1 ML annealing vertical hetero-molecular systems with PTCDA on Ag(111) up to 570 K results in a single layer of mixed hetero-molecular films with lateral long range order. In this way the system CuPc + PTCDA/Ag(111) is prepared and then characterized as a proper system for a detailed analysis with RPES. Additional annealing experiments of hetero-organic films consisting of F4TCNQ and PTCDA molecules on Ag(110) with an F4TCNQ coverage of 1.0 ML (and above) end in a submonolayer (sub-ML) film of F4TCNQ/Ag(110) that exhibits a contribution of amorphous carbon. Consequently, it can be concluded that at elevated temperatures part of the F4TCNQ molecules decompose.

In the second part of this thesis homo-molecular multilayer samples and (sub-)ML films on single crystalline metal surfaces are investigated with RPES in order to enable the final RPES study of vertical and lateral hetero-molecular interface systems. First a photon energy ($h\nu$) dependent intensity variation of (groups of) molecular orbital signals of exemplary multilayer films (NTCDA and coronene) is studied and explained on the basis of the local character of the electronic transitions in near edge x-ray absorption fine structure (NEXAFS) spectroscopy in combination with the real space probability density of the contributing molecular orbitals. This simple approach is found to be able to correctly describe relative intensity variations by orders of magnitude while it fails for $h\nu$ dependent relative intensity changes in the same order of magnitude. After that the $h\nu$ dependent line-shape evolution of an energetically separated molecular orbital signal of a CuPc multilayer is discussed in relation to small molecules in the gas phase and explained with an effect of electron vibration coupling. Through a comparison of the $h\nu$ dependent line-shape evolution of the highest occupied molecular orbital (HOMO) of a

CuPc with a SnPc multilayer the molecule specific character of this effect is identified. Then the same effect with either two (or more) electronic transitions or multiple coupling vibrational modes is observed for a coronene multilayer. Thereafter the influence of the adsorption on metal surfaces on this effect is studied and discussed with special emphasis on a possible contribution by features which are related to dynamical interface CT. For a sub-ML of SnPc/Au(111) no variation with respect to a SnPc multilayer film is detected while for a sub-ML of CuPc/Au(111) less intensity is distributed into the high binding energy (E_B) part of the HOMO signal with respect to the corresponding multilayer film. In the RPES data of a sub-ML of coronene/Ag(111) a resonance specific variation of the $h\nu$ dependent line-shape evolution of the HOMO signal is found by the revelation of a change of this effect with respect to the coronene multilayer data in only one of the two NEXAFS resonances. All these findings are consistently explained within one effect and a common set of parameters, namely all quantities that characterize the potential energy surfaces involved in the RPES process. Through that an alternative explanation that relies on dynamical CT can be excluded which influences the following CT analysis with RPES.

Three criteria for such an analysis of dynamical interface CT with RPES are identified. In the system coronene on Ag(111) a low E_B feature is related to metal-molecule interface CT through the assignment of a particular final state and hence named CT state. In the E_B region of the frontier molecular orbital signals of the molecule-metal interface systems with a signal from the lowest unoccupied molecular orbital (LUMO) in direct valence PES a broad line-shape is measured in RPES. This finding is related to interface CT by a possible explanation that emerges through the comparison to the line-shape of the CT state. The constant kinetic energy (E_K) features detected for several molecule-metal interfaces constitute the third criterion for a CT analysis with RPES. For the molecule-metal interface systems without a LUMO signal in direct valence PES the energy of these features can be calculated with the assignment of the responsible decay channel in combination with explicitly given simplifying assumptions. Through that the involvement of metal-molecule interface CT in the generation of these constant E_K features is demonstrated. The RPES data of the lateral and the vertical hetero-molecular interface, identified in the first part, is then scanned for these three CT criteria. Thereby neither for the lateral hetero-molecular system CuPc + PTCDA/Ag(111) nor for the vertical hetero-molecular system CuPc/1 ML PTCDA/Ag(111) dynamical hetero-molecular interface CT can be confirmed. In the former system the molecule-metal interface interaction is found to dominate the physics of the system in RPES while in the latter system no hints for a significant hybridization at the CuPc-PTCDA interface can be revealed.

Zusammenfassung

Diese Dissertation besteht aus zwei Hauptteilen, in denen neue experimentelle Ergebnisse präsentiert, ausgewertet und interpretiert werden. Das Ziel dieser Arbeit ist es, dynamischen Ladungstransfer an einer Heteroorganikgrenzfläche mit resonanter Photoelektronenspektroskopie (RPES) zu untersuchen. Um dies zu ermöglichen, musste erst eine solche Heteroorganikgrenzfläche, mit den geforderten strukturellen Eigenschaften, gefunden werden, die außerdem noch ein geeignetes Spektrum des Valenzbereichs in direkter Photoelektronenspektroskopie (PES) aufweist. Zusätzlich erforderte die angestrebte Ladungstransferanalyse mit RPES vorausgehende RPES Messungen an homomolekularen Systemen. Das dadurch erlangte Wissen konnte dann für die Interpretation von RPES Messungen heteromolekularer Grenzflächenschichten benutzt werden.

Der erste Teil dieser Arbeit befasst sich mit der Charakterisierung von heteromolekularen Filmen auf Silbereinkristalloberflächen durch hochauflösende PES der Rumpfzustände und PES der Valenzzustände. Die Reproduktion der Spektren der Rumpfzustände mit PES Referenzspektren homomolekularer Filme ermöglicht es herauszufinden welches Molekül direkt auf der Silberoberfläche liegt und welches in höheren Lagen (nicht der ersten) adsorbiert ist. Außerdem können dadurch Signale in PES Spektren des Valenzbereiches gewissen Zuständen zugeordnet werden, da ein direkter Zusammenhang von PES der Rumpfzustände und der Valenzzustände existiert. Dieser wiederum ermöglicht es, durch die Analyse der Daten der Rumpfzustände, herauszufinden, welche Beiträge im Spektrum des Valenzbereichs enthalten sein müssen. Mit der Analyse der PES Spektren der Rumpfzustände wird gezeigt, dass die Systeme PTCDA auf einer Monolage (ML) SnPc auf Ag(111) und CuPc/1 ML PTCDA/Ag(111) bei 300 K stabil sind. Somit kann ein signifikanter Austausch von Molekülen zwischen den beiden Lagen dieser vertikalen Heteroschichten ausgeschossen werden. Dampft man hingegen PTCDA Moleküle auf eine 1 ML CuPc/Ag(111) Schicht auf, so wird ein Austausch von CuPc Molekülen mit PTCDA Molekülen beobachtet. Für eine PTCDA Bedeckung von bis zu 0.5 ML diffundieren alle PTCDA Moleküle in die erste Lage, ersetzen die dort befindlichen CuPc Moleküle und zwingen diese in höhere Lagen. Oberhalb einer PTCDA Bedeckung von 0.5 ML adsorbieren diese Moleküle auch in höheren Lagen. Um weitere Systeme zu finden, die für die geplanten RPES Messungen geeignet sind, werden anschließend ebenfalls heteromolekulare Filme, bestehend aus F4TCNQ und PTCDA Molekülen auf Ag(110), mit der gleichen Methode untersucht. Ähnlich dem Verhalten des Systems PTCDA/1 ML CuPc/Ag(111) wird hierbei ein Austausch von PTCDA Molekülen durch F4TCNQ Moleküle in der ersten Lage des Systems F4TCNQ/1 ML PTCDA/Ag(110) beobachtet. Kehrt man die Präparationsreihenfolge hingegen um, kann bei 300 K ein stabiler Film von PTCDA/1.0 ML F4TCNQ/Ag(110) erzeugt werden. Das System CuPc auf 1 ML PTCDA/Ag(111) wird als einziges stabiles heteromolekulares System identifiziert, welches sowohl bei 300 K das benötigte benetzende Wachstum der ersten beiden Lagen,

als auch ein PES Spektrum des Valenzbereichs mit energetisch trennbaren Molekülorbitalsignalen im gleichen Intensitätsbereich aufweist. Somit ist gezeigt, dass dieses System für eine detaillierte Analyse mit RPES geeignet ist.

Der unerwartete Befund, dass bei einigen heteromolekularen Filmen ein vertikaler Austausch stattfindet, motiviert eine Studie des Verhaltens aller heteromolekularen Filme bei höheren Temperaturen. Dabei wird gezeigt, dass ein 1 ML SnPc/Ag(111) Film entsteht, wenn eine 1.5 ML SnPc/1 ML PTCDA/Ag(111) und eine 1.0 ML PTCDA/1 ML SnPc/Ag(111) Probe auf eine Temperatur erhitzt werden, bei der Moleküle, welche nicht direkt auf der Ag(111) Oberfläche adsorbiert sind, desorbieren. Bei erhöhter Temperatur (oberhalb ca. 420 K) verdrängen also SnPc Moleküle PTCDA Moleküle aus der ersten Lage auf der Ag(111) Oberfläche. Wird die Temperatur weiter erhöht (oberhalb ca. 470 K), so desorbieren PTCDA und SnPc Moleküle, welche sich nicht in der ersten Lage befinden, von dem entstandenen 1 ML SnPc/Ag(111) Film. Das Erhitzen aller heteromolekularen Filme, die aus PTCDA und CuPc Molekülen bestehen, auf eine Endtemperatur von 570 K resultiert in einer Probe, bei der sowohl CuPc als auch PTCDA Moleküle in der ersten, und einzigen Lage, adsorbiert sind. Abhängig von der anfänglichen CuPc Bedeckung entstehen verschiedene Verhältnisse der beiden Moleküle. Eine anfängliche CuPc Bedeckung von genau einer ML, oder darüber, führt zu einem Film mit einer PTCDA Bedeckung von ca. 0.1–0.2 ML. Aus den Heizexperimenten am System CuPc/1 ML PTCDA/Ag(111) folgt also, dass bei erhöhten Temperaturen CuPc Moleküle den Platz von PTCDA Molekülen in der ersten Lage einnehmen. Gleichermaßen wird der Austausch, der für das System PTCDA/1 ML CuPc/Ag(111) bei 300 K erfolgt ist, wieder rückgängig gemacht. Das Erhitzen einer heteromolekularen Probe mit PTCDA Molekülen und SnPc bzw. CuPc Bedeckungen unterhalb einer ML auf 570 K resultiert in einer gemischten heteromolekularen ML, die eine langreichweitige laterale Ordnung besitzt. Auf diese Art und Weise kann das System CuPc + PTCDA/Ag(111) präpariert werden. Die Charakterisierung dieses Systems zeigt, dass es sich für eine detaillierte Analyse mit RPES eignet. In weiteren Experimenten werden heteromolekulare Filme, bestehend aus F4TCNQ und PTCDA Molekülen auf Ag(110) mit einer F4TCNQ Bedeckung von 1.0 ML, und darüber, erhitzt. Hierbei werden Submonolagenfilme von F4TCNQ auf Ag(110) erzeugt, die zusätzlich noch amorphen Kohlenstoff enthalten. Daraus lässt sich schließen, dass ein Teil der F4TCNQ Moleküle beim Erhitzen auf diese Temperaturen zersetzt werden.

Im zweiten Teil dieser Arbeit werden homomolekulare Multilagen-, Monolagen und Submololagenfilme auf einkristallinen Metalloberflächen mit RPES untersucht, um die dadurch erlangten Ergebnisse auf RPES Messungen an heteromolekularen Filmen anzuwenden. Als erstes wird anhand von Messungen an Multilagenfilmen zweier Modellmoleküle (NTCDA und Coronen) die Abhängigkeit der Intensitätsvariation (einer Gruppe) von Molekülorbitalsignalen von der Photonenenergie ($h\nu$) untersucht. Die gewonnenen Daten werden durch den lokalen Charakter der elektronischen Übergänge in der Nahkantenröntgenabsorptionsfeinstrukturspektroskopie (NEXAFS) und der Realraumwahrscheinlichkeitsdichte der beitragenden Molekülorbitale erklärt. Mit diesem vereinfachten Denkansatz können relative Intensitätsvariationen über Größenordnungen be-

schrieben werden, bei relativen Veränderungen der Intensität innerhalb der selben Größenordnung versagt diese Erklärung allerdings. Daraufhin wird die $h\nu$ Abhängigkeit der Linienformentwicklung von einem energetisch trennbaren Molekülorbitalsignal einer CuPc Multilage im Vergleich zu kleinen Molekülen in der Gasphase diskutiert und auf einen Effekt der Kopplung von Vibrationen an elektronische Übergänge zurückgeführt. Ein anschließender Vergleich dieser $h\nu$ Abhängigkeit der Linienformentwicklung des höchsten besetzten Molekülorbitals (HOMO) von CuPc und SnPc Multilagen offenbart den molekülspezifischen Charakter dieses Effekts. Danach wird gezeigt, dass für eine Multilage Coronen der selbe Effekt, allerdings mit der Beteiligung zweier (oder mehrerer) elektronischer Übergänge oder aneinander koppelnder Vibrationsmoden, zu sehen ist. Im Anschluss wird der Einfluss durch die Adsorption auf einer Metalloberfläche auf diesen Effekt untersucht und im Hinblick auf eine mögliche Beteiligung von Signalen diskutiert, in deren Entstehung Ladungstransfer beteiligt ist. Der Vergleich der RPES Messung eines Submonolagenfilms von SnPc auf Au(111) und den entsprechenden Daten einer SnPc Multilage zeigt keinerlei sichtbare Veränderung. Demgegenüber wird für eine Submonolage CuPc auf Au(111) eine verminderte Intensitätsumverteilung in den Teil größerer Bindungsenergie (E_B) des HOMO, im Vergleich zur einer CuPc Multilage, festgestellt. Vergleicht man die RPES Daten von einer Submonolage Coronen/Ag(111) mit denen des entsprechenden Multilagenfilms, erkennt man eine resonanzspezifische Veränderung der $h\nu$ Abhängigkeit der Linienformentwicklung, da sich nur in einer der beiden NEXAFS Resonanzen eine Veränderung dieses Effekts zwischen dem Submonolagen- und dem Multilagenfilm zeigt. Alle diese experimentellen Befunde können mit einem einzigen Effekt und einem gemeinsamen Parametersatz erklärt werden. Dies sind alle Parameter, die benötigt werden, um die Potentialenergieoberflächen zu beschreiben, welche im RPES Prozess involviert sind. Dadurch kann eine Alternativerklärung, die auf dynamischem Ladungstransfer beruht, ausgeschlossen werden, was wiederum die folgende Ladungstransferanalyse mit RPES entscheidend beeinflusst.

Eine solche Ladungstransferanalyse mit RPES kann durch den Nachweis von drei verschiedenen mit dynamischem Ladungstransfer assoziierten Signalen durchgeführt werden. Ein in den RPES Daten von einer Submonolage Coronen/Ag(111) detektiertes Signal bei niedriger E_B kann, durch die Zuordnung eines spezifischen Endzustandes, mit Ladungstransfer über die Grenzfläche zwischen Molekül und Metall hinweg in Verbindung gebracht werden. Folglich wird dieses Signal Ladungstransferzustand genannt. Im E_B Bereich der am schwächsten gebundenen Molekülorbitalsignale zeigen RPES Messungen eine verbreiterte Linienform für diejenigen Molekülmetallgrenzflächensysteme, welche ein Signal des niedrigsten unbesetzten Molekülorbitals (LUMO) in direkter PES aufweisen. Durch den Vergleich mit der Linienform des Ladungstransferzustandes kann eine mögliche Erklärung für diesen experimentellen Befund entwickelt werden, die diesen mit Ladungstransfer in Verbindung bringt. Als drittes Signal, das für eine Ladungstransferanalyse mit RPES herangezogen werden kann, dienen Signale konstanter kinetische Energie (E_K), welche sich in den RPES Daten einiger Molekülmetallgrenzflächensysteme zeigen. Die gemessene Energie dieser Signale kann für die

Molekülmetallgrenzflächensysteme, welche kein Signal des LUMO in direkter PES aufweisen, durch die Zuordnung des verantwortlichen Zerfallskanals und explizit angeführte Vereinfachungen erfolgreich berechnet werden. Dadurch wird die Beteiligung von Ladungstransfer über die Grenzfläche zwischen Molekül und Metall im Erzeugungsprozess dieser Signale konstanter E_K gezeigt. In den RPES Daten der lateralen und vertikalen heteromolekularen Grenzflächensysteme, die im ersten Teil dieser Arbeit identifiziert wurden, wird dann letztendlich nach einem Beitrag dieser drei mit Ladungstransfer assoziierten Signale gesucht. Weder für das laterale heteromolekulare System CuPc + PTCDA/Ag(111) noch für das vertikale heteromolekulare System CuPc auf 1 ML PTCDA/Ag(111) kann, durch die Detektion eines dieser Signale, Ladungstransfer entlang der heteromolekularen Grenzfläche bestätigt werden. Als entscheidender Faktor für die physikalische Beschreibung von RPES am ersten System wird die Wechselwirkung zwischen Molekül und Metall identifiziert. Das zentrale Ergebnis für das zweite System ist, dass keine Hinweise auf eine signifikante Hybridisierung an der Grenzfläche zwischen CuPc und PTCDA entdeckt werden können.

Appendix

A Supporting data for chapter 3

Angular dependence of core level PES of 1 ML PTCDA/Ag(111)

Fig. A1 shows the angular dependence of the C1s and O1s core level PES spectra of 1 ML PTCDA/Ag(111). With varying electron emission angle ϕ the integrated intensity (Fig. A1(a) and (b)) and the line-shape (Fig. A1(c) and (d)) of both core level PES spectra changes.

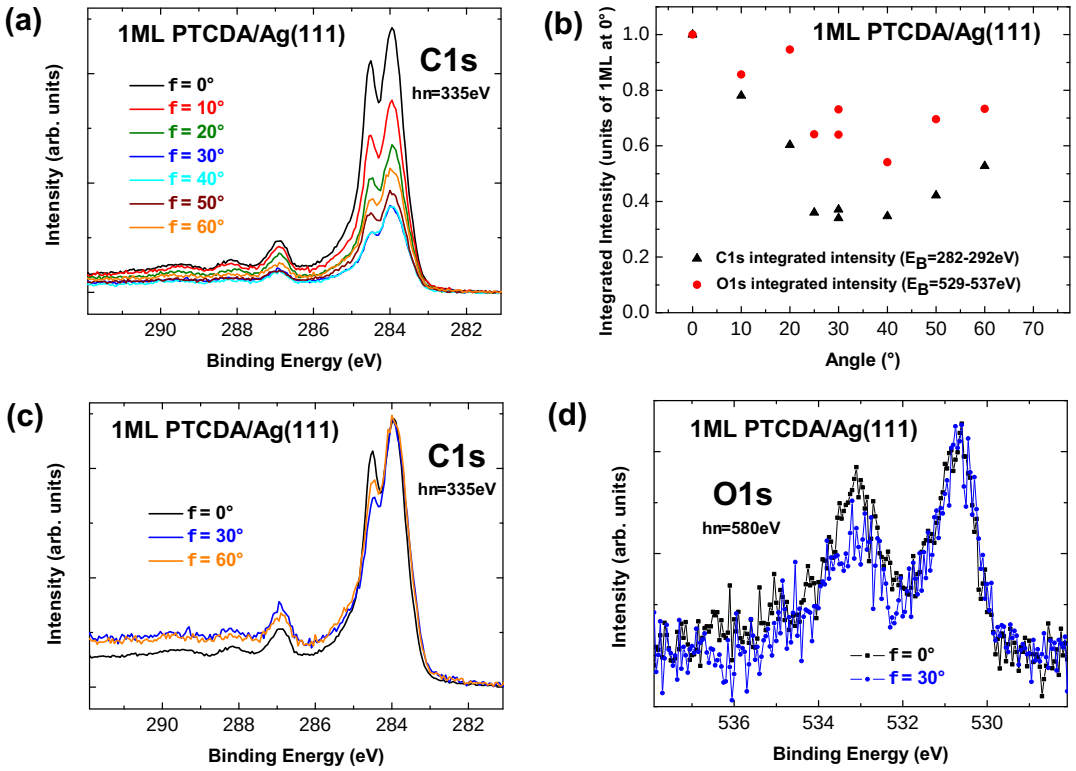

Figure A1: Angular dependence of C1s and O1s core level PES data of 1 ML PTCDA/Ag(111). For the C1s spectra a linear and for the O1s spectra a power law background is subtracted. **(a)** Selected C1s core level PES spectra for different electron emission angles ϕ (with respect to the surface normal, see section 3.1). The data is normalized at the pre-peak plateau at $E_B \approx 280$ eV (see section 3.3). **(b)** Integrated intensity of all C1s and O1s core level PES spectra normalized to the integrated intensity value of the spectrum with $\phi = 0°$. **(c)** Comparison of the line shape of selected C1s core level PES spectra. For comparison the spectra are scaled for matching intensity of the peak at the smallest E_B. **(d)** Comparison of the line shape of selected O1s core level PES spectra analogue to panel (c).

B Supporting data for chapter 4

Coverage dependence of PTCDA/1 ML SnPc/Ag(111) and hints for a layer exchange

In Fig. A2 PES data of PTCDA/1 ML SnPc/Ag(111) is presented. In Fig A2(a) representative C1s core level spectra corresponding to the valence PES spectra in Fig A2(b) are displayed. With the PTCDA multilayer reference spectrum (purple line in Fig A2(c)) the PES intensity which grows with PTCDA coverage in the C1s spectrum in Fig A2(a) can be identified to originate from multilayer-like PTCDA molecules. Hence the PES intensity growing with PTCDA coverage in Fig A2(b) can be assigned to the PTCDA HOMO of multilayer-like PTCDA molecules. In Fig A2(c) a C1s core level spectrum (open circles) is shown for which the rising edge of the main peak at $E_B \approx 284$ eV cannot be reproduced with the scaled reference spectra of 1 ML SnPc/Ag(111) (cyan line) and a PTCDA multilayer (purple line). This spectrum is not representative for the 0.35 ML PTCDA/1 ML SnPc/Ag(111) sample since for the five C1s spectra on other sample spots the reproduction works (as in Fig. 4.1(a)). In the O1s core level PES spectrum of the 0.35 ML PTCDA/1 ML SnPc/Ag(111) sample (see Fig A2(d)) additional intensity with respect to the PTCDA multilayer reference spectrum is visible at the rising edge of the main peak at $E_B \approx 530.5$ eV. Both deviations from the reference spectra could be a consequence of a 1 ML PTCDA/Ag(111) contribution.

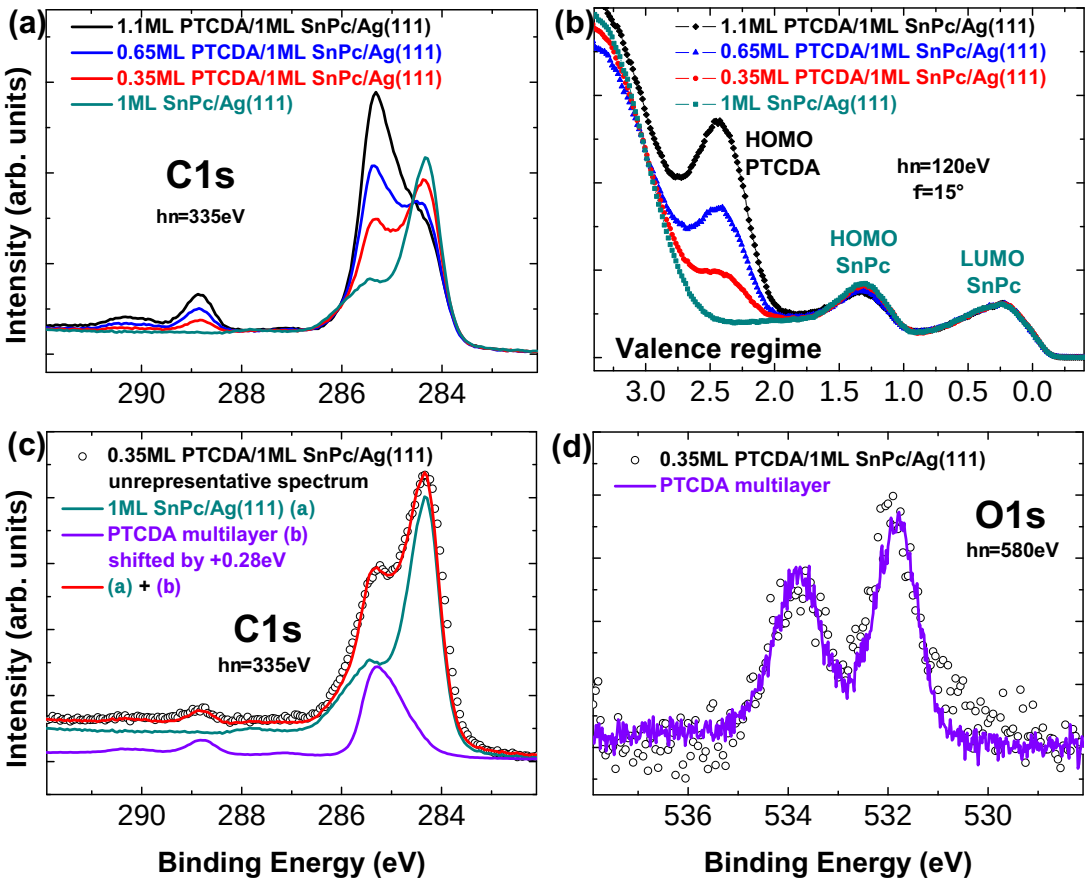

Figure A2: PES data of PTCDA/1 ML SnPc/Ag(111). **(a)** Representative C1s core level PES spectra of different PTCDA coverages together with a reference spectrum of 1 ML SnPc/Ag(111) (cyan line). **(b)** Valence PES data corresponding to the C1s core level PES spectra of panel (a). **(c)** C1s core level PES spectrum of 0.35 ML PTCDA/1 ML SnPc/Ag(111) (open circles) together with scaled reference spectra of 1 ML SnPc/Ag(111) (cyan line) and a PTCDA multilayer (purple line). The red line is the sum of both reference spectra. This spectrum is not representative for the sample. **(d)** O1s core level PES spectrum of 0.35 ML PTCDA/1 ML SnPc/Ag(111) (open circles) in comparison to a scaled multilayer PTCDA reference spectrum (purple line).

Further annealing experiments of SnPc/1 ML PTCDA/Ag(111)

In Fig. A3 PES data of 1.5 ML SnPc/1 ML PTCDA/Ag(111) annealed at 430 K is shown. The successful reproduction of the measured C1s core level PES spectrum in Fig. A3(a) requires the use of multilayer and ML reference spectra of both molecules. For a successful reproduction of the N1s core level PES spectrum in Fig. A3(b) a SnPc multilayer and a 1 ML SnPc/Ag(111) reference are necessary. These findings lead to the conclusion that PTCDA and SnPc are both situated in the first and in higher layers.

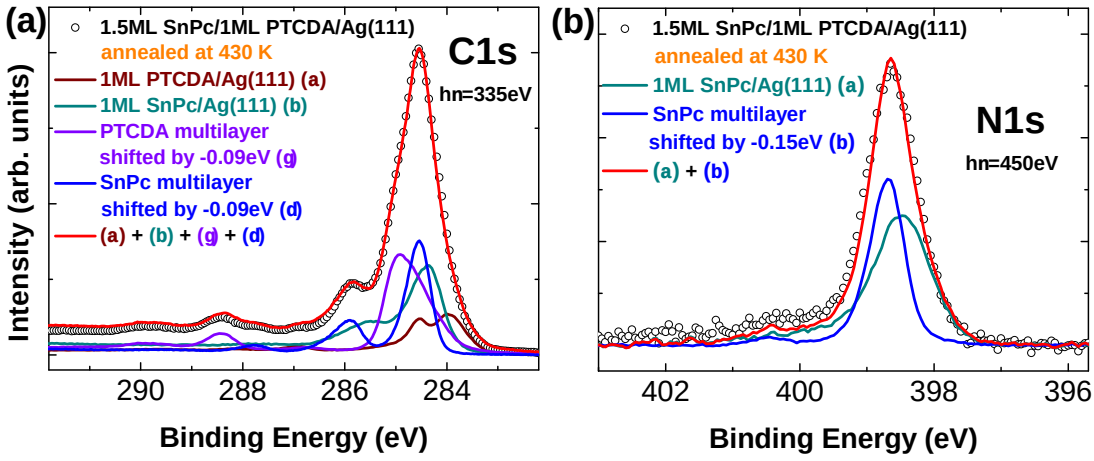

Figure A3: PES data of 1.5 ML SnPc/1 ML PTCDA/Ag(111) annealed at 430 K. **(a)** C1s core level PES spectrum (open circles) together with scaled reference spectra of 1 ML PTCDA/Ag(111) (brown line), 1 ML SnPc/Ag(111) (cyan line), a PTCDA multilayer (purple line), and a SnPc multilayer (blue line). **(b)** N1s core level PES spectrum (open circles) together with scaled reference spectra of 1 ML SnPc/Ag(111) (cyan line) and a CuPc multilayer (blue line). In both panels the red line is the sum of all reference spectra.

The C1s core level PES spectrum displayed in Fig. A4(a) is an example spectrum of a SnPc/1 ML PTCDA/Ag(111) hetero-organic film for which no PTCDA reference spectrum is needed in order to achieve a successful reproduction of the measured spectrum. Only a 1 ML SnPc/Ag(111) and a SnPc multilayer reference spectrum are necessary to reproduce all features of the measured line-shape of the C1s core level PES spectrum of 4 ML SnPc/1 ML PTCDA/Ag(111) annealed at 470 K. The O1s core level PES spectrum of the same sample (filled back squares) is illustrated in Fig. A4(b) in comparison to a 1 ML PTCDA/Ag(111) reference (filled brown circles). The PES intensity found for the O1s core level PES spectrum of 4 ML SnPc/1 ML PTCDA/Ag(111) annealed at 470 K (filled back squares) is too small for an evaluation of the line-shape. Comparing the intensity of the O1s core level PES spectrum of the annealed hetero-organic film (filled back squares) to the intensity of a O1s core level PES spectrum of 1 ML PTCDA/Ag(111) (filled brown circles) I can conclude that the amount of PTCDA molecules in the hetero-organic film is vanishingly small. Hence either almost all PTCDA molecules are desorbed from this sample or large pure SnPc domains are measured in both core level spectra of Fig. A4.

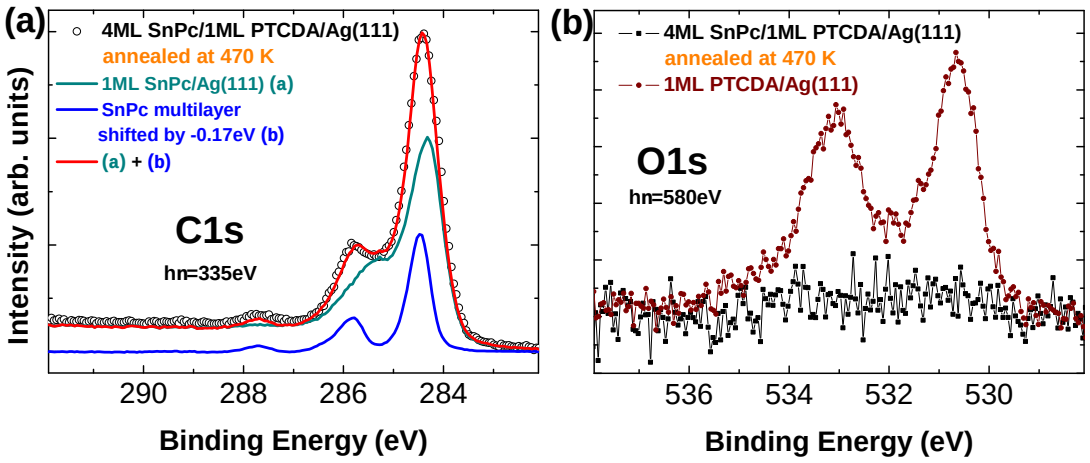

Figure A4: PES data of 4 ML SnPc/1 ML PTCDA/Ag(111) annealed at 470 K. **(a)** C1s core level PES spectrum (open circles) together with scaled reference spectra of 1 ML SnPc/Ag(111) (cyan line) and a SnPc multilayer (blue line). The red line is the sum of both reference spectra. **(b)** O1s core level PES spectrum (filled back squares) together with a reference spectrum of 1 ML PTCDA/Ag(111) (filled brown circles).

Simulation of different origins of an E_B shift of a LUMO signal

Fig. A5 demonstrates how a change in the background can lead to an apparent E_B shift of a Gaussian peak at constant E_B that is cut by a Fermi function. From the simulated valence PES spectrum in Fig. A5(a) to the one in Fig. A5(b) the slope of the linear background is changed which results in an apparent E_B shift of the LUMO peak maximum by $\Delta E_B = 120$ meV. From the simulated valence PES spectrum in Fig. A5(a) to the one in Fig. A5(c) E_B of the LUMO peak is changed by $\Delta E_B = 120$ meV which results in an actual E_B shift of the LUMO peak maximum by $\Delta E_B = 120$ meV. In Fig. A5(d) the simulated valence PES spectrum in Fig. A5(b) is directly compared to the simulated valence PES spectrum in Fig. A5(c). In a measured valence PES EDC differences of the background (substrate s-p bands) of two spectra might not be obvious due to a change of the PES intensity of other signals. Hence it is very difficult to distinguish between an apparent E_B shift of a peak maximum (like in Fig. A5(b)) and an actual E_B shift of a peak maximum (like in Fig. A5(c)) in such a situation.

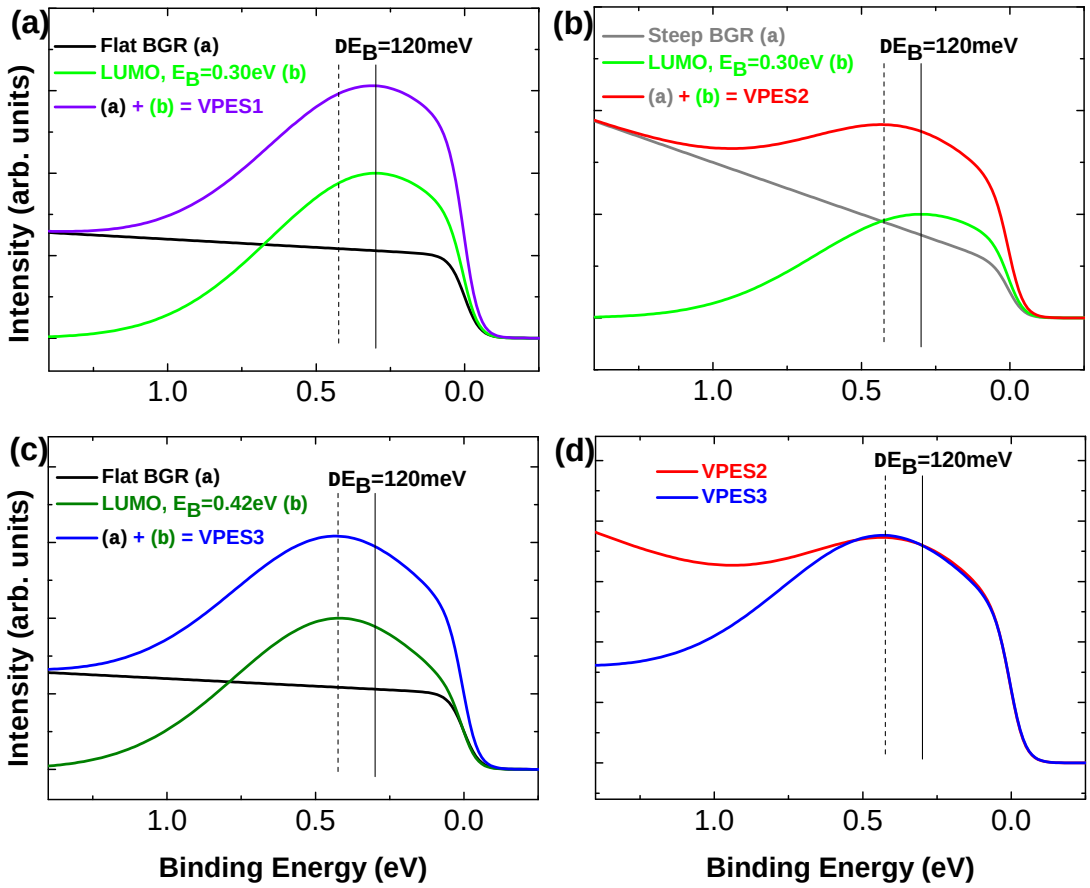

Figure A5: Simulation of valence PES data of a Gaussian LUMO signal and a linear background (BGR) which are both cut by a Fermi function. **(a)** A flat BGR (α) and a LUMO signal with $E_B = 0.30$ eV (β) add up to a valence PES spectrum (VPES1). **(b)** A steep BGR (α) and a LUMO signal with $E_B = 0.30$ eV (β) add up to a valence PES spectrum (VPES2) for which the apparent LUMO peak maximum appears shifted by $\Delta E_B = 120$ meV with respect to VPES1. **(c)** A flat BGR (α) and a LUMO signal with $E_B = 0.42$ eV (β) add up to a valence PES spectrum (VPES3) for which the actual LUMO peak maximum is shifted by $\Delta E_B = 120$ meV with respect to VPES1. **(d)** Direct comparison of VPES2 and VPES3.

Line-shapes of C1s core level PES spectra of homo-molecular F4TCNQ and a *fingerprint approach* analysis of 1.0 ML F4TCNQ/1 ML PTCDA/Ag(110)

In Fig. A6(a) the line-shapes of a F4TCNQ multilayer C1s core level PES spectrum prepared and measured at 100 K (green line) and a 1.0 ML F4TCNQ/Ag(110) spectrum (orange line) are compared to each other. Both C1s PES line-shapes are significantly different with respect to each other. Fig. A6(b) shows the C1s core level PES spectrum of a 1.0 ML F4TCNQ/1 ML PTCDA/Ag(110) sample. The measured C1s PES spectrum of this hetero-organic system (open circles) is successfully reproduced by reference spectra of 1 ML PTCDA/Ag(110) (brown line), 1.0 ML F4TCNQ/Ag(110) (orange line), a PTCDA multilayer (purple line), and a F4TCNQ multilayer (green line).

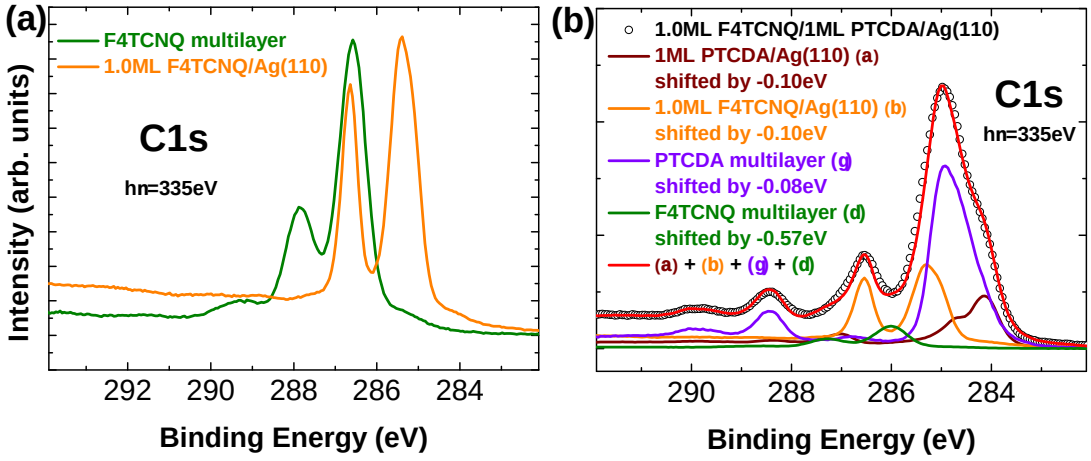

Figure A6: **(a)** C1s core level PES spectrum of a F4TCNQ multilayer prepared and measured at 100 K (green line) in comparison to a 1.0 ML F4TCNQ/Ag(110) spectrum (orange line). The spectrum of the F4TCNQ multilayer is scaled for best comparison of the line-shapes of both spectra. **(b)** C1s core level PES spectrum of 1.0 ML F4TCNQ/1 ML PTCDA/Ag(110) (open circles) together with scaled reference spectra of 1 ML PTCDA/Ag(110) (brown line), 1.0 ML F4TCNQ/Ag(110) (orange line), a PTCDA multilayer (purple line), and an F4TCNQ multilayer (green line). The red line is the sum of all reference spectra.

Coverage dependent E_B shifts of F4TCNQ/Ag(110)

Fig. A7 illustrates the coverage dependent E_B shifts of F4TCNQ on Ag(110). E_B of all core level PES spectra and all valence PES signals continuously increases with increasing F4TCNQ coverage.

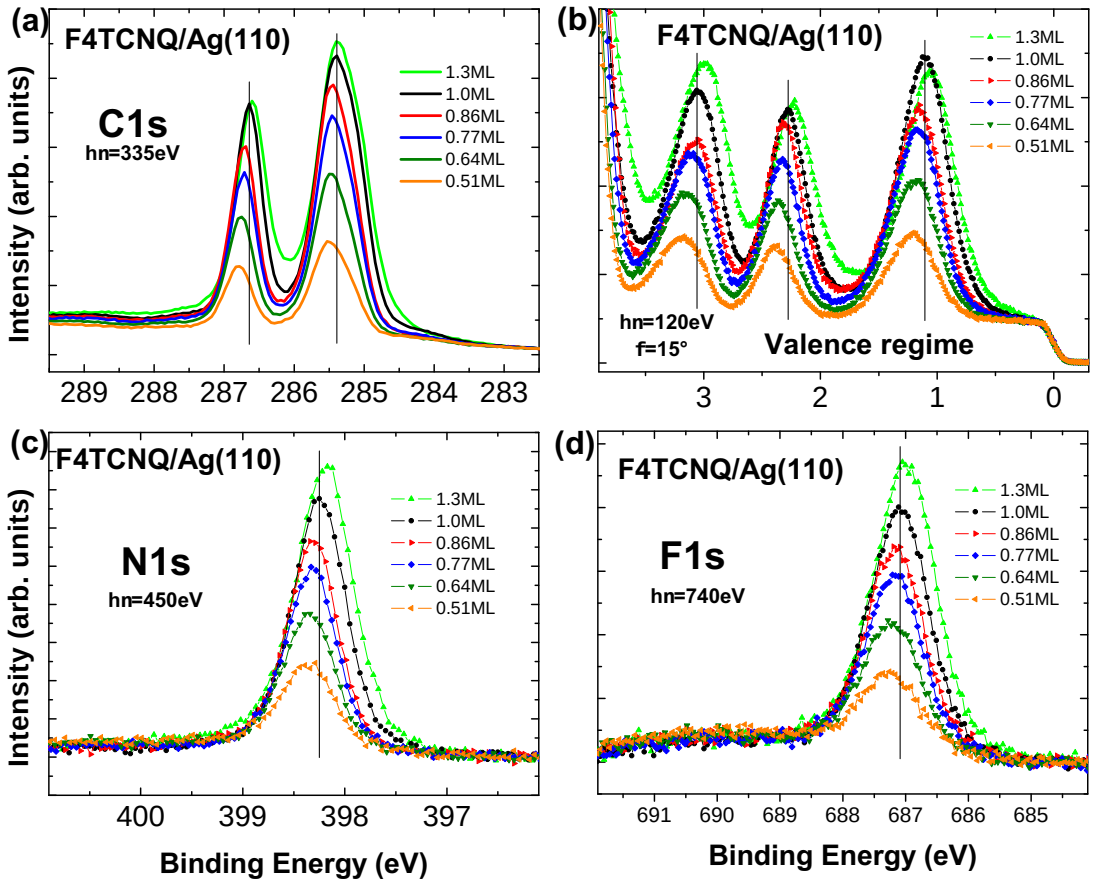

Figure A7: PES data of F4TCNQ/Ag(110) for different coverages. The black vertical lines are a guide to the eye which facilitates the observation of the coverage dependent E_B shifts. **(a)** C1s core level PES spectra of different F4TCNQ coverages. **(b)** Valence PES spectra of different F4TCNQ coverages. **(c)** N1s core level PES spectra of different F4TCNQ coverages. **(d)** F1s core level PES spectra of different F4TCNQ coverages.

C Supporting data for chapter 5

Direct valence PES data of an NTCDA multilayer and an ML NTCDA/Ag(111)

Fig. A8 displays the valence PES spectra of a flat lying Frank-van-der-Merwe-like grown NTCDA multilayer and an ML NTCDA/Ag(111). The E_B region of the CIS 1 and CIS 2 spectra in Fig. 5.1 is bounded by the orange (CIS 1) and blue (CIS 2) vertical lines in Fig. A8(a). These E_B regions are selected in order to include the PES intensity maxima originating from a group of resonantly enhanced molecular orbital signals in the PES overview map in Fig. 5.1(a). The only molecular orbital signal in Fig. A8(a) that can be attributed to a single molecular orbital signal is the HOMO signal. All other molecular orbital signals are energetically overlapping with each other. In the valence PES spectrum of an ML NTCDA/Ag(111) illustrated in Fig. A8(b) the LUMO signal, the HOMO signal, and the PES signal of the HOMO-1 can be assigned to a peak or a shoulder (HOMO-1) in the PES spectrum.

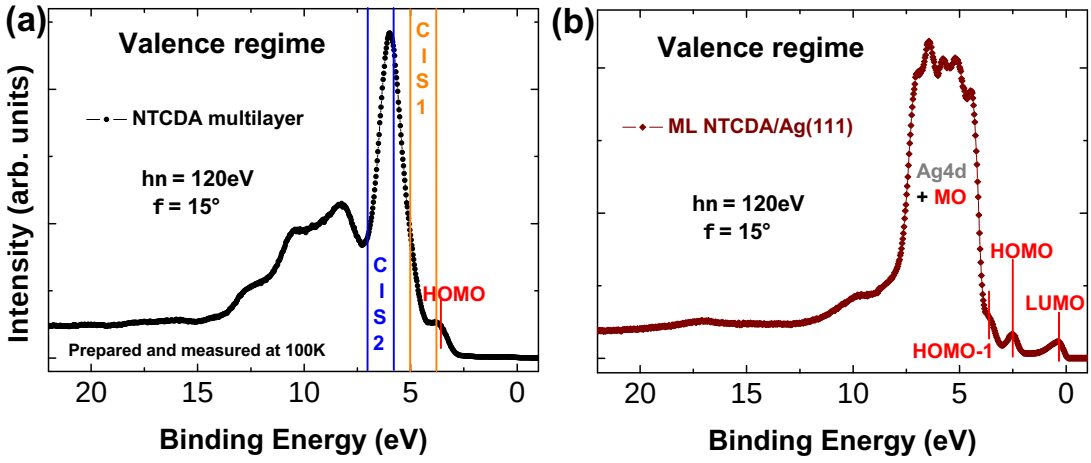

Figure A8: Valence PES spectra of NTCDA for different coverages. The red vertical lines denote the E_B of the indicated molecular orbital signals. **(a)** Valence PES spectrum of an NTCDA multilayer prepared and measured at 100 K. The E_B region within the orange and blue vertical lines corresponds to the E_B region of the CIS 1 and CIS 2 spectrum in Fig. 5.1, respectively. **(b)** Valence PES spectrum of an ML NTCDA/Ag(111) in the E_B region corresponding to panel (a).

Calculated real space probability densities of the frontier molecular orbitals of coronene

Fig. A9 displays the real space probability densities of the two molecular orbital signals with the lowest E_B in direct valence PES obtained by DFT calculations. The pictures are taken from Fig. A4 of Ref. [59]. Details about these DFT calculations can be found in Ref. [59]. In Fig. A9(a) the real space probability density of the HOMO is presented while Fig. A9(b) shows the corresponding result for the HOMO-1.

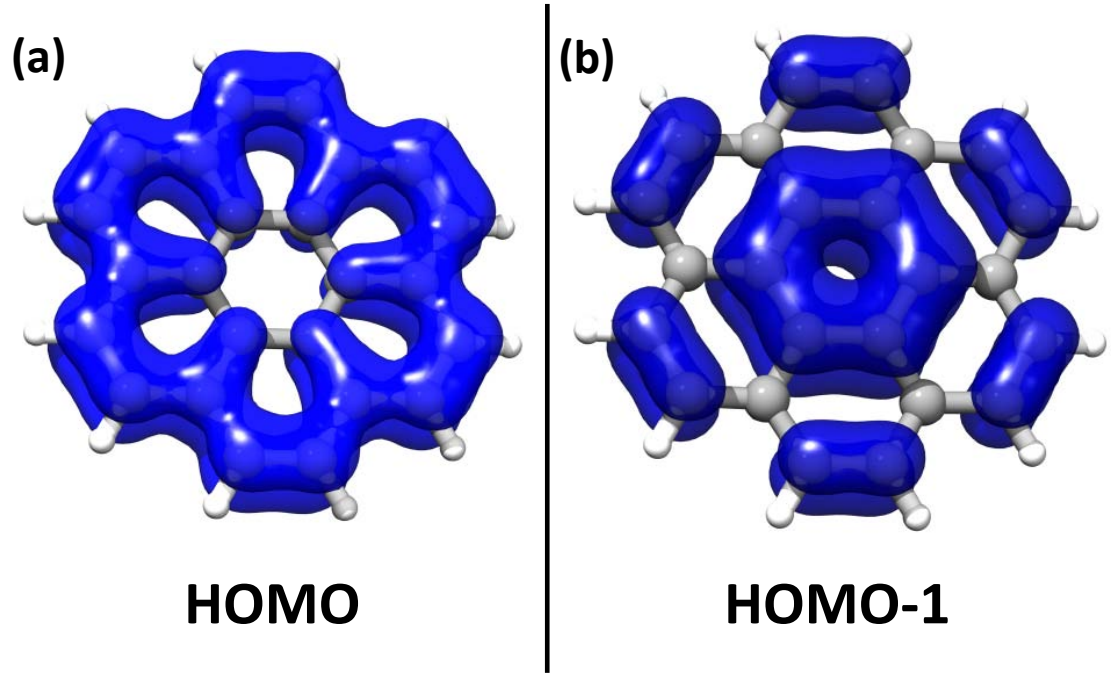

Figure A9: Real space probability densities of the frontier molecular orbitals of coronene taken from Fig. A4 of Ref. [59]. For details of the DFT calculations see Ref. [59]. **(a)** Real space probability density of the HOMO. **(b)** Real space probability density of the HOMO-1.

Direct valence PES data of multilayer CuPc/Ag(111)

Fig. A10 shows a comparison of direct valence PES spectra of a multilayer of CuPc molecules at 100 K (filled blue diamonds) and at 300 K (filled red circles) on Ag(111). A difference in E_B of the HOMO signals of both films of 70 meV is observed. The same difference in E_B of these HOMO signals is found in the RPES data illustrated in Fig. 5.5(a). The difference in the PES intensity of the two HOMO signals is a consequence of the normalization of both spectra at the pre-peak plateau at $E_B = 0.8$ eV and the different growth modes of the two samples. For the Frank-van-der-Merwe-like grown film at 100 K the s-p bands of the Ag(111) substrate are more attenuated than for the Stranski-Krastanow grown film at 300 K.

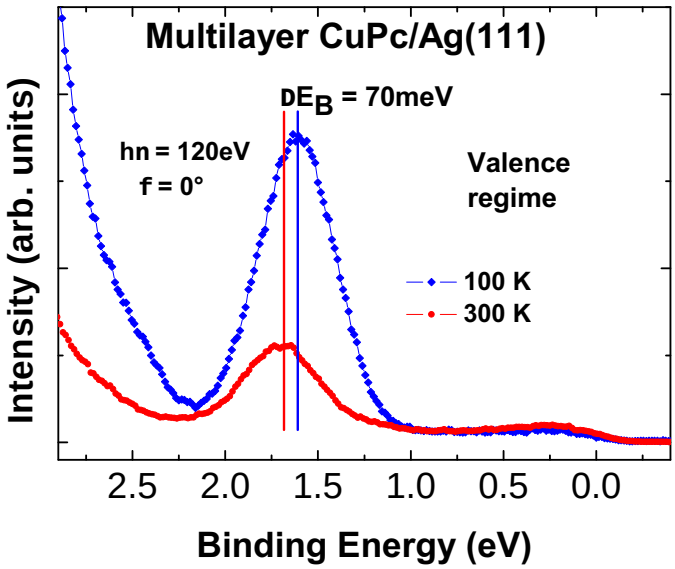

Figure A10: Comparison of direct valence PES spectra of multilayer CuPc/Ag(111) at 100 K (filled blue diamonds) and at 300 K (filled red circles). The spectra are normalized with respect to each other at $E_B = 0.8$ eV. The vertical lines in the same color as the particular valence PES spectrum denote the E_B position of the HOMO signal of this spectrum.

Resonant photoelectron spectroscopy data of CO in the gas phase

In Fig. A11 RPES data at the carbon K-edge of CO molecules in the gas phase is presented together with calculations. The pictures illustrated in panels (a) and (b) are taken from Ref. [63] and the ones in panels (c) and (d) from Ref. [62]. In Fig. A11(a) the NEXAFS spectrum is displayed which demonstrates to which intermediate state vibrational level ν_n a particular $h\nu$ corresponds. Fig. A11(b) shows that with increasing ν_n more relative intensity is distributed into the part of smaller E_K of the frontier molecular orbital signals. This effect becomes even clearer in the RPES data illustrated in Fig. A11(c) and (d). Therein a comparison to calculations reveals that the intensity in the part of smaller E_K of the particular molecular orbital signal corresponds to higher final state vibrational levels ν_f. In the lowest panels of Fig. A11(c) and (d) the direct (thick line) and the interference parts (thin line) of the calculations are presented separately. For details about the measurement of this data see Refs. [62, 63]. For details about the presented calculations see Ref. [62].

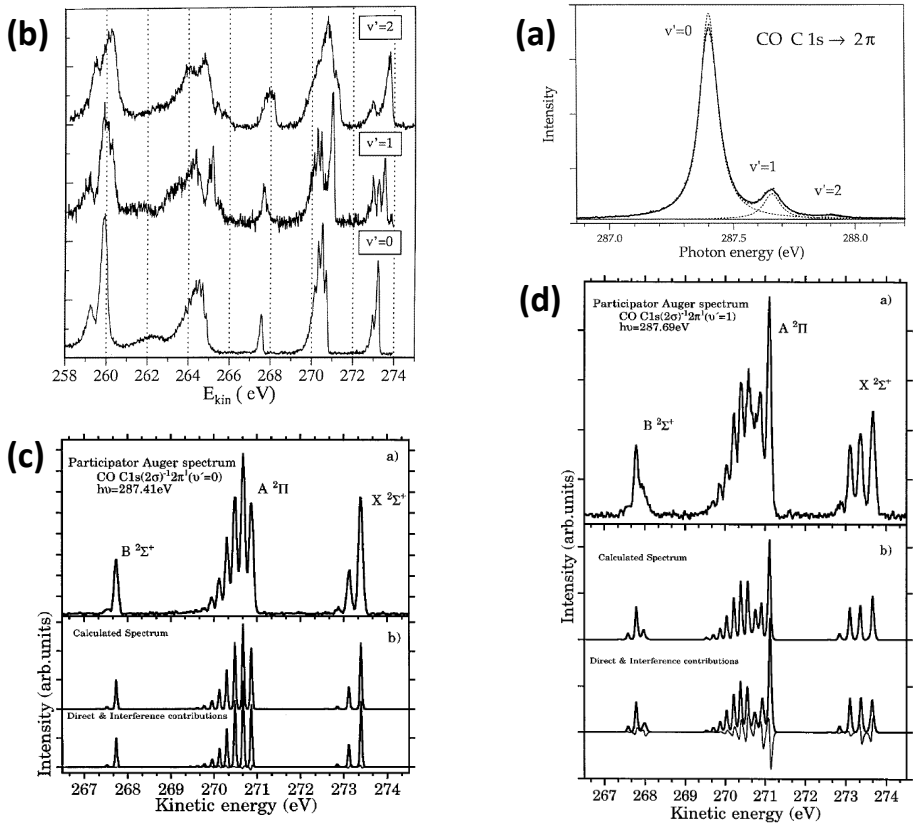

Figure A11: RPES data at the carbon K-edge of CO in the gas phase. The pictures presented in panels (a) and (b) are taken from Ref. [63] and the ones in panels (c) and (d) are taken from Ref. [62]. For details about the measurement of this data see Refs. [62, 63]. For details about the presented calculations see Ref. [62]. **(a)** NEXAFS spectrum of the $h\nu$ region of the C1s to 2π resonance. **(b)** RPES data recorded with $h\nu$ corresponding to the intermediate state vibrational levels $\nu_n = 0,1,2$. **(c)** RPES data recorded with $h\nu$ corresponding to $\nu_n = 0$ together with calculations. **(d)** Analogue figure to panel (c) for $h\nu$ corresponding to $\nu_n = 1$.

Direct valence PES EDCs of coronene/Ag(111) at high symmetry points

In Fig. A12 EDCs of the 1 ML coronene/Ag(111) data cube presented and discussed in Refs. [121] and [59] are illustrated. The two EDCs are extracted at high symmetry points (K-point and M-point) of the surface Brilluin zone (for details see Refs. [121] and [59]). In Fig. A12(a) a large E_B region is presented that shows the angular intensity variation of the HOMO signal. Neither in Fig. A12(a) nor in Fig. A12(b) a LUMO signal can be detected. The upper limit of the value of the relative intensity of the LUMO signal with respect to the HOMO signal of 1% given in Eq. 5.1 is estimated from the noise level of the extracted EDCs in the E_B region of interest.

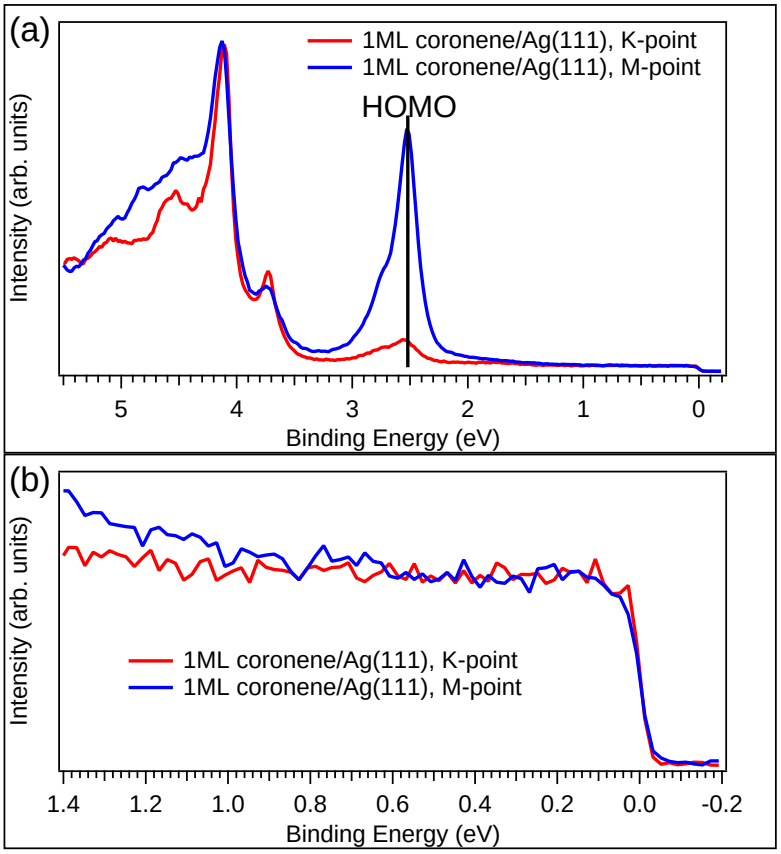

Figure A12: Valence PES spectra of 1 ML coronene/Ag(111) taken from the ARPES data cube of Refs. [121] and [59]. For details about the experiment and data evaluation see Refs. [121] and [59]. **(a)** EDCs at the K-point (red line) and the M-point (blue line) on a large E_B scale. **(b)** Zoom of panel (a) into the E_B region where a LUMO signal could emerge.

Absence of constant kinetic energy features in the RPES data of multilayer samples

In Figs. A13 and A14 the RPES data of the corresponding multilayer samples to the systems illustrated in Figs. 5.18, 5.19, and 5.20 is presented. In contrast to the (sub-)ML films on Ag(111) (see Figs. 5.18 and 5.19) and Au(111) (see Fig. 5.20) no constant E_K features are observed for the multilayer samples in Figs. A13 and A14.

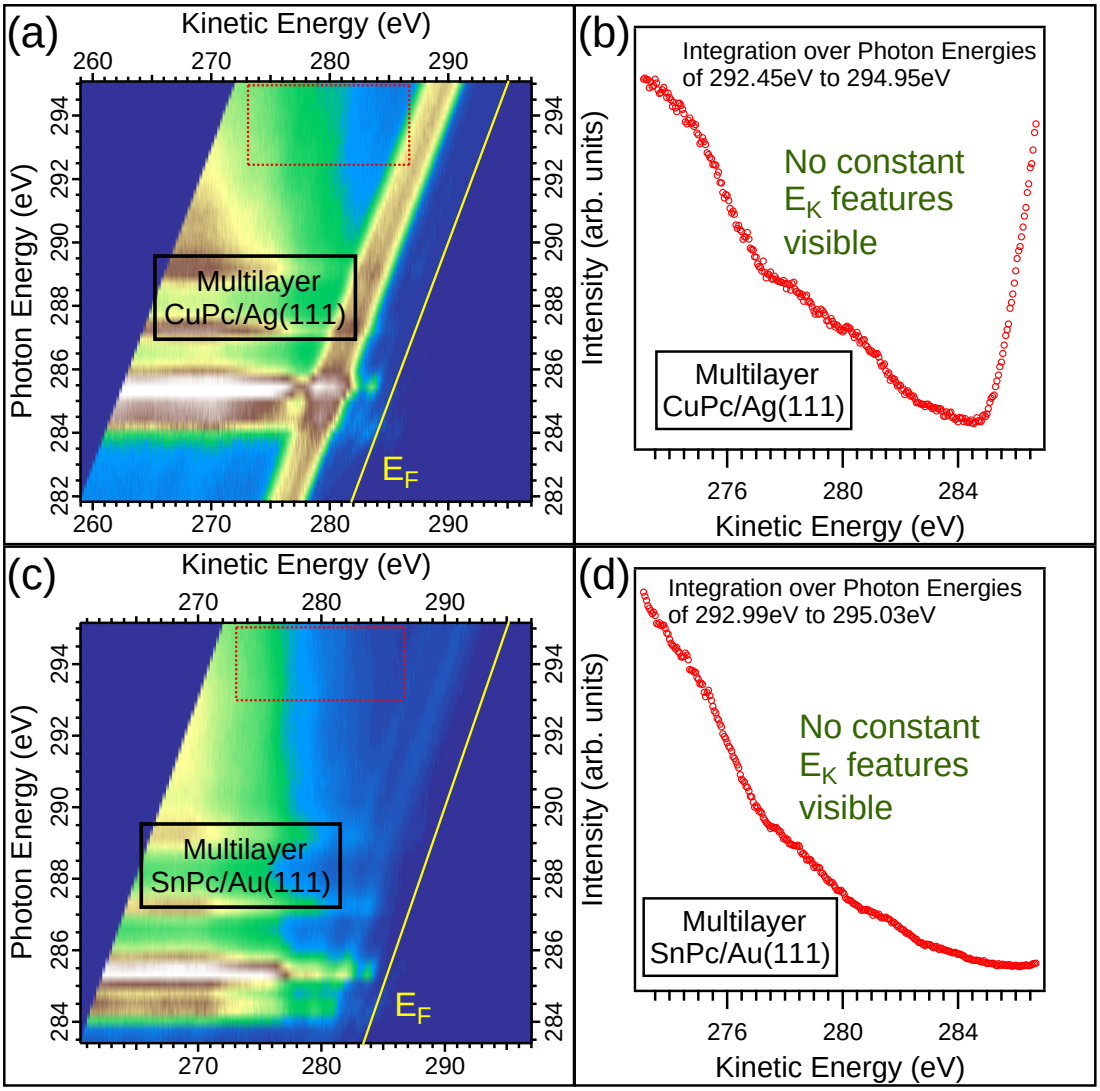

Figure A13: RPES data at the carbon K-edge of a multilayer CuPc/Ag(111) and a multilayer SnPc/Au(111). **(a)** PES overview map of a multilayer CuPc/Ag(111) with an $h\nu$ increment of 250 meV and an E_K increment of 50 meV presented on an E_K scale. The red dashed box illustrates the area from which the $h\nu$ integrated EDC originates and the E_K region in which it is presented in panel (b). The yellow line represents E_F. **(b)** $h\nu$ integrated EDC of a multilayer CuPc/Ag(111) obtained by integration over $h\nu$ in the area of the red dashed box in the PES overview map in panel (a). **(c)** PES overview map of a multilayer SnPc/Au(111) analog to panel (a). **(d)** $h\nu$ integrated EDC of a multilayer SnPc/Au(111) analog to panel (b).

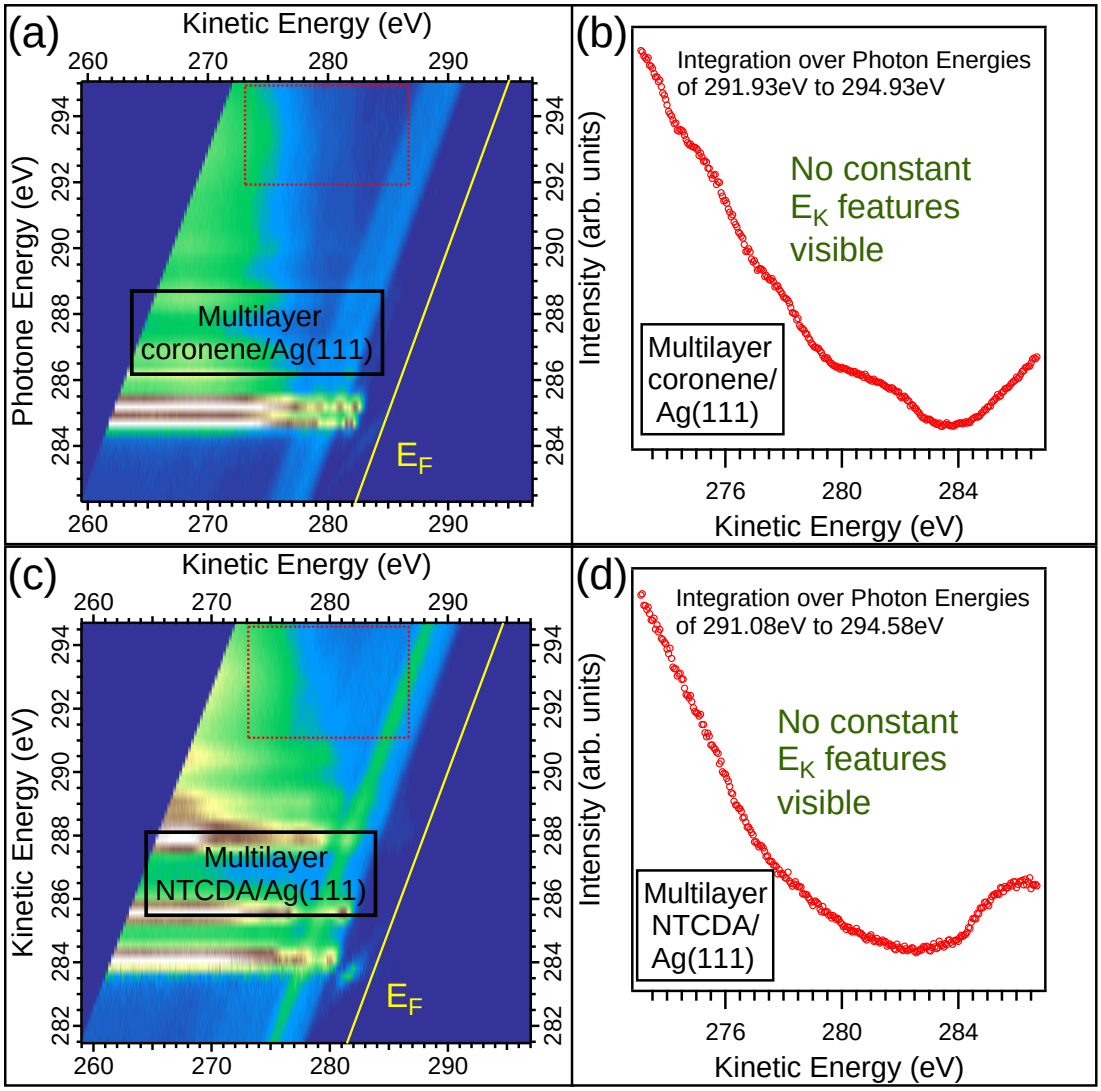

Figure A14: RPES data at the carbon K-edge of a multilayer coronene/Ag(111) and a multilayer NTCDA/Ag(111). **(a)** PES overview map of a multilayer coronene/Ag(111) with an $h\nu$ increment of 250 meV and an E_K increment of 50 meV presented on an E_K scale. The red dashed box illustrates the area from which the $h\nu$ integrated EDC originates and the E_K region in which it is presented in panel (b). The yellow line represents E_F. **(b)** $h\nu$ integrated EDC of a multilayer coronene/Ag(111) obtained by integration over $h\nu$ in the area of the red dashed box in the PES overview map in panel (a). **(c)** PES overview map of a multilayer NTCDA/Ag(111) analog to panel (a). **(d)** $h\nu$ integrated EDC of a multilayer NTCDA/Ag(111) analog to panel (b).

Direct valence PES data of 0.8 ML coronene/Ag(111)

In Fig. A15 EDCs of direct valence PES data of the system 0.8 ML coronene/Ag(111) is presented. Valence PES overview spectra recorded with emission angles of $\phi = 0°$ and $\phi = 15°$ are illustrated in Fig. A15(a). For the spectrum recorded with $\phi = 15°$ a larger PES intensity of the molecular orbital signals, especially the HOMO signal, with respect to the Ag(111) s-p bands is observed than for the spectrum recorded with $\phi = 0°$. This is due to the angular dependency of the PES intensity of molecular orbitals of coronene (for a detailed study of this effect in the system coronene on Ag(111) see Ref. [121]). In Fig. A15(b) a direct valence PES detail spectrum recorded with a smaller pass energy than the valence PES overview spectra in Fig. A15(a) is displayed. The smaller E_K resolution of the valence PES spectrum in Fig. A15(b) allows the detection of the HOMO-1 signal which is hardly visible in the valence PES overview spectra in Fig. A15(a). So E_B of the HOMO and the HOMO-1 signal can be determined with the direct valence PES detail spectrum in Fig. A15(b). The obtained values are used for the calculation of $E_{K,theo}(\text{CFS } m)$ with Eq. 5.15 in subsection 5.3.3.

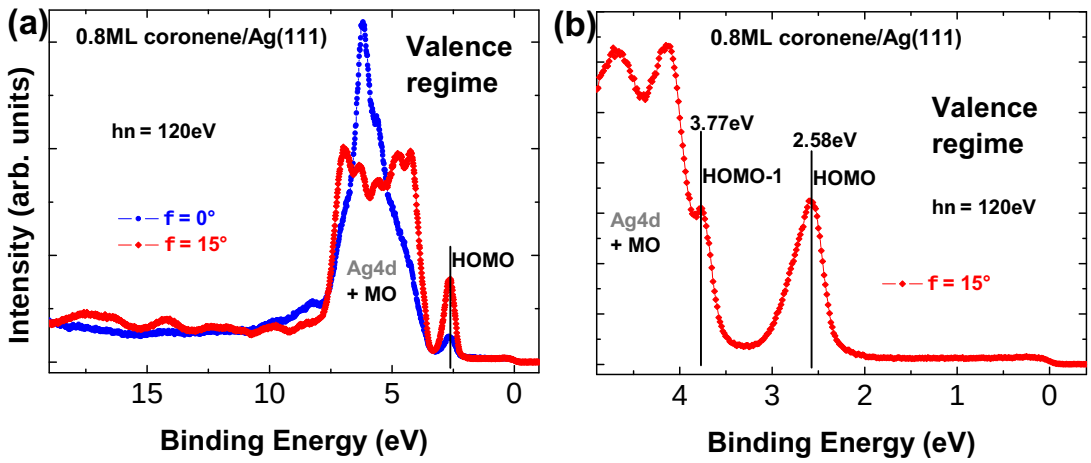

Figure A15: Valence PES spectra of 0.8 ML coronene/Ag(111) recorded with different angles ϕ and different pass energies. The black vertical lines denote E_B of the indicated molecular orbital signals. **(a)** Valence PES overview spectrum for $\phi = 0°$ and $\phi = 15°$ recorded with a pass energy of 50 eV. The spectra are normalized with respect to each other so that both exhibit an equal intensity for the Ag(111) s-p bands at $E_B \approx 0-2$ eV. **(b)** Valence PES detail spectrum for $\phi = 15°$ recorded with a pass energy of 20 eV.

Bibliography

[1] C. J. Brabec, V. Dyakonov, J. Parisi, N. S. Sariciftci, *Organic Photovoltaics*. Springer-Verlag, 2003.

[2] W. Brütting, *Physics of Organic Semiconductors*. Wiley-VCH, 2005.

[3] S.-S. Sun, N. Serdar Sariciftci, *Organic Photovoltaics: Mechanisms, Materials, and Devices*. Taylor and Francis, 2005.

[4] W. R. Salanek, K. Seki, A. Kahn, J.-J. Pireaux, *Conjugated Polymer and Molecular Interfaces: Science and Technology for Photonic and Optoelectronic Applications*. Marcel Dekker, 2002.

[5] C. Wöll, *Physical and Chemical Aspects of Organic Electronics*. Wiley-VCH, 2009.

[6] P. Peumans, A. Yakimov, and S. R. Forrest, "Small molecular weight organic thin-film photodetectors and solar cells," *J. Appl. Phys.*, vol. 93, no. 7, pp. 3693–3723, 2003.

[7] J. Wagner, M. Gruber, A. Hinderhofer, A. Wilke, B. Bröker, J. Frisch, P. Amsalem, A. Vollmer, A. Opitz, N. Koch, F. Schreiber, and W. Brütting, "High Fill Factor and Open Circuit Voltage in Organic Photovoltaic Cells with Diindenoperylene as Donor Material," *Adv. Funct. Mater.*, vol. 20, no. 24, pp. 4295–4303, 2010.

[8] R. Fitzner, E. Reinold, A. Mishra, E. Mena-Osteritz, H. Ziehlke, C. Körner, K. Leo, M. Riede, M. Weil, O. Tsaryova, A. Weiß, C. Uhrich, M. Pfeiffer, and P. Bäuerle, "Dicyanovinyl-Substituted Oligothiophenes: Structure-Property Relationships and Application in Vacuum-Processed Small Molecule Organic Solar Cells," *Adv. Funct. Mater.*, vol. 21, no. 5, pp. 897–910, 2011.

[9] P. A. Brühwiler, O. Karis, and N. Mårtensson, "Charge-transfer dynamics studied using resonant core spectroscopies," *Rev. Mod. Phys.*, vol. 74, no. 3, pp. 703–740, 2002.

[10] A. Föhlisch, S. Vijayalakshmi, A. Pietzsch, M. Nagasono, W. Wurth, P. Kirchmann, P. Loukakos, U. Bovensiepen, M. Wolf, M. Tchaplyguine, and F. Hennies, "Charge transfer dynamics in molecular solids and adsorbates driven by local and non-local excitations," *Surf. Sci.*, vol. 606, no. 11–12, pp. 881–885, 2012.

[11] A. Föhlisch, P. Feulner, F. Hennies, A. Fink, D. Menzel, D. Sanchez-Portal, P. M. Echenique, and W. Wurth, "Direct observation of electron dynamics in the attosecond domain," *Nature*, vol. 436, no. 7049, pp. 373–376, 2005.

[12] A. Föhlisch, "Ultrafast charge transfer and nuclear dynamics studied with resonant X-ray spectroscopy," *Appl. Phys. A*, vol. 85, no. 4, pp. 351–359, 2006.

[13] A. Föhlisch, S. Vijayalakshmi, F. Hennies, W. Wurth, V. Medicherla, and W. Drube, "Verification of the core-hole-clock method using two different time references: Attosecond charge transfer in c(4x2)S/Ru(0001)," *Chem. Phys. Lett.*, vol. 434, no. 4–6, pp. 214–217, 2007.

[14] W. Chen, H. Huang, S. Chen, L. Chen, H. L. Zhang, X. Y. Gao, and A. T. S. Wee, "Molecular orientation of 3,4,9,10-perylene-tetracarboxylic-dianhydride thin films at organic heterojunction interfaces," *Appl. Phys. Lett.*, vol. 91, p. 114102, 2007.

[15] W. Chen, H. Huang, S. Chen, X. Y. Gao, and A. T. S. Wee, "Low-Temperature Scanning Tunneling Microscopy and Near-Edge X-ray Absorption Fine Structure Investigations of Molecular Orientation of Copper(II) Phthalocyanine Thin Films at Organic Heterojunction Interfaces," *J. Phys. Chem. C*, vol. 112, no. 13, pp. 5036–5042, 2008.

[16] D. Kasemann, C. Wagner, R. Forker, T. Dienel, K. Müllen, and T. Fritz, "Line-on-Line Organic-Organic Heteroepitaxy of Quaterrylene on Hexa-peri-hexabenzocoronene on Au(111)," *Langmuir*, vol. 25, no. 21, pp. 12569–12573, 2009.

[17] M. Häming, M. Greif, M. Wießner, A. Schöll, and F. Reinert, "Characterization of ultrathin organic hetero-interfaces - SnPc/PTCDA/Ag(111)," *Surf. Sci.*, vol. 604, no. 19–20, pp. 1619–1622, 2010.

[18] M. Häming, M. Greif, C. Sauer, A. Schöll, and F. Reinert, "Electronic structure of ultrathin heteromolecular organic-metal interfaces: SnPc/PTCDA/Ag(111) and SnPc/Ag(111)," *Phys. Rev. B*, vol. 82, no. 23, p. 235432, 2010.

[19] L. Sun, C. Liu, D. Queteschiner, G. Weidlinger, and P. Zeppenfeld, "Layer inversion in organic heterostructures," *Phys. Chem. Chem. Phys.*, vol. 13, pp. 13382–13386, 2011.

[20] B. Stadtmüller, T. Sueyoshi, G. Kichin, I. Kröger, S. Soubatch, R. Temirov, F. S. Tautz, and C. Kumpf, "Commensurate registry and chemisorption at a hetero-organic interface," *Phys. Rev. Lett.*, vol. 108, no. 10, p. 106103, 2012.

[21] C. Kleimann, B. Stadtmüller, S. Schröder, and C. Kumpf, "Electrostatic Interaction and Commensurate Registry at the Heteromolecular F16CuPc-CuPc Interface," *J. Phys. Chem. C*, vol. 118, no. 3, pp. 1652–1660, 2014.

[22] L. Chen, W. Chen, H. Huang, H. L. Zhang, J. Yuhara, and A. T. S. Wee, "Tunable Arrays of C60 Molecular Chains," *Adv. Mater.*, vol. 20, no. 3, pp. 484–488, 2008.

[23] J. Niederhausen, P. Amsalem, A. Wilke, R. Schlesinger, S. Winkler, A. Vollmer, J. P. Rabe, and N. Koch, "Doping of C_{60} (sub)monolayers by Fermi-level pinning induced electron transfer," *Phys. Rev. B*, vol. 86, no. 8, p. 081411, 2012.

[24] P. Amsalem, J. Niederhausen, A. Wilke, G. Heimel, R. Schlesinger, S. Winkler, A. Vollmer, J. P. Rabe, and N. Koch, "Role of charge transfer, dipole-dipole interactions, and electrostatics in Fermi-level pinning at a molecular heterojunction on a metal surface," *Phys. Rev. B*, vol. 87, no. 3, p. 035440, 2013.

[25] C. Bobisch, T. Wagner, A. Bannani, and R. Möller, "Ordered binary monolayer composed of two organic molecules: Copperphthalocyanine and 3,4,9,10-perylene-tetra-carboxylic-dianhydride on Cu(111)," *J. Chem. Phys.*, vol. 119, no. 18, p. 9804, 2003.

[26] E. Barrena, D. G. de Oteyza, H. Dosch, and Y. Wakayama, "2D Supramolecular Self-Assembly of Binary Organic Monolayers," *ChemPhysChem*, vol. 8, no. 13, pp. 1915–1918, 2007.

[27] M. Cottin, J. Schaffert, A. Sonntag, H. Karacuban, R. Möller, and C. Bobisch, "Supramolecular architecture of organic molecules: PTCDA and CuPc on a Cu(111) substrate," *Appl. Surf. Sci.*, vol. 258, no. 6, pp. 2196–2200, 2012.

[28] A. El-Sayed, D. J. Mowbray, J. M. Garcia-Lastra, C. Rogero, E. Goiri, P. Borghetti, A. Turak, B. P. Doyle, M. Dell'Angela, L. Floreano, Y. Wakayama, A. Rubio, J. E. Ortega, and D. G. de Oteyza, "Supramolecular Environment-Dependent Electronic Properties of Metal-Organic Interfaces," *Jour. Phys. Chem. C*, vol. 116, no. 7, pp. 4780–4785, 2012.

[29] T. N. Krauss, E. Barrena, H. Dosch, and Y. Wakayama, "Supramolecular Assembly of a 2D Binary Network of Pentacene and Phthalocyanine on Cu(100)," *ChemPhysChem*, vol. 10, no. 14, pp. 2445–2448, 2009.

[30] B. Stadtmüller, D. Lüftner, M. Willenbockel, E. M. Reinisch, T. Sueyoshi, G. Koller, S. Soubatch, M. G. Ramsey, P. Puschnig, F. S. Tautz, and C. Kumpf, "Unexpected interplay of bonding height and energy level alignment at heteromolecular hybrid interfaces," *Nat. Commun.*, vol. 5, no. 3685, pp. 1–7, 2014.

[31] C. Wagner, R. Franke, T. Dienel, R. Forker, R. Jacob, and T. Fritz, "Degradation and segregation: Thermal stability and highly ordered epitaxial thin films of large aromatic molecules," *Appl. Phys. Lett.*, vol. 91, no. 11, p. 113111, 2007.

[32] N. Wintjes, J. Lobo-Checa, J. Hornung, T. Samuely, F. Diederich, and T. A. Jung, "Two-Dimensional Phase Behavior of a Bimolecular Porphyrin System at the Solid-Vacuum Interface," *J. Am. Chem. Soc.*, vol. 132, no. 21, pp. 7306–7311, 2010.

[33] C. Sauer, M. Wießner, A. Schöll, and F. Reinert, "Interface originated modification of electron-vibration coupling in resonant photoelectron spectroscopy," *Phys. Rev. B*, vol. 89, no. 7, p. 075413, 2014.

[34] S. Hüfner, *Photoelectron Spectroscopy - Principles and Applications*. Springer-Verlag, 3rd ed., 2003.

[35] F. Reinert and S. Hüfner, "Photoemission Spectroscopy with Very High Energy Resolution: Studying the Influence of Electronic Correlations on the Millielectronvolt Scale," in *Very High Resolution Photoelectron Spectroscopy* (S. Hüfner, ed.), vol. 715 of *Lecture Notes in Physics*, pp. 13–53, Springer Berlin Heidelberg, 2007.

[36] J. Stöhr, *NEXAFS spectroscopy*. Springer-Verlag Berlin Heidelberg, 1992.

[37] A. Einstein, "Über einen die Erzeugung und Verwandlung des Lichtes betreffenden heuristischen Gesichtspunkt," *Ann. Phys.*, vol. 322, no. 6, pp. 132–148, 1905.

[38] F. Schwabl, *Quantenmechanik - Eine Einführng*. Springer-Verlag, 2007.

[39] P. A. M. Dirac, "The quantum theory of the emission and absorption of radiation," *Royal Society of London Proceedings Series A*, vol. 114, pp. 243–265, 1927.

[40] M. Weinelt, A. Nilsson, M. Magnuson, T. Wiell, N. Wassdahl, O. Karis, A. Föhlisch, N. Mårtensson, J. Stöhr, and M. Samant, "Resonant Photoemission at the 2p Edges of Ni: Resonant Raman and Interference Effects," *Phys. Rev. Lett.*, vol. 78, no. 5, pp. 967–970, 1997.

[41] N. Mårtensson, M. Weinelt, O. Karis, M. Magnuson, N. Wassdahl, A. Nilsson, J. Stöhr, and M. Samant, "Coherent and incoherent processes in resonant photoemission," *Appl. Phys. A*, vol. 65, no. 2, pp. 159–167, 1997.

[42] U. Fano, "Effects of Configuration Interaction on Intensities and Phase Shifts," *Phys. Rev.*, vol. 124, no. 6, pp. 1866–1878, 1961.

[43] L. C. Davis and L. A. Feldkamp, "New Mechanism for Resonant Photoemission," *Phys. Rev. Lett.*, vol. 44, no. 10, pp. 673–676, 1980.

[44] L. C. Davis and L. A. Feldkamp, "Resonant photoemission involving super-Coster-Kronig transitions," *Phys. Rev. B*, vol. 23, no. 12, pp. 6239–6253, 1981.

[45] J. Schmidt-May, F. Gerken, R. Nyholm, and L. C. Davis, "Resonant photoemission of oxidized Yb: Experiment and theory," *Phys. Rev. B*, vol. 30, no. 10, pp. 5560–5565, 1984.

[46] C. O. Almbladh and L. Hedin, "Beyond the one-electron model: many-body effects in atoms, molecules and solids," in *Handbook on Synchrotron Radiation* (E. E. Koch, ed.), vol. 1b, pp. 607–904, North-Holland Publishing Company, 1983.

[47] J. J. Sakurai, *Modern Quantum Mechanics Revised Edition*. Addison-Wesley Publishing Company, 1994.

[48] V. Carravetta, F. K. Gel'mukhanov, H. Ågren, S. Sundin, S. J. Osborne, A. Naves de Brito, O. Björneholm, A. Ausmees, and S. Svensson, "Excitation-energy-dependent resonant photoemission: C 1s-π^* spectra of carbon monoxide," *Phys. Rev. A*, vol. 56, no. 6, pp. 4665–4674, 1997.

[49] F. Gel'mukhanov and H. Ågren, "Resonant X-ray Raman scattering," *Physics Reports*, vol. 312, no. 3–6, pp. 87–330, 1999.

[50] S. R. Mishra, T. R. Cummins, G. D. Waddill, W. J. Gammon, G. van der Laan, K. W. Goodman, and J. G. Tobin, "Nature of Resonant Photoemission in Gd," *Phys. Rev. Lett.*, vol. 81, no. 6, pp. 1306–1309, 1998.

[51] S. Hüfner, F. Schumann, E. Rotenberg, J. Tobin, S.-H. Yang, B. S. Mun, S. Morton, J. Schäfer, and D. Ehm, "3*d* and 4*d* resonant photoemission in Pr and Nd metal," *Phys. Rev. B*, vol. 63, no. 8, p. 085106, 2001.

[52] C. Guillot, Y. Ballu, J. Paigné, J. Lecante, K. P. Jain, P. Thiry, R. Pinchaux, Y. Pétroff, and L. M. Falicov, "Resonant Photoemission in Nickel Metal," *Phys. Rev. Lett.*, vol. 39, no. 25, pp. 1632–1635, 1977.

[53] S. Hüfner, S.-H. Yang, B. S. Mun, C. S. Fadley, J. Schäfer, E. Rotenberg, and S. D. Kevan, "Observation of the two-hole satellite in Cr and Fe metal by resonant photoemission at the 2p absorption energy," *Phys. Rev. B*, vol. 61, no. 19, pp. 12582–12585, 2000.

[54] M. López, C. Laubschat, A. Gutiérrez, A. Höhr, M. Domke, G. Kaindl, and M. Abbate, "Resonant photoemission at the 2p thresholds of Fe, Co, and Ni metal," *Z. Phys. B*, vol. 95, no. 1, pp. 9–12, 1994.

[55] O. Karis, A. Nilsson, M. Weinelt, T. Wiell, C. Puglia, N. Wassdahl, N. Mårtensson, M. Samant, and J. Stöhr, "One-Step and Two-Step Description of Deexcitation Processes in Weakly Interacting Systems," *Phys. Rev. Lett.*, vol. 76, no. 8, pp. 1380–1383, 1996.

[56] M. Born and R. Oppenheimer, "Zur Quantentheorie der Molekeln," *Annalen der Physik*, vol. 389, no. 20, pp. 457–484, 1927.

[57] N. Ueno and S. Kera, "Electron spectroscopy of functional organic thin films: Deep insights into valence electronic structure in relation to charge transport property," *Prog. Surf. Sci.*, vol. 83, pp. 490–557, 2008.

[58] S. Kera, H. Yamane, and N. Ueno, "First-principles measurements of charge mobility in organic semiconductors: Valence hole-vibration coupling in organic ultrathin films," *Prog. Surf. Sci.*, vol. 84, pp. 135–154, 2009.

[59] M. Wießner, *Isolierte Moleküle und delokalisierte Zustände: Einblick in die elektronische Struktur organischer Adsorbate mittels winkelaufgelöster Photoemission*. PhD thesis, University of Würzburg, 2013.

[60] F. Holch, *Investigation of Intermolecular Interaction in organic thin films by means of NEXAFS Spectroscopy*. PhD thesis, University of Würzburg, 2009.

[61] M. Scholz, *Energy-Dispersive NEXAFS: A Novel Tool for the Investigation of Intermolecular Interaction and Structural Phase Dynamics*. PhD thesis, University of Würzburg, 2013.

[62] S. Osborne, A. Ausmees, S. Svensson, A. Kivimäki, O. Sairanen, A. N. de Brito, H. Aksela, and S. Aksela, "The vibrationally resolved participator Auger spectra of selectively excited C1s(2σ) 2π vibrational states in carbon monoxide," *J. Chem. Phys.*, vol. 102, pp. 7317–7324, 1995.

[63] M. N. Piancastelli, M. Neeb, A. Kivimäki, B. Kempgens, H. M. Köppe, K. Maier, A. M. Bradshaw, and R. F. Fink, "Vibrationally resolved decay spectra of CO at the C and O K - edges: experiment and theory," *J. Phys. B: At. Mol. Opt. Phys.*, vol. 30, pp. 5677–5692, 1997.

[64] S. Kera, S. Hosoumi, K. Sato, H. Fukagawa, S.-i. Nagamatsu, Y. Sakamoto, T. Suzuki, H. Huang, W. Chen, A. T. S. Wee, V. Coropceanu, and N. Ueno, "Experimental Reorganization Energies of Pentacene and Perfluoropentacene: Effects of Perfluorination," *Jour. Phys. Chem. C*, vol. 117, no. 43, pp. 22428–22437, 2013.

[65] J.-L. Brédas, D. Beljonne, V. Coropceanu, and J. Cornil, "Charge-Transfer and Energy-Transfer Processes in Π-Conjugated Oligomers and Polymers: A Molecular Picture," *Chem. Rev.*, vol. 104, pp. 4971–5003, 2004.

[66] D. Hübner, F. Holch, M. Rocco, K. Prince, S. Stranges, A. Schöll, E. Umbach, and R. Fink, "Isotope effects in high-resolution NEXAFS spectra of naphthalene," *Chem. Phys. Lett.*, vol. 415, no. 1–3, pp. 188–192, 2005.

[67] A. Schöll, Y. Zou, L. Kilian, D. Hübner, D. Gador, C. Jung, S. G. Urquhart, T. Schmidt, R. Fink, and E. Umbach, "Electron-Vibron Coupling in High-Resolution X-Ray Absorption Spectra of Organic Materials: NTCDA on Ag(111)," *Phys. Rev. Lett.*, vol. 93, no. 14, p. 146406, 2004.

[68] V. Kimberg, A. Lindblad, J. Söderström, O. Travnikova, C. Nicolas, Y. P. Sun, F. Gel'mukhanov, N. Kosugi, and C. Miron, "Single-Molecule X-Ray Interferometry: Controlling Coupled Electron-Nuclear Quantum Dynamics and Imaging Molecular Potentials by Ultrahigh-Resolution Resonant Photoemission and Ab Initio Calculations," *Phys. Rev. X*, vol. 3, no. 1, p. 011017, 2013.

[69] M. Neeb, J.-E. Rubensson, M. Biermann, and W. Eberhardt, "Coherent excitation of vibrational wave functions observed in core hole decay spectra of O_2, N_2 and CO," *J. Electron Spectrosc. and Relat. Phenom.*, vol. 67, no. 2, pp. 261–274, 1994.

[70] O. Travnikova, C. Miron, M. Bässler, R. Feifel, M. Piancastelli, S. Sorensen, and S. Svensson, "Resonant Auger decay study of core-excited OCS," *J. Electron Spectrosc. and Relat. Phenom.*, vol. 174, no. 1–3, pp. 100–106, 2009.

[71] O. Gunnarsson and K. Schönhammer, "Photoemission from Ce Compounds: Exact Model Calculation in the Limit of Large Degeneracy," *Phys. Rev. Lett.*, vol. 50, no. 8, pp. 604–607, 1983.

[72] O. Gunnarsson and K. Schönhammer, "Electron spectroscopies for Ce compounds in the impurity model," *Phys. Rev. B*, vol. 28, no. 8, pp. 4315–4341, 1983.

[73] P. W. Anderson, "Localized Magnetic States in Metals," *Phys. Rev.*, vol. 124, no. 1, pp. 41–53, 1961.

[74] O. Gunnarsson, K. Schönhammer, J. C. Fuggle, F. U. Hillebrecht, J. M. Esteva, R. C. Karnatak, and B. Hillebrand, "Occupancy and hybridization of the f level in Ce compounds," *Phys. Rev. B*, vol. 28, no. 12, pp. 7330–7333, 1983.

[75] J. Allen, S. Oh, O. Gunnarsson, K. Schönhammer, M. Maple, M. Torikachvili, and I. Lindau, "Electronic structure of cerium and light rare-earth intermetallics," *Advances in Physics*, vol. 35, no. 3, pp. 275–316, 1986.

[76] M. Klein, J. Kroha, H. v. Löhneysen, O. Stockert, and F. Reinert, "Echo of the quantum phase transition of $CeCu_{6-x}Au_x$ in XPS: Breakdown of Kondo screening," *Phys. Rev. B*, vol. 79, no. 7, p. 075111, 2009.

[77] F. Schwabl, *Quantenmechanik für Fortgeschrittene*. Springer-Verlag, 2005.

[78] Y. Zou, L. Kilian, A. Schöll, T. Schmidt, R. Fink, and E. Umbach, "Chemical bonding of PTCDA on Ag surfaces and the formation of interface states," *Surf. Sci.*, vol. 600, no. 6, pp. 1240–1251, 2006.

[79] L. Kilian, A. Hauschild, R. Temirov, S. Soubatch, A. Schöll, A. Bendounan, F. Reinert, T. L. Lee, F. S. Tautz, M. Sokolowski, and E. Umbach, "Role of Intermolecular Interactions on the Electronic and Geometric Structure of a Large Π-Conjugated Molecule Adsorbed on a Metal Surface," *Phys. Rev. Lett.*, vol. 100, no. 13, p. 136103, 2008.

[80] J. Ziroff, F. Forster, A. Schöll, P. Puschnig, and F. Reinert, "Hybridization of Organic Orbitals with Substrate States at Interfaces: PTCDA on Silver," *Phys. Rev. Lett.*, vol. 104, p. 233004, 2010.

[81] A. Bendounan, F. Forster, A. Schöll, D. Batchelor, J. Ziroff, E. Umbach, and F. Reinert, "Electronic structure of 1 ML NTCDA/Ag(111) studied by photoemission spectroscopy," *Surf. Sci.*, vol. 601, pp. 4013–4017, 2007.

[82] I. Kröger, B. Stadtmüller, C. Stadler, J. Ziroff, M. Kochler, A. Stahl, F. Pollinger, T. L. Lee, J. Zegenhagen, F. Reinert, and C. Kumpf, "Submonolayer growth of copper-phthalocyanine on Ag(111)," *New J. Phys.*, vol. 12, p. 083038, 2010.

[83] M. Häming, C. Scheuermann, A. Schöll, F. Reinert, and E. Umbach, "Coverage dependent organic-metal interaction studied by high-resolution core level spectroscopy: SnPc (sub)monolayers on Ag(111)," *J. Electron Spectrosc. Relat. Phenom.*, vol. 174, no. 1–3, pp. 59–64, 2009.

[84] M. Häming, A. Schöll, E. Umbach, and F. Reinert, "Adsorbate-substrate charge transfer and electron-hole correlation at adsorbate/metal interfaces," *Phys. Rev. B*, vol. 85, no. 23, p. 235132, 2012.

[85] A. Schöll, Y. Zou, T. Schmidt, R. Fink, and E. Umbach, "High-Resolution Photoemission Study of Different NTCDA Monolayers on Ag(111): Bonding and Screening Influences on the Line Shapes," *J. Phys. Chem. B*, vol. 108, no. 38, pp. 14741–14748, 2004.

[86] A. Schöll, L. Kilian, Y. Zou, J. Ziroff, S. Hame, F. Reinert, E. Umbach, and R. H. Fink, "Disordering of an Organic Overlayer on a Metal Surface Upon Cooling," *Science*, vol. 329, no. 5989, pp. 303–305, 2010.

[87] J. Ziroff, S. Hame, M. Kochler, A. Bendounan, A. Schöll, and F. Reinert, "Low-energy scale excitations in the spectral function of organic monolayer systems," *Phys. Rev. B*, vol. 85, p. 161404(R), 2012.

[88] R. Temirov, A. Lassise, F. B. Anders, and F. S. Tautz, "Kondo effect by controlled cleavage of a single-molecule contact," *Nanotechnology*, vol. 19, no. 065401, pp. 1–13, 2008.

[89] A. Greuling, M. Rohlfing, R. Temirov, F. S. Tautz, and F. B. Anders, "Ab initio study of a mechanically gated molecule: From weak to strong correlation," *Phys. Rev. B*, vol. 84, no. 12, p. 125413, 2011.

[90] M. Mugarza, C. Krull, R. Robles, S. Stepanow, G. Ceballos, and P. Gambardella, "Spin coupling and relaxation inside molecule-metal contacts," *Nat. Commun.*, vol. 2, p. 490, 2011.

[91] A. Mugarza, R. Robles, C. Krull, R. Korytár, N. Lorente, and P. Gambardella, "Electronic and magnetic properties of molecule-metal interfaces: Transition-metal phthalocyanines adsorbed on Ag(100)," *Phys. Rev. B*, vol. 85, no. 15, p. 155437, 2012.

[92] D. Cahen and A. Kahn, "Electron Energetics at Surfaces and Interfaces: Concepts and Experiments," *Adv. Mater.*, vol. 15, no. 4, pp. 271–277, 2003.

[93] H. Ishii, K. Sugiyama, E. Ito, and K. Seki, "Energy Level Alignment and Interfacial Electronic Structures at Organic/Metal and Organic/Organic Interfaces," *Adv. Mater.*, vol. 11, no. 8, pp. 605–625, 1999.

[94] A. Kahn, N. Koch, and W. Gao, "Electronic Structure and Electrical Properties of Interfaces between Metals and Π-Conjugated Molecular Films," *Jour. Pol. Sci. B*, vol. 41, pp. 2529–2548, 2003.

[95] J. Hwang, A. Wan, and A. Kahn, "Energetics of metal-organic interfaces: New experiments and assessment of the field," *Mater. Sci. Engin. R*, vol. 63, pp. 1–31, 2009.

[96] A. Schöll *et al.*, Würzburg, unpublished (2008).

[97] K. Glöckler, C. Seidel, A. Soukopp, M. Sokolowski, E. Umbach, M. Böhringer, R. Berndt, and W.-D. Schneider, "Highly ordered structures and submolecular scanning tunnelling microscopy contrast of PTCDA and DM-PBDCI monolayers on Ag(111) and Ag(110)," *Surf. Sci.*, vol. 405, no. 1, pp. 1–20, 1998.

[98] C. Seidel, J. Poppensieker, and H. Fuchs, "Real-time monitoring of phase transitions of vacuum deposited organic films by molecular beam deposition LEED," *Surf. Sci.*, vol. 408, no. 1–3, pp. 223–231, 1998.

[99] M. Wießner, D. Hauschild, A. Schöll, F. Reinert, V. Feyer, K. Winkler, and B. Krömker, "Electronic and geometric structure of the PTCDA/Ag(110) interface probed by angle-resolved photoemission," *Phys. Rev. B*, vol. 86, no. 4, p. 045417, 2012.

[100] S. Kera, S. Tanaka, H. Yamane, D. Yoshimura, K. Okudaira, K. Seki, and N. Ueno, "Quantitative analysis of photoelectron angular distribution of single-domain organic monolayer film: NTCDA on GeS(001)," *Chem. Phys.*, vol. 325, no. 1, pp. 113–120, 2006.

[101] P. Puschnig, S. Berkebile, A. J. Fleming, G. Koller, K. Emtsev, T. Seyller, J. D. Riley, C. Ambrosch-Draxl, F. P. Netzer, and M. G. Ramsey, "Reconstruction of Molecular Orbital Densities from Photoemission Data," *Science*, vol. 326, no. 5953, pp. 702–706, 2009.

[102] J.-M. Imer and E. Wuilloud, "A simple model calculation for XPS, BIS and EELS 4f-excitations in Ce and La compounds," *Z. Phys. B - Condensed Matter*, vol. 66, no. 2, pp. 153–160, 1987.

[103] A. Fujimori and F. Minami, "Valence-band photoemission and optical absorption in nickel compounds," *Phys. Rev. B*, vol. 30, no. 2, pp. 957–971, 1984.

[104] A. Fujimori, F. Minami, and S. Sugano, "Multielectron satellites and spin polarization in photoemission from Ni compounds," *Phys. Rev. B*, vol. 29, no. 9, pp. 5225–5227, 1984.

[105] R. Zimmermann, *Experimentelle Untersuchungen zur elektronischen Struktur von 3d - Übergangsmetalloxiden, ihre Beschreibung im Rahmen des Clustermodells und Vergleich mit Bantstrukturrechnungen*. PhD thesis, Universität des Saarlandes, 1996.

[106] R. Zimmermann, "XPS-Untersuchungen der elektronischen Struktur von Halogeniden und Oxiden der 3d-übergangsmetalle Mangan und Kupfer und ihre Erklärung im Rahmen des Charge Transfer-Modells," Diploma Thesis, Universität des Saarlandes, 1991.

[107] D. Batchelor, T. Schmidt, R. Follath, C. Jung, R. Fink, M. Knupfer, A. Schöll, T. Noll, F. Siewert, B. Büchner, and E. Umbach, "An energy-dispersive VUV beamline for NEXAFS and other CFS/CIS studies," *Nucl. Instrum. Methods Phys. Res., Sect. A*, vol. 575, no. 3, pp. 470–475, 2007.

[108] M. L. M. Rocco, M. Haeming, D. R. Batchelor, R. Fink, A. Schöll, and E. Umbach, "Electronic relaxation effects in condensed polyacenes: A high-resolution photoemission study," *J. Chem. Phys.*, vol. 129, no. 7, p. 074702, 2008.

[109] H. Petersen, "The high energy plane grating monochromators at BESSY," *Nucl. Instrum. Methods Phys. Res., Sect. A*, vol. 246, no. 1–3, pp. 260–263, 1986.

[110] R. Follath, "The versatility of collimated plane grating monochromators," *Nucl. Instrum. Methods Phys. Res., Sect. A*, vol. 467–468, Part 1, no. 0, pp. 418–425, 2001.

[111] J. A. Venables, *Introduction to Surface and Thin Film Processes*. Cambridge University Press, 2000.

[112] J. A. Venables, "Atomic processes in crystal growth," *Surf. Sci.*, vol. 299–300, no. 0, pp. 798–817, 1994.

[113] C. R. Braatz, G. Öhl, and P. Jakob, "Vibrational properties of the compressed and the relaxed 1,4,5,8-naphthalene-tetracarboxylic dianhydride monolayer on Ag(111)," *Jour. Chem. Phys.*, vol. 136, no. 13, p. 134706, 2012.

[114] M. Scholz, C. Sauer, M. Wiessner, N. Nguyen, A. Schöll, and F. Reinert, "Structure formation in organic thin films observed in real time by energy dispersive near-edge x-ray absorption fine-structure spectroscopy," *New J. Phys.*, vol. 15, no. 8, p. 083052, 2013.

[115] J. Weimer, E. Umbach, and D. Menzel, "The properties of K and coadsorbed CO + K on Ru(001): I. Adsorption, desorption, and structure," *Surf. Sci.*, vol. 155, no. 1, pp. 132–152, 1985.

[116] S. Kneitz, J. Gemeinhardt, H. Koschel, G. Held, and H.-P. Steinrück, "Energy and temperature dependent sticking coefficients of CO on ultrathin copper layers on Ru(001)," *Surf. Sci.*, no. 0, pp. 27–31, 1999.

[117] U. Stahl, D. Gador, A. Soukopp, R. Fink, and E. Umbach, "Coverage-dependent superstructures in chemisorbed NTCDA monolayers: a combined LEED and STM study," *Surf. Sci.*, vol. 414, no. 3, pp. 423–434, 1998.

[118] L. Kilian, U. Stahl, I. Kossev, M. Sokolowski, R. Fink, and E. Umbach, "The commensurate-to-incommensurate phase transition of an organic monolayer: A high resolution LEED analysis of the superstructures of NTCDA on Ag(111)," *Surf. Sci.*, vol. 602, no. 14, pp. 2427–2434, 2008.

[119] A. Schöll, Y. Zou, T. Schmidt, R. Fink, and E. Umbach, "Energy calibration and intensity normalization in high-resolution NEXAFS spectroscopy," *J. Electron Spectrosc. and Relat. Phenom.*, vol. 129, no. 1, pp. 1–8, 2003.

[120] T. Graber, F. Forster, A. Schöll, and F. Reinert, "Experimental determination of the attenuation length of electrons in organic molecular solids: The example of PTCDA," *Surf. Sci.*, vol. 605, no. 9–10, pp. 878–822, 2011.

[121] M. Wießner, N. S. R. Lastra, J. Ziroff, F. Forster, P. Puschnig, L. Dössel, K. Müllen, A. Schöll, and F. Reinert, "Different views on the electronic structure of nanoscale graphene: aromatic molecule versus quantum dot," *New J. Phys.*, vol. 14, no. 11, p. 113008, 2012.

[122] M. Kochler, "Hochauflösende Photoelektronenspektroskopie an dünnen CuPc-Filmen auf Edelmetall(111)-Oberflächen," Diploma Thesis, University of Würzburg, 2009.

[123] M. Häming, L. Weinhardt, A. Schöll, and F. Reinert, "Vibronic structure in resonant Auger Raman spectroscopy of large π-conjugated molecules," *Chem. Phys. Lett.*, vol. 510, no. 1–3, pp. 82–86, 2011.

[124] M. Grünewald, "Organische Heteroepitaxie von PTCDA und SnPc auf einkristallinem Silber," Diploma Thesis, Friedrich-Schiller-Universität Jena, 2011.

[125] C. Stadler, S. Hansen, I. Kröger, C. Kumpf, and E. Umbach, "Tuning intermolecular interaction in long-range-ordered submonolayer organic films," *Nat. Phys.*, vol. 5, no. 2, pp. 153–158, 2009.

[126] C. Stadler, S. Hansen, F. Pollinger, C. Kumpf, E. Umbach, T.-L. Lee, and J. Zegenhagen, "Structural investigation of the adsorption of SnPc on Ag(111) using normal-incidence x-ray standing waves," *Phys. Rev. B*, vol. 74, no. 3, p. 035404, 2006.

[127] R. Woolley, C. Martin, G. Miller, V. Dhanak, and P. Moriarty, "Adsorbed molecular shuttlecocks: An NIXSW study of Sn phthalocyanine on Ag(111) using Auger electron detection," *Surf. Sci.*, vol. 601, no. 5, pp. 1231–1238, 2007.

[128] B. Stadtmüller, M. Willenbockel, E. M. Reinisch, T. Ules, F. C. Bocquet, S. Soubatch, P. Puschnig, G. Koller, M. G. Ramsey, F. S. Tautz, and C. Kumpf, "Orbital tomography for highly symmetric adsorbate systems," *EPL*, vol. 100, no. 2, p. 26008, 2012.

[129] C. H. Schwalb, S. Sachs, M. Marks, A. Schöll, F. Reinert, E. Umbach, and U. Höfer, "Electron lifetime in a shockley-type metal-organic interface state," *Phys. Rev. Lett.*, vol. 101, no. 14, p. 146801, 2008.

[130] M. Marks, N. L. Zaitsev, B. Schmidt, C. H. Schwalb, A. Schöll, I. A. Nechaev, P. M. Echenique, E. V. Chulkov, and U. Höfer, "Energy shift and wave function overlap of metal-organic interface states," *Phys. Rev. B*, vol. 84, no. 8, p. 081301, 2011.

[131] H. Marchetto, U. Groh, T. Schmidt, R. Fink, H.-J. Freund, and E. Umbach, "Influence of substrate morphology on organic layer growth: PTCDA on Ag(111)," *Chem. Phys.*, vol. 325, no. 1, pp. 178–184, 2006.

[132] F. Tautz, "Structure and bonding of large aromatic molecules on noble metal surfaces: The example of PTCDA," *Prog. Surf. Sci.*, vol. 82, no. 9–12, pp. 479–520, 2007.

[133] M. Wießner, J. Ziroff, F. Forster, M. Arita, K. Shimada, P. Puschnig, A. Schöll, and F. Reinert, "Substrate-mediated band-dispersion of adsorbate molecular states," *Nat. Commun.*, vol. 4, p. 1514, 2013.

[134] B. Stadtmüller, *Study of intermolecular interactions in hetero-organic thin films*. PhD thesis, RWTH Aachen University, 2012.

[135] Private communication with Marco Grünewald, Friedrich-Schiller-Universität Jena.

[136] C. Seidel, C. Awater, X. Liu, R. Ellerbrake, and H. Fuchs, "A combined STM, LEED and molecular modelling study of PTCDA grown on Ag(110)," *Surf. Sci.*, vol. 371, no. 1, pp. 123–130, 1997.

[137] M. Böhringer, W.-D. Schneider, K. Glöckler, E. Umbach, and R. Berndt, "Adsorption site determination of PTCDA on Ag(110) by manipulation of adatoms," *Surf. Sci.*, vol. 419, no. 1, pp. L95–L99, 1998.

[138] M. Willenbockel, B. Stadtmüller, K. Schönauer, F. C. Bocquet, D. Lüftner, E. M. Reinisch, T. Ules, G. Koller, C. Kumpf, S. Soubatch, P. Puschnig, M. G. Ramsey, and F. S. Tautz, "Energy offsets within a molecular monolayer: the influence of the molecular environment," *New J. Phys.*, vol. 15, no. 3, p. 033017, 2013.

[139] G. M. Rangger, O. T. Hofmann, L. Romaner, G. Heimel, B. Bröker, R.-P. Blum, R. L. Johnson, N. Koch, and E. Zojer, "F4TCNQ on Cu, Ag, and Au as prototypical example for a strong organic acceptor on coinage metals," *Phys. Rev. B*, vol. 79, no. 16, p. 165306, 2009.

[140] W. Gao and A. Kahn, "Electronic structure and current injection in zinc phthalocyanine doped with tetrafluorotetracyanoquinodimethane: Interface versus bulk effects," *Organic Electronics*, vol. 3, no. 2, pp. 53–63, 2002.

[141] Private communication with Benjamin Stadtmüller, Forschungszentrum Jülich.

[142] F. Bruckner, "Elektronische Struktur von homo- und heteromolekularen Adsorbatsystemen an Ag(111)-Oberflächen," Diploma Thesis, University of Würzburg, 2012.

[143] Private communication with Michael Wießner, University of Würzburg.

[144] A. Hinderhofer and F. Schreiber, "Organic-Organic Heterostructures: Concepts and Applications," *ChemPhysChem*, vol. 13, no. 3, pp. 628–643, 2012.

[145] Y. L. Huang, E. Wruss, D. A. Egger, S. Kera, N. Ueno, W. A. Saidi, T. Bucko, A. T. Wee, and E. Zojer, "Understanding the Adsorption of CuPc and ZnPc on Noble Metal Surfaces by Combining Quantum-Mechanical Modelling and Photoelectron Spectroscopy," *Molecules*, vol. 19, no. 3, pp. 2969–2992, 2014.

[146] V. G. Ruiz, W. Liu, E. Zojer, M. Scheffler, and A. Tkatchenko, "Density-Functional Theory with Screened van der Waals Interactions for the Modeling of Hybrid Inorganic-Organic Systems," *Phys. Rev. Lett.*, vol. 108, no. 14, p. 146103, 2012.

[147] J. Ziroff, P. Gold, A. Bendounan, F. Forster, and F. Reinert, "Adsorption energy and geometry of physisorbed organic molecules on Au(111) probed by surface-state photoemission," *Surf. Sci.*, vol. 603, no. 2, pp. 354–358, 2009.

[148] C. Wagner, N. Fournier, F. S. Tautz, and R. Temirov, "Measurement of the Binding Energies of the Organic-Metal Perylene-Teracarboxylic-Dianhydride/Au(111) Bonds by Molecular Manipulation Using an Atomic Force Microscope," *Phys. Rev. Lett.*, vol. 109, no. 7, p. 076102, 2012.

[149] Presentation at the DPG Spring Meeting 2012 of Gregor Öhl, Philipps-Universität Marburg.

[150] J. Schnadt, P. A. Bruhwiler, L. Patthey, J. N. O'Shea, S. Sodergren, M. Odelius, R. Ahuja, O. Karis, M. Bassler, P. Persson, H. Siegbahn, S. Lunell, and N. Martensson, "Experimental evidence for sub-3-fs charge transfer from an aromatic adsorbate to a semiconductor," *Nature*, vol. 418, no. 6898, pp. 620 – 623, 2002.

[151] M. P. de Jong, R. Friedlein, S. L. Sorensen, G. Öhrwall, W. Osikowicz, C. Tengsted, S. K. M. Jönsson, M. Fahlman, and W. R. Salaneck, "Orbital-specific dynamic charge transfer from Fe(II)-tetraphenylporphyrin molecules to molybdenum disulfide substrates," *Phys. Rev. B*, vol. 72, no. 3, p. 035448, 2005.

[152] W. Chen, L. Wang, D. Chen Qi, S. Chen, X.-Y. Gao, and A. Thye Shen Wee, "Probing the ultrafast electron transfer at the CuPc/Au(111) interface," *Applied Physics Letters*, vol. 88, no. 18, pp. 184102–184102–3, 2006.

[153] L. Cao, Y.-Z. Wang, T.-X. Chen, W.-H. Zhang, X.-J. Yu, K. Ibrahim, J.-O. Wang, H.-J. Qian, F.-Q. Xu, D.-C. Qi, and A. T. S. Wee, "Charge transfer dynamics of 3,4,9,10-perylene-tetracarboxylic-dianhydride molecules on Au(111) probed by resonant photoemission spectroscopy," *J. Chem. Phys.*, vol. 135, no. 17, p. 174701, 2011.

[154] J. Ben Taylor, L. C. Mayor, J. C. Swarbrick, J. N. O'Shea, C. Isvoranu, and J. Schnadt, "Adsorption and charge transfer dynamics of bi-isonicotinic acid on Au(111)," *J. Chem. Phys.*, vol. 127, no. 13, p. 134707, 2007.

[155] L. Cao, Y.-Z. Wang, J.-Q. Zhong, Y.-Y. Han, W.-H. Zhang, X.-J. Yu, F.-Q. Xu, D.-C. Qi, and A. T. S. Wee, "Molecular Orientation and Site Dependent Charge Transfer Dynamics at PTCDA/TiO2(110) Interface Revealed by Resonant Photoemission Spectroscopy," *J. Phys. Chem. C*, vol. 118, no. 8, pp. 4160–4166, 2014.

[156] R. Friedlein, S. Braun, M. de Jong, W. Osikowicz, M. Fahlman, and W. Salaneck, "Ultrafast charge transfer in organic electronic materials and at hybrid interfaces studied using the core-hole clock technique," *J. Electron Spectrosc. Relat. Phenom.*, vol. 183, no. 1–3, pp. 101–106, 2011.

[157] L. Wang, W. Chen, and A. T. S. Wee, "Charge transfer across the molecule/metal interface using the core hole clock technique," *Surf. Sci. Rep.*, vol. 63, no. 11, pp. 465–486, 2008.

[158] D. Gador, C. Buchberger, R. Fink, and E. Umbach, ""Manipulation" of molecular orientation in ultrathin organic films: NTCDA on Ag(111)," *EPL*, vol. 41, no. 2, p. 231, 1998.

[159] D. Gador, C. Buchberger, R. Fink, and E. Umbach, "Characterization of high-quality NTCDA films on metal substrates," *J. Electron Spectrosc. Relat. Phenom.*, vol. 96, no. 1–3, pp. 11–17, 1998.

[160] A. Schoell, Y. Zou, D. Huebner, S. G. Urquhart, T. Schmidt, R. Fink, and E. Umbach, "A comparison of fine structures in high-resolution x-ray-absorption spectra of various condensed organic molecules," *J. Chem. Phys.*, vol. 123, no. 4, p. 044509, 2005.

[161] M. Scholz, F. Holch, C. Sauer, M. Wiessner, A. Schöll, and F. Reinert, "Core hole-electron correlation in coherently coupled molecules," *Phys. Rev. Lett.*, vol. 111, no. 4, p. 048102, 2013.

[162] M. Dauth, T. Körzdörfer, S. Kümmel, J. Ziroff, M. Wiessner, A. Schöll, F. Reinert, M. Arita, and K. Shimada, "Orbital Density Reconstruction for Molecules," *Phys. Rev. Lett.*, vol. 107, no. 5, p. 193002, 2011.

[163] H. Oji, R. Mitsumoto, E. Ito, H. Ishii, Y. Ouchi, K. Seki, T. Yokoyama, T. Ohta, and N. Kosugi, "Core hole effect in NEXAFS spectroscopy of polycyclic aromatic hydrocarbons: Benzene, chrysene, perylene, and coronene," *J. Chem. Phys.*, vol. 109, no. 23, p. 10409, 1998.

[164] L. Kjeldgaard, T. Kääambre, J. Schiessling, I. Marenne, J. N. O'Shea, J. Schnadt, C. J. Glover, M. Nagasono, D. Nordlund, M. G. Garnier, L. Qian, J.-E. Rubensson, P. Rudolf, N. Mårtensson, J. Nordgren, and P. A. Brühwiler, "Intramolecular vibronic dynamics in molecular solids: C60," *Phys. Rev. B*, vol. 72, no. 20, p. 205414, 2005.

[165] S. Sundin, F. Kh. Gel'mukhanov, H. Ågren, S. J. Osborne, A. Kikas, O. Björneholm, A. Ausmees, and S. Svensson, "Collapse of Vibrational Structure in the Auger Resonant Raman Spectrum of CO by Frequency Detuning," *Phys. Rev. Lett.*, vol. 79, no. 8, pp. 1451–1454, 1997.

[166] F. Evangelista, V. Carravetta, G. Stefani, B. Jansik, M. Alagia, S. Stranges, and A. Ruocco, "Electronic structure of copper phthalocyanine: An experimental and theoretical study of occupied and unoccupied levels," *J. Chem. Phys.*, vol. 126, p. 124709, 2007.

[167] M. Linares, S. Stafström, Z. Rinkevicius, H. Ågren, and P. Norman, "Complex Polarization Propagator Approach in the Restricted Open-Shell, Self-Consistent Field Approximation: The Near K-Edge X-ray Absorption Fine Structure Spectra of Allyl and Copper Phthalocyanine," *J. Phys. Chem. B*, vol. 115, no. 18, pp. 5096–5102, 2011.

[168] R. De Francesco, M. Stener, and G. Fronzoni, "Theoretical Study of Near-Edge X-ray Absorption Fine Structure Spectra of Metal Phthalocyanines at C and N K-Edges," *J. Phys. Chem. A*, vol. 116, no. 11, pp. 2885–2894, 2012.

[169] V. Y. Aristov, O. V. Molodtsova, V. V. Maslyuk, D. V. Vyalikh, V. M. Zhilin, Y. A. Ossipyan, T. Bredow, I. Mertig, and M. Knupfer, "Electronic structure of the organic semiconductor copper phthalocyanine: Experiment and theory," *J. Chem. Phys.*, vol. 128, p. 034703, 2008.

[170] G. Remmers, M. Domke, A. Puschmann, T. Mandel, C. Xue, G. Kaindl, E. Hudson, and D. A. Shirley, "High-resolution K-shell photoabsorption in formaldehyde," *Phys. Rev. A*, vol. 46, no. 7, pp. 3935–3944, 1992.

[171] J. Bozek, S. Canton, E. Kukk, and N. Berrah, "Vibrationally resolved resonant Auger spectroscopy of formaldehyde at the C1s-1π resonance," *Chem. Phys.*, vol. 289, no. 1, pp. 149–161, 2003.

[172] E. Kukk, G. Snell, J. D. Bozek, W.-T. Cheng, and N. Berrah, "Vibrational structure and partial rates of resonant Auger decay of the N1s to 2pi core excitations in nitric oxide," *Phys. Rev. A*, vol. 63, no. 6, p. 062702, 2001.

[173] M. Wießner, J. Kübert, V. Feyer, P. Puschnig, A. Schöll, and F. Reinert, "Lateral band formation and hybridization in molecular monolayers: NTCDA on Ag(110) and Cu(100)," *Phys. Rev. B*, vol. 88, no. 7, p. 075437, 2013.

[174] M. Häming, *Electronic Many-Body Effects in organic Thin Films and Interfaces*. PhD thesis, University of Würzburg, 2010.

[175] A. J. Britton, A. Rienzo, J. N. O'Shea, and K. Schulte, "Charge transfer between the Au(111) surface and adsorbed C60: Resonant photoemission and new core-hole decay channels," *J. Chem. Phys.*, vol. 133, no. 9, p. 094705, 2010.

[176] J. Ziroff *et al.*, Würzburg, unpublished (2011).

Own publications

1. **C. Sauer**, and G. Blumberg, "Screening of the Raman response in multiband superconductors: Application to iron pnictides", *Phys. Rev. B*, vol. 82, p. 014525, 2010.
2. M. Häming, M. Greif, **C. Sauer**, A. Schöll, and F. Reinert, "Electronic structure of ultrathin heteromolecular organic-metal interfaces: SnPc/PTCDA/Ag(111) and SnPc/Ag(111)", *Phys. Rev. B*, vol. 82, p. 235432, 2010.
3. M. Scholz, F. Holch, **C. Sauer**, M. Wiessner, A. Schöll, and F. Reinert, "Core Hole-Electron Correlation in Coherently Coupled Molecules", *Phys. Rev. Lett.*, vol. 111, p. 048102, 2013
4. M. Scholz, **C. Sauer**, M. Wiessner, N. Nguyen, A. Schöll, and F. Reinert, "Structure formation in organic thin films observed in real time by energy dispersive near-edge x-ray absorption fine-structure spectroscopy", *New J. Phys.*, vol. 15, p. 083052, 2013.
5. **C. Sauer**, M. Wießner, A. Schöll, and F. Reinert, "Interface originated modification of electron-vibration coupling in resonant photoelectron spectroscopy", *Phys. Rev. B*, vol. 89, p. 075413, 2014.
6. M. Wießner, D. Hauschild, **C. Sauer**, V. Feyer, A. Schöll, and F. Reinert, "Complete determination of molecular orbitals by measurement of phase symmetry and electron density", *Nat. Commun.*, vol. 5, p. 4156, 2014.

Abbreviations

Physical quantities

E_B	binding energy
E_F	Fermi energy
E_K	kinetic energy
$h\nu$	photon energy

Acronyms

CFS	**c**onstant **f**inal **s**tate
CIS	**c**onstant **i**nitial **s**tate
CT	**c**harge **t**ransfer
DFT	**d**ensity **f**unctional **t**heory
DRS	**d**ifferential **r**eflectance **s**pectroscopy
EDC	**e**nergy **d**istribution **c**urve
HOMO	**h**ighest **o**ccupied **m**olecular **o**rbital
LEED	**l**ow **e**nergy **e**lectron **d**iffraction
LUMO	**l**owest **u**noccupied **m**olecular **o**rbital
ML	**m**ono**l**ayer
NEXAFS	**n**ear **e**dge **x**-ray **a**bsorption **f**ine **s**tructure
PES	**p**hoto**e**lectron **s**pectroscopy
RPES	**r**esonant **p**hoto**e**lectron **s**pectroscopy
STM	**s**canning **t**unneling **m**icroscopy
sub-ML	**sub**mono**l**ayer

Abbreviations of molecular names

CuPc	copper-phthalocyanine
F4TCNQ	2,3,5,6-tetrafluoro-7,7,8,8-tetracyanoquinodimethane
NTCDA	1,4,5,8-naphthalene-tetracarboxylic-dianhydride
PTCDA	3,4,9,10-perylene-tetracarboxylic-dianhydride
SnPc	tin-phthalocyanine

Danksagung

In der Wissenschaft ist es so gut wie immer Teamarbeit, die letztendlich zu den präsentierten Ergebnissen führt. So wäre auch diese Arbeit nicht in der entsprechenden Form entstanden, wenn nicht viele Leute, auf die ein oder andere Weise, einen Beitrag geleistet hätten. Bei diesen vielen Helfern möchte ich mich an dieser Stelle bedanken.

Als erstes möchte ich mich bei PD Dr. Achim Schöll für das Betreuen dieser Arbeit bedanken. Von Anfang an hat er mir, trotz meiner noch geringen Erfahrung in der Experimentalphysik, ermöglicht beim Durchführen von Messzeiten Verantwortung zu tragen. Des Weiteren danke ich ihm für die Möglichkeit zwei interessante und umfangreiche Themengebiete, die Charakterisierung organischer Heteroschichten und resonante Photoelektronenspektroskopie, zu bearbeiten. Ohne sein Vertrauen in meine Fähigkeiten und sein erfolgreiches Beantragen von Messzeit an der UE52-PGM bei BESSY hätte ich nicht in die Situation des "Luxusproblems" einer solch enormen Datenmenge kommen können. Bei der gemeinsamen Diskussion dieser Daten habe ich stets von seiner großen Erfahrung auf dem Gebiet der Untersuchung von organischen Materialen mit Synchrotronstrahlung profitieren können. Weitere interessante Aspekte aus der Festkörperphysik wurden von Prof. Dr. Friedrich Reinert zu diesen Diskussionen beigetragen. Von seinem Wissen über Photoelektronenspektroskopie und resonante Photoelektronenspektroskopie konnte ich hierbei sehr viel lernen. Des Weiteren danke ich ihm für die Aufnahme in seine Arbeitsgruppe und ebenfalls die Übernahme von Betreuungsaufgaben dieser Arbeit. Die Kombination aus diesen beiden Betreuern, welche zusammen Expertenwissen aus verschiedenen Fachbereichen vereinen, hat das Betrachten der Daten aus verschiedenen Perspektiven, was ein zentraler Aspekt diese Arbeit ist, erst möglich gemacht.

Für die Bereitschaft das Zweitgutachten für diese zugegebenermaßen recht umfangreiche Doktorarbeit zu erstellen, geht mein Dank an Prof. Dr. Matthias Bode. Außerdem möchte ich Prof. Dr. Giorgio Sangiovanni für die Übernahme der Aufgabe des dritten Prüfers im Promotionskolloquium danken.

Auch auf den Messzeiten bei BESSY standen mir viele Personen tatkräftig zur Seite. Ich danke den BESSY Mitarbeitern Stephan Pohl, Dr. Stefan Krause und Dr. Patrick Hoffmann für technische und wissenschaftliche Unterstützung. Für das Weitergeben seines Spezialwissens über die UE52-PGM Beamline und seine Arbeiten an dieser Beamline vor meiner Zeit als Experimentator danke ich Dr. David Batchelor. Besonderer Dank geht an Dr. Michael Wießner, Holger Wetzstein, Sina Gusenleitner, Dr. Markus Scholz, Florian Bruckner, Than-Nam Nguyen, Dr. Benjamin Stadtmüller, Evelyn Handick und Marco Grünewald, die während der Messzeiten bei BESSY die Experimente mit mir

zusammen durchgeführt haben. Vielen Dank, dass ihr bei diesen langen und anstrengenden Tag- und Nachtschichten mit mir Vollgas gegeben habt.

Meine ersten Schritte ins Ultrahochvakuum durfte ich im Labor in Würzburg zusammen mit Michael Greif und zusätzlicher Hilfe von Dr. Markus Scholz unternehmen. Vielen Dank an euch zwei für die Einweisung in die Kunst der Erzeugung von luftleerem Raum.

Des Weiteren möchte ich den Kollaborationspartnern von der Friedrich-Schiller-Universität Jena danken. Marco Grünewald, Dr. Roman Forker und Prof. Dr. Torsten Fritz sei hiermit herzlich für die Zusammenarbeit an und die Diskussionen zu organischen Heteroschichten gedankt. Marco Grünewald möchte ich an dieser Stelle noch einmal herzlich für die gemeinsame Durchführung der letzten beiden Messzeiten bei BESSY danken. Auf Grund der engen Personalsituation bei der EP 7 hat seine Hilfe die erfolgreiche und effektive Datenproduktion bei diesen Messzeiten erst möglich gemacht. Für eine Kollaboration zu Beginn meiner Promotion sei Dr. Benjamin Stadtmüller und Prof. Dr. Christian Kumpf vom PGI-3 des Forschungszentrums Jülich gedankt.

Für die Möglichkeit des interdisziplinären Austauschs danke ich dem GREKOS Projekt, welches mir zu interessanten Diskussionen und dem Besuch des "Statusseminar Organische Photovoltaik" des BMBF verholfen hat. Dadurch konnte ich einen Einblick in die Anwendungsmöglichkeiten von heteroorganischen Grenzflächen gewinnen. Für interessante Vorträge in der Ringvorlesung, die Teilnahme an der Konferenz 2011 in Würzburg, sowie der Klausurtagung 2012 im Kloster Schöntal danke ich dem Graduiertenkolleg GRK 1221.

Während meiner Promotion hatte ich das Vergnügen die Bachelorarbeit von Henriette Maaß und die Diplomarbeit von Florian Bruckner zu betreuen. Beiden danke ich für die angenehme Zusammenarbeit und die großartigen Leistungen, welche letztendlich auch zu tollen Ergebnissen geführt haben.

Wichtige experimentelle Vorarbeiten zu dieser Dissertation über Heteroorganikschichten und resonante Photoelektronenspektroskopie hat Dr. Marc Häming geleistet. Für diese sowie gemeinsame Diskussionen über die Durchführung und Auswertung von Synchrotronmesszeiten, Photoelektronenspektroskopie, Röntgenabsorption und resonante Photoelektronenspektroskopie möchte ich ihm danken. Leider hatte ich nie die Möglichkeit gemeinsam mit ihm eine Messzeit durchzuführen und so direkt von ihm zu lernen. Weiterer Dank gilt Johannes Ziroff für gemeinsame Diskussionen über resonante Photoelektronenspektroskopie, den Kondoeffekt und organische Moleküle auf Metalloberflächen im Allgemeinen. Auch Dr. Mattia Mulazzi möchte ich danken für Diskussionen zu Photoelektronenspektroskopie, Festkörperphysikkonzepten und vor allem die Kunst der nonverbalen Kommunikation. Des Weiteren geht mein Dank an Holger Schwab für Diskussionen über resonante Photoelektronenspektroskopie und das Gunnarsson-Schönhammer Modell, Frank Meyer und Andreas Benkert für Diskussionen über resonante Photoelektronenspektroskopie im Vergleich zu inelastischer Röntgenstreuung sowie Dr. Hendrik Bentmann für Diskussionen zu Oberflächenzuständen.

Im speziellen sei noch ein weiteres Mal Dr. Michael Wießner für das Anfertigen der Bilder von Molekülen und von DFT Rechnungen geladener Moleküle gedankt. Letztere haben es auf Grund von methodischen Schwierigkeiten leider nicht in diese Arbeit geschafft. Frank Meyer danke ich für Rechnungen zur Röntgenabsorption an Coronen, die mit den in der Literatur verfügbaren Rechnungen verglichen werden konnten. Marco Grünewald sei nochmals gedankt für den Einblick in LEED Messungen an SnPc + PTCDA/Ag(111) Heteromonolagen, STM Messungen an PTCDA/1 ML CuPc/Ag(111) Heteroschichten und vielen DRS Datensätzen. Der Vergleich unserer Ergebnisse hat mich in meiner Arbeit an vielen Stellen weitergebracht. Gleichermaßen danke ich Dr. Benjamin Stadtmüller für den Einblick in LEED Messungen an einer 1.5 ML SnPc auf 1 ML PTCDA auf Ag(111) Probe vor und nach dem Erhitzen auf 570 K und Massenspektrometerdaten während des Heizvorganges. Johannes Ziroff danke ich im speziellen noch für die Bereitstellung der Daten von resonanter Photoelektronenspektroskopie an 1 ML PTCDA auf Ag(111), welche ich für die Differenzspektren für die entsprechenden Daten des Systems CuPc auf 1 ML PTCDA auf Ag(111) benutzt habe.

Meinen beiden langjährigen Bürokollegen Dr. Michael Wießner und Patrick Bayersdorfer möchte ich noch ganz besonders für die lockere und lustige Stimmung im "Gemeinschaftsbüro" danken. Viele wissenschaftliche und auch die ein oder andere nichtwissenschaftliche Unterhaltung mit euch hat mir den Arbeitsalltag verschönert. Zuletzt ist noch Sonja Schatz hinzugekommen, die mit ihrer enormen Begeisterungsfähigkeit und ihrem stets freundlichen Wesen für sehr gute Stimmung gesorgt hat. Vielen Dank dafür. Auch allen anderen, die über die Jahre zur Arbeitsgruppe EP 7 und anfangs EP 2 gehört haben, sei für die angenehme Atmosphäre und die Zusammenarbeit gedankt. Unserem Admin Dirk Hauschild möchte ich im speziellen noch für die IT-Betreuung danken.

Zu guter Letzt geht noch ganz besonderer Dank an meine Freunde und Familie, ohne deren Unterstützung diese Arbeit nicht möglich gewesen wäre. An dieser Stelle die Namen all derer zu nennen, die mir in dieser Zeit mir immer wieder den nötigen Ausgleich zur Arbeit an der Promotion ermöglicht haben, würde den Rahmen dieser Danksagung sprengen. In einigen Fällen wäre eine explizite Begründung für das Danke sagen auch in einer Dissertation ein wenig Fehl am Platz. Vielen, vielen Dank!

Eidesstattliche Erklärung

gemäß § 5, Abs. 2, Ziff. 2 und 5 der
Promotionsordnung der
Fakultät für Physik und Astronomie der
Julius-Maximilians-Universität Würzburg

Hiermit erkläre ich an Eides statt, dass ich die vorliegende Dissertation eigenständig, d.h. insbesondere selbstständig und ohne Hilfe einer kommerziellen Promotionsberatung angefertigt und keine anderen als die von mir angegebenen Quellen und Hilfsmittel benutzt habe und dass ich die Gelegenheit zum Promotionsvorhaben nicht kommerziell vermittelt bekommen habe und insbesondere nicht eine Person oder Organisation eingeschaltet habe, die gegen Entgelt Betreuer bzw. Betreuerinnen für die Anfertigung von Dissertationen sucht.

Hiermit erkläre ich zudem, dass ich die Regeln der Universität Würzburg über gute wissenschaftliche Praxis eingehalten habe und dass ich die Dissertation in gleicher oder anderer Form nicht bereits in einem anderen Prüfungsfach vorgelegt habe.

Würzburg, den 27.08.2014

Christoph Sauer